Relativistic corrections of Fermi surface instabilities

And you run and you run to catch up with the sun but it's sinking.
Racing around to come up behind you again.
The sun is the same in a relative way, but you're older.
Shorter of breath and one day closer to death.

PINK FLOYD, TIME

Dissertation zur Erlangung des
naturwissenschaftlichen Doktorgrades der
Julius-Maximilians-Universität Würzburg

vorgelegt von TILMAN SCHWEMMER

betreut von

Prof. Dr. Ronny Thomale &
Prof. Dr. Domenico di Sante

Relativistic corrections of Fermi surface instabilities

Dissertation zur Erlangung des

naturwissenschaftlichen Doktorgrades

der Julius-Maximilians-Universität Würzburg

vorgelegt von

Tilman Schwemmer

aus Bremen

Würzburg 2023

Eingereicht am 17.01.2023
bei der Fakultät für Physik und Astronomie

1. Gutachter: Prof. Dr. Ronny Thomale
2. Gutachter: Prof. Dr. Giorgio Sangiovanni
3. Gutachter: Prof. Dr. Walter Metzner
der Dissertation

Vorsitzender:

1. Prüfer: Prof Dr. Ronny Thomale
2. Prüfer: Prof. Dr. Giorgio Sangiovanni
3. Prüfer: Prof. Dr. Matthias Bode
im Promotionskolloquium

Tag des Promotionskolloquiums: 04.05.2023

Doktorurkunde ausgehändigt am:

Dedicated to my grandparents,

Die Naturwissenschaft braucht der Mensch zum Erkennen, den Glauben zum Handeln.

Max Planck

Abstract

Relativistic effects crucially influence the fundamental properties of many quantum materials. In the accelerated reference frame of an electron, the electric field of the nuclei is transformed into a magnetic field that couples to the electron spin. The resulting interaction between an electron spin and its orbital angular momentum, known as spin-orbit coupling (SOC), is hence fundamental to the physics of many condensed matter phenomena. It is particularly important quantitatively in low-dimensional quantum systems, where its coexistence with inversion symmetry breaking can lead to a splitting of spin degeneracy and spin momentum locking. Using the paradigm of Landau Fermi liquid theory, the physics of SOC can be adequately incorporated in an effective single particle picture. In a weak coupling approach, electronic correlation effects beyond single particle propagator renormalization can trigger Fermi surface instabilities such as itinerant magnetism, electron nematic phases, superconductivity, or other symmetry broken states of matter.

In this thesis, we use a weak coupling-based approach to study the effect of SOC on Fermi surface instabilities and, in particular, superconductivity. This encompasses a weak coupling renormalization group formulation of unconventional superconductivity as well as the random phase approximation. We propose a unified formulation for both of these two-particle Green's function approaches based on the notion of a generalized susceptibility.

In the half-Heusler semimetal and superconductor LuPtBi, both SOC and electronic correlation effects are prominent, and thus indispensable for any concise theoretical description. The metallic and weakly dispersive surface states of this material feature spin momentum locked Fermi surfaces, which we propose as a possible domain for the onset of unconventional surface superconductivity. Using our framework for the analysis of Fermi surface instability and combining it with *ab-initio* density functional theory calculations, we analyse the surface band structure of LuPtBi, and particularly its propensity towards Cooper pair formation. We study how the presence of strong SOC modifies the classification of two-electron wave functions as well as the screening of electron-electron interactions. Assuming an electronic mechanism, we identify a chiral super-

conducting condensate featuring Majorana edge modes to be energetically favoured over a wide range of model parameters.

Zusammenfassung

Relativistische Effekte bestimmen die Eigenschaften vieler Quantenmaterialien entscheidend. Im beschleunigten Bezugssystem eines Elektrons transformiert das elektrische Feld des Kerns in ein magnetisches Feld, welches an den Spin des Elektrons koppelt. Die daraus resultierende Wechselwirkung zwischen dem Spin eines Elektrons und seinem Bahndrehimpuls, bekannt als Spin-Bahn-Kopplung (*engl.* spin-orbit coupling SOC), ist für die Physik vieler Phänomene der kondensierten Materie von grundlegender Bedeutung. Dieser Effekt ist in niedrigdimensionalen Quantensystemen, wo seine Koexistenz mit Inversionssymmetriebrechung zu einer Aufspaltung der Spinentartung und Kopplung des Spins an den Impulsfreiheitsgrad führen kann besonders wichtig. Mit dem Paradigma von Landaus Fermi-Flüssigkeits-Theorie lässt sich die Physik des SOC in einem effektiven Ein-Teilchenbild gut modellieren. Ausgehend von einem schwach gekoppelten Bild können elektronische Korrelationseffekte, die über diese einfache Theorie hinausgehen, eine Instabilität der Fermi-Fläche auslösen, die zu Magnetismus, elektronisch-nematischen Phasen, Supraleitung oder anderen symmetriegebrochenen Materialzuständen führt.

In dieser Dissertation verwenden wir einen auf schwacher Kopplung basierenden Ansatz, um die Wirkung von SOC auf Instabilitäten der Fermi-Fläche und insbesondere auf Supraleitung zu untersuchen. Wir betrachten eine störungstheoretische Renormierungsgruppenformulierung für unkonventionellen Supraleitung die Random-Phase-Approximation (RPA). Auf Grundlage der verallgemeinerten Suszeptibilität entwickeln wir eine einheitliche Formulierung für diese beiden Ansätze.

In dem Halb-Heusler-Halbmetall und Supraleiter LuPtBi sind sowohl SOC- als auch elektronische Korrelationseffekte für jede theoretische Beschreibung von großer Bedeutung. Der metallische und schwach dispersive Oberflächenzustand dieses Materials weist Fermi-Flächen mit gekoppeltem Spin und Impuls auf, die wir als mögliche Domäne für den Beginn unkonventioneller Oberflächensupraleitung vorschlagen. Wir kombinieren *ab-initio* Dichtefunktionaltheorieberechnungen für die Oberflächenbandstruktur von LuPtBi mit der Renormierungsgruppe und der RPA

für eine Analyse der Fermi-Oberflächeninstabilitäten and der Kristalloberfläche. Wir untersuchen, wie die Existenz von starkem SOC die Klassifizierung von Zwei-Elektronen-Wellenfunktionen sowie die Abschirmung von Elektron-Elektronen-Wechselwirkungen modifiziert. Unter der Annahme eines elektronischen Mechanismus identifizieren wir ein chirales supraleitendes Kondensat mit Majorana-Randmoden, das über einen weiten Bereich von Modellparametern energetisch begünstigt ist.

Table of contents

Introduction

Superconductors are fascinating materials of both technological relevance and academic interest. Already in the year 1911, Kammerlingh Onnes discovered that electrical resistivity of mercury vanishes when the material is cooled to liquid helium temperatures ($T \approx -270\,^{\circ}\mathrm{C}$). It was quickly established that this phenomenon is not unique to mercury as a material [1]. This property of superconductors, namely their perfect conductivity, forms the basis of the most widely spread use of superconductors today in high-field magnets for particle accelerators and magnetic resonance imaging machines [2]. From the viewpoint of fundamental research, it is neither the vanishing resistivity nor the perfect diamagnetism exhibited by the superconducting state of matter that make it so remarkable. Rather, it is the fundamentally quantum mechanical nature of this macroscopic phenomenon.

Quantum mechanics is instrumental to our modern understanding of atoms, molecules, and materials. Nevertheless, we can describe almost all macroscopic systems perfectly by using classical mechanics and electromagnetism. This is due to the fact that the quantum mechanical wavefunction in most systems is localized to the span of a few atoms [3]. This limits the direct observation of quantum effects to experiments that are either extremely sensitive to, or explicitly probe microscopic length scales. Superconductivity is a notable exception to this observation. If a superconductor is cooled below its critical temperature at which the phase transition to the superconducting state occurs, a macroscopic fraction of the electrons inside the material condense into a single quantum state that necessitates a description via a single quantum mechanical wave function [4, 5]. The multiple occupation of a single quantum state requires the formation of bound states between pairs of electrons, known as Cooper pairs. In 1972 the Nobel prize in physics was awarded to J. Bardeen, L. N. Cooper, and J. R. Schrieffer for their theory of superconductivity, commonly known as BCS theory. In their work they derive a unified theory from the microscopic forces binding the Cooper pairs to the phase coherence of the macroscopic condensate. This

phase coherence of the emerging state provides a natural explanation for the vanishing resistivity and perfect diamagnetism of the superconductor.

In conventional BCS superconductors like mercury or niobium the bound states of electrons form due to an attractive potential between them that results from their coupling to the crystal's lattice vibrations (phonons). Due to this, the superconducting transition temperature T_c correlates with the electron phonon coupling in these materials. An effect that can be demonstrated by comparing the T_c of different isotopes of the same element [6]. Notably, the attractive potential generated by the phonon modes of materials like the layered copper-oxides is insufficient to explain their "high-T_c" and a new explanation for the pairing mechanism is needed [7].

Long before the discovery of "high-T_c" superconductivity in the cuprates by J. G. Bednorz and K. A. Müller in 1986 [8], W. Kohn and J. M. Luttinger realized that the repulsive Coulomb potential between two electrons may support the formation of Cooper pairs inside a solid state material [9]. Their result rests on two important insights: (i) Cooper pairs may have finite angular momentum; (ii) Screening of the long-range Coulomb potential can lead to attractive interaction channels in a harmonic decomposition of the effective interaction.

Combining these ideas leads to the conclusion that superconductivity can arise from the repulsive Coulomb interaction between electrons alone. Cooper pairs with distinguishable angular momentum result in different superconducting states of matter and, therefore, relate to different order parameters. This mechanism forms the basis for the current understanding of the pairing mechanism in the "high-T_c" superconducting material classes of the cuprates and iron-pnictides [10–12].

While more generally valid, the theory of Kohn and Luttinger as well as the BCS theory of superconductivity were initially applied to relatively isotropic three dimensional systems (a sensible assumption for most conventional phonon based superconductors). The mentioned "high-T_c" superconductivity arises in layered materials *i.e.*, materials with a large anisotropy in their chemical and electronic structure. For the example of "high-T_c" copper-oxide materials, the ratio of the conductivity in the doped copper-oxide planes is up to three orders of magnitude higher than in the perpendicular direction [13].

From a theoretical point of view, the dimensionality of a physical system does not only influence its description via certain models but critically determines the relevance of interactions between the constituent particles. Some intuition for this can be gained when we consider a one-dimensional system of electrons interacting via the Coulomb potential induced by their identical charges. Clearly, the particles in such a system can never switch places, thus emphasizing the importance of their potential energy U over their kinetic energy T. While the argument is more involved for higher dimensions, it is still possible to show that electron correlations for systems of identical particle density are stronger in two spatial dimensions than in three [14]. This

significance of correlations in low dimensional systems naively suggests that interaction driven spontaneous symmetry breaking is enhanced in these systems. It is important to note that this intuition has to be complemented by various arguments and proofs that exclude the possibility of true long-range ordering *i.e.*, spontaneous symmetry breaking of a continuous symmetry in one spatial dimension (two spatial dimensions at finite temperatures), often referred to as Mermin-Wagner-Hohenberg (MWH) theorem [15–17].

For fully three-dimensional layered bulk systems such as the copper-oxide superconductors and layered iron pnictides, the MWH theorem is clearly irrelevant as they develop long-range magnetic (breaking the spin-rotation symmetry) or superconducting order (breaking the $U(1)$ gauge symmetry associated with particle number conservation) depending on the parameters of the system [8, 18, 19]. Nevertheless, the theoretical modelling of these systems often neglects the interaction and movement of particles between different layers of the system *i.e.*, the dispersion of the system is assumed to be perfectly two-dimensional [11, 12]. For the case of the copper-oxide superconductors, it is widely believed that their properties can be sufficiently captured by a single-orbital, square-lattice tight-binding model with additional onsite interactions between the particles [11]. This model was introduced already in 1963 as a simple model describing the physics of electrons in narrow bands formed by d or f orbitals by J. Hubbard [20] and became one of the paradigmatic models of correlated electron physics.

While the Hubbard model has so far eluded an exact solution, its various exactly understood limiting cases exhibiting a wide range of physical phenomena drive continuous interest [21]. In its simplest form the model is characterized by two parameters: The first is the ratio U/t of the hopping amplitude t between nearest-neighbour sites on the lattice and the potential energy penalty U that is associated with doubly occupied sites. The second parameter $0 < n < 2$ counts the average number of electrons per unit cell. Despite its parametric simplicity, this basic model seems to provide an adequate description of the copper-oxide materials at various doping levels (corresponding to different values of n in the model), while being complex enough to necessitate approximations or parameter fine tuning to obtain physical insights from it [22].

Unfortunately, the copper-oxide materials are best described at intermediate or large values U/t, where perturbative treatments are not justified [11]. The experimental observation of quasi-two-dimensional superconductivity, however, has not been limited to this regime. In fact, even the superconducting state of copper-oxides with larger than optimal hole doping may be properly described as emerging from of a correlated metal state that is well described by the Hubbard model in the limit of small U/t [22]. For this situation an exact solution for $U/t \to 0$ is possible [23]. A reasonable expectation would be that conclusions from such an analysis hold even for the onset of finite interactions. This is indeed confirmed when employing more involved (but less controlled)

approximations such as the random phase approximation (RPA) or the functional renormalization group (fRG) [24, 25].

While most of these approximation techniques are not limited to the simplest Hubbard model per se, adapting them to extended-Hubbard type models is still challenging on an implementation level. Including longer range hopping and nearest neighbour repulsion terms, adding orbital degrees of freedom, or putting the model of interest on a more complex lattice geometry make it a versatile tool for the description of various realistic material systems. This approach has been employed in the past for the investigation of multiple strongly-correlated metals such as the iron-pnictide superconductors and Sr_2RuO_4 among others.

Recently, the inclusion of spin-orbit coupling (SOC) into theoretical models has become particularly relevant for the description of real materials of experimental interest [26, 27]. SOC is one of two leading order relativistic effects in atomic theory, the other being the spin-spin interaction between different electrons. It is most intuitively understood in the accelerated reference frame of an electron orbiting the atomic nucleus. From this point of view, the electric field of the moving nucleus gives rise to a magnetic field that couples to the electrons spin via the Zeemann interaction. Compared to the spin-spin interaction, SOC is significantly more relevant for condensed matter systems as the associated energy scale is related to the host atoms atomic number Z. For a hydrogen like atom with central charge Ze, the SOC interaction scales as $\Delta E_{\mathrm{SOC}} \sim Z^4$. Correcting for the screening charges in heavy atoms, one still obtains an approximate scaling of $\Delta E_{\mathrm{SOC}} \sim Z^2$ [28, 29]. While calculating spin-orbit effects on the band structure of real materials is standard in modern density functional theory implementations like the Vienna *ab-initio* simulation package [30], its interplay with electronic correlations in general and unconventional superconductivity in particular is an ongoing research effort [31–34].

Hubbard models for realistic materials

Here, we want to highlight three instances of generalized Hubbard models that form a significant part of the research during my PhD before continuing to the main part of the thesis. The highlighted problems include the investigation of lattice geometries different from the square lattice, the inclusion of additional orbital degrees of freedom, and the influence of a third spatial dimension.

Layered Kagome materials AV_3Sb_5

One of the most natural extensions of the single-band square-lattice Hubbard model is its adaptation to different lattice geometries. A prime example of the rich physics resulting from such a

simple change is the emergence of unconventional charge and spin order as well as spin triplet f-wave superconductivity in the Kagome Hubbard model [35, 36]. In 2013, this phenomenology was established in a purely theoretical study of the Kagome Hubbard model, without realistic material analogues in sight.

The discovery of the layered Kagome metals AV_3Sb_5 (where A is one of the Alkali metals *i.e.*, potassium, rubidium or caesium) in 2019 constituted the starting point for the experimental investigation of correlated Kagome systems in the metallic regime. Like the high-T_c superconductors discussed above, these materials display a layered structure in which the vanadium atoms form a Kagome lattice in each plane shown, in Figure 1 [37]. Additionally, the chemistry of the system conspires with the crystal field in the vicinity of the vanadium atoms in a way such that the vanadium 3d orbitals are part of the relevant low-energy degrees of freedom. Due to the comparably small volume of these orbitals and resulting confinement of the electrons, one can expect strong correlation effects in such a system. The resulting tendency for spontaneous symmetry breaking due to residual quasiparticle interactions is further enhanced by the large density of states at and around the Fermi-level in these materials. This feature is facilitated by the systems chemical potential being tuned close to multiple van Hove singularities in the pristine *i.e.*, non doped stoichiometry.

Combining the two-dimensional character, metallic nature and relevance of electronic correlations of the vanadium d-orbitals, it is not surprising that the layered Kagome metals have recently emerged as a prime candidate for exotic Fermi-surface instabilities in general and potentially unconventional superconductivity in particular [38–40]. The interest in the material class is further enhanced by the fact that three compounds were found to be superconducting with critical temperatures of $T_c = 0.93\,\mathrm{K}$ (KV_3Sb_5), $T_c = 0.92\,\mathrm{K}$ (RbV_3Sb_5), $T_c = 2.5\,\mathrm{K}$ (CsV_3Sb_5) [38, 41, 42] and that various unconventional charge density wave (CDW) orders have been experimentally identified in these materials.

In a recent letter [43], we developed an effective Hubbard type tight-binding model for the analysis of the superconductivity in AV_3Sb_5. Our model is able to encompass the necessary complexity of multiple van Hove singularities in the vicinity of the Fermi-surface as well as the Kagome lattices special sublattice decoration, while still allowing for a thorough analysis of its pairing instabilities. One of the central insights of our model building was that the two van-Hove singularities (vHs) in the Kagome lattices band structure feature two distinct sublattice structures. While the non-trivial sublattice structure of the Kagome tight-binding model and its influence on the superconducting instabilities of the related Hubbard model have been discussed earlier [44], this more subtle point was not clarified there.

The energy eigenstates of a nearest-neighbour Honeycomb lattice tight-binding (TB) model are formed from perfect super positions of the two sublattices *i.e.*, the probability of a given energy

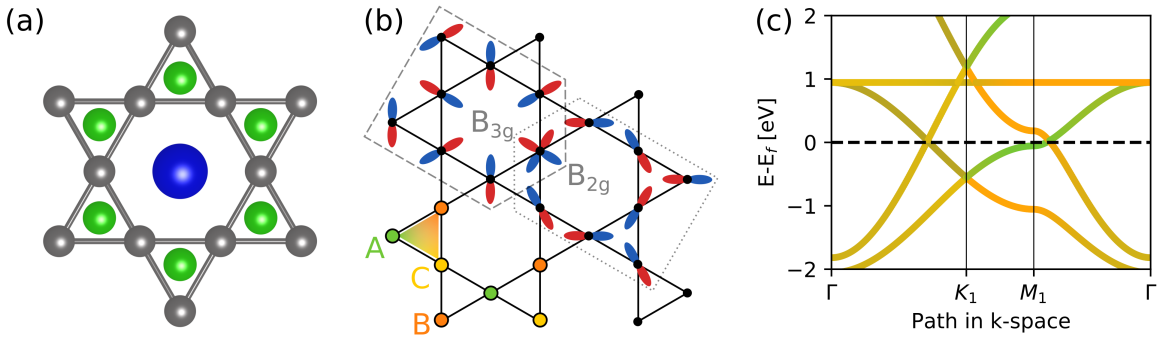

Figure 1: (a) Top view of the KV_3Sb_5 crystal structure. The blue atom in the center represents the alkali metal (potassium (K) in this case), the vanadium (V) atoms in silver form the Kagome net and the antimony (Sb) atoms organize themselves in an interlacing honeycomb lattice. The top view hides the fact that not all atoms reside in the same plane. (b) Sketch of the sublattice structure and orbital model of the Kagome V planes. The sign structure of the d_{xz} and d_{yz} orbitals (shown from above) is depicted in blue and red. The red, yellow, and orange colouring indicates the three Kagome sublattices. (c) Band structure of our 2 orbital × 3 sublattice effective model along the conventional high-symmetry path through momentum space (k-space) and in vicinity to the Fermi-level. The color coding is used to depict the sublattice support of the energy eigenstates at each momentum.

eigenstate to be measured on sublattice A is identical to the probability for the other sublattice B. We call this even sublattice occupation. In contrast, the energy eigenstates of the Kagome TB model vary between an equal split between all three sublattices and the pure occupation of a single sublattice degree of freedom. In particular, two different types of van Hove singularities exist in Kagome systems, which we call sublattice mixing (*m*-type) and sublattice pure (*p*-type) and they relate to the lower and upper van-Hove singularity of the simple three-band Kagome model, respectively.

In principle, the modelling of an AV_3Sb_5 band structure around the Fermi-level would require at least 17 distinct orbital/sublattice degrees of freedom per unit cell. This number is comprised of the five d-orbitals for each of the three distinct vanadium atoms per unit cell forming the Kagome structure and the contribution of two antimony p_z orbitals. In order to dramatically decrease the numerical cost associated with our analysis and still preserve the complexity of multiple *p*- and *m*-type van Hove singularities, we decided to constrain our model to the vanadium $d_{xz/yz}$ orbitals. Figure 1 shows a top view of KV_3Sb_5s crystal structure as well as the real space sketch of our tight-binding-model. In panel (c) the band structure in the vicinity of the Fermi-level is presented. One can clearly identify the *p*- type (*m*-type) vHs located just below (above) the Fermi-level at the M point of the Brillouin zone.

Using this tight binding model as the basis for an extended Hubbard model with long-range interactions and analysing it via the random-phase-approximation (RPA) based approach for unconventional superconductivity discussed in the methods section of this thesis, we were able to identify strong competition between various exotic superconducting states. We further highlighted how the interplay between nearest neighbour repulsion and the sublattice structure resulting from the different types of van Hove singularities gives rise to the possibility of inter sublattice triplet f-wave pairing.

Infinite-layer nickel oxides with three-dimensional characteristics

The infinite-layer nickel oxides (nickelates) $RNiO_2$ (R being a placeholder for rare earth atoms *e.g.* La, Pr or Nd) and their hole doped versions are another promising class of materials for the investigation of unconventional superconductivity [45–47]. In these compounds, the unusual +1 oxidation state of the nickel atoms results in a d^9 electronic configuration, analogous to the copper-oxide superconductors. As a result, the key low-energy degrees of freedom are formed by the Ni $d_{x^2-y^2}$ orbitals hybridizing in the systems NiO_2-planes. While this feature is similar to the copper-oxide planes, the contribution of the interstitial rare earth atoms to the low-energy degrees of freedom is unique to the nickelate system. The charge transfer gap between the oxygen p and nickel d-orbitals is also significantly enhanced. In summary, the electronic structure of the infinite-layer nickelates provides a perfect testing ground for the crucial ingredients of unconventional superconductivity due to its similarities and differences to the "high-T_c" copper-oxide materials. The possibility of rare earth atom substitution constitutes an additional tuning parameter in the system that can be used to test our understanding of the superconducting mechanism at play.

In [47], we studied an extended Hubbard model of selected Ni and Nd orbitals that allowed us to adequately capture the low-energy electronic degrees of freedom in the infinite-layer nickelate $NdNiO_2$. Using the RPA in the fluctuation-exchange parametrization we identified its dominant pairing instability to be in the $d_{x^2-y^2}$ channel, making the connection to the copper-oxide superconductors even stronger. Another key result of our analysis is the presence of an intrinsic hole doping of the systems Ni d-orbital Fermi-surface that is facilitated by the two small electron-like pockets formed by Nd d-orbitals. The expected stronger correlation between Ni 3d-orbitals compared to the Nd 5d-orbitals, combined with symmetry constraints on the coupling between them, restrict the relevance of these states to this self doping effect, justifying an effective two-dimensional modelling of the system a posteriori.

Multi-orbital effects in transition metal oxides

Prior to the discovery of the infinite-layer nickelates discussed in the previous section, nickelate heterostructures were suggested as a potential avenue for the realization of an electronic structure resembling the "high-T_c" copper-oxide materials [48]. For the specific case of the $LaNiO_3$ / $LaAlO_3$ heterostructure discussed there, a quasi-two-dimensional electronic structure comprised of Ni 3d-orbitals in a tetragonal crystal field was proposed. In contrast to conventional copper-oxide superconductors, however, the Ni $3d^7$ configuration and weak crystal-field splitting between the two e_g-orbitals require the consideration of both orbital degrees of freedom. Similarly, the reduction of the apical oxygen distance in $BaCuO_{3+\delta}$ necessitates the consideration of such an e_g two orbital model for the description of its low-energy degrees of freedom.

Despite the similarities in the low-energy electronic structure between these compounds, experiments reveal $BaCuO_{3+\delta}$ as a "high-T_c" superconductor with $T_c \approx 70\,\mathrm{K}$ while superconductivity has not been observed in $LaNiO_3$ / $LaAlO_3$ heterostructures and the T_c of related structures has not exceeded 3 K. We were able to explain this striking difference in critical temperatures from calculations on a unifying two-orbital Hubbard-like model. Using a variety of many-body methods we identified the differences in e_g-orbital splitting and band filling between both material platforms as the critical parameters that drive/ inhibit the superconducting transition temperature.

Two dimensional quantum-material platforms

While superconductivity in the cuprates, nickelates and Kagome metal systems can be understood as quasi-two-dimensional, due to the weak-coupling between parallel layers of strong hybridization, their real material instances are bulk systems with a macroscopic number of layers. In this sense, they fundamentally differ from truly two-dimensional systems. From a theoretical standpoint, two-dimensional superconductivity is constrained by the Mermin-Wagner-Hohenberg (MWH) theorem [15], that prohibits true long-range correlations of the superconducting order parameter in less than three spatial dimensions. Nevertheless, the system can form quasi-long-range ordered correlations in the order parameter via the Kosterlitz-Thouless-Berezinskii (KTB) transition and a zero resistance state with perfect diamagnetism *i.e.*, superconductivity can still appear without violating the MWH theorem [49, 50].

Experimentally, the pronounced relevance of disorder for the superconducting transition in two-dimensional systems makes its observation challenging, especially since the system is dominated by its interfaces / surfaces in the residual spatial dimension in this limit. The crossover regime between two and three-dimensional superconductors has been studied since the 1970s [51] via the investigation of superconducting thin films of elemental metals such as lead or bismuth on

insulating substrates. In these systems, a superconductor-insulator (S-I) transition was observed as a function of the sheet resistance (correlated with the film thickness) [52]. Other experiments present evidence for the existence of a KTB transition via analysing the scaling of a thin films resistance as a function of temperature in the vicinity of the phase transition [53].

Owing to the fact that one of the two critical length scales in a superconductor, the superconducting coherence length ξ (next to the London penetration depth), is of the order of a few hundred nano meters for conventional BCS superconductors, the thickness of a two-dimensional superconductor may exceed the atomic-scale thickness. This is in fact what was observed in the previously mentioned works [52, 53].

Recent advances in material fabrication further led to the discovery of two-dimensional superconductivity in systems of atomic scale thickness, such as single atomic layers deposited on insulating substrates, electronic states forming at the interface between different materials and even specifically engineered systems composed of several atomic-monolayers [54–56]. In contrast to the previously discussed systems, the superconducting properties of these systems can't be understood as a thin-film limit of three dimensional materials. The main reason here is the simple lack of three-dimensional extensions of these materials. Phrased from a different point of view, the unique possibilities for the design of electronic parent states in two-spatial dimensions provide an arena for the emergence superconductivity that exceeds the three dimensional systems significantly. Most interestingly, the superconductivity in a variety of systems such as atomic monolayers of FeSe, magic-angle twisted bilayer Graphene (MATBG) or, most recently, a monolayer of Sn deposited on Si(111) have been suggested to be of unconventional origin [54, 56–61].

The discussed sensitivity of two-dimensional superconductors to disorder as well as difficulties in consistent sample preparation pose significant experimental challenges in all of these systems. A possible avenue towards simpler sample manufacturing and preparation is to circumvent the need for multiple materials and the artificial creation of atomically sharp interfaces by using the simplest interface available in any material: its surface to the vacuum. The broken translational symmetry perpendicular to this interface generically allows for additional electronic states confined to the surface [62] that may then (under the right conditions) form dispersive bands parallel to the surface of a given crystal. While the resulting surface bands may be linked to a non-trivial topology of the bulk band structure as present in topological insulators or semimetals, such a structure is no prerequisite for the formation of metallic surface states. They can be easily understood as an effect of the change in boundary and, therefore, normalizability conditions on the electronic wavefunction [62]. From a complementary point of view, one may consider the missing bonding partners at the crystal surface and resulting changes to the local electronic structure as key ingredients for explaining these additional states. Due to their ubiquitous nature and com-

paratively simple experimental realization, metallic surface states provide a perfect avenue for the investigation of two-dimensional superconductivity.

In contrast to the two-dimensional material platforms discussed above, the possibility of unconventional surface superconductivity seems to be theoretically unexplored. While experiments evidencing superconducting states constrained to the surface of the sample are numerous and cover a wide array of materials [63–68], the interpretation of the results seems to be limited to conventional *s*-wave order parameters and phonon-based mechanisms.

In this thesis, we will demonstrate that the enhanced nesting effects in two-spatial dimensions may conspire with electronic correlations to induce unconventional superconductivity in such a metallic surface state. A prime material candidate for this endeavour is LuPtBi. This material is experimentally known to feature a metallic surface state with a significant density of states on top of a semimetallic bulk. Additionally, the combination of the non-centro-symmetric space-group, large spin-orbit coupling effects and superconductivity in LuPtBi and it's close cousin YPtBi have already triggered enormous interest and several interesting bulk superconducting states have already been proposed for them [69–71].

Outline

The discussion of the specific case of the potential for unconventional surface superconductivity in LuPtBi is going to be prefaced with two more general chapters focusing on the methodology employed for this and the other projects mentioned in this introduction.

The first chapter starts with a definition of the class of generalized Hubbard type models we want to consider. Subsequently, we develop a formalism for analysing the propensity towards Fermi-surface instabilities caused by the electronic correlation effects in these models. A particular focus is given to unconventional superconducting instabilities. The discussed framework is based on the calculations of generalized linear response susceptibilities and provides a unified viewpoint on random-phase-approximation (RPA) calculations and the weak-coupling renormalization group (wcRG) approach to unconventional superconductivity. We show how this angle of approaching the problem can be exploited in order to achieve a numerically efficient and gauge invariant implementation of the necessary calculations in generic models.

Based on the formalism developed in the first chapter, we benchmark our numerical implementation in the second chapter. Here we start by reproducing literature results for the Hubbard model on the square and triangular lattice and continue with exploring the effects of spin-orbit coupling on the correlated electron physics in these models.

Chapter three, finally uses the developed formalism to investigate the potential for unconventional surface superconductivity in LuPtBi. Starting from an *ab-initio* calculation for the electronic structure of the material, we construct a generalized Hubbard model for the description of its metallic surface. We continue by dissecting the spin and charge fluctuations of the model and calculate the effective electron-electron interaction in the Cooper channel of the model. Finally, we identify the superconducting instability implied by our analysis and close with a discussion of potential experiments that may provide evidence for surface superconductivity in general, and the particular superconducting ground state predicted by us in general.

The formalistic and computational toolkit developed during my PhD allows for and led to the the study of many realistic quantum materials as outlined above. Nevertheless, I decided to focus the application part of the thesis to the problem of unconventional surface superconductivity as its study necessitates the inclusion of spin-orbit coupling into the microscopic description on a methodological level and constitutes a novel arena for unconventional superconducting mechanisms conceptually.

Methodology

In this part, we introduce the theoretical and numerical framework used to study the quantum many body problems introduced in the following chapters. The contents of this part of the thesis are partially included in Reference [72].

Methodology

The introduction of this thesis highlighted the fact that Fermi-liquids can undergo a superconducting transition driven by electronic correlation effects [9]. In fact, condensed matter research over the past decades has led to the discovery of a variety of superconducting materials featuring a metallic parent state and a pairing mechanism which is likely driven by electronic correlations rather than electron-phonon coupling [22].

Starting from a Fermi-liquid description of the metallic state, an initial perturbative treatment of the residual correlation effects is appropriate. This picture was the starting point for an analysis by Kohn and Luttinger in 1965 [9]. They found that the ubiquitous presence of particle-hole (PH) fluctuations in a metallic state introduces an additional momentum dependence into the effective (screened) electron-electron interaction already on perturbative level. This modified interaction generically supports the emergence of an unconventional superconducting condensate, as the existence of a single attractive channel with infinitesimal strength can drive the Cooper instability of a Fermi-liquid. Decades later, their argument was re-established in a more systematic way for generic lattice models [23, 73], resulting in the application of the theory to numerous toy models and materials [44, 74–77]. We henceforth label this approach as weak coupling renormalization group (wcRG) as it relies heavily on a 1-loop perturbative treatment of the electron-electron interaction (for a detailed review see *e.g.* [73]). Its central motif is to retain analytical control over the divergence in the particle-particle (PP) channel via the introduction of a cutoff. Subsequently one can show that the physical results are independent of this calculational device and obtains a rigorous formulation of unconventional pairing in the limit of vanishing coupling.

A related, but somewhat less rigorous approach to unconventional superconductivity arising from particle-hole fluctuations is given by the random-phase approximation. Both experimental and theoretical studies have established such particle-hole fluctuations, mostly in the form of spin-fluctuations, as a common thread between many unconventional superconductors [22]. For a material system close to a (magnetic) instability, such fluctuations can, within a leading approx-

imation, be well described by the random-phase-approximation (RPA). One can then proceed to analyze the pairing interactions induced by these fluctuations [24, 78, 79]. While a rigorous convergence radius for the RPA has not been established so far, it is clear that the error will usually increase with the electronic coupling strength, as all vertex corrections and other higher order diagrammatic components are neglected. If we start from the hypothesis that the pairing is driven by particle-hole fluctuations however, their resummation to arbitrary order should yield a valid description even beyond the limit of perturbative coupling strengths, making the RPA a useful tool for the qualitative analysis of superconductivity beyond the analytically controlled limit of the wcRG.

In this chapter, we will start by establish a general class of extended Hubbard models and proceed to briefly summarize the fermionic coherent state path integral formulation of the quantum many-body problem, the theoretical basis upon which the wcRG and RPA rest. The emergence of unconventional superconductivity in these models is first discussed via a generalized formulation of the wcRG that natively allows for the inclusion of spin-orbit coupling terms, does not necessitate an analytically solvable tight-binding model and enables efficient interaction phase-diagram scans. Subsequently we discuss how the central building block of this formulation, the generalized non-local particle-hole susceptibility $\aleph$, relates to correlation functions and susceptibilities of general two-particle operators. We finally present a generalized formulation of the RPA based on this object before discussing numerical aspects of its efficient computation.

1.1 Generalized Hubbard model

The formalism described here concerns generalized Hubbard type models. The spinful (s_i) electrons in our models can occupy different orbital and sublattice degrees of freedom denoted by a fused index w_i. The kinetic part of the Hamiltonian generically is of tight-binding type

$$H_0 = \sum_{\mathbf{r}_0,\mathbf{r}_2} \sum_{a_0,a_2} t_{a_2 a_0}(\mathbf{r}_2 - \mathbf{r}_0) c_2^\dagger c_0 \,, \tag{1.1}$$

where $a_i = (w_i, s_i)$ is a fused spin, orbital and sublattice index, $c_i^\dagger$ denotes the creation operator of an electron with indices a_i on a lattice site $\mathbf{r}_i$ and the amplitudes t_{ij} parametrize translation invariant hopping processes between states $c_i^\dagger |0\rangle$ and $c_j^\dagger |0\rangle$.

Using the translation invariance of the model via Fourier transformation we we find

$$H_0 = \sum_{\mathbf{k}} \sum_{a_0,a_2} \Big(\sum_{\mathbf{r}} t_{a_2 a_0}(\mathbf{r}) \mathrm{e}^{-\mathrm{i}\mathbf{k}\mathbf{r}} \Big) c^\dagger_{a_2,\mathbf{k}} c_{a_0,\mathbf{k}} \,. \tag{1.2}$$

While the matrix $t_{a_2a_0}(\mathbf{r})$ may not allow for a closed analytical solution for generic systems, we can always find a numerical eigenmode decomposition

$$\begin{aligned} h_{a_2a_0}(\mathbf{k}) &= \sum_{\mathbf{r}_k} t_{a_2a_0}(\mathbf{r}_k)\mathrm{e}^{-\mathrm{i}\mathbf{k}\mathbf{r}_k} \\ &= \sum_{\alpha_i} v_{a_2\alpha_i}(\mathbf{k})\epsilon_{\alpha_i}(\mathbf{k})v^*_{a_0\alpha_i}(\mathbf{k})\,. \end{aligned} \tag{1.3}$$

The solution of the eigenvalue problem is parametrized by (possibly degenerate) band energies $\epsilon_{\alpha_i}(\mathbf{k})$ (eigenvalues) and a complete set of orthonormal eigenvectors $v_{a_i\alpha_i}(\mathbf{k})$ of the matrix, which encode the orbital-spin structure of the energy eigenstates. We note that the Fourier transformation of systems with multiple sites in the unit cell should be done in "proper" gauge as defined in [80] in order to ensure full periodicity of $h(\mathbf{k})$ across all Brillouin zones (BZ). The proper gauge a choice of basis which appears as if all orbital positions lie in the center of the unit cell, eliminating the possibility for terms with fractional real-space lattice vectors in the Hamiltonian. This allows the definition of all other operations and in particular integrations without explicit specialization of the BZ in which to evaluate, as they are all equivalent.

An important detail we want to stress here is the fact that the orbital band transformations $v_{a_i\alpha_i}(\mathbf{k})$ are only defined up to gauge transformations *i.e.*, $\mathrm{e}^{\mathrm{i}\varphi_{\alpha_i}(\mathbf{k})}v_{a_i\alpha_i}(\mathbf{k})$ are equally valid solutions to the eigenvalue problem given by Equation 1.3. Additional care must be taken in the case of degenerate bands where not only the phase but also the choice of basis in the degenerate subspace is not specified by the eigenvalue problem. While the second issue is easily circumvented by analytical separation of the spin degree of freedom in the case of non spin-orbit coupled systems, the first issue is ubiquitous and particularly relevant for models requiring a numerical solution of Equation 1.3. This ambiguity in the choice of eigenstates poses difficulties in the analysis of Hubbard type models due to the resulting gauge-dependence of the bare interaction in band space as we will elaborate now.

Notwithstanding these arguments, a representation of Equation 1.1 in terms of energy eigenstates

$$H_0 = \sum_{\mathbf{k}}\sum_{\alpha} \epsilon_\alpha(\mathbf{k})c^\dagger_{\alpha,\mathbf{k}}c_{\alpha,\mathbf{k}}\,, \tag{1.4}$$

with

$$c^\dagger_{\alpha,\mathbf{k}} = \sum_a v_{a\alpha}(\mathbf{k})c^\dagger_{a,\mathbf{k}} \tag{1.5}$$

proves to be an computationally useful device.

A general translation-invariant two-particle interaction is denoted by a quartic Hamiltonian of the form

$$H_I = \sum_{\{\mathbf{r}_i\}} \sum_{\{a_i\}} U_{a_0 a_1 a_2 a_3}(\hat{\mathbf{r}}_1, \hat{\mathbf{r}}_2, \hat{\mathbf{r}}_3) c_2^\dagger c_3^\dagger c_1 c_0 \,, \tag{1.6}$$

where we define $\hat{\mathbf{r}}_i = \mathbf{r}_i - \mathbf{r}_0$ to compactify notation and emphasize translational invariance. We further employ $\{x_i\} = x_0, x_1, x_2, x_3$ as a shorthand notation for multiple sums. Using the same Fourier transform (in proper gauge) as before we find

$$H_I = \sum_{\{\mathbf{k}_i\}} \sum_{\{a_i\}} U_{\{a_i\}}(\{\mathbf{k}_i\}) c^\dagger_{a_2,\mathbf{k}_2} c^\dagger_{a_3,\mathbf{k}_3} c_{a_1,\mathbf{k}_1} c_{a_0,\mathbf{k}_0} \tag{1.7}$$

where we introduced the definition

$$\begin{aligned} U_{\{a_i\}}(\{\mathbf{k}_i\}) = \; & \delta(\mathbf{k}_0 + \mathbf{k}_1 - \mathbf{k}_2 - \mathbf{k}_3) \\ & \sum_{\hat{\mathbf{r}}_1, \hat{\mathbf{r}}_2, \hat{\mathbf{r}}_3} U_{\{a_i\}}(\hat{\mathbf{r}}_1, \hat{\mathbf{r}}_2, \hat{\mathbf{r}}_3) \mathrm{e}^{+\mathrm{i}(\mathbf{k}_1 \hat{\mathbf{r}}_1 - \mathbf{k}_2 \hat{\mathbf{r}}_2 - \mathbf{k}_3 \hat{\mathbf{r}}_3)} \,. \end{aligned} \tag{1.8}$$

Analogous to the single particle Hamiltonian, a subsequent transformation into band space results in

$$\begin{aligned} U_{\{\alpha_i\}}(\{\mathbf{k}_i\}) = \sum_{\{a_i\}} & v_{a_2\alpha_2}(\mathbf{k}_2) v_{a_3\alpha_3}(\mathbf{k}_3) \\ & v^*_{a_1\alpha_1}(\mathbf{k}_1) v^*_{a_0\alpha_0}(\mathbf{k}_0) U_{\{a_i\}}(\{\mathbf{k}_i\}) \,. \end{aligned} \tag{1.9}$$

Our previous discussion on the gauge freedom in the definition of the eigenvectors $v_{a_i\alpha_i}$ make it clear that this expression is manifestly gauge variant. Due to this it may be a useful analytical device in some cases, but not a computationally advantageous quantity for general models. While one can trivially avoid this issue by considering the interaction in orbital space only, this is not commonly done in the wcRG and functional renormalization group (fRG) literature. There, calculations in band space are standard since they enable a restriction of the effective interaction to the bands crossing the Fermi-level. While performing calculations in orbital space can in principle be fused with such an approximation, the performance of the established Fermi surface patch formulation of the fRG is significantly reduced in such a hybrid approach. The reason is that a restriction of the interaction to the Fermi surface is most useful if the interaction is constrained to one band at the Fermi surface, resulting in a reduction of the vertex function by a factor of N_{orb}^4 [81, 82]. Nevertheless, our formulation of the wcRG via the generalized susceptibility does not allow for such a reduction, but in turn allows for gauge invariant calculations of two-particle scattering amplitudes. Note that fRG calculations in orbital space are possible and have been suc-

cessfully employed in the analysis of electronic instabilities in the Honeycomb Hubbard model and the square lattice Hubbard model with added Rashba spin-orbit interactions [34, 80, 83–85].

Before continuing with a discussion of the wcRG and RPA methodology, we want to provide some additional context to the applicability and relevance of our models to real materials. Landau's Fermi-liquid theory tells us that the metallic phase of a material can be described in terms of non-interacting quasi-particle excitations [86]. This crucially does not mean that that the Coulomb interaction between the "bare" constituent electrons is neglected. Instead the statement implies that it is possible to describe the low-energy excitations of a metal as non-interacting. Throughout this thesis we adopt the point of view that the residual, and therefore weak, interactions between such low-energy quasi-particle excitations drive the system into a spontaneously symmetry breaking, many-body correlated phase. The generalized Hubbard models discussed above can be viewed as an intermediate construction between the full electronic structure of a real material and such a low-energy effective theory. While realistic materials are generically formed from multiple atoms per unit cell with many valence electrons, the analysis of bond-chemistry and crystal field effects often results in the insight that only a small subsection of electronic degrees of freedom are relevant for the low-energy physics at the Fermi-level. Such a simplification can be used to provide a connection between toy-models and real materials *e.g.* the one-band square lattice Hubbard model description of the "high-T_c" cuprates as mentioned in the introduction. As a next step, one can use results of *ab-initio* density functional theory (DFT) calculations as the input for the calculation of maximally localized Wannier functions which can then be used to construct low-energy effective models for realistic materials [87]. This provides a low-energy model with a constrained number of orbitals as well as the matrix elements $t_{a_2 a_0}(\mathbf{r})$ governing the transitions between them. Interactions can be added to such a model "by hand" as a phenomenological parameter. Alternatively it is possible to compute them via *ab-initio* methods in the constrained random-phase-approximation, where the low-energy sector chosen for the minimal model and the full DFT results are used as an input (see *e.g.* [88] and references therein). Since this thesis is focused on the methodological development of the analysis of unconventional superconductivity in the resulting models, we constrain ourselves to scenarios where the interaction is treated as a small phenomenological parameter. In the following Chapter 2 we will apply our methodological toolbox to toy model Hubbard models on the square and triangular lattice. Chapter 3 investigates the possibility for unconventional surface superconductivity in LuPtBi on the basis of an *ab-initio* electronic structure calculation of its surface state.

Prior to an investigation of these models we will now proceed with a brief summary of the fermionic coherent state path integrals that will be the basis for both the wcRG and RPA described subsequently.

1.2 Path integral formulation for generalized Hubbard models

Instead of the microscopic dynamics of every single particle of the system, we are interested in the thermodynamic properties of its collective modes. Such a scenario is conveniently captured by the partition function

$$\mathcal{Z} = \mathrm{Tr}\, \mathrm{e}^{-\beta H}\,, \tag{1.10}$$

where the trace indicates a sum over all possible microscopic states and $\beta = 1/(k_\mathrm{B}T)$ is the inverse temperature in units of Energy [89] (with the Boltzmann constant $k_\mathrm{B} \approx 1.381 \times 10^{-23}\,\mathrm{J\,K^{-1}} \approx 86.17\,\mu\mathrm{eV\,K^{-1}}$).

One common approach to evaluate this partition function for interacting Fermion systems of the type discussed in the previous chapter is via fermionic path integrals [73, 90, 91]. In the case of a theory described by Equation 1.1 and Equation 1.6 the conventional procedure is to start with a set of coherent states

$$|\psi_\alpha(\mathbf{k})\rangle = |0\rangle - \psi_\alpha(\mathbf{k})\,|\alpha, \mathbf{k}\rangle \tag{1.11}$$

that are based on the solution Equation 1.4 of the non-interacting problem and obey the eigenvalue equations

$$c_{\alpha,\mathbf{k}}\,|\psi_\alpha(\mathbf{k})\rangle = \psi_\alpha(\mathbf{k})\,|\psi_\alpha(\mathbf{k})\rangle\ . \tag{1.12}$$

Importantly such states can not be constructed using conventional complex numbers but require the $\psi_\alpha(\mathbf{k})$ to be anticommuting Grassmann numbers

$$\psi_\alpha(\mathbf{k})\psi_\beta(\mathbf{k}') = -\psi_\beta(\mathbf{k}')\psi_\alpha(\mathbf{k}) \quad \rightarrow \quad \psi_\alpha^2(\mathbf{k}) = 0\,, \tag{1.13}$$

in order to uphold the fermionic antisymmetry of the wavefunction. We can therefore write the coherent states with an exponential function

$$|\psi_\alpha(\mathbf{k})\rangle = \exp\Big\{-\psi_\alpha(\mathbf{k})c_\alpha^\dagger(\mathbf{k})\Big\}\,|0\rangle\ . \tag{1.14}$$

We will refrain from a complete review of the properties of Grassmann numbers, *e.g.* their behaviour under integration and differentiation and the resulting coherent states (check [73] for a nice review in the context of correlated electrons and the renormalization group, the textbook references [86, 90, 91] including bosonic path integrals or my Master thesis [92] for a more elaborate summary in similar notation) and simply state one of the most important results: Using adjoint coherent states

$$\langle\bar\psi_\alpha(\mathbf{k})|\, c_{\alpha,\mathbf{k}}^\dagger = \langle\bar\psi_\alpha(\mathbf{k})|\,\bar\psi_\alpha(\mathbf{k}) \tag{1.15}$$

it is possible to formulate a resolution of unity for the complete Fock space from coherent states

$$\mathbb{1} = \int \prod_{\alpha,\mathbf{k}} \mathrm{d}\bar{\psi}_\alpha(\mathbf{k}) \mathrm{d}\psi_\alpha(\mathbf{k})\, \mathrm{e}^{-\bar{\psi}_\alpha(\mathbf{k})\psi_\alpha(\mathbf{k})}\, |\psi_\alpha(\mathbf{k})\rangle \langle\bar{\psi}_\alpha(\mathbf{k})| \ . \tag{1.16}$$

Note that the adjoint Grassmann numbers $\bar{\psi}_\alpha(\mathbf{k})$ are a new set of independent variables, unrelated to $\psi_\alpha(\mathbf{k})$ The product over all integrals α and $\mathbf{k}$ is often abbreviated by introducing ψ as a vector of Grassmann numbers and writing

$$\mathbb{1} = \int \mathrm{d}\bar{\psi}\mathrm{d}\psi\ |\psi\rangle \langle\bar{\psi}| \prod_{\alpha,\mathbf{k}} \mathrm{e}^{-\bar{\psi}_\alpha(\mathbf{k})\psi_\alpha(\mathbf{k})} = \int \mathrm{d}\bar{\psi}\mathrm{d}\psi\ |\psi\rangle \langle\bar{\psi}|\ \mathrm{e}^{-\sum_{\alpha,\mathbf{k}} \bar{\psi}_\alpha(\mathbf{k})\psi_\alpha(\mathbf{k})} . \tag{1.17}$$

Notice that we have been careful to only commute pairs of Grassmann variables during all operations. Using this shorthand notation it is possible to calculate the partition function in terms of coherent states

$$\mathcal{Z} = \mathrm{Tr}\, \mathrm{e}^{-\beta H} = \int \mathrm{d}\bar{\psi}\mathrm{d}\psi\, \mathrm{e}^{-\sum_{\alpha,\mathbf{k}} \bar{\psi}_\alpha(\mathbf{k})\psi_\alpha(\mathbf{k})} \langle -\bar{\psi}|\, \mathrm{e}^{-\beta H}\, |\psi\rangle \ , \tag{1.18}$$

where the additional minus sign in the bra-type coherent state arises due to the anti-commuting nature of the Grassmann variables. For a normal ordered operator $A(c^\dagger_{\alpha,\mathbf{k}}, c_{\alpha,\mathbf{k}})$ the matrix element $\langle -\bar{\psi}|\, A\, |\psi\rangle$ is simply evaluated by replacing all fermionic annihilation and creation operators with the respective coherent state eigenvalues $\psi_\alpha(\mathbf{k})$ $[\bar{\psi}_\alpha(\mathbf{k})]$. For the exponential of a normal ordered operator this is not possible as one can see from a second order Taylor expansion. In the path-integral approach, this problem is solved by splitting the exponential

$$\mathrm{e}^{-\beta H} = \lim_{N\to\infty} \left(\mathrm{e}^{-\frac{\beta}{N}H}\right)^N = \lim_{N\to\infty} \left(1 - \frac{\beta}{N} H\right)^N , \tag{1.19}$$

into $N \to \infty$ parts and performing a first order Taylor expansion in β/N. Adding an additional resolution of unity

$$\mathbb{1} = \int \mathrm{d}\bar{\psi}_i \mathrm{d}\psi_i\ |\psi\rangle_i \langle\bar{\psi}_i|\ \mathrm{e}^{-\sum_{\alpha,\mathbf{k}} \bar{\psi}_{i,\alpha}(\mathbf{k})\psi_{i,\alpha}(\mathbf{k})} \tag{1.20}$$

between each of the N factors then removes all operators and matrix elements from the formulation and we are left with the evaluation of $2N$ integrals over Grassmann vectors ψ_i

$$\mathcal{Z} = \lim_{N\to\infty} \int \prod_{i=1}^{N} \mathrm{d}\bar{\psi}_i \mathrm{d}\psi_i \mathrm{e}^{-\sum_{\alpha,\mathbf{k}} \bar{\psi}_{\alpha,i}(\mathbf{k})\psi_{\alpha,i}(\mathbf{k})} \Big(1 - \frac{\beta}{N} H(\bar{\psi}_{\alpha,i+1}(\mathbf{k}), \psi_{\alpha,i}(\mathbf{k}))\Big) \langle\bar{\psi}_{i+1}|\psi_i\rangle \ . \tag{1.21}$$

Crucially we had to implement the periodic boundary conditions

$$\bar{\psi}_{N+1} = -\bar{\psi}_1 \quad \text{and} \quad \psi_{N+1} = -\psi_1 \tag{1.22}$$

for this compact notation to work. Calculation of

$$\langle\bar{\psi}_{i+1}|\psi_i\rangle = \exp\{\bar{\psi}_{i+1}\psi_i\} = \exp\left\{\sum_{\alpha,\mathbf{k}}\bar{\psi}_{\alpha,i+1}(\mathbf{k})\psi_{\alpha,i}(\mathbf{k})\right\} \tag{1.23}$$

and rewriting the term $1-\beta/NH(\psi)$ back into exponential form yields

$$\mathcal{Z} = \lim_{N\to\infty}\int\prod_{i=1}^{N}\left[\mathrm{d}\bar{\psi}_i\mathrm{d}\psi_i\right]\exp\left\{-\frac{\beta}{N}\sum_{i=1}^{N}\sum_{\alpha,\mathbf{k}}\left(\frac{\bar{\psi}_{\alpha,i}(\mathbf{k})-\bar{\psi}_{\alpha,i+1}(\mathbf{k})}{\beta/N}\psi_{\alpha,i}(\mathbf{k})+H(\bar{\psi}_{\alpha,i+1}(\mathbf{k}),\psi_{\alpha,i}(\mathbf{k}))\right)\right\}. \tag{1.24}$$

Before taking the limit $N\to\infty$ in the partition function we consider the continuous set of Grassmann numbers

$$\begin{aligned}\psi_\alpha(\mathbf{k},\tau_i) &= \psi_{\alpha,i}(\mathbf{k})\\ \bar{\psi}_\alpha(\mathbf{k},\tau_i) &= \bar{\psi}_{\alpha,i}(\mathbf{k})\,.\end{aligned} \tag{1.25}$$

These functions of τ are anti-periodic in β

$$\psi_\alpha(\mathbf{k},\tau+\beta) = -\psi_\alpha(\mathbf{k},\tau) \tag{1.26}$$

in order to fulfill the periodic boundary conditions in Equation 1.22 and may therefore be represented via a discrete Fourier series

$$\begin{aligned}\psi_\alpha(\mathbf{k},\tau) &= \sum_n \mathrm{e}^{-\mathrm{i}\omega_n\tau}\psi_\alpha(\mathbf{k},\omega_n)\\ \bar{\psi}_\alpha(\mathbf{k},\tau) &= \sum_n \mathrm{e}^{+\mathrm{i}\omega_n\tau}\bar{\psi}_\alpha(\mathbf{k},\omega_n)\,.\end{aligned} \tag{1.27}$$

The anti-symmetry is now encoded in the fact that only odd frequencies

$$\omega_n = \pi\frac{2n+1}{\beta} \tag{1.28}$$

contribute to the series expansion.

As a final preparation for the "continuous" path integral formulation of the partition function, we investigate the properties of our Grassmann valued function at an infinitesimally incremented time $\tau+\delta$

$$\bar{\psi}_\alpha(\mathbf{k},\tau+\delta) = \sum_n \mathrm{e}^{+\mathrm{i}\omega_n\tau}\mathrm{e}^{+\mathrm{i}\omega_n\delta}\bar{\psi}_\alpha(\mathbf{k},\omega_n) = \sum_n \mathrm{e}^{+\mathrm{i}\omega_n\tau}\Big(1+O(\omega_n\delta)\Big)\bar{\psi}_\alpha(\mathbf{k},\omega_n) = \bar{\psi}_\alpha(\mathbf{k},\tau)+\sum_n O(\omega_n\delta)\,. \tag{1.29}$$

From this result we can deduce that disregarding terms of order δ restricts the validity of our analysis to frequencies smaller $1/\delta$. Since infinitely many frequencies may contribute to the partition function, taking the limit $N \to \infty$ is therefore not sufficient to obtain an exact result for the partition function if we simply replace $\bar{\psi}(\tau + \beta/N)$ by $\bar{\psi}(\tau)$. Fortunately we are only interested in the correlations functions at low-energy and thus small frequency of our model and the approximation holds for this case [73].

By replacing

$$\sum_{i=1}^{N} f_i \frac{\beta}{N} \to \int_0^\beta f(\tau)\mathrm{d}\tau \quad \text{and} \quad \frac{f_{i+1} - f_i}{\beta/N} \to \frac{\partial}{\partial\tau} f(\tau) \tag{1.30}$$

we read of the continuous action

$$S(\psi, \bar{\psi}) = \sum_{\alpha,\mathbf{k}} \int_0^\beta H\Big(\bar{\psi}_\alpha(\mathbf{k},\tau), \psi_\alpha(\mathbf{k},\tau)\Big) - \Big(\frac{\partial}{\partial\tau}\bar{\psi}_\alpha(\mathbf{k},\tau)\Big)\psi_\alpha(\mathbf{k},\tau)\,\mathrm{d}\tau \tag{1.31}$$

from Equation 1.24. The conventional form for the action is obtained via partial integration with vanishing boundary terms (guaranteed by the anti-symmety of $\psi(\tau)$)

$$S(\psi, \bar{\psi}) = \sum_{\alpha,\mathbf{k}} \int_0^\beta \bar{\psi}_\alpha(\mathbf{k},\tau)\frac{\partial}{\partial\tau}\psi_\alpha(\mathbf{k},\tau) + H\Big(\bar{\psi}_\alpha(\mathbf{k},\tau), \psi_\alpha(\mathbf{k},\tau)\Big)\,\mathrm{d}\tau\,. \tag{1.32}$$

Introducing the shorthand notation

$$\int \prod_{i=1}^{\infty} \Big[\mathrm{d}\bar{\psi}_i \mathrm{d}\psi_i\Big] = \int \mathcal{D}(\bar{\psi}(\tau), \psi(\tau))\,, \tag{1.33}$$

we find the following expression for the partition function:

$$\mathcal{Z} = \int \mathcal{D}(\bar{\psi}(\tau), \psi(\tau)) \exp\{-S(\psi, \bar{\psi})\}\,. \tag{1.34}$$

Example calculations for the free theory

To illustrate the benefits of our previous calculations, we start by calculating some basic properties of the non-interacting problem and perturbatively add the interactions in a second step. For the free theory, the action reads

$$S_0 = \sum_{\alpha,\mathbf{k}} \int_0^\beta \bar{\psi}_\alpha(\mathbf{k},\tau)\frac{\partial}{\partial\tau}\psi_\alpha(\mathbf{k},\tau) + \bar{\psi}_\alpha(\mathbf{k},\tau)\epsilon_\alpha(\mathbf{k})\psi_\alpha(\mathbf{k},\tau)\,\mathrm{d}\tau\,. \tag{1.35}$$

Using the orthogonality relation of different Fourier components

$$\int_0^\beta \mathrm{e}^{i\omega_n\tau}\mathrm{e}^{-i\omega_m\tau}\,\mathrm{d}\tau = \beta\delta_{mn} \tag{1.36}$$

we use the Fourier transformation given by Equation 1.29 and find

$$S_0 = \beta\sum_n\sum_{\alpha,\mathbf{k}}\bar{\psi}_\alpha(\mathbf{k},\omega_n)\Big(-\mathrm{i}\omega_n+\epsilon_\alpha(\mathbf{k})\Big)\psi_\alpha(\mathbf{k},\omega_n)\,. \tag{1.37}$$

This transformations Jacobian is unity, therefore we can rewrite the partition function in terms of a path-integral over fields at different frequencies instead of "time-slices" τ

$$\mathcal{Z} = \int \mathcal{D}(\bar{\psi}(\omega_n),\psi(\omega_n))\exp\left\{-\beta\sum_n\sum_{\alpha,\mathbf{k}}\bar{\psi}_\alpha(\mathbf{k},\omega_n)\Big(-\mathrm{i}\omega_n+\epsilon_\alpha(\mathbf{k})\Big)\psi_\alpha(\mathbf{k},\omega_n)\right\}. \tag{1.38}$$

We have decoupled the path integral completely into the problem of independent fermionic oscillators and obtain a path-integral free representation for the partition function by using the definitions for Grassmann integration [90, 92]

$$\begin{aligned}\mathcal{Z} &= \prod_{\alpha,\mathbf{k}}\prod_n\int \mathrm{d}\bar{\psi}_\alpha(\mathbf{k},\omega_n)\mathrm{d}\psi_\alpha(\mathbf{k},\omega_n)\exp\Big\{-\beta\bar{\psi}_\alpha(\mathbf{k},\omega_n)\Big(-\mathrm{i}\omega_n+\epsilon_\alpha(\mathbf{k})\Big)\psi_\alpha(\mathbf{k},\omega_n)\Big\}\\ &= \prod_{\alpha,\mathbf{k}}\prod_n\beta\Big(-\mathrm{i}\omega_n+\epsilon_\alpha(\mathbf{k})\Big)\,.\end{aligned} \tag{1.39}$$

Using this result we can calculate an intermediate result that will prove to be valuable in the calculation of any thermal expectation values. Consider the expression

$$\begin{aligned}&\int \mathcal{D}\Big(\bar{\psi}(\omega_n),\psi(\omega_n)\Big)\,\bar{\psi}_{\alpha_1}(\mathbf{k}_1,\omega_{n_1})\psi_{\alpha_0}(\mathbf{k}_0,\omega_{n_0})\exp\Big\{-S_0\Big(\bar{\psi}(\omega_n),\psi(\omega_n)\Big)\Big\}\\ =&\int \mathcal{D}\Big(\bar{\psi}(\omega_n),\psi(\omega_n)\Big)\,\bar{\psi}_{N_1}\psi_{N_0}\exp\Big\{-S_0\Big(\bar{\psi}_N,\psi_N\Big)\Big\}\\ =&\prod_N\Big[-\delta_{NN_0}\delta_{N_0N_1}+(1-\delta_{NN_0})(1-\delta_{NN_1})\beta\Big(-\mathrm{i}\omega_n+\epsilon_{\alpha_n}(\mathbf{k}_n)\Big)\Big]\\ =&\delta_{N_0N_1}(-1)\cdot\prod_{N\neq N_0}\beta\Big(-\mathrm{i}\omega_n+\epsilon_{\alpha_n}(\mathbf{k}_n)\Big)\\ =&\frac{-\delta_{N_0N_1}}{\beta\Big(-\mathrm{i}\omega_{n_0}+\epsilon_{\alpha_0}(\mathbf{k}_0)\Big)}\prod_N\beta\Big(-\mathrm{i}\omega_n+\epsilon_{\alpha_n}(\mathbf{k}_n)\Big)\\ =&\frac{\delta_{N_0N_1}}{\beta\Big(\mathrm{i}\omega_{n_0}-\epsilon_{\alpha_0}(\mathbf{k}_0)\Big)}\mathcal{Z} = \mathcal{Z}\,\frac{\delta_{\alpha_0\alpha_1}\delta(\mathbf{k}_0-\mathbf{k}_1)\delta(\omega_{n_0}-\omega_{n_1})}{\beta\Big(\mathrm{i}\omega_{n_0}-\epsilon_{\alpha_0}(\mathbf{k}_0)\Big)}\,.\end{aligned} \tag{1.40}$$

Since the result is again proportional to the partition function, one usually uses the shorthand notation

$$\left\langle A(\psi,\bar{\psi})\right\rangle_0 = \frac{1}{\mathcal{Z}_0}\int \mathcal{D}\left(\bar{\psi}(\omega_n),\psi(\omega_n)\right) A(\psi,\bar{\psi}) \exp\left\{-S_0\left(\bar{\psi}(\omega_n),\psi(\omega_n)\right)\right\} \tag{1.41}$$

for "expectation values" of Grassmann valued functions $A(\psi,\bar{\psi})$. The index $\langle\rangle_0$ denotes averaging over the bare action S_0. For the previous expression 1.40 we can therefore write

$$\left\langle \bar{\psi}_{\alpha_1}(\mathbf{k}_1,\omega_{n_1})\psi_{\alpha_0}(\mathbf{k}_0,\omega_{n_0})\right\rangle_0 = \frac{\delta_{\alpha_0\alpha_1}\delta(\mathbf{k}_0-\mathbf{k}_1)\delta(\omega_{n_0}-\omega_{n_1})}{\beta\left(\mathrm{i}\omega_{n_0}-\epsilon_{\alpha_0}(\mathbf{k}_0)\right)}\,. \tag{1.42}$$

This object is called the imaginary time Green's function in Matsubara frequency representation.

Using this result we can calculate the thermal expectation value of any normal ordered operator. As an example we consider the mean-particle occupation at momentum $\mathbf{k}_0$

$$\hat{n}(\mathbf{k}_0) = \sum_{\alpha_0} c^\dagger_{\alpha_0,\mathbf{k}_0} c_{\alpha_0,\mathbf{k}_0}\,. \tag{1.43}$$

The thermal expectation value of this operator is given by [89]

$$\left\langle \hat{n}(\mathbf{k}_0)\right\rangle = \mathrm{Tr}\;\hat{n}(\mathbf{k}_0)\mathrm{e}^{-\beta H}\,. \tag{1.44}$$

We can now employ fermionic coherent states to evaluate the trace, use the path integral discretization for the exponential and replace the operators in $\hat{n}$ by the corresponding Grassmann numbers at imaginary "time" $\tau = 0$

$$\left\langle \hat{n}(\mathbf{k}_0)\right\rangle_0 = \frac{1}{\mathcal{Z}}\sum_{\alpha_0}\int \mathcal{D}(\bar{\psi}(\tau),\psi(\tau))\,\bar{\psi}_{\alpha_0}(\mathbf{k}_0,\tau=0+\delta)\psi_{\alpha_0}(\mathbf{k}_0,\tau=0)\exp\{-S_0(\psi,\bar{\psi})\}\,. \tag{1.45}$$

Note that we were careful to include the fact that the creation operator $c^\dagger_{\alpha_0,\mathbf{k}_0}$ acting on the left coherent state is applied to a "time" slice at $\tau = 0+\delta$ (slightly "later") while the annihilation operator acts on the coherent state at $\tau = 0$ as defined by Equation 1.21. In the next step we insert the Fourier representation of $\psi(\tau)$ and employ Equation 1.42

$$\begin{aligned}
\left\langle \hat{n}(\mathbf{k}_0)\right\rangle_0 &= \frac{1}{\mathcal{Z}}\sum_{\alpha_0}\sum_{m_0,n_0}\int \mathcal{D}(\bar{\psi}(\omega_n),\psi(\omega_n))\,\mathrm{e}^{\mathrm{i}\omega_{m_0}\delta}\bar{\psi}_{\alpha_0}(\mathbf{k}_0,\omega_{m_0})\psi_{\alpha_0}(\mathbf{k}_0,\omega_{n_0})\exp\{-S_0(\psi,\bar{\psi})\}\\
&= \sum_{\alpha_0}\sum_{n_0,m_0}\mathrm{e}^{\mathrm{i}\omega_{m_0}\delta}\frac{\delta_{\alpha_0\alpha_0}\delta(\mathbf{k}_0-\mathbf{k}_0)\delta(\omega_{n_0}-\omega_{m_0})}{\beta\left(\mathrm{i}\omega_{n_0}-\epsilon_{\alpha_0}(\mathbf{k}_0)\right)}\\
&= \sum_{\alpha_0}\sum_{n_0}\frac{\mathrm{e}^{\mathrm{i}\omega_{n_0}\delta}}{\beta\left(\mathrm{i}\omega_{n_0}-\epsilon_{\alpha_0}(\mathbf{k}_0)\right)}\,.
\end{aligned} \tag{1.46}$$

The evaluation of our expectation value has been reduced to a standard Matsubara frequency summation (for details see *e.g.* [90] or [93]) with the well known result

$$\frac{1}{\beta}\sum_n \frac{\mathrm{e}^{\mathrm{i}\omega_n 0^+}}{\mathrm{i}\omega_n - \xi} = \frac{1}{\mathrm{e}^{\beta\xi}+1} = n_F\big(\beta\xi\big) \tag{1.47}$$

and we find

$$\big\langle \hat{n}(\mathbf{k}_0)\big\rangle_0 = \sum_{\alpha_0} n_F\big(\beta\epsilon_{\alpha_0}(\mathbf{k}_0)\big) \tag{1.48}$$

for the mean-particle occupation.

Linear response theory for static perturbations

In order to gain insight into the phenomenology of a physical system in (thermal) equilibrium, theorists and experimentalists alike perturb the equilibrium slightly and monitor the changes to some of the characteristic observables. Often it is sufficient to model a systems response to such a perturbation to linear order in order to capture the essential properties of the state at hand.

In the framework developed so far we describe a perturbation to the system by adding a term to the Hamiltonian

$$H = H_0 + H_I + \lambda\hat{A} \tag{1.49}$$

where the scalar λ controls the strength of the perturbation and the operator $\hat{A}$ governs the action of the perturbation on our system. A general overview over such perturbation operators as well as common examples are discussed in Section 1.4.1. Here we want to focus on how we can calculate the response of our system to such a perturbation by considering how it changes the expectation value of a different operator $\hat{B}$.

We have seen in the previous section how such an expectation value is calculated using path integrals. The addition of a new term into the Hamiltonian can be described by an added term in the action

$$S_A = \int_0^\beta A(\psi(\tau),\bar{\psi}(\tau))\,\mathrm{d}\tau\,. \tag{1.50}$$

The expectation value of some operator $\hat{B}$ in the presence of this additional action is

$$\big\langle B\big\rangle_{\lambda A} = \frac{1}{\mathcal{Z}_{\lambda A}}\int \mathcal{D}\big(\bar{\psi}(\tau),\psi(\tau)\big)\,B(\psi,\bar{\psi})\exp\Big\{-S\left(\bar{\psi}(\tau),\psi(\tau)\right) - \lambda S_A\big(\bar{\psi}(\tau),\psi(\tau)\big)\Big\}\,. \tag{1.51}$$

We expand $\mathcal{Z}_{\lambda A}$ to linear order in λ

$$\mathcal{Z}_{\lambda A} \approx \int \mathcal{D}\big(\bar{\psi}(\tau),\psi(\tau)\big)\big(1-\lambda S_A\big)\exp\Big\{-S\left(\bar{\psi}(\tau),\psi(\tau)\right)\Big\} = \mathcal{Z} - \lambda\big\langle S_A\big\rangle_0\mathcal{Z} = \mathcal{Z}\Big[1-\lambda\big\langle S_A\big\rangle\Big] \tag{1.52}$$

and conclude that

$$\left\langle B\right\rangle_{\lambda A} = \left\langle B\right\rangle + \lambda\left\langle B\right\rangle\left\langle S_A\right\rangle - \lambda\left\langle BS_A\right\rangle + O(\lambda^2)\,. \tag{1.53}$$

This is conventionally re-written into the form

$$\lim_{\lambda\to 0}\frac{\partial\langle B\rangle_{\lambda A}}{\partial\lambda} = \left\langle B\right\rangle\left\langle S_A\right\rangle - \left\langle BS_A\right\rangle := -\left\langle BS_A\right\rangle_{\text{conn}} := \chi_{A,B}\,. \tag{1.54}$$

The subscript "conn" denotes the fact that only the connected Feynman diagrams contribute to the expression for the susceptibility since one has to subtract the product $\langle B\rangle_0\langle S_A\rangle_0$. We will elaborate on this notion of connected diagrams in the following section about the Wick theorem. Finally we note that our expression for the static susceptibility can be written as

$$\chi_{A,B} = -\int_0^\beta \left\langle B(\psi(\tau=0),\bar\psi(\tau=\delta))A(\psi(\tau'),\bar\psi(\tau'+\delta))\right\rangle_{\text{conn}}\mathrm{d}\tau'\,, \tag{1.55}$$

with the previously discussed regularization δ arising from the path integral formulation. Readers familiar with such expressions may wonder about the absence of an imaginary time-ordering operator. Since we understand all expectation values to be defined by the path-integral expression Equation 1.41 which already performs such a time-ordering by construction, no explicit time-ordering is necessary here.

Wick theorem for the interacting theory

Inspired by the preceding linear response calculation we will now continue with the analysis of the interaction term H_I via a Taylor expansion. This treatment lies at the heart of the Feynman diagram approach to interacting many-body systems and is not restricted to the application in perturbation theory as we will see in Section 1.3 and Section 1.4.

Recall that our system is described by a kinetic Hamiltonian (see Equation 1.4 and following)

$$H_0 = \sum_{\mathbf{k}}\sum_{\alpha}\epsilon_\alpha(\mathbf{k})c^\dagger_{\alpha,\mathbf{k}}c_{\alpha,\mathbf{k}}\,, \tag{1.56}$$

and an interaction part

$$H_I = \sum_{\{\mathbf{k}_i\}}\sum_{\{\alpha_i\}}U_{\{\alpha_i\}}(\{\mathbf{k}_i\})c^\dagger_{\alpha_2,\mathbf{k}_2}c^\dagger_{\alpha_3,\mathbf{k}_3}c_{\alpha_1,\mathbf{k}_1}c_{\alpha_0,\mathbf{k}_0}\,. \tag{1.57}$$

Both parts are already normal ordered so that we can replace the operators with their corresponding Grassmann fields $\psi(\tau)$. The additional derivative arising in the path integral formulation is

quadratic in the fields and therefore added to the kinetic part and we define two seperate actions

$$S_0 = \sum_{\alpha,\mathbf{k}} \int_0^\beta \bar{\psi}_\alpha(\mathbf{k},\tau)\Big[\frac{\partial}{\partial\tau} + \epsilon_\alpha(\mathbf{k})\Big]\psi_\alpha(\mathbf{k},\tau)\,\mathrm{d}\tau\,, \tag{1.58}$$

and

$$S_I = \sum_{\{\mathbf{k}_i\}}\sum_{\{\alpha_i\}} U_{\{\alpha_i\}}(\{\mathbf{k}_i\}) \int_0^\beta \bar{\psi}_{\alpha_2}(\mathbf{k}_2,\tau)\bar{\psi}_{\alpha_3}(\mathbf{k}_3,\tau)\psi_{\alpha_1}(\mathbf{k}_1,\tau)\psi_{\alpha_0}(\mathbf{k}_0,\tau)\,\mathrm{d}\tau\,. \tag{1.59}$$

We have already solved the non-interacting problem via Fourier transformation. Employing the same expansion for the interacting part yields

$$\begin{aligned} S_I &= \sum_{\{\mathbf{k}_i\}}\sum_{\{\alpha_i\}} U_{\{\alpha_i\}}(\{\mathbf{k}_i\}) \sum_{\{\omega_{n_i}\}} \beta\bar{\psi}_{\alpha_2}(\mathbf{k}_2,\omega_{n_2})\bar{\psi}_{\alpha_3}(\mathbf{k}_3,\omega_{n_3})\psi_{\alpha_1}(\mathbf{k}_1,\omega_{n_1})\psi_{\alpha_0}(\mathbf{k}_0,\omega_{n_0})\delta(\omega_{n_2}+\omega_{n_3}-\omega_{n_1}-\omega_{n_0}) \\ &= \beta\sum_{\{\mathbf{k}_i\}}\sum_{\{\alpha_i\}}\sum_{\{\omega_{n_i}\}} U_{\{\alpha_i\}}(\{\mathbf{k}_i\},\{\omega_{n_i}\})\bar{\psi}_{\alpha_2}(\mathbf{k}_2,\omega_{n_2})\bar{\psi}_{\alpha_3}(\mathbf{k}_3,\omega_{n_3})\psi_{\alpha_1}(\mathbf{k}_1,\omega_{n_1})\psi_{\alpha_0}(\mathbf{k}_0,\omega_{n_0}) \\ &= \beta\sum_{\mathbf{0},\mathbf{1},\mathbf{2},\mathbf{3}} U_{\mathbf{0},\mathbf{1},\mathbf{2},\mathbf{3}}\bar{\psi}_{\mathbf{2}}\bar{\psi}_{\mathbf{3}}\psi_{\mathbf{1}}\psi_{\mathbf{0}}\,. \end{aligned} \tag{1.60}$$

Here we have absorbed the energy conserving delta function that results from the integration over τ into the coupling function U and introduced a multi-index $\mathbf{i} = (\alpha_i, \mathbf{k}_i, \omega_{n_i})$ in the last line. Using this notation the kinetic part of the action (quadratic in fields) reads

$$S_0 = \beta\sum_{\mathbf{0}}\Big(-\mathrm{i}\omega_{n_0} + \epsilon_{\alpha_0}(\mathbf{k}_0)\Big)\bar{\psi}_{\mathbf{0}}\psi_{\mathbf{0}}\,. \tag{1.61}$$

Inspired by Equation 1.42 we define the reciprocal Green's function

$$G^{-1}_{\mathbf{02}} = \delta_{\alpha_0\alpha_2}\delta(\mathbf{k}_0-\mathbf{k}_2)\delta(\omega_{n_0}-\omega_{n_2})\Big(-\mathrm{i}\omega_{n_0} + \epsilon_{\alpha_0}(\mathbf{k}_0)\Big) \tag{1.62}$$

and write

$$S_0 = \beta\sum_{\mathbf{0},\mathbf{2}} G^{-1}_{\mathbf{02}}\bar{\psi}_{\mathbf{2}}\psi_{\mathbf{0}}\,. \tag{1.63}$$

Now we represent the partition function of the interacting system via a Taylor series expansion of e^{-S_I}. This results in a sum of expectation values that are calculated with respect to S_0

$$\begin{aligned}\mathcal{Z} &= \mathcal{Z}_0 \frac{1}{\mathcal{Z}_0} \int \mathcal{D}\left(\bar{\psi},\psi\right) \exp\left\{-S_I\left(\bar{\psi},\psi\right)\right\} \exp\left\{-S_0\left(\bar{\psi},\psi\right)\right\} \\ &= \mathcal{Z}_0 \frac{1}{\mathcal{Z}_0} \int \mathcal{D}\left(\bar{\psi},\psi\right) \left[1 - S_I\left(\bar{\psi},\psi\right) + \frac{1}{2}\left(S_I\left(\bar{\psi},\psi\right)\right)^2 + O\left((S_I)^3\right)\right] \exp\left\{-S_0\left(\bar{\psi},\psi\right)\right\} \\ &= \mathcal{Z}_0 \left[\left\langle 1\right\rangle_0 - \left\langle S_I\right\rangle_0 + \frac{1}{2}\left\langle (S_I)^2\right\rangle_0 + \left\langle O\left((S_I)^3\right)\right\rangle_0\right].\end{aligned} \tag{1.64}$$

The first term in this expansion just gives $\mathcal{Z}_0$ as expected. For all following terms we see that we will have to calculate expectation values of type

$$\left\langle \bar{\psi}_{\mathbf{1}}\bar{\psi}_{\mathbf{3}}\bar{\psi}_{\mathbf{5}}\ldots\psi_{\mathbf{4}}\psi_{\mathbf{2}}\psi_{\mathbf{0}}\right\rangle_0 . \tag{1.65}$$

We have previously (compare Equation 1.42) seen that

$$\left\langle \bar{\psi}_{\mathbf{2}}\psi_{\mathbf{0}}\right\rangle_0 = \frac{\delta_{\mathbf{02}}}{\beta\left(\mathrm{i}\omega_{n_0} - \epsilon_{\alpha_0}(\mathbf{k}_0)\right)} = G_{\mathbf{02}} \tag{1.66}$$

and it is simple to show by explicit calculation (see *e.g.* [92]) of the Grassmann integrals that

$$\left\langle \bar{\psi}_{\mathbf{2}}\bar{\psi}_{\mathbf{3}}\psi_{\mathbf{1}}\psi_{\mathbf{0}}\right\rangle_0 = \left\langle \bar{\psi}_{\mathbf{2}}\psi_{\mathbf{0}}\right\rangle_0 \left\langle \bar{\psi}_{\mathbf{3}}\psi_{\mathbf{1}}\right\rangle_0 - \left\langle \bar{\psi}_{\mathbf{3}}\psi_{\mathbf{0}}\right\rangle_0 \left\langle \bar{\psi}_{\mathbf{2}}\psi_{\mathbf{1}}\right\rangle_0 = G_{\mathbf{02}}G_{\mathbf{13}} - G_{\mathbf{03}}G_{\mathbf{12}} . \tag{1.67}$$

In general we see that each field necessitates a conjugate partner with identical quantum numbers as one expects for particle conserving systems and one finds the general formula to be [94]

$$\left\langle \bar{\psi}_{\mathbf{1}}\bar{\psi}_{\mathbf{3}}\ldots\bar{\psi}_{\mathbf{2n+1}}\psi_{\mathbf{2n}}\ldots\psi_{\mathbf{2}}\psi_{\mathbf{0}}\right\rangle_0 = \sum_{\text{all pairings } P} (-1)^{(n_P)} \left\langle \bar{\psi}_{P(\mathbf{1})}\psi_{P(\mathbf{0})}\right\rangle_0 \left\langle \bar{\psi}_{P(\mathbf{3})}\psi_{P(\mathbf{2})}\right\rangle_0 \ldots \left\langle \bar{\psi}_{P(\mathbf{2n+1})}\psi_{P(\mathbf{2n})}\right\rangle_0 , \tag{1.68}$$

known as Wick's theorem for fermions. Note that we have to sum over all possible pairings P of the $2n$ Grassmann fields while n_P keeps track of the number of permutations needed to achieve a given combination, resulting in an antisymmetric expression under particle exchange.

Using these results we can estimate the energy cost of adding an interaction U to our theory by calculating the expectation value

$$\left\langle H_I\right\rangle_0 = \Big\langle \sum_{\mathbf{0,1,2,3}} U_{\mathbf{0,1,2,3}} c_{\mathbf{2}}^\dagger c_{\mathbf{3}}^\dagger c_{\mathbf{1}} c_{\mathbf{0}}\Big\rangle_0 = \sum_{\mathbf{0,1,2,3}} U_{\mathbf{0,1,2,3}} \left\langle \bar{\psi}_{\mathbf{2}}\bar{\psi}_{\mathbf{3}}\psi_{\mathbf{1}}\psi_{\mathbf{0}}\right\rangle_0 = \sum_{\mathbf{0,1,2,3}} U_{\mathbf{0,1,2,3}} \left(G_{\mathbf{02}}G_{\mathbf{13}} - G_{\mathbf{03}}G_{\mathbf{12}}\right). \tag{1.69}$$

Using the antisymmetry of the interaction matrix elements with respect to particle exchange

$$\begin{aligned} +U_{\mathbf{0,1,2,3}} &= -U_{\mathbf{1,0,2,3}} \\ &= -U_{\mathbf{0,1,3,2}} = +U_{\mathbf{1,0,3,2}} \end{aligned} \tag{1.70}$$

the expression can be simplified to a single term and subsequently evaluated analogous to Equation 1.48

$$\begin{aligned} \left\langle H_I \right\rangle_0 &= 2 \sum_{\mathbf{0,1,2,3}} U_{\mathbf{0,1,2,3}} G_{\mathbf{02}} G_{\mathbf{13}} = 2 \sum_{\mathbf{0,1}} U_{\mathbf{0,1,0,1}} \frac{1}{\beta\left(\omega_{n_0} - \epsilon_{\alpha_0}(\mathbf{k}_0)\right)} \frac{1}{\beta\left(\omega_{n_1} - \epsilon_{\alpha_1}(\mathbf{k}_1)\right)} \\ &= 2 \sum_{\mathbf{k}_0,\mathbf{k}_1} \sum_{\alpha_0,\alpha_1} U_{\alpha_0\alpha_1\alpha_0\alpha_1}(\mathbf{k}_0, \mathbf{k}_1, \mathbf{k}_0, \mathbf{k}_1)\, n_F(\epsilon_{\alpha_0}(\mathbf{k}_0))\, n_F(\epsilon_{\alpha_1}(\mathbf{k}_1))\,. \end{aligned} \tag{1.71}$$

While it is clear that analogous calculations can in principle be done to arbitrary order in S_I / U, we note that the number of terms to track grows in a combinatorial fashion and the number of frequency and momentum integrals is proportional to the number of interactions in each term.

A convenient way to track all of these different contributions is by using Feynman diagrams. Instead of listing a precise set of rules for the translation between such diagrams and expressions of the type considered here we will refer the reader to the extensive literature (*e.g.* [86, 90, 91]) and focus on examples of associated formulas and symbols. Single particle Green's functions are replaced by lines with an arrow indicating which Fermion is created (annihilated)

$$G_{\mathbf{02}} = \mathbf{0} \longrightarrow \mathbf{2} \tag{1.72}$$

$$\left\langle c_2^\dagger c_3^\dagger c_1 c_0 \right\rangle_0 = \quad \begin{matrix} \mathbf{0} \longrightarrow \mathbf{2} \\ \\ \mathbf{1} \longrightarrow \mathbf{3} \end{matrix} \quad - \quad \begin{matrix} \mathbf{0} & & \mathbf{2} \\ & \times & \\ \mathbf{1} & & \mathbf{3} \end{matrix} \tag{1.73}$$

while interaction vertices are replaced by black dots to distinguish them from accidental crossings of propagator lines induced by the diagrams topology

$$U_{\mathbf{0,1,2,3}} = \quad \begin{matrix} \mathbf{0} & U & \mathbf{2} \\ & \bullet & \\ \mathbf{1} & & \mathbf{3} \end{matrix} \tag{1.74}$$

$$\left\langle H_I \right\rangle_0 = 2 \sum_{\mathbf{0,1,2,3}} U_{\mathbf{0,1,2,3}} G_{\mathbf{02}} G_{\mathbf{13}} = 2$$

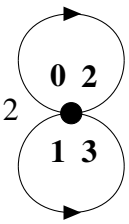

. (1.75)

Note that free indices are indicated by open ended Fermion lines, while closed Fermion loops imply a summation over all internal indices. At interaction vertices and along all Fermion lines momentum and energy are conserved, greatly reducing the number of required summations.

In contrast, an arbitrary external operator may break these conservation laws. We represent this by an additional line that we label with the introduced degrees of freedom. For example we may represent a two fermion operator

$$\hat{A}(\mathbf{q}, l) = \sum_{\mathbf{0,1}} A_{\mathbf{01}}(\mathbf{q}, l) c^\dagger_{\mathbf{1}} c_{\mathbf{0}} \tag{1.76}$$

via the diagram

$$A_{\mathbf{01}}(\mathbf{q}, l) =$$

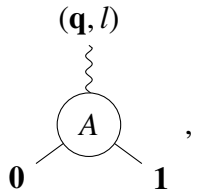

, (1.77)

where $\mathbf{q}$ is the momentum inserted into the diagram by the operator and l is a placeholder index for all potential sub-lattice or spin-degrees of freedom. For the time independent observables and perturbations considered in this thesis, the external line does not carry energy such that energy conservation holds between the fermion indices $\mathbf{0}$ and $\mathbf{1}$.

Having established a framework for the calculation of scattering amplitudes in the interacting theory via perturbation theory, we proceed by investigating the impact of the interactions on the ground state of our non-interacting model via the perturbative renormalization group.

1.3 Weak coupling renormalization group (wcRG)

The weak coupling renormalization group (wcRG) approach to unconventional superconductivity centers on the motiv of perturbative coupling strength. This not only justifies a perturbative expansion of the interaction as presented in the previous section but further enables us to use analytically established arguments about the systems ground state.

If we restrict our interest to the scenario $U/W \to 0$ (where U is the largest interaction parameter in the problem and W the bandwidth of the non-interacting theory), we can truncate any perturbative calculation at second order in perturbation theory and neglect all diagrams of higher order without loss of accuracy. Techniques that allow for th retention of higher orders in the interaction will be discussed in Section 1.4.

Further, it is analytically established that a generic (not fine tuned) Fermi-liquid subject to infinitesimal repulsive interaction always has a superconducting and a superconducting instability only. The fact that such an instability exists generically has been first pointed out by Kohn and Luttinger [9]. It's existence as well as the absence of particle-hole instabilities in this particular limit can be understood in the language of the perturbative renormalization group developed by Shankar and Polchinksi for weakly interacting electron systems [73, 95]. Raghu *et al.* [23] used this formulation as the basis for calculations of the Kohn-Luttinger effect in lattice models. Here we present a generalized formulation of their method applicable to the generic tight-binding Hamiltonian presented in Equation 1.1. Crucially, our formulation allows for a straightforward generalization to random-phase approximation calculations as will be explained in Section 1.4.

The wcRG is formulated at temperature $T = 0$ via the introduction of an artificial cutoff Ω_0 into the problem [23]. Ω_0 is constrained from below such that the most divergent terms in the perturbative expansion of the partition function *i.e.*, the Cooper logarithms are still small in the first step of the RG calculation. This allows us to neglect many-body effects on the renormalization of the bare interaction and truncate its perturbative expansion at second order. The cutoff is further restricted from above by the relevant interaction scales for the the magnetic and charge channels and we can neglect it for the calculation of particle-hole fluctuations [74]. To state this in a more quantitative way:

If ρ denotes the density of states at the Fermi level, the cutoff Ω_0 is restricted to a parameter range

$$W \gg \rho U^2 \gg \Omega_0 \gg \left(\epsilon(\mathbf{k}_F) - \min_{\mathbf{k}} \epsilon(\mathbf{k})\right) \exp\left[-(\rho U)^{-1}\right]. \tag{1.78}$$

The first part of this inequality allows us to calculate an effective interaction including the renormalization effects of modes with energies larger than Ω_0 via second order perturbation theory in U/W. Due to our lower bound for Ω_0 it is also guaranteed that the resulting interaction will still be small enough for the application of one loop renormalization group equations to the new theory. Since we define all energies $\epsilon(\mathbf{k})$ to be defined relative to the Fermi energy, $\epsilon(\mathbf{k}_F) - \min_{\mathbf{k}} \epsilon(\mathbf{k})$ simply is the Fermi energy in our system.

In the established path integral formulation of the fermionic many body problem we now start by dividing the action into fast modes $\psi_f, \bar{\psi}_f$ with Matsubara frequency indices $\omega_{n_f} > \Omega_0$ and the

remaining slow modes $\psi_s, \bar{\psi}_s$

$$S = S_0(\psi_s, \bar{\psi}_s) + S_0(\psi_f, \bar{\psi}_f) + S_I(\psi_s, \bar{\psi}_s, \psi_f, \bar{\psi}_f) = S_{0s} + S_{0f} + S_I\,. \tag{1.79}$$

Notice that energy conservation implies a separability of the non-interacting part of the action S_0, while S_I couples slow and fast modes. Since the path integral measure is given by a product over Grassmann fields at different frequencies we can now rewrite our expression for the partition function and find [96]

$$\mathcal{Z} = \int \mathcal{D}\big(\bar{\psi}_s, \psi_s\big)\, \mathrm{e}^{-S_{0s}} \int \mathcal{D}\big(\bar{\psi}_f, \psi_f\big)\, \mathrm{e}^{-S_I} \mathrm{e}^{-S_{0f}} = \int \mathcal{D}\big(\bar{\psi}_s, \psi_s\big)\, \mathrm{e}^{-S'_I} \mathrm{e}^{-S_{0s}}\,, \tag{1.80}$$

where S'_I constitutes an effective action for a theory that only includes the slow modes. We can read of how to calculate this effective interaction from Equation 1.80

$$\mathrm{e}^{-S'_I} = \int \mathcal{D}\big(\bar{\psi}_f, \psi_f\big)\, \mathrm{e}^{-S_I} \mathrm{e}^{-S_{0f}} = \langle \mathrm{e}^{-S_I} \rangle_{0f} \mathcal{Z}_{0f} \tag{1.81}$$

and perform an expansion up to second order in S_I

$$\begin{aligned}
S'_I(\psi_s, \bar{\psi}_s) &= -\log\langle \mathrm{e}^{-S_I} \rangle_{0f} - \log \mathcal{Z}_{0f} \\
&= -\log\left\langle 1 + \sum_{n=1}^{\infty} \frac{(-S_I)^n}{n!} \right\rangle_{0f} + \text{const.} = -\left\langle \sum_{n=1}^{\infty} \frac{(-S_I)^n}{n!} \right\rangle_{0f} + \frac{1}{2}\left\langle \sum_{n=1}^{\infty} \frac{(-S_I)^n}{n!} \right\rangle_{0f}^2 + O(S_I^3) + \text{const.} \\
&= -\Big\langle -S_I \Big\rangle_{0f} - \frac{1}{2}\Big\langle (S_I)^2 \Big\rangle_{0f} + \frac{1}{2}\Big\langle -S_I \Big\rangle_{0f}^2 + O(S_I^3) + \text{const.} \\
&= \Big\langle S_I \Big\rangle_{0f} - \frac{1}{2}\Big(\Big\langle (S_I)^2 \Big\rangle_{0f} - \Big\langle S_I \Big\rangle_{0f}^2 \Big) + O(S_I^3) + \text{const.}\,.
\end{aligned} \tag{1.82}$$

The first order contributions to the effective action S'_I are given by the bare interaction S_I evaluated between slow modes as well as self-energy corrections which can be neglected in the limit of infinitesimal coupling strengths [23, 73]. At second order, we are left with the connected diagrams only, as all disconnected diagrams are canceled by the square of the first order term. Taking all contributions with four external slow modes into account, we find a diagrammatic expression for the effective interaction between the low-energy fermions

$$U^{\text{eff}}_{\mathbf{0,1,2,3}} =$$ 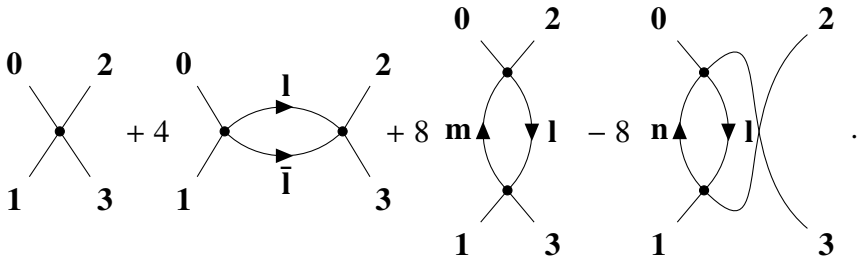

. (1.83)

We have labeled the internal propagators to be integrated over (fast modes) by $\mathbf{l}$ and $\bar{\mathbf{l}}, \mathbf{m}, \mathbf{n}$ and note that the momentum and frequency indices of the latter three are restricted by their respective conservation laws at each vertex. They can therefore be expressed as a function of external legs and $\mathbf{l}$

$$\begin{aligned} \bar{\mathbf{l}} &= \mathbf{0} + \mathbf{1} - \mathbf{l} \\ \mathbf{m} &= \mathbf{2} - \mathbf{0} + \mathbf{l} \\ \mathbf{n} &= \mathbf{3} - \mathbf{0} + \mathbf{l}. \end{aligned} \tag{1.84}$$

The resulting theory is now composed of modes restricted to a small annulus of size Ω_0 around the Fermi energy $\epsilon(\mathbf{k}_F)$ that interact via the weak renormalized interaction U^{eff} such that one can easily apply the standard Fermi-liquid RG procedure by Shankar and Polchinksi to it [73, 95]. Raghu *et al.* have shown by explicit calculations up to fourth order in perturbation theory that this two-step procedure removes any dependence of physical observables on the intermediate and artificial cutoff Ω_0 [23]. From their calculations one can also see that the central property governing the low energy physics is the effective interaction in the Cooper channel $U^{\text{eff}}_{\{\alpha_i\}}(\mathbf{k}_F, \mathbf{q}_F)$, while contributions with deviating momentum structure and self-energy effects can be safely neglected. From the restrictions we chose for Ω_0 it is clear that it is sufficient to restrict ourselves to momenta $\mathbf{k}_F, \mathbf{q}_F$ from the Fermi surface since these are the only degrees of freedom present in the second step of the renormalization. We thus adapt our notation to reflect this constraint to the Cooper channel

$$\begin{aligned} U^{\text{eff}}_{\mathbf{0,1,2,3}} &= U_{\{\alpha_i\},\{\omega_{n_i}\}}(\mathbf{k}_0, \mathbf{k}_1, \mathbf{k}_2, \mathbf{k}_3) \\ U_{\{\alpha_i\}}(\mathbf{k}_F, \mathbf{q}_F) &:= U_{\{\alpha_i\},\{\omega_{n_i}=0\}}(\mathbf{k}_F, -\mathbf{k}_F, \mathbf{q}_F, -\mathbf{q}_F) \end{aligned} \tag{1.85}$$

where $\mathbf{k}_F$ and $\mathbf{q}_F$ are restricted to lie on the Fermi surface and we are only interested in band indices α_i corresponding to zero energy modes at these momenta. In the following we will see how this effective interaction between Cooper pairs is calculated numerically.

1.3.1 Calculation of the effective Cooper pair interaction

From Equation 1.83 we see that the effective Cooper pair interaction at second order in perturbation theory is given by

$$\begin{aligned} U^{\text{eff}}_{\{\alpha_i\}}(\mathbf{k}_F, \mathbf{q}_F) = U^{\text{bare}}_{\{\alpha_i\}}(\mathbf{k}_F, \mathbf{q}_F) \\ + U^{\text{2nd order}}_{\{\alpha_i\}}(\mathbf{k}_F, \mathbf{q}_F)\,, \end{aligned} \tag{1.86}$$

and second order corrections are given by the particle-particle (PP), direct (D) particle-hole (PH) and crossed particle-hole (cPH) diagrams

$$\begin{aligned} U^{\text{2nd order}}_{\{\alpha_i\}}(\mathbf{k}_F, \mathbf{q}_F) = +4U^{\text{PP}}_{\{\alpha_i\}}(\mathbf{k}_F, \mathbf{q}_F) \\ +8U^{\text{PH}}_{\{\alpha_i\}}(\mathbf{k}_F, \mathbf{q}_F) \\ -8U^{\text{cPH}}_{\{\alpha_i\}}(\mathbf{k}_F, \mathbf{q}_F)\,. \end{aligned} \tag{1.87}$$

In the band space notation we previously introduced the different contributions are given by the integrals

$$U^{\text{PP}}_{\{\alpha_i\}} = \sum_{\beta_l,\beta_o} \int_{\Omega_0} \mathrm{d}\mathbf{l}\, U^{\mathbf{k}_F,-\mathbf{k}_F,\mathbf{l},-\mathbf{l}}_{\alpha_0\alpha_1\beta_l\beta_o} L^{\text{PP}}_{\beta_l\beta_o}(\mathbf{l})\, U^{\mathbf{l},-\mathbf{l},\mathbf{q}_F,-\mathbf{q}_F}_{\beta_l\beta_o\alpha_2\alpha_3} \tag{1.88}$$

$$U^{\text{PH}}_{\{\alpha_i\}} = \sum_{\beta_l,\beta_m} \int \mathrm{d}\mathbf{l}\, U^{\mathbf{k}_F,\mathbf{m},\mathbf{q}_F,\mathbf{l}}_{\alpha_0\beta_m\alpha_2\beta_l} L^{\text{PH}}_{\beta_l\beta_m}(\mathbf{l},\mathbf{m})\, U^{\mathbf{l},-\mathbf{k}_F,\mathbf{m},-\mathbf{q}_F}_{\beta_l\alpha_1\beta_m\alpha_3} \tag{1.89}$$

$$U^{\text{cPH}}_{\{\alpha_i\}} = \sum_{\beta_l,\beta_n} \int \mathrm{d}\mathbf{l}\, U^{\mathbf{k}_F,\mathbf{n},-\mathbf{q}_F,\mathbf{l}}_{\alpha_0\beta_n\alpha_3\beta_l} L^{\text{PH}}_{\beta_l\beta_n}(\mathbf{l},\mathbf{n})\, U^{\mathbf{l},-\mathbf{k}_F,\mathbf{n},\mathbf{q}_F}_{\beta_l\alpha_1\beta_n\alpha_2} \tag{1.90}$$

where

$$\begin{aligned} \mathbf{m} &= \mathbf{l} - \mathbf{k}_F + \mathbf{q}_F \quad \text{and} \\ \mathbf{n} &= \mathbf{l} - \mathbf{k}_F - \mathbf{q}_F \end{aligned} \tag{1.91}$$

due to momentum conservation [23, 33, 73].

Using the fact that the bare interaction is constant in imaginary time and restricting our focus to the zero energy sector of the effective interaction, we can absorb all frequency summations into L^{PH} and L^{PP}. Standard Matsubara summation techniques can then be used solve the frequency dependence analytically which reduces the propagator pairs to the well known fractions

$$L^{\text{PP}}_{\alpha_l\alpha_o}(\mathbf{l}) = \frac{n_F(-\beta\epsilon_{\alpha_l}(\mathbf{l})) - n_F(\beta\epsilon_{\alpha_o}(-\mathbf{l}))}{\epsilon_{\alpha_l}(\mathbf{l}) + \epsilon_{\alpha_o}(-\mathbf{l})} \tag{1.92}$$

and

$$L^{\mathrm{PH}}_{\alpha_l\alpha_m}(\mathbf{l},\mathbf{m}) = \frac{n_F(\beta\epsilon_{\alpha_l}(\mathbf{l})) - n_F(\beta\epsilon_{\alpha_m}(\mathbf{m}))}{\epsilon_{\alpha_l}(\mathbf{l}) - \epsilon_{\alpha_m}(\mathbf{m})} \tag{1.93}$$

with the Fermi Dirac distribution $n_F(x)$

$$n_F(x) = \frac{1}{\mathrm{e}^x + 1}\,. \tag{1.94}$$

Using the property $n_F(-x) = 1 - n_F(x)$ one can convert the nominators of these fractions to the computationally disadvantageous but easier to interpret expressions

$$\begin{aligned} n_F(-\beta\epsilon_{\alpha_l}(\mathbf{l})) - n_F(\beta\epsilon_{\alpha_o}(-\mathbf{l})) &= \Big(n_F(\beta\epsilon_{\alpha_l}(\mathbf{l})) - 1\Big)\Big(n_F(\beta\epsilon_{\alpha_o}(-\mathbf{l})) - 1\Big) - n_F(\beta\epsilon_{\alpha_l}(\mathbf{l}))n_F(\beta\epsilon_{\alpha_o}(-\mathbf{l})) \\ n_F(\beta\epsilon_{\alpha_l}(\mathbf{l})) - n_F(\beta\epsilon_{\alpha_m}(\mathbf{m})) &= \Big(n_F(\beta\epsilon_{\alpha_l}(\mathbf{l})) - 1\Big)n_F(\beta\epsilon_{\alpha_m}(\mathbf{m})) - n_F(\beta\epsilon_{\alpha_l}(\mathbf{l}))\Big(n_F(\beta\epsilon_{\alpha_m}(\mathbf{m})) - 1\Big)\,, \end{aligned} \tag{1.95}$$

where each factor of $n_F(E)$ $[1 - n_F(E)]$ describes the probability of finding an filled [empty] state at energy E. This way it is clear that we can interpret Equations 1.92 and 1.93 as the summary of all processes in second order perturbation theory that correspond to the intermediate excitation of PP and hole-hole like or the two different particle-hole like excitations respectively.

While the wcRG is formulated in the limit of zero temperature *i.e.*, $\beta \to \infty$, we retain the temperature dependence as it provides a physical smoothing parameter as well as providing an even more natural connection to two-particle susceptibilities. Note that the PP diagram in Equation 1.88 is explicitly regularized by restricting its integration to modes $\mathbf{l}$ respecting $|\epsilon_{\beta_l}(\pm\mathbf{l})| > \Omega_0$ while no such restriction is needed in the particle-hole diagrams due to the careful choice of Ω_0. Nevertheless, the denominator of L^{PH} may vanish for the case of $\mathbf{l} = \mathbf{m}$ and $\alpha_l = \alpha_m$, resulting in

$$L^{\mathrm{PH}}_{\alpha_l\alpha_l}(\mathbf{l},\mathbf{l}) = n_F'(\beta\epsilon_{\alpha_l}(\mathbf{l})) \xrightarrow{\beta\to\infty} \delta(\epsilon_{\alpha_l}(\mathbf{l})) \tag{1.96}$$

which requires special treatment in the numerical evaluation. We can explicitly calculate these edge cases via a line integral along the FS using

$$\int_{\mathrm{BZ}} \mathrm{d}\mathbf{l}\,\delta(\epsilon_{\beta_\mathbf{l}}(\mathbf{l})) = \int \mathrm{d}\epsilon_{\beta_\mathbf{l}}\,\frac{1}{\nabla_\mathbf{l}\epsilon_{\beta_\mathbf{l}}}\,\delta(\epsilon_{\beta_\mathbf{l}}(\mathbf{l})) = \int_{\mathrm{FS}_{\beta_\mathbf{l}}} \frac{\mathrm{d}\mathbf{l}}{v_{F_{\beta_\mathbf{l}}}(\mathbf{l})}\,, \tag{1.97}$$

where $v_{F_{\beta_\mathbf{l}}}(\mathbf{l})$ denotes the Fermi velocity on band $\beta_\mathbf{l}$.

The calculation of the PP diagram in Equation 1.88 would indeed require a careful implementation of the cutoff. Closer inspection of the formula yields the insight that the vanishing total momentum of Cooper pairs disallows the emergence of new momentum dependencies $\mathbf{k}_F$ or $\mathbf{q}_F$. Additionally, the diagram scales with U^2 compared to U for the bare interaction. Combining these

facts one can draw the conclusion that the PP diagram merely rescales the bare interaction and neglect it completely in the limit of vanishing U [23, 74]. While this approach was adopted for the remainder of this thesis, we would like to point out that the interaction structure of multi-orbital systems is not momentum dependent, posing a potential loophole for the argument. Furthermore, the calculation of the PP diagram is restricted to the $\mathbf{q} = 0$ transfer momentum, making the numerical cost of calculating this diagram negligible compared to the particle-hole diagrams. Therefore a simple sanity check for the presented argument could always be implemented in any numerical scheme with negligible cost.

As we have seen, the formulation of the diagrams in band space is useful for the analysis of models with a closed analytical solution for H_0 as well as the presented path-integral derivation. For models where H_0 can only be solved by numerical matrix diagonalization, the gauge variance discussed in Sect. 1.1, requires particular care. Inserting the orbital band transformation matrices from Equation 1.9 into the expression for the direct particle-hole bubble above we can arrive at gauge invariant and therefore numerically preferable quantities

$$\begin{aligned} U^{\mathrm{PH}}_{\{\alpha_i\}}(\mathbf{k}_F, \mathbf{q}_F) = \sum_{\beta_l,\beta_m} \int \mathrm{d}\mathbf{l} \sum_{\{a_i\}} \sum_{\{b_i\}} & L^{\mathrm{PH}}_{\beta_l\beta_m}(\mathbf{l}, \mathbf{m}) \\ & v^*_{a_0\alpha_0}(\mathbf{k}_F) v^*_{b_1\beta_m}(\mathbf{m}) U^{\mathbf{k}_F,\mathbf{m},\mathbf{q}_F,\mathbf{l}}_{a_0b_1a_2b_3} v_{a_2\alpha_2}(\mathbf{q}_F) v_{b_3\beta_l}(\mathbf{l}) \\ & v^*_{b_0\beta_l}(\mathbf{l}) v^*_{a_1\alpha_1}(-\mathbf{k}_F) U^{\mathbf{l},-\mathbf{k}_F,\mathbf{m},-\mathbf{q}_F}_{b_0a_1b_2a_3} v_{b_2\beta_m}(\mathbf{m}) v_{a_3\alpha_3}(-\mathbf{q}_F) \\ = \sum_{\{a_i\}} & v^*_{a_0\alpha_0}(\mathbf{k}_F) v^*_{a_1\alpha_1}(-\mathbf{k}_F) v_{a_2\alpha_2}(\mathbf{q}_F) v_{a_3\alpha_3}(-\mathbf{q}_F) \\ \sum_{\{b_i\}} & \int \mathrm{d}\mathbf{l}\, U^{\mathbf{k}_F,\mathbf{m},\mathbf{q}_F,\mathbf{l}}_{a_0b_1a_2b_3} U^{\mathbf{l},-\mathbf{k}_F,\mathbf{m},-\mathbf{q}_F}_{b_0a_1b_2a_3} \\ \sum_{\beta_l,\beta_m} & v^*_{b_1\beta_m}(\mathbf{m}) v_{b_2\beta_m}(\mathbf{m}) L^{\mathrm{PH}}_{\beta_l\beta_m}(\mathbf{l}, \mathbf{m}) v^*_{b_0\beta_l}(\mathbf{l}) v_{b_3\beta_l}(\mathbf{l})\,. \end{aligned} \tag{1.98}$$

For the special case of momentum independent interactions, we are able to pull the interaction terms in orbital space in front of the $\mathbf{l}$ integration and the object to integrate is the generalized susceptibility known from random phase approximation calculations

$$\chi_{a_0a_1a_2a_3}(\mathbf{l} - \mathbf{m}) = \chi_{a_0a_1a_2a_3}(\mathbf{k}_F - \mathbf{q}_F) = -\int \mathrm{d}\mathbf{l} \sum_{\beta,\gamma} v^*_{a_0\beta}(\mathbf{l}) v_{a_2\beta}(\mathbf{l}) L^{\mathrm{PH}}_{\beta\gamma}(\mathbf{l}, \mathbf{m}) v^*_{a_1\gamma}(\mathbf{m}) v_{a_3\gamma}(\mathbf{m})\,. \tag{1.99}$$

We now generalize this idea to momentum dependent interactions $U_{\{a_i\}}(\{\mathbf{k}_i\})$ *i.e.*, non-local interactions. To this end we first introduce the integrand of this generalized susceptibility as

$$X_{a_0a_1a_2a_3}(\mathbf{l}, \mathbf{m}) = \sum_{\beta,\gamma} v^*_{a_0\beta}(\mathbf{l}) v_{a_2\beta}(\mathbf{l}) L^{\mathrm{PH}}_{\beta\gamma}(\mathbf{l}, \mathbf{m}) v^*_{a_1\gamma}(\mathbf{m}) v_{a_3\gamma}(\mathbf{m})\,. \tag{1.100}$$

In the next step we explicitly write our bare interaction in the direct particle-hole channel (D-channel) representation of the singular-mode and truncated-unity functional renormalization group [97, 98] approaches

$$U_{\{a_i\}}(\{\mathbf{k}_i\}) = \delta(\mathbf{k}_0 + \mathbf{k}_1 - \mathbf{k}_2 - \mathbf{k}_3) \sum_{i,j} U^{ij}_{\{a_i\}}(\mathbf{k}_0 - \mathbf{k}_2) f^*_i(\mathbf{k}_0) f_j(\mathbf{k}_3)\,, \tag{1.101}$$

where the $f_i(\mathbf{k})$ denote a finite set of envelope functions that can be adapted to the specifics of the input interaction and are commonly known as form factors. In App. A we show that such a reformulation is generically possible for reasonable translationally invariant interactions involving a finite number of bonds and that the number of form factors is bounded by the number of sites involved in the interaction with a reference site.

Inserting Equation 1.101 into our gauge invariant expression for the direct particle-hole diagram yields

$$\begin{aligned} U^{\mathrm{PH}}_{\{\alpha_i\}}(\mathbf{k}_F, \mathbf{q}_F) = &\sum_{\{a_i\}} v^*_{a_0\alpha_0}(\mathbf{k}_F) v^*_{a_1\alpha_1}(-\mathbf{k}_F) v_{a_2\alpha_2}(\mathbf{q}_F) v_{a_3\alpha_3}(-\mathbf{q}_F) \\ &\sum_{\{b_i\}} \sum_{\{g_i\}} U^{g_0 g_2}_{a_0 b_1 a_2 b_3}(\mathbf{k}_F - \mathbf{q}_F) U^{g_1 g_3}_{b_0 a_1 b_2 a_3}(\mathbf{k}_F - \mathbf{q}_F) \\ &\int \mathrm{d}\mathbf{l}\, X_{b_1 b_0 b_2 b_3}(\mathbf{l}, \mathbf{m}) f^*_{g_0}(\mathbf{k}_F) f_{g_2}(\mathbf{l}) f^*_{g_1}(\mathbf{l}) f_{g_3}(-\mathbf{q}_F)\,. \end{aligned} \tag{1.102}$$

This motivates us to define

$$\aleph^{gh}_{b_0 b_1 b_2 b_3}(\mathbf{k}_F, \mathbf{q}_F) = \int \mathrm{d}\mathbf{l}\, f^*_g(\mathbf{l}) X_{b_0 b_1 b_2 b_3}(\mathbf{l}, \mathbf{l} - \mathbf{k}_\mathrm{F} + \mathbf{q}_\mathrm{F}) f_h(\mathbf{l}) \tag{1.103}$$

as an even more generalized susceptibility. Here we chose the Hebrew letter $\aleph$ (Aleph) due to its similarity with the Greek letter χ. Repeating this calculation for the crossed particle-hole channel reduces to the same integral. In conclusion, the knowledge of $\aleph$ for all points $\mathbf{k}_F$ and $\mathbf{q}_F$ on the discretized Fermi surface is sufficient for the calculation of both the PH and cPH diagrams without further integration. In particular, this allows for an efficient calculation of phase diagram scans in all possible values of $U^{g_0 g_2}_{\mathbf{0123}}$ for a given single-particle Hamiltonian H_0.

As we will see in Section 1.4, the structure of our generalized susceptibility also allows for a straightforward calculation of all particle-hole like diagrams contributing to the random phase approximation. In fact our proposed form factor decomposition is formally equivalent to a procedure which has been previously utilized to incorporate long range Coulomb interactions in FLEX implementations [99]. We further note that it is straightforward to express the momentum depen-

dence of the bare interaction in the PP channel and thereby facilitate a similar structure for the remaining diagram.

We have now established a gauge invariant formulation for the numerically expensive momentum integration. The gauge of the effective interaction in band space, however, is not yet fixed. We tackle this problem by enforcing the calculation of the pair interaction between time reversal partner states. This is possible for generic models as the time reversal operator $\hat{T}$ does not affect the real space, orbital or sublattice degrees of freedom and can always be represented by

$$\hat{T} = \mathrm{i}\sigma_y \mathcal{K}\,, \tag{1.104}$$

where σ_y acts in spin space, $\mathcal{K}$ represents complex conjugation and the orbital sublattice structure is trivial. Instead of calculating the effective interaction between Cooper pairs created by operators $c^\dagger_{\mathbf{k}\alpha} c^\dagger_{-\mathbf{k}\beta}$, we consider an interaction between states created by

$$\begin{aligned} c^\dagger_{\mathbf{k}\alpha} \hat{T} c^\dagger_{\mathbf{k}\beta} \hat{T}^{-1} &= \sum_{a,b} v_{a\alpha}(\mathbf{k}) v^*_{b\beta}(\mathbf{k}) c^\dagger_{\mathbf{k}a} \hat{T} c^\dagger_{\mathbf{k}b} \hat{T}^{-1} \\ &= \sum_{a,b} v_{a\alpha}(\mathbf{k}) v^*_{b\beta}(\mathbf{k}) c^\dagger_{\mathbf{k}a} \sum_c \mathcal{D}^\dagger_{cb}(T) c^\dagger_{-\mathbf{k}c} \\ &= \sum_{a,b} V^{\mathrm{pair}}_{\alpha\beta,ab}(\mathbf{k}) c^\dagger_{\mathbf{k}a} c^\dagger_{-\mathbf{k}b}\,. \end{aligned} \tag{1.105}$$

Here we have defined the quantity

$$V^{\mathrm{pair}}_{\alpha\beta,ab}(\mathbf{k}) = v_{a\alpha}(\mathbf{k}) \sum_c \mathcal{D}^\dagger_{cb}(T) v^*_{c\beta}(\mathbf{k})\,, \tag{1.106}$$

which has the advantage that it is invariant under gauge transformations of the type

$$v_{a\alpha}(\mathbf{k}) \to \mathrm{e}^{\mathrm{i}\varphi(\mathbf{k})} v_{a\alpha}(\mathbf{k})\,. \tag{1.107}$$

$\mathcal{D}^\dagger_{cb}(T)$ represents the unitary part of the time-reversal symmetry operator in orbital-spin-space and is given by a tensor product of $\mathrm{i}\sigma_y$ in spin and $\mathbb{1}$ in orbital-sublattice space. Our construction eliminates possible gauge differences between states at $\mathbf{k}$ and $-\mathbf{k}$ arising from numerics by using the state at $\mathbf{k}$ to define the state at $-\mathbf{k}$ in a natural way.

Equation 1.107 is sufficient to solve the gauge-problem for the case of non-degenerate bands at the Fermi surface, as we generically expect inter-band (*i.e.*, finite frequency) Cooper pairing to be negligible. For degenerate Fermi surfaces that naturally arise in the context of fully spin-rotation symmetric models or spin-orbit coupled systems that respect inversion symmetry, Cooper pairing between different band indices $\alpha \neq \beta$ at zero energy needs to be taken into account. While we can

fix the relative gauge between the degenerate states at a given momentum $\mathbf{k}$ as well as their time-reversal partners at $-\mathbf{k}$, the choice of the pseudo-spin basis is not fixed by this procedure leaving a residual gauge degree of freedom. In order to relate Cooper pair scattering amplitudes between states at different momenta in a meaningful way (an operation that is necessary for symmetry operations), a consistent choice for the pseudo-spin basis along the Fermi surface has to be made. For band degeneracies originating from spin rotational invariance this choice is naturally given as the spin sector decouples trivially from the theory. In the case of centrosymmetric spin-orbit coupling, a consistent definition of the pseudo-spin basis may be found by analytic and manual diagonalization of $h_{ab}\mathbf{k}$ into a block diagonal structure. Spin-orbit coupled three band models for Sr_2RuO_4, where rearranging the orbital spin basis properly renders the Hamiltonian block diagonal [100] are an example of this. Fink [81] has proposed to solve the problem for generic systems by adiabatically switching on the spin-orbit interaction, implying a smooth and traceable evolution of the natural spin basis. Another promising approach to the problem could be the choice of Cooper pair states that are simultaneous eigenstates to $\hat{H}_0$, $\hat{T}$ and the inversion operator $\hat{I}$. The central problem with this approach is the fact that the specific representation of $\hat{I}$ depends on the single particle basis in a non-generic way. In particular, electrons in orbitals with odd (even) angular momentum (do not) acquire a minus sign under inversion and maximally localized Wannier functions may not necessarily respect inversion symmetry on their own. Since we are interested in the case of strong inversion symmetry breaking, we continue without solving this issue in all generality.

Combining the gauge invariance of the $\aleph$ object and our choice of Cooper pair states, we summarize the formulas for the particle-hole diagrams contributing to the effective interaction in the Cooper channel as

$$\begin{aligned} U^{\mathrm{PH}}_{\{\alpha_i\}}(\mathbf{k}_F, \mathbf{q}_F) = \sum_{\{g_i\}} & f^*_{g_0}(\mathbf{k}_F) f_{g_3}(-\mathbf{q}_F)\,. \\ & \sum_{\{a_i\}} \left(V^{\mathrm{pair}}_{\alpha_0\alpha_1,a_0a_1}(\mathbf{k}_F)\right)^* V^{\mathrm{pair}}_{\alpha_2\alpha_3,a_2a_3}(\mathbf{q}_F) \\ & \sum_{\{b_i\}} U^{g_0g_2,(\mathbf{k}_F-\mathbf{q}_F)}_{a_0b_1a_2b_3} \aleph^{g_1g_2}_{b_1b_0b_2b_3}(\mathbf{k}_F, \mathbf{q}_F) U^{g_1g_3,(\mathbf{k}_F-\mathbf{q}_F)}_{b_0a_1b_2a_3} \end{aligned} \tag{1.108}$$

and

$$U^{\mathrm{cPH}}_{\{\alpha_i\}}(\mathbf{k}_F, \mathbf{q}_F) = \sum_{\{g_i\}} f^*_{g_0}(\mathbf{k}_F) f_{g_3}(+\mathbf{q}_F)\,. \\ \sum_{\{a_i\}} \left(V^{\mathrm{pair}}_{\alpha_0\alpha_1,a_0a_1}(\mathbf{k}_F)\right)^* V^{\mathrm{pair}}_{\alpha_2\alpha_3,a_2a_3}(\mathbf{q}_F) \\ \sum_{\{b_i\}} U^{g_0g_2,(\mathbf{k}_F+\mathbf{q}_F)}_{a_0b_1a_3b_3} \aleph^{g_1g_2}_{b_1b_0b_2b_3}(\mathbf{k}_F, -\mathbf{q}_F) U^{g_1g_3,(\mathbf{k}_F+\mathbf{q}_F)}_{b_0a_1b_2a_2}\,. \tag{1.109}$$

Let us reiterate the benefits of this formulation:

- $\aleph$ only contains information about the kinetic model chosen and the set of form factors used.
- $\aleph$ is a gauge invariant quantity.
- By using a basis of time reversal partner states for the calculation we fix the $U(1)$ gauge of the effective interaction completely.
- Knowledge of $\aleph$ allows for detailed scans of the interaction parameter phase diagram without the necessity to calculate momentum space integrals.
- We will see that a form invariant expression can be used to calculate the effective Cooper pair interaction in the random phase approximation.

In the next section we will see how the obtained effective interaction relates to the dominant superconducting instability of the model.

1.3.2 Renormalization group analysis of unconventional superconductivity

In the second step of the wcRG scheme, we perform an analytical 1-loop RG flow from our theory at cutoff Ω_0 to even lower cutoff energies. This can be done by using standard one-loop Fermi-liquid RG since the action generated by the first step is of the form required for the input of these approaches:

- All states in the theory are confined to a small annulus of width Ω_0 around the Fermi surface, allowing a linearization of the dispersion.
- The effective interaction between the states is small, allowing for the a truncation of the RG equations at one-loop.

At the tree-level analysis of the RG flow one finds that most interaction parameters are exponentially suppressed due to the phase space restrictions imposed during the the flow [73, 92, 95]. The remaining parameters are either Fermi-liquid parameters or interactions in the Cooper channel. The Fermi liquid parameters are marginal in the RG language *i.e.*, do not renormalize under the flow from Ω_0 to low energy (smaller cutoffs) [73, 95] and can be neglected in the wcRG approach. Cooper channel interactions, however, renormalize significantly and their flow is given by the one loop RG equations arising from the PP diagram to be

$$\mathrm{d}g_{ik} = \sum_j -g_{ij}g_{jk}\ \mathrm{d}[\log(\Omega_0/\Omega)]\,. \tag{1.110}$$

Here, the indices i, j, k run over all degrees of freedom for Cooper pairs on the Fermi surface and the integration measure is absorbed into the definition of

$$\begin{aligned} g_{(\alpha_0\alpha_1,\mathbf{k}_F),(\alpha_2\alpha_3,\mathbf{q}_F)} = \sqrt{\rho_{\alpha_0}\rho_{\alpha_2}}\sqrt{\frac{\bar{v}_{F\alpha_0}\bar{v}_{F\alpha_2}}{v_{F\alpha_0}(\mathbf{k}_F)v_{F\alpha_2}(\mathbf{q}_F)}} \\ \sqrt{\frac{A_{F\alpha_0}(\mathbf{k}_F)A_{F\alpha_2}(\mathbf{q}_F)}{A_{F\alpha_0}A_{F\alpha_2}}}U_{\{\alpha_i\}}(\mathbf{k}_F,\mathbf{q}_F)\,, \end{aligned} \tag{1.111}$$

where $A_{F\alpha}(\mathbf{k}_F)$ and $v_{F\alpha}(\mathbf{k}_F)$ denote the Fermi surface area and Fermi velocity associated with each discretized point $\mathbf{k}_F$ on the Fermi surface, α only runs over the bands at zero energy for these points. ρ_α and $A_{F\alpha}$ meanwhile denote the total density of states and total Fermi surface area contributed by a specific band α. The mean of the Fermi velocity on a band is defined via an inverse average

$$\bar{v}_{F\alpha} = \left(\sum_{\mathbf{k}_F\in\alpha}\frac{A_{F\alpha}(\mathbf{k}_F)}{A_{F\alpha}}\frac{1}{v_{F\alpha}(\mathbf{k}_F)}\right)^{-1} \tag{1.112}$$

over all Fermi surface momenta on this band. The flow equation Equation 1.110 can now be solved via matrix diagonalization of

$$g_{ij} = \sum_n \phi^*_{in}\lambda_n\phi_{jn} \tag{1.113}$$

by realizing that all eigenvalues renormalize independently due to the orthonormality of eigenvectors. We find

$$\mathrm{d}\lambda_n = -\lambda_n^2\ \mathrm{d}[\log(\Omega_0/\Omega)]\,, \tag{1.114}$$

and see that all positive eigenvalues (corresponding to repulsive interactions g) renormalize to zero und this flow equation. Negative eigenvalues, on the other hand, correspond to attractive in-

teraction channels and grow indefinitely under the RG flow and indicate an instability of the Fermi surface. The smallest (*i.e.*, most negative) eigenvalue λ_0 indicates the strongest superconducting instability and we will refer to it as the leading eigenvalue in the following. From the definition of g we can see that it is a dimensionless matrix that scales with $U\rho$. Since U_0 is purely repulsive we can expect its attractive eigenvalues λ to scale with $U^2\rho/W$, with the bandwidth W arising due to the PP loop in Equation 1.109. Accordingly it is conventional to calculate λ and $V_{\text{eff}} = |\lambda|/\rho$ in units of t/U^2 or W/U^2. A link between $|\lambda|$ and an estimate for the superconducting transition temperature that is independent of Ω_0 can be given as [23]

$$T_c \sim W \exp\left[-1/|\lambda|\right] = W \exp\left[-1/(\rho V_{\text{eff}})\right]. \tag{1.115}$$

The eigenvector ϕ_{j0} corresponding to λ_0 encodes the information about the full structure of the leading superconducting instability's gap function on the Fermi surface

$$\Delta^{\text{SC}}_{\alpha_0\alpha_1}(\mathbf{k}_F) \propto \sqrt{\frac{\bar{v}_{F\alpha}}{v_{F\alpha_0}(\mathbf{k}_F)}}\phi_0(\alpha_0\alpha_1, \mathbf{k}_F), \tag{1.116}$$

which we can subsequently analyze in terms of momentum structure, orbital/sublattice content and singlet / triplet character. The central information extracted in our analysis is the symmetry character of the gap function.

An equivalent (but slightly less rigorous) approach to the analysis of our low energy theory below Ω_0 is given by a straightforward superconducting mean field theory. We present details of its derivation in Appendix B and only state the result here. The self consistency equation for the superconducting the mean field reads

$$\Delta^{\text{SC}}_{\alpha_0\alpha_1}(\mathbf{k}_F) = \int_{\Omega_0} \mathrm{d}\mathbf{q} \sum_{\alpha_2,\alpha_3} U^{\text{eff}}_{\{\alpha_i\}}(\mathbf{k}_F, \mathbf{q}) L^{PP,\Delta}_{\alpha_2,\alpha_3}(\mathbf{q}) \Delta^{\text{SC}}_{\alpha_2\alpha_3}(\mathbf{q}). \tag{1.117}$$

As we have already integrated out all high-energy modes with $\omega_n > \Omega_0$ in the first RG step, the integral only runs over modes with $\epsilon(\mathbf{q}) < \Omega_0$. Furthermore, the PP loop $L^{PP,\Delta}$ has to be evaluated with respect to the energy spectrum in the (potential) presence of a finite superconducting gap Δ which acts as a regulator to the bare PP loop at temperatures $T < T_c$. Close to the superconducting transition $T \approx T_c$, the superconducting gap vanishes and $L^{PP,\Delta} \approx L^{PP}$ *i.e.*, we can calculate the PP loop using the normal state dispersion. This limit yields the linearized gap equation and for small values of Ω_0 we can write

$$\Delta^{\text{SC}}_{\alpha_0\alpha_1}(\mathbf{k}_F) = \frac{1}{K} \sum_{\alpha_2,\alpha_3} \left\langle U^{\text{eff}}_{\{\alpha_i\}}(\mathbf{k}_F, \mathbf{q}_F) \Delta^{\text{SC}}_{\alpha_2\alpha_3}(\mathbf{q}_F) \right\rangle_{\mathbf{q}_F}, \tag{1.118}$$

where the integral d$\mathbf{q}$ has been replaced by a density of states weighted integral over the Fermi surface and κ is a constant that only depends on the temperature, cutoff and density of states at the Fermi level [82]. Clearly, Equation 1.113 is a discretized version of the linearized gap equation, a fact that is expected as the validity of the one-loop RG flow breaks down when $U \times L^{PP} \sim 1$. In summary, the shape of the superconducting gap function $\Delta_{\alpha_2\alpha_3}(\mathbf{k})$ can be extracted by diagonalization of the effective low-energy interaction between Cooper pairs and the corresponding eigenvalues of Equation 1.113 are a cutoff independent measure of the superconducting pairing strength. In order to extract information about the superconducting condensation energy at zero temperature as well as differentiating between degenerate superconducting instabilities, a self consistent solution of Equation 1.117 is necessary.

The presented formulation of the wcRG enables a generic and numerically efficient implementation of the wcRG for the complete class of models discussed in Sect. 1.1. The key ingredients necessary for such an implementation are the discretization of the Fermi surface and an efficient solver for the integral in Equation 1.103. Our approach to these problems as well as a reduction of the computational effort via the use of symmetries is discussed in [72].

In the following we will discuss the random phase approximation approach to unconventional superconductivity and emphasize its connection to the wcRG.

1.4 Random phase approximation

The random phase approximation (RPA) was first introduced by Bohm and Pines [101–104] in an attempt to describe an electron gas interacting via the long range Coulomb interaction. The eponymous random phases between single electron excitations motivated the authors to develop a theory of collective description of the electronic interactions. Later, Gell-Mann and Brueckner [105] showed that their approach can understood as a summation of the most highly divergent terms of the perturbative expansion introduced in Equation 1.82. Notably, this formulation of the RPA not only explains that the bare Coulomb interaction is screened by internal dynamics of the interacting electron gas, but enables a more quantitative calculation of correlation energy in this system.

Here we will refrain from a detailed motivation of the RPA or a review of the key results and only point the reader to literature references such as Ch. 14 of Ref. [93]. Instead we will generalize the RPA evaluation of particle-hole susceptibilities by identifying the most highly divergent diagrams in an analogous way. In particular we point out the connection between unconventional particle-hole instabilities, long-range interactions and the generalized susceptibilities introduced in Section 1.3.

1.4.1 Linear response and generalized susceptibilities

Before engaging in the RPA resummation of diagrams including the interaction, we will consider two-particle linear response functions of the kinetic model. We start by considering models without a sublattice basis and absent SU(2) symmetry. Here we can introduce perturbing scalar and vector fields of Zeemann type

$$H_P = \sum_{\mathbf{r}} \mathcal{E}(\mathbf{r}) \sum_{\sigma} c^\dagger_{\mathbf{r},\sigma} c_{\mathbf{r},\sigma} + \sum_{\mathbf{r}} \sum_{i} \mathcal{B}_i(\mathbf{r}) \sum_{\sigma_0\sigma_2} c^\dagger_{\mathbf{r},\sigma_0} \sigma^i_{\sigma_0,\sigma_2} c_{\mathbf{r},\sigma_2} \,, \tag{1.119}$$

and perform a Fourier transformation yielding

$$\begin{aligned} H_P &= \sum_{\mathbf{r}} \mathcal{E}(\mathbf{r}) \sum_{\sigma} \sum_{\mathbf{k}_0\mathbf{k}_2} c^\dagger_{\mathbf{k}_2,\sigma} c_{\mathbf{k}_0,\sigma} \mathrm{e}^{-i\mathbf{r}(\mathbf{k}_2-\mathbf{k}_0)} + \sum_{\mathbf{r}} \sum_{i} \mathcal{B}_i(\mathbf{r}) \sum_{\sigma_0\sigma_2} \sum_{\mathbf{Qk}} c^\dagger_{\mathbf{k}+\mathbf{Q},\sigma_2} \sigma^i_{\sigma_0,\sigma_2} c_{\mathbf{k},\sigma_0} \mathrm{e}^{-i\mathbf{r}\mathbf{Q}} \\ &= \sum_{\mathbf{Q}} \mathcal{E}(\mathbf{Q}) \sum_{\sigma,\mathbf{k}} c^\dagger_{\mathbf{k}+\mathbf{Q},\sigma} c_{\mathbf{k},\sigma} + \sum_{\mathbf{Q}} \sum_{i} \mathcal{B}_i(\mathbf{Q}) \sum_{\sigma_0\sigma_2} \sum_{\mathbf{k}} c^\dagger_{\mathbf{k}+\mathbf{Q},\sigma_2} \sigma^i_{\sigma_0,\sigma_2} c_{\mathbf{k},\sigma_0} \,, \end{aligned} \tag{1.120}$$

where we defined

$$\begin{aligned}\mathcal{E}(\mathbf{Q}) &= \sum_{\mathbf{r}} \mathcal{E}(\mathbf{r}) \mathrm{e}^{-i\mathbf{r}\mathbf{Q}} \quad \text{and} \\ \mathcal{B}_i(\mathbf{Q}) &= \sum_{\mathbf{r}} \mathcal{B}_i(\mathbf{r}) \mathrm{e}^{-i\mathbf{r}\mathbf{Q}} \,.\end{aligned} \tag{1.121}$$

$\sigma^i_{\sigma\sigma'}$ are the three Pauli matrices and we will later use $\sigma^0_{\sigma\sigma'} = \delta_{\sigma\sigma'}$ as the "0th" Pauli matrix. The intuition for these simple site dependent potential terms for the accumulated charge and spin is clear and we can also use these operators as observables due to the hermiticity of the operators for real potentials $\mathcal{E}(\mathbf{r})$ and $\mathcal{B}_i(\mathbf{r})$. For their Fourier transforms the hermiticity conditions $\mathcal{E}(-\mathbf{Q}) = \mathcal{E}^*(\mathbf{Q})$ and $\mathcal{B}_i(-\mathbf{Q}) = \mathcal{B}_i^*(\mathbf{Q})$ hold.

Already for this simple single band model a further generalization of the fields suggests itself by encompassing modifications to certain inter-site matrix elements. Consider the following perturbation

$$H_P = \sum_{\mathbf{r},\mathbf{d}} \mathcal{E}(\mathbf{r},\mathbf{d}) \sum_{\sigma} c^\dagger_{\mathbf{r}+\mathbf{d}/2,\sigma} c_{\mathbf{r}-\mathbf{d}/2,\sigma} = \sum_{\mathbf{Q},\mathbf{k}} \mathcal{E}(\mathbf{Q},\mathbf{k}) \sum_{\sigma} c^\dagger_{\mathbf{k}+\mathbf{Q}/2,\sigma} c_{\mathbf{k}-\mathbf{Q}/2,\sigma} \,, \tag{1.122}$$

where

$$\mathcal{E}(\mathbf{Q},\mathbf{k}) = \sum_{\mathbf{r},\mathbf{d}} \mathcal{E}(\mathbf{r},\mathbf{d}) \mathrm{e}^{-i\mathbf{r}\mathbf{Q}} \mathrm{e}^{-i\mathbf{d}\mathbf{k}} \,, \tag{1.123}$$

which can be analogously extended to the spin sector. This modification to the systems hopping terms is restricted by the hermiticity conditions

$$\begin{aligned}\mathcal{E}(\mathbf{Q},\mathbf{k}) &= \mathcal{E}^*(-\mathbf{Q},\mathbf{k}) \quad \text{and} \\ \mathcal{B}_i(\mathbf{Q},\mathbf{k}) &= \mathcal{B}_i^*(-\mathbf{Q},\mathbf{k}) \,.\end{aligned} \tag{1.124}$$

At this point one may wonder why a separation of the "electric" and "magnetic" fields is necessary if the discussed constraints do not differ. A related question could concern the highlighted treatment of the spin degree of freedom over the previously fused discussion of spin-sublattice and orbital degrees of freedom. The answer to both of these questions lies in the spin's non-trivial transformation behavior under time-reversal symmetry. Considering the real space expression in Equation 1.119, it becomes clear that any hermitian term proportional to $\tilde{E}$ will transform trivially under time-reversal symmetry while terms proportional to $\tilde{B}$ will acquire a minus sign *i.e.*, break time-reversal symmetry; expected for a magnetic field. This is not a problem per se since probing the response of a time-reversal invariant system with a time-reversal symmetry breaking field still results in a sensible response function. It does however make sense to treat the E and B fields

separately. The issue becomes more subtle for fields that modify hopping terms as these can be complex without breaking hermiticity (*e.g.* spin-orbit coupling terms), leading to a non-trivial transformation behavior of $\tilde{E}$ and $\tilde{B}$ under time reversal symmetry. We find that

$$\begin{aligned} \mathcal{E}(\mathbf{Q},\mathbf{k}) &\to +\mathcal{E}^*(-\mathbf{Q},-\mathbf{k}) = +\,\mathcal{E}(\mathbf{Q},-\mathbf{k}) \quad \text{and} \\ \mathcal{B}_i(\mathbf{Q},\mathbf{k}) &\to -\mathcal{B}_i^*(-\mathbf{Q},-\mathbf{k}) = -\mathcal{B}_i(\mathbf{Q},-\mathbf{k})\,. \end{aligned} \tag{1.125}$$

Considering the $\mathbf{Q} = 0$ sector, this corresponds to the well known statement that hermitian and time reversal symmetry respecting hoppings have to be odd (even) functions of momentum if they do (not) depend on the spin of the hopping electron.

We summarize $\mathcal{E}$ and $\mathcal{B}_i$ into a four component field $\mathcal{A}_\eta$ where $\mathcal{A}_0 = \mathcal{E}$ and $\mathcal{A}_i = \mathcal{B}_i$ ($i = 1,2,3 = x,y,z$) and proceed to generalize to systems with sublattice or orbital degrees of freedom with label o_i. The most general two operator perturbation can then be written as

$$\begin{aligned} H_P &= \sum_{\mathbf{r},\mathbf{d}} \sum_{\eta,o_0,o_2} \mathcal{A}_{\eta,o_0o_2}(\mathbf{r},\mathbf{d}) \sum_{\{\sigma_i\}} c^\dagger_{\mathbf{r}+\mathbf{d}/2,\sigma,o_2} \sigma^\eta_{\sigma_0,\sigma_2} c_{\mathbf{r}-\mathbf{d}/2,\sigma,o_0} \\ &= \sum_{\mathbf{r},\mathbf{d}} \sum_{\eta,m} \mathcal{A}_{\eta,m}(\mathbf{r},\mathbf{d}) \sum_{\{\sigma_i\},\{o_i\}} c^\dagger_{\mathbf{r}+\mathbf{d}/2,\sigma_0,o_2} O^m_{o_0,o_2} \sigma^\eta_{\sigma_0,\sigma_2} c_{\mathbf{r}-\mathbf{d}/2,\sigma_2,o_0} \\ &= \sum_{\mathbf{Q},\mathbf{k}} \sum_{\eta,m} \mathcal{A}_{\eta,m}(\mathbf{Q},\mathbf{k}) \sum_{\{\sigma_i\},\{o_i\}} c^\dagger_{\mathbf{k}+\mathbf{Q}/2,\sigma_0,o_2} O^m_{o_0,o_2} \sigma^\eta_{\sigma_0,\sigma_2} c_{\mathbf{k}-\mathbf{Q}/2,\sigma_2,o_0}\,. \end{aligned} \tag{1.126}$$

As for the spin degree of freedom an expansion of $A_{\eta,ou}$ in terms of a complete set of hermitian matrices $O_{m,ou}$ in the form of

$$\mathcal{A}_{\eta,ou} = \sum_m \mathcal{A}_{\eta m} O^m_{ou} \tag{1.127}$$

seems natural as it provides the remaining $A_{\eta m}$ with a simple transformation behaviour under hermiticity and allows for an interpretation in terms of a a field coupling to (local) hermitian operators. Considering the transformation behaviour under time reversal results in an additional seperation into real and complex (or alternatively symmetric and anti-symmetric) matrices due to the trivial transformation behaviour of orbital and sublattice degrees of freedom under this symmetry. Using Equation 1.124 it is clear that the hermiticity condition generalizes to

$$\mathcal{A}_{\eta m}(\mathbf{Q},\mathbf{k}) = \mathcal{A}^*_{\eta m}(-\mathbf{Q},\mathbf{k})\,. \tag{1.128}$$

Finally we will reduce the generality of our real space considerations slightly by restricting d to small distances. We constrain our analysis to product functions $\mathcal{A}(\mathbf{r},\mathbf{d}) = \sum_f \mathcal{A}_f(\mathbf{r})\phi_f(\mathbf{d})$ as we are interested in modifications to specific short range hopping integrals. Clearly $\tilde{\phi}_0(\mathbf{d}) = \delta(\mathbf{d})$

results in the less general Equation 1.119 while expressions like

$$\phi_j(\mathbf{d}) = \delta(\mathbf{d}-\mathbf{x}) + \delta(\mathbf{d}+\mathbf{x}) - \delta(\mathbf{d}-\mathbf{y}) - \delta(\mathbf{d}+\mathbf{y}) \tag{1.129}$$

allow us to probe the systems response to an assymmetry in the nearest neighbour hopping integrals *i.e.*, nematicity. Fourier transformation according to Equation 1.123 results in

$$\mathcal{A}_{\eta m}(\mathbf{Q},\mathbf{k}) = \sum_f \mathcal{A}_{\eta m f}(\mathbf{Q})\phi_f(\mathbf{k}) \tag{1.130}$$

where

$$\phi_f(\mathbf{k}) = \sum_{\mathbf{d}} \phi_f(\mathbf{d})\mathrm{e}^{-\mathbf{i}\mathbf{d}\mathbf{k}}\,. \tag{1.131}$$

Putting everything together we define a set of operators

$$A_{\eta,m,f}(\mathbf{Q}) = \sum_{\mathbf{k}}\sum_{\sigma_0,\sigma_2}\sum_{o_0,o_2} \phi_f(\mathbf{k}) c^\dagger_{\mathbf{k}+\mathbf{Q}/2,\sigma_2,o_2} O^m_{o_0o_2}\sigma^\eta_{\sigma_0\sigma_2} c_{\mathbf{k}-\mathbf{Q}/2,\sigma_0,o_0}\,, \tag{1.132}$$

with hermitian adjoint

$$A^\dagger_{\eta,m,f}(\mathbf{Q}) = \sum_{\mathbf{k}}\sum_{\sigma_0,\sigma_2}\sum_{o_0,o_2} \phi^*_f(\mathbf{k}) c^\dagger_{\mathbf{k}-\mathbf{Q}/2,\sigma_2,o_2} O^m_{o_0o_2}\sigma^\eta_{\sigma_0\sigma_2} c_{\mathbf{k}+\mathbf{Q}/2,\sigma_0,o_0}\,. \tag{1.133}$$

If we define $O^0_{ou} = \delta_{ou}$ and $\phi_0(\mathbf{k}) = 1$, we can write common examples for these operators like the Fourier transform of the electron density

$$n(\mathbf{Q}) = A_{0,0,0}(\mathbf{Q}) \tag{1.134}$$

and the mean spin direction of our system

$$S_i(\mathbf{Q}=\mathbf{0}) = A_{i,0,0}(\mathbf{0}) \tag{1.135}$$

in precisely this form. An antiferromagnetic pattern on the square lattice Hubbard model would be result in a finite expectation value of

$$S_i(\mathbf{Q}=(\pi,\pi)) = A_{i,0,0}((\pi,\pi))\,, \tag{1.136}$$

while

$$n_i(\mathbf{Q}=(\pi,0)) = A_{0,0,0}((\pi,0)) \tag{1.137}$$

indicates charge stripe order. More exotic particle-hole instabilities have been classified in Ref. [106]. In particular, charge $\eta = 0$ and spin $\eta = i$ bond order states with wave-vector $\mathbf{Q}$ will have signatures for non-trivial form factors $\phi_f(\mathbf{k} \neq \text{const.})$.

We also note that PP operator pairs may be classified analogously. Here it is convention to consider time-reversal partners, which leads to the addition of a matrix $\mathrm{i}\sigma^y$ into the definition

$$P^\dagger_{\eta,m,f}(\mathbf{Q}) = \sum_{\mathbf{k}} \sum_{\sigma_0,\sigma_0,\sigma_2} \sum_{o_0,o_2} \phi^*_f(\mathbf{k}) c^\dagger_{\mathbf{k}+\mathbf{Q}/2,\sigma_0,o_0} O^m_{o_0 o_2} \sigma^\eta_{\sigma_0\sigma_1} (\mathrm{i}\sigma^y_{\sigma_1\sigma_2}) c^\dagger_{-\mathbf{k}+\mathbf{Q}/2,\sigma_2,o_2} \,. \tag{1.138}$$

Clearly this operator is not self-adjoint. A conventional s-wave superconducting mean-field may be added into a Hamiltonian via the term

$$H_{SC} = \Delta P^\dagger_{0,0,0}(\mathbf{0}) + \Delta^* P_{0,0,0}(\mathbf{0}) \,, \tag{1.139}$$

while non-trivial form factor dependencies denote unconventional superconducting condensates with potentially finite angular momentum and finite momenta $\mathbf{Q} \neq \mathbf{0}$ correspond to pair density waves.

Having established a general notation and some first classification of different electron-hole operators we can now proceed to the calculation of the system's response functions for these operators. To this end we will use the set of operators A not only as perturbations but also track the change of their expectation value in response to the perturbation.

From Section 1.2, we know that

$$\chi_{A,B} = -\int_0^\beta \left\langle B(\psi(\tau = 0), \bar{\psi}(\tau = \delta)) A(\psi(\tau'), \bar{\psi}(\tau' + \delta)) \right\rangle_{\text{conn}} \mathrm{d}\tau' \,, \tag{1.140}$$

for general (time-independent and normal ordered) operators A and B. In order to particularize this to the class of operators $A^\dagger_{\eta,m,f}(\mathbf{Q})$ introduced above we introduce a shorthand notation

$$\begin{aligned} A &= A^\dagger_{\eta,m,f}(\mathbf{q}) = \sum_{0,3} A_{0,3} c^\dagger_3 c_0 \\ B &= A_{\eta',m',f'}(\mathbf{q}') = \sum_{1,2} B_{1,2} c^\dagger_2 c_1 \end{aligned} \tag{1.141}$$

with multi indices $i = (\alpha_i, \mathbf{k}_i)$ carrying all band space quantum numbers except for a frequency index. Explicit calculation involving Equation 1.5 yields

$$\begin{aligned} A_{0,3} &= \delta(\mathbf{k}_3 + \mathbf{q} - \mathbf{k}_0) \sum_{\sigma_0,\sigma_3} \sum_{o_0,o_3} \phi^*_f(\mathbf{k}_3) O^m_{o_0 o_3} \sigma^\eta_{\sigma_0\sigma_3} v_{a_3=(\sigma_3,o_3),\alpha_3}(\mathbf{k}_3) v^*_{a_0=(\sigma_0,o_0),\alpha_0}(\mathbf{k}_0) \\ B_{1,2} &= \delta(\mathbf{k}_1 + \mathbf{q}' - \mathbf{k}_2) \sum_{\sigma_1,\sigma_2} \sum_{o_1,o_2} \phi_{f'}(\mathbf{k}_1) O^{m'}_{o_1 o_2} \sigma^{\eta'}_{\sigma_1\sigma_2} v_{a_2=(\sigma_2,o_2),\alpha_2}(\mathbf{k}_2) v^*_{a_1=(\sigma_1,o_1),\alpha_1}(\mathbf{k}_1)\,. \end{aligned} \tag{1.142}$$

Note that while both $A_{0,3}$ and $B_{1,2}$ are gauge-variant quantities with respect to the choice of eigenstates, the susceptibility will turn out to be gauge invariant as A and B are gauge invariant and observable operators.

We now perform a Fourier transformation of the field operators and introduce $\mathbf{i} = (i, \omega_{n_i})$ yielding

$$\begin{aligned} \chi_{A,B} &= -\sum_{\{i\}} B_{1,2} A_{0,3} \int_0^\beta \left\langle \bar\psi_2(\tau = \delta)\psi_1(\tau = 0)\bar\psi_3(\tau' + \delta)\psi_1(\tau') \right\rangle_{\text{conn}} \mathrm{d}\tau' \\ &= -\sum_{\{\mathbf{i}\}} B_{1,2} A_{0,3} \int_0^\beta \mathrm{e}^{\mathrm{i}(\omega_{n_1} - \omega_{n_2})\tau'} \,\mathrm{d}\tau' \left\langle \bar\psi_{\mathbf{2}}\psi_{\mathbf{1}}\bar\psi_{\mathbf{3}}\psi_{\mathbf{0}} \right\rangle_{\text{conn}} \mathrm{e}^{\mathrm{i}\omega_{n_2}\delta} \mathrm{e}^{\mathrm{i}\omega_{n_3}\delta} \\ &= -\beta \sum_{\{\mathbf{i}\}} B_{1,2} A_{0,3} \delta_{\omega_{n_0}\omega_{n_3}} \left\langle \bar\psi_{\mathbf{2}}\psi_{\mathbf{1}}\bar\psi_{\mathbf{3}}\psi_{\mathbf{0}} \right\rangle_{\text{conn}} \mathrm{e}^{\mathrm{i}\omega_{n_2}\delta} \mathrm{e}^{\mathrm{i}\omega_{n_3}\delta}\,. \end{aligned} \tag{1.143}$$

Note that the complete discussion up to this point does not depend on the specific form of the action furnishing the expectation value $\langle \bar\psi_{\mathbf{1}}\psi_{\mathbf{2}}\bar\psi_{\mathbf{0}}\psi_{\mathbf{3}}\rangle_{\text{conn}}$, *i.e.*, our result is exact for the interacting problem. We have to remember that we shall only consider contributions to the expectation value where A and B are connected *i.e.*, diagrams that can not be reduced to products of expectation values $\langle A\rangle\langle B\rangle = \langle \bar\psi_{\mathbf{1}}\psi_{\mathbf{2}}\rangle\langle \bar\psi_{\mathbf{0}}\psi_{\mathbf{3}}\rangle$. Explicitly reintroducing the momentum dependency of A and B, as well as the field variables $\psi_{\mathbf{i}}$ yields

$$\chi_{A(\mathbf{q}),B(\mathbf{q}')} \propto \langle \bar\psi_{\mathbf{1},\mathbf{l}}\psi_{\mathbf{2},\mathbf{l}+\mathbf{q}}\bar\psi_{\mathbf{0},\mathbf{l}'+\mathbf{q}'}\psi_{\mathbf{3},\mathbf{l}'}\rangle_{\text{conn}} \tag{1.144}$$

and a perturbative expansion of the interaction up yields is most conveniently done in terms of Feynman diagrams and presented in the next section.

For the non-interacting theory, however, the susceptibility is given by a single contribution that can be represented by the Feynman diagram

$\chi^0_{AB}(\mathbf{q}) =$ 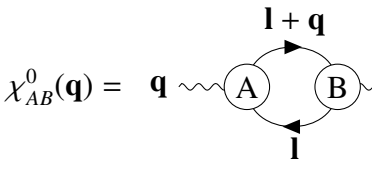

, (1.145)

and evaluated as

$$\begin{aligned}\chi^0_{AB}(\mathbf{q}) &= -\beta \sum_{\{\mathbf{i}\}} B_{1,2} A_{0,3} \delta_{\omega_{n_0}\omega_{n_3}} \left\langle \bar{\psi}_{\mathbf{2}} \psi_{\mathbf{0}} \right\rangle_0 \mathrm{e}^{\mathrm{i}\omega_{n_2}\delta} \left\langle \psi_{\mathbf{1}} \bar{\psi}_{\mathbf{3}} \right\rangle_0 \mathrm{e}^{\mathrm{i}\omega_{n_3}\delta} \\ &= \beta \sum_{\{\mathbf{i}\}} B_{1,2} A_{0,3} \delta_{\omega_{n_0}\omega_{n_3}} G_{\mathbf{02}} G_{\mathbf{13}} \mathrm{e}^{\mathrm{i}\omega_{n_2}\delta} \mathrm{e}^{\mathrm{i}\omega_{n_3}\delta} \\ &= \sum_{\{i\}} B_{1,2} A_{0,3} \beta \sum_{\omega_n} G_{0,2}(\omega_n) G_{1,3}(\omega_n) \mathrm{e}^{\mathrm{i}\omega_n\delta} \\ &= \sum_{0,1} B_{1,0} A_{0,1} L^{\mathrm{PH}}_{\alpha_0\alpha_1}(\mathbf{k}_0, \mathbf{k}_1)\,.\end{aligned} \tag{1.146}$$

The explicit energy conservation $\omega_{n_0} = \omega_{n_3}$ conspires with the energy conservation along propagator lines to leave a single frequency summation which is readily evaluated using the residue theorem and the Fermi-Dirac distribution. We can now insert the expressions for $A_{0,3}$ and $B_{1,2}$ and find

$$\begin{aligned}&\chi^0\left(A^\dagger_{\eta,m,f}(\mathbf{q}), A_{\eta',m',f'}(\mathbf{q}')\right) = \\ &= \sum_{\mathbf{k}_0,\mathbf{k}_1} \sum_{\alpha_0,\alpha_1} \delta(\mathbf{k}_1 + \mathbf{q} - \mathbf{k}_0)\delta(\mathbf{k}_1 + \mathbf{q}' - \mathbf{k}_0) \sum_{\{\sigma_i\}} \sum_{\{o_i\}} \phi^*_f(\mathbf{k}_1)\phi_{f'}(\mathbf{k}_1) O^m_{o_0o_3} O^{m'}_{o_1o_2} \sigma^\eta_{\sigma_0\sigma_3} \sigma^{\eta'}_{\sigma_1\sigma_2} \\ &\quad v_{a_3,\alpha_1}(\mathbf{k}_1) v^*_{a_0,\alpha_0}(\mathbf{k}_0) v_{a_2,\alpha_0}(\mathbf{k}_0) v^*_{a_1,\alpha_1}(\mathbf{k}_1) L^{\mathrm{PH}}_{\alpha_0\alpha_1}(\mathbf{k}_0, \mathbf{k}_1) \\ &= \sum_{\mathbf{k}_1} \delta(\mathbf{k}_1 + \mathbf{q}' - \mathbf{k}_1 - \mathbf{q}) \sum_{\{\sigma_i\}} \sum_{\{o_i\}} \phi^*_f(\mathbf{k}_1)\phi_{f'}(\mathbf{k}_1) O^m_{o_0o_3} O^{m'}_{o_1o_2} \sigma^\eta_{\sigma_0\sigma_3} \sigma^{\eta'}_{\sigma_1\sigma_2} X_{a_0a_1a_2a_3}(\mathbf{k}_0, \mathbf{k}_1) \\ &= \delta(\mathbf{q}' - \mathbf{q}) \sum_{\{\sigma_i\}} \sum_{\{o_i\}} O^m_{o_0o_3} O^{m'}_{o_1o_2} \sigma^\eta_{\sigma_0\sigma_3} \sigma^{\eta'}_{\sigma_1\sigma_2} \sum_{\mathbf{l}} \phi^*_f(\mathbf{l})\phi_{f'}(\mathbf{l}) X_{a_0a_1a_2a_3}(\mathbf{l} + \mathbf{q}, \mathbf{l}) \\ &= \delta(\mathbf{q}' - \mathbf{q}) \sum_{\{\sigma_i\}} \sum_{\{o_i\}} O^m_{o_0o_3} O^{m'}_{o_1o_2} \sigma^\eta_{\sigma_0\sigma_3} \sigma^{\eta'}_{\sigma_1\sigma_2} \aleph^{ff'}_{a_0a_1a_2a_3}(\mathbf{q}, \mathbf{0})\,.\end{aligned} \tag{1.147}$$

Here we have made use of previously introduced shorthand notations for the particle-hole bubble calculation given by Eqs. 1.100 and 1.103. Our result provides further motivation for the definition of the generalized susceptibility $\aleph$ and shows that the conventional susceptibility is simply given by its limiting case for on-site particle-hole fluctuations. We can see that translational invariance decouples particle-hole fluctuations with different momenta $\mathbf{q}$ and that this result will hold upon including any momentum conserving interaction. As the description of particle-hole operators in terms of Equation 1.132 seems to be useful, we will employ it to the analysis of general interaction terms in the next section.

1.4.2 Particle-Hole decomposition of general interactions

While considering a general translation invariant two-particle interaction (compare Equation 1.8)

$$H_I = \sum_{\{\mathbf{k}_i\}} \sum_{\{a_i\}} U_{\{a_i\}}(\{\mathbf{k}_i\}) c^\dagger_{a_2,\mathbf{k}_2} c^\dagger_{a_3,\mathbf{k}_3} c_{a_1,\mathbf{k}_1} c_{a_0,\mathbf{k}_0} \,, \tag{1.148}$$

we have previously (Equation 1.101) seen that it may be useful to parametrize this interaction as

$$U_{\{a_i\}}(\{\mathbf{k}_i\}) = \delta(\mathbf{k}_0 + \mathbf{k}_1 - \mathbf{k}_2 - \mathbf{k}_3) \sum_{i,j} U^{ij}_{\{a_i\}}(\mathbf{k}_0 - \mathbf{k}_2) \phi^*_i(\mathbf{k}_0) \phi_j(\mathbf{k}_3) \,. \tag{1.149}$$

A different way to phrase this decomposition is in terms of the general particle-hole operators introduced in the previous section. Note that we have to pick a slightly less physical gauge choice for the Fourier transformation here and $\mathbf{k}$ is no longer dual to the center of mass independent relative coordinate $\mathbf{d}$ from the previous section. If we start with

$$\mathcal{A}_{\eta,m}(\mathbf{Q},\mathbf{k}) \sum_{\{\sigma_i\},\{o_i\}} c^\dagger_{\mathbf{k}+\mathbf{Q},\sigma_0,o_2} O^m_{o_0,o_2} \sigma^\eta_{\sigma_0,\sigma_2} c_{\mathbf{k},\sigma_2,o_0} \tag{1.150}$$

and consider the operator

$$\begin{aligned} \sum_{\mathbf{Q}} \sum_{\eta\eta',mm',ff'} V_{\eta\eta',mm',ff'}(\mathbf{Q}) A^\dagger_{\eta,m,f}(\mathbf{Q}) A_{\eta',m',f'}(\mathbf{Q}) = \\ \sum_{\mathbf{Q}} \sum_{\eta\eta',mm',ff'} V_{\eta\eta',mm',ff'}(\mathbf{Q}) \sum_{\{\sigma_i\}} \sum_{\{o_i\}} \sum_{\mathbf{k},\mathbf{k}'} \phi^*_f(\mathbf{k}) \phi_{f'}(\mathbf{k}') O^m_{o_0 o_2} O^{m'}_{o_1 o_3} \sigma^\eta_{\sigma_0\sigma_2} \sigma^{\eta'}_{\sigma_1\sigma_3} \\ c^\dagger_{\mathbf{k},\sigma_2,o_2} c^\dagger_{\mathbf{k}'+\mathbf{Q},\sigma_3,o_3} c_{\mathbf{k}',\sigma_1,o_1} c_{\mathbf{k}+\mathbf{Q},\sigma_0,o_0} \end{aligned} \tag{1.151}$$

and compare term by term with the previous expressions we find that if we let

$$U^{ij}_{\{a_i\}}(\mathbf{k}_0 - \mathbf{k}_2) = \sum_{\eta\eta',mm'} V_{\eta\eta',mm',ij}(\mathbf{k}_0 - \mathbf{k}_2) O^m_{o_0 o_2} O^{m'}_{o_1 o_3} \sigma^\eta_{\sigma_0\sigma_2} \sigma^{\eta'}_{\sigma_1\sigma_3} \,, \tag{1.152}$$

we can write

$$H_I = \sum_{\mathbf{Q}} \sum_{\eta\eta',mm',ff'} V_{\eta\eta',mm',ff'}(\mathbf{Q}) A^\dagger_{\eta,m,f}(\mathbf{Q}) A_{\eta',m',f'}(\mathbf{Q}) \,. \tag{1.153}$$

It is important to notice that this decomposition of H_I into two pairs of fermion operators is not unique. A decomposition in terms of particle-pair operators $P^\dagger \propto c^\dagger c^\dagger$ is clearly possible as well. Another way to phrase the bias introduced here is by considering other options for the "emphasized" transfer momentum $\mathbf{Q} = \mathbf{k}_0 - \mathbf{k}_2$. Taking into account momentum conservation one realizes that three unique choices for transfer momenta constructed from two-fermionic momenta

exist:

$$\begin{aligned}\mathbf{Q}_D &= \mathbf{k}_0 - \mathbf{k}_2 = \mathbf{k}_3 - \mathbf{k}_1 \\ \mathbf{Q}_P &= \mathbf{k}_0 + \mathbf{k}_1 = \mathbf{k}_2 + \mathbf{k}_3 \\ \mathbf{Q}_C &= \mathbf{k}_0 - \mathbf{k}_3 = \mathbf{k}_2 - \mathbf{k}_1 \,.\end{aligned} \tag{1.154}$$

These three are commonly called direct particle-hole (D), particle-particle (P) and crossed particle-hole (C) channel in the fRG literature [97, 98]. Nevertheless, the decomposition given by Equation 1.153 is sufficient for the calculation of all diagrams contributing to the PH channel in the RPA approximation. This crucially depends on the insight that any short ranged two-particle interaction can be exactly expressed in this form via a finite number of form-factor functions ϕ_i. Such a statement is only possible for the bare interaction, while a general effective interaction at an intermediate scale may acquire long-range momentum dependencies in $\mathbf{Q}_D$,$\mathbf{Q}_P$ AND $\mathbf{Q}_P$. Due to this the number of form-factors required for an exact mapping between the three channels grows during a functional renormalization group flow.

In order to illustrate our construction for the bare interaction we particularize to a model without sublattice or orbital degrees of freedom and consider the bare Coulomb interaction with a Yukawa-type regularization α for its long range convergence and an explicit exclusion of the diverging on site contribution

$$H_I = \sum_{\{\mathbf{k}_i\}} \delta(\mathbf{k}_0 + \mathbf{k}_1 - \mathbf{k}_2 - \mathbf{k}_3) \sum_{\mathbf{d}\neq\mathbf{0}} \frac{\mathrm{e}^{-\alpha|\mathbf{d}|}}{|\mathbf{d}|} \mathrm{e}^{\mathrm{i}\mathbf{d}(\mathbf{k}_0-\mathbf{k}_2)} \sum_{\{\sigma_i\}} \delta_{\sigma_0\sigma_2}\delta_{\sigma_1\sigma_3} c^\dagger_{\sigma_2,\mathbf{k}_2} c^\dagger_{\sigma_3,\mathbf{k}_3} c_{\sigma_0,\mathbf{k}_0} c_{\sigma_1,\mathbf{k}_1} \,. \tag{1.155}$$

Here the sum over $\mathbf{d}$ runs over all possible distances between lattice sites. The lattice discretization makes an analytic evaluation of the Fourier transform non-trivial. The continuous integral in three dimensions gives

$$\int_{\mathbb{R}} \mathrm{d}\mathbf{r} \frac{\mathrm{e}^{-\alpha|\mathbf{r}|}}{|\mathbf{r}|} \mathrm{e}^{\mathrm{i}\mathbf{r}\mathbf{Q}} = \frac{4\pi}{\alpha^2 + \mathbf{Q}^2} \,, \tag{1.156}$$

where the divergence for $\mathbf{Q} \to 0$ and $\alpha \to 0$ indicates the long range nature of the interaction. Inspired by this observation we investigate the lattice interaction in the limit $\mathbf{Q} \to 0$ via Taylor expansion

$$\begin{aligned}\sum_{\mathbf{d}\neq\mathbf{0}} \frac{\mathrm{e}^{-\alpha|\mathbf{d}|}}{|\mathbf{d}|} \mathrm{e}^{\mathrm{i}\mathbf{d}\mathbf{Q}} &\approx \sum_{\mathbf{d}\neq\mathbf{0}} \frac{\mathrm{e}^{-\alpha|\mathbf{d}|}}{|\mathbf{d}|} \left(1 + \mathrm{i}|\mathbf{d}||\mathbf{Q}|\cos\Theta_{\mathbf{d}\mathbf{Q}}\right) = \sum_{\mathbf{d}\neq\mathbf{0}} \frac{\mathrm{e}^{-\alpha|\mathbf{d}|}}{|\mathbf{d}|} + \mathrm{i}|\mathbf{Q}| \sum_{\mathbf{d}\neq\mathbf{0}} \mathrm{e}^{-\alpha|\mathbf{d}|}\cos\Theta_{\mathbf{d}\mathbf{Q}} \\ &\approx \frac{2\pi}{\alpha} + O(|\mathbf{Q}|) + O(|\mathbf{Q}|\alpha)\end{aligned} \tag{1.157}$$

and find a similar divergence for the true Coulomb case $\alpha \to 0$. Due to the periodicity similar divergences appear for all transfer momenta with $\mathbf{Qd} = 2\pi$ of which only a single one is included in the first Brillouin zone used for integration. We will come back to this divergence in the next section.

Naively one would simply read of

$$V_{\eta\eta',ij}(\mathbf{Q}) = \delta_{\eta 0}\delta_{\eta\eta'}\delta_{i0}\delta_{ij}\sum_{\mathbf{d}\neq\mathbf{0}}\frac{\mathrm{e}^{-\alpha|\mathbf{d}|}}{|\mathbf{d}|}\mathrm{e}^{\mathrm{i}\mathbf{dQ}}\,, \tag{1.158}$$

from Equation 1.155 where

$$\begin{aligned}\phi_{i=0}(\mathbf{k}) &= 1\\ \sigma^{\eta=0}_{\sigma_0\sigma_2} &= \delta_{\sigma_0\sigma_2}\end{aligned} \tag{1.159}$$

as previously and we omit the index m due to the absent residual degrees of freedom. Unfortunately the situation is complicated due to the presence of the exchange interaction terms *i.e.*, [] the antisymmetry constraints on V. Clearly we can write

$$H_I = -\sum_{\{\mathbf{k}_i\}}\delta(\mathbf{k}_0+\mathbf{k}_1-\mathbf{k}_2-\mathbf{k}_3)\sum_{\mathbf{d}\neq\mathbf{0}}\frac{\mathrm{e}^{-\alpha|\mathbf{d}|}}{|\mathbf{d}|}\mathrm{e}^{\mathrm{i}\mathbf{d}(\mathbf{k}_1-\mathbf{k}_2)}\sum_{\{\sigma_i\}}\delta_{\sigma_0\sigma_3}\delta_{\sigma_1\sigma_2}c^\dagger_{\sigma_2,\mathbf{k}_2}c^\dagger_{\sigma_3,\mathbf{k}_3}c_{\sigma_1,\mathbf{k}_1}c_{\sigma_0,\mathbf{k}_0}\,, \tag{1.160}$$

but it is non-trivial to make the connection to Equation 1.153 here. Using momentum conservation and the completeness relation of the Pauli matrices

$$\sum_\eta \sigma^\eta_{\sigma_0\sigma_2}\sigma^\eta_{\sigma_1\sigma_3} = 2\delta_{\sigma_0\sigma_3}\delta_{\sigma_1\sigma_2} \tag{1.161}$$

we find

$$H_I = -\sum_{\{\mathbf{k}_i\}}\delta(\mathbf{k}_0+\mathbf{k}_1-\mathbf{k}_2-\mathbf{k}_3)\sum_{\mathbf{d}\neq\mathbf{0}}\frac{\mathrm{e}^{-\alpha|\mathbf{d}|}}{|\mathbf{d}|}\mathrm{e}^{\mathrm{i}\mathbf{d}(\mathbf{k}_3-\mathbf{k}_0)}\frac{1}{2}\sum_\eta\sum_{\{\sigma_i\}}\sigma^\eta_{\sigma_0\sigma_2}\sigma^\eta_{\sigma_1\sigma_3}c^\dagger_{\sigma_2,\mathbf{k}_2}c^\dagger_{\sigma_3,\mathbf{k}_3}c_{\sigma_1,\mathbf{k}_1}c_{\sigma_0,\mathbf{k}_0}\,. \tag{1.162}$$

In this representation, the matrix elements do not depend on the transfer momentum $\mathbf{k}_0 - \mathbf{k}_2$. Instead, the momentum dependence has been transferred into the form factors. If we define an infinite set of form factors

$$\phi_i(\mathbf{k}) = \mathrm{e}^{\mathrm{i}\mathbf{d}_i\mathbf{k}}\,, \tag{1.163}$$

which arises due to the long range nature of the assumed interaction, we can write

$$H_I = -\sum_{\{\mathbf{k}_i\}} \delta(\mathbf{k}_0 + \mathbf{k}_1 - \mathbf{k}_2 - \mathbf{k}_3) \sum_{i\neq 0} \frac{\mathrm{e}^{-\alpha|\mathbf{d}_i|}}{|\mathbf{d}_i|} \phi_i^*(\mathbf{k}_0)\phi_i(\mathbf{k}_3) \frac{1}{2} \sum_{\eta} \sum_{\{\sigma_i\}} \sigma^{\eta}_{\sigma_0\sigma_2} \sigma^{\eta}_{\sigma_1\sigma_3} c^{\dagger}_{\sigma_2,\mathbf{k}_2} c^{\dagger}_{\sigma_3,\mathbf{k}_3} c_{\sigma_1,\mathbf{k}_1} c_{\sigma_0,\mathbf{k}_0} \,. \tag{1.164}$$

From this equation we can would deduce

$$V_{\eta\eta',ij}(\mathbf{Q}) = -\frac{1}{2}\delta_{\eta\eta'}(1-\delta_{i0})\delta_{ij}\frac{\mathrm{e}^{-\alpha|\mathbf{d}_i|}}{|\mathbf{d}_i|} \,. \tag{1.165}$$

While Equation 1.158 and Equation 1.165 are seemingly at odds with each other, their combination

$$V_{\eta\eta',ij}(\mathbf{Q}) = \delta_{\eta\eta'}\delta_{ij}\Big(\delta_{\eta 0}\delta_{i0}\sum_{k\neq 0}\frac{\mathrm{e}^{-\alpha|\mathbf{d}_k|}}{|\mathbf{d}_k|}\mathrm{e}^{\mathrm{i}\mathbf{d}_k\mathbf{Q}} - \frac{1}{2}(1-\delta_{i0})\frac{\mathrm{e}^{-\alpha|\mathbf{d}_i|}}{|\mathbf{d}_i|}\Big) \tag{1.166}$$

results in a manifestly antisymmetric interaction tensor

$$\begin{aligned} U_{\{a_i\}}(\{\mathbf{k}_i\}) &= \delta(\mathbf{k}_0 + \mathbf{k}_1 - \mathbf{k}_2 - \mathbf{k}_3) \sum_{i,j} \sum_{\eta\eta',mm'} V_{\eta\eta',mm',ij}(\mathbf{k}_0 - \mathbf{k}_2) O^{m}_{o_0o_2} O^{m'}_{o_1o_3} \sigma^{\eta}_{\sigma_0\sigma_2} \sigma^{\eta'}_{\sigma_1\sigma_3} \phi_i^*(\mathbf{k}_0)\phi_j(\mathbf{k}_3) \\ &= -U_{a_1a_0a_2a_3}(\mathbf{k}_1,\mathbf{k}_0,\mathbf{k}_2,\mathbf{k}_3) \,. \end{aligned} \tag{1.167}$$

Since this antisymmetry is not obvious from the result we will also show the result for momentum independent (onsite) interactions

$$\begin{aligned} U_{\{a_i\}}(\{\mathbf{k}_i\}) &= U\Big(\delta_{\sigma_0\sigma_2}\delta_{\sigma_1\sigma_3} - \delta_{\sigma_1\sigma_2}\delta_{\sigma_0\sigma_3}\Big)\delta(\mathbf{k}_0 + \mathbf{k}_1 - \mathbf{k}_2 - \mathbf{k}_3) \\ &= U\sum_{\eta\eta'}\Big(\delta_{\eta\eta'}\delta_{\eta_0} - \frac{1}{2}\delta_{\eta\eta'}\Big)\sigma^{\eta}_{\sigma_0\sigma_2}\sigma^{\eta'}_{\sigma_1\sigma_3}\delta(\mathbf{k}_0 + \mathbf{k}_1 - \mathbf{k}_2 - \mathbf{k}_3) \\ V_{\eta\eta',ij}(\mathbf{Q}) &= U\delta_{\eta\eta'}\delta_{ij}\delta_{i0}\Big(\delta_{\eta 0} - \frac{1}{2}\Big) = U\frac{1}{2}\delta_{\eta\eta'}\delta_{ij}\delta_{i0}\Big(\delta_{\eta 0} - \delta_{\eta,\{x,y,z\}}\Big) \,. \end{aligned} \tag{1.168}$$

This case does not necessitate the introduction of form factor dependencies due to the locality of the interaction, while the antisymmetry requirement still results in a non-trivial form for V. We have used the identify $1 = \delta_{\eta 0} + \delta_{\eta\{x,y,z\}}$ in order to simplify the expression. With the same replacement we can separate our result for the long range interaction into a spin and charge component

$$\begin{aligned} V_{\eta\eta',ij}(\mathbf{Q}) &= \frac{1}{2}\delta_{\eta\eta'}\delta_{ij}\Big\{\delta_{\eta 0}\Big(\delta_{i0}\sum_{k\neq 0}2C_k - (1-\delta_{i0})C_i\Big) - \delta_{\eta\{x,y,z\}}(1-\delta_{i0})C_i\Big\} \\ C_i &= \frac{\mathrm{e}^{-\alpha|\mathbf{d}_i|}}{|\mathbf{d}_i|}\mathrm{e}^{\mathrm{i}\mathbf{d}_i\mathbf{Q}} \end{aligned} \tag{1.169}$$

1.4.3 Susceptibilities in interacting theories

In Section 1.4.1, we have seen how to calculate the bare susceptibility of our Hubbard type models for generic two-particle operators. Here we will use the separation of H_I in terms of these operators to motivate the calculation of these susceptibilities for an interacting model in the random-phase approximation.

Using the notation from above we recall that

$$\chi_{A,B} = -\beta \sum_{\{\mathbf{i}\}} B_{1,2} A_{0,3} \delta_{\omega_{n_0}\omega_{n_3}} \left\langle \bar{\psi}_{\mathbf{2}} \psi_{\mathbf{1}} \bar{\psi}_{\mathbf{3}} \psi_{\mathbf{0}} \right\rangle_{\text{conn}} \mathrm{e}^{\mathrm{i}\omega_{n_2}\delta} \mathrm{e}^{\mathrm{i}\omega_{n_3}\delta}, \tag{1.170}$$

and proceed with a perturbative expansion of the expectation value in terms of the interacting part of the action S_I. Some but certainly not all diagrams of up to order $(S_I)^2$ are given by

$\chi_{AB}(\mathbf{q}) =$

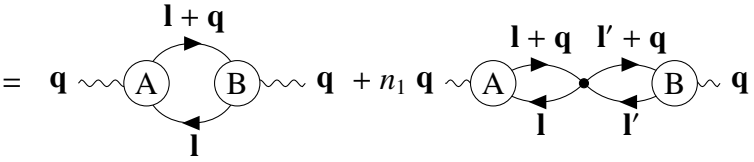

(1.171)

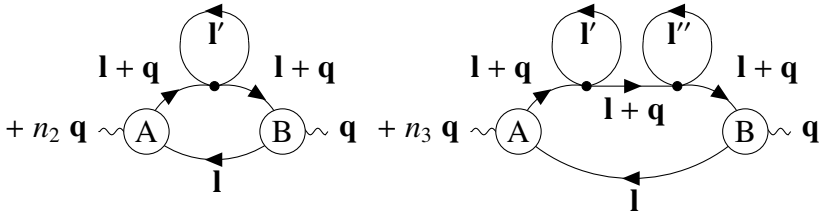

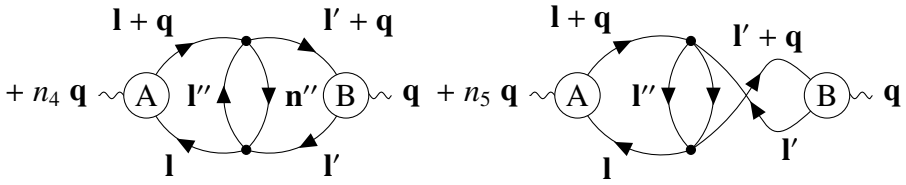

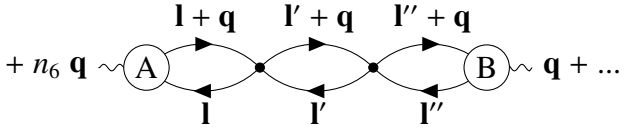

where we have indicated the different symmetry prefactors via n_i. With each added interaction vertex, the number of loop integrations grows by one. We have denoted each momentum to be integrated over by $\mathbf{l}$, $\mathbf{l}'$ or $\mathbf{l}''$ while other momenta like $\mathbf{l}+\mathbf{q}$ or $\mathbf{n}''$ are constrained by momentum conservation.

The first term in the expansion is the only term occurring in a non-interacting theory and was already calculated explicitly in Section 1.4.1. Interestingly, the following diagram with prefactor n_1 has a strikingly similar momentum structure and the integrals over multi indices $\mathbf{l}$ and $\mathbf{l}'$ are only coupled by the interaction term. The two diagrams with prefactor n_2 and n_3 can be reproduced from the first diagram with a modified propagator line and are conventionally called self energy diagrams. While these diagrams are omitted in the susceptibility calculation on RPA level they can be included in frequency dependent fluctuation exchange (FLEX) calculations, where the frequency dependent self-energy is included explicitly. In the third line, we see that diagrams with a more complicated topology can introduce highly linked momentum integrals. For example $\mathbf{n}'' = \mathbf{l}'' + \mathbf{l} - \mathbf{l}'$ in order to enforce momentum conservation at each vertex making it impossible to factorize integrations over $\mathbf{l}$, $\mathbf{l}'$ and $\mathbf{l}''$ even for momentum independent interactions. Nevertheless, these types of diagrams are implicitly included in functional renormalization group (fRG) calculations via the iterative structure of the functional flow equation. In contrast, the last diagram with symmetry prefactor n_6 can be factorized in equivalent fashion to the diagrams in the first line as we will now see.

Using results obtained during the calculation of the bare susceptibility and some previously established shorthand notation we can calculate the first diagram including an interaction term as

$$\begin{aligned}
\chi^{\text{part}}_{AB}(\mathbf{q}) &= \beta \sum_{\{\mathbf{i}\}} \delta_{\omega_{n_0}\omega_{n_2}} A_{0,2} G_{\mathbf{04}} G_{\mathbf{62}} U_{\mathbf{4576}} G_{\mathbf{73}} G_{\mathbf{15}} B_{1,3} \\
&= \sum_{\{i\}} A_{0,2}\delta_{0,4}\delta_{7,3}\delta_{6,2}\delta_{1,5} L^{\text{PH}}_{\alpha_0\alpha_2}(\mathbf{k}_0, \mathbf{k}_2) U_{\alpha_0\alpha_1\alpha_2\alpha_3}(\{\mathbf{k}_i\}) L^{\text{PH}}_{\alpha_3\alpha_1}(\mathbf{k}_3, \mathbf{k}_1) B_{1,3} \\
&= \sum_{\{\alpha_i\}} \sum_{\mathbf{l},\mathbf{l}'} A_{l+q,l} L^{\text{PH}}_{\alpha_0\alpha_2}(\mathbf{l}+\mathbf{q}, \mathbf{l}) U_{\alpha_0\alpha_1\alpha_2\alpha_3}(\mathbf{l}+\mathbf{q}, \mathbf{l}', \mathbf{l}, \mathbf{l}'+\mathbf{q}) L^{\text{PH}}_{\alpha_3\alpha_1}(\mathbf{l}'+\mathbf{q}, \mathbf{l}') B_{l',l'+q} \,.
\end{aligned} \tag{1.172}$$

Up to this point the calculation is most conveniently performed in band space and similar expressions are readily obtained for all diagrams in Equation 1.171 due to the static nature of the bare interaction. The remaining momentum space integrals, however, take an especially simple structure for this specific diagram. If we insert the D-channel decomposition of the interaction we find

$$\chi^{\text{part}}_{AB}(\mathbf{q}) = \sum_{\{\alpha_i\}} \sum_{\mathbf{l},\mathbf{l}'} \sum_{gg'} A_{l+q,l} L^{\text{PH}}_{\alpha_0\alpha_2}(\mathbf{l}+\mathbf{q}, \mathbf{l}) \phi^*_g(\mathbf{l}) U^{gg'}_{\alpha_0\alpha_1\alpha_2\alpha_3}(\mathbf{q}) \phi^*_{g'}(\mathbf{l}') L^{\text{PH}}_{\alpha_3\alpha_1}(\mathbf{l}'+\mathbf{q}, \mathbf{l}') B_{1,2} \,. \tag{1.173}$$

and realize that the result decouples in $\mathbf{q}$ and into two independent integrals over $\mathbf{l}$ and $\mathbf{l}'$. Finally we transform everything from band space back into orbital space and find

$$\begin{aligned}\chi^{\text{part}}\left(A^{\dagger}_{\eta,m,f}(\mathbf{q}), A_{\eta',m',f'}(\mathbf{q})\right) &= \\ &= \sum_{\{\sigma_i\}}\sum_{\{o_i\}}\sum_{gg'} O^{m}_{o_0o_3}\sigma^{\eta}_{\sigma_0\sigma_3}\aleph^{fg}_{a_0a_7a_4a_3}(\mathbf{q},\mathbf{0})U^{gg'}_{a_4a_5a_7a_6}(\mathbf{q})\aleph^{g'f'}_{a_6a_1a_2a_5}(\mathbf{q},\mathbf{0})O^{m'}_{o_1o_2}\sigma^{\eta'}_{\sigma_1\sigma_2}\,.\end{aligned} \tag{1.174}$$

An equivalent calculation can be performed for the last diagram shown in Equation 1.171 and for the equivalent diagram at all orders in U. These diagrams are the only diagrams considered in the RPA and we will from now on refer to them as RPA diagrams. Similar structures in the loop can most likely be employed for some self-energy diagrams, while the diagrams with symmetry factors n_4 and n_5 can not be factored into independent integrals and the double momentum space integrals have to be carried out explicitly.

Clearly the RPA diagrams turn out to be easily calculated due to their simple analytic structure. We introduce yet another set of multi-indices $\mathcal{A}_0 = (f_0, a_0, b_0$ for notational convenience and thereby rewrite the "central" part of the previous equation as a matrix product

$$\aleph^{f_0f_1}_{a_0a_1b_1b_0}(\mathbf{q})U^{f_1f_2}_{b_1b_2a_1a_2}(\mathbf{q})\aleph^{f_2f_3}_{a_2a_3b_3b_2}(\mathbf{q}) = \aleph\mathcal{A}_0\mathcal{A}_1(\mathbf{q})U\mathcal{A}_1\mathcal{A}_2(\mathbf{q})\aleph\mathcal{A}_2\mathcal{A}_3(\mathbf{q})\,. \tag{1.175}$$

Each $\mathcal{A}_i$ can be viewed as a PH pair and $\aleph_{\mathcal{AB}}$ can be interpreted as coherent particle-hole propagation in the system while $U_{\mathcal{AB}}$ describes particle-hole scattering at the interaction vertex. All RPA type diagrams can be written in terms of these matrix products. We therefore consider the infinite series

$$\begin{aligned}\aleph^{\text{RPA}}_{\mathcal{A}_0\mathcal{A}_1}(\mathbf{q}) = \aleph_{\mathcal{A}_0\mathcal{A}_1}(\mathbf{q}) &- \aleph_{\mathcal{A}_0\mathcal{B}_1}(\mathbf{q})U_{\mathcal{B}_1\mathcal{B}_2}(\mathbf{q})\aleph_{\mathcal{B}_2\mathcal{A}_1}(\mathbf{q}) \\ &+ \aleph_{\mathcal{A}_0\mathcal{B}_1}(\mathbf{q})U_{\mathcal{B}_1\mathcal{B}_2}(\mathbf{q})\aleph_{\mathcal{B}_2\mathcal{B}_3}(\mathbf{q})U_{\mathcal{B}_3\mathcal{B}_4}(\mathbf{q})\aleph_{\mathcal{B}_4\mathcal{A}_1}(\mathbf{q}) \\ &- \aleph_{\mathcal{A}_0\mathcal{B}_1}(\mathbf{q})U_{\mathcal{B}_1\mathcal{B}_2}(\mathbf{q})\aleph_{\mathcal{B}_2\mathcal{B}_3}(\mathbf{q})U_{\mathcal{B}_3\mathcal{B}_4}(\mathbf{q})\ldots\,,\end{aligned} \tag{1.176}$$

with all repeated multi-indices denoting implicit summation over them. Note that the alternating sign originates from the varying definition of the generalized susceptibility Equation 1.103 compared to common RPA convention Equation 1.99 [79]. This can be simplified to a recursive expression

$$\aleph^{\text{RPA}}_{\mathcal{A}_0\mathcal{A}_1}(\mathbf{q}) = \aleph_{\mathcal{A}_0\mathcal{A}_1}(\mathbf{q}) - \aleph_{\mathcal{A}_0\mathcal{B}_1}(\mathbf{q})U_{\mathcal{B}_1\mathcal{B}_2}(\mathbf{q})\aleph^{\text{RPA}}_{\mathcal{B}_2\mathcal{A}_1}(\mathbf{q})\,, \tag{1.177}$$

which is commonly solved by a resummation of the geometric series

$$\aleph^{\text{RPA}}_{\mathcal{A}_0\mathcal{A}_1}(\mathbf{q}) = \frac{\aleph_{\mathcal{B}_2\mathcal{A}_1}(\mathbf{q})}{\mathbf{1} + \aleph_{\mathcal{A}_0\mathcal{B}_1}(\mathbf{q})U_{\mathcal{B}_1\mathcal{B}_2}(\mathbf{q})\,.} \tag{1.178}$$

The fraction implies a matrix inversion of the denominator. Note that inserting the result back into Equation 1.108 and Equation 1.109 yields the effective interaction in the fluctuation exchange approximation [47, 72].

In order to motivate the importance of RPA type diagrams over others, we will now attempt to classify the importance of diagrams in the interacting theory in analogy to a justification of the RPA given by Bruus and Flensberg in [93]. We start our reasoning from the assumption of weak enough electron-electron interactions such that $U/W < 1$. Since $\aleph \propto G_{\mathbf{01}} \propto W^{-1}$, it is clear that diagrams with a lower number of interaction vertices will contribute less to the overall susceptibility in Equation 1.171 in this limit. In a next step we try to compare the relevance of different diagrams in the same order of interaction strength. While this is generically not possible prior to an actual calculation of the diagrams, we can use the fact that $V(\mathbf{Q})$ diverges for small transfer momenta $\mathbf{Q}$ in the case of the long-range interactions introduced in Section 1.4.2 to craft an argument. For $\mathbf{Q} \to \mathbf{0}$, an RPA diagram of order n will diverge as α^{-n} while any diagram of non-RPA type will at least involve one interaction $V(\mathbf{p} \neq \mathbf{Q})$, depending on a momentum $\mathbf{p}$ that is integrated out. The singularity at $\mathbf{p} \to \mathbf{0}$ is of measure zero in these integrals, and the diagram will diverge more weakly with at worst α^{n-1}. In conclusion, the long-range singularity of the Coulomb potential provides one avenue to justify a restriction to the RPA diagrams. Following this argument, the PH susceptibility of a given system diverges at each order in perturbation theory for a sufficiently long range interaction. Coincidentally, the geometric series of RPA type diagrams to all order n, cures this divergence as one can easily from Equation 1.178. This fact can be understood as a self-screening of the system that is facilitated by PH fluctuations.

For lattice systems, a similar argument for the importance of RPA diagrams could be made by assuming the existence of a perfect nesting vector $\mathbf{Q}$ driving a divergence in the bare susceptibility $\aleph_0$ at this momentum and at zero temperature. Clearly this situation can be analysed analogously and the RPA diagrams are easily identified as the most divergent diagrams at each order in U/W. The RPA is therefore an especially suitable approximation close to a PH instability [107]. Despite these reasons, the RPA remains a crude approximation for generic Hubbard type Hamiltonians and is most easily justified by numerical applicability and a posteriori comparison to more sophisticated methods like the fRG.

1.4.4 RPA analysis of unconventional Fermi surface instabilities

We have previously seen in Sect. 1.3, that Hubbard type models become superconducting for low enough temperatures due to the presence of an effectively attractive interaction channel and the diverging PP diagram [5]. The two most relevant assumptions in our argument were the absence of fine-tuning and an infinitesimal coupling strength. This allowed us to perform calculations in one

loop perturbation theory and to neglect the possibility for growing couplings in the PH channel. Accordingly, lifting these assumptions necessitates a reconsideration of the possibilities for spontaneous symmetry breaking in our models. One possibility for treating PH and PP instabilities on equal footing is to calculate a one loop renormalization group flow starting from the full bandwidth W instead of the small intermediate scale Ω_0 introduced previously [73, 108–113]. Such a calculation can be either done analytically by singling out a small number of physically motivated coupling functions [76, 114–117] or numerically via a discretization of the vertex function, an approach known as functional renormalization group (fRG) [82, 118–123].

Here we will pursue an alternative, numerically much less demanding, approach. We have seen that $\aleph^{\mathrm{RPA}}$ is associated to our systems linear response functions with respect to an exhaustive set of PH perturbation operators and from Equation 1.178 it is clear that $\aleph^{\mathrm{RPA}}$ diverges if

1. the nominator diverges, a scenario that is associated with small temperatures and fine tuned Fermi surfaces with perfect nesting.

2. the denominator vanishes *i.e.*, the matrix $\aleph_{\mathcal{A}_0\mathcal{B}_1}(\mathbf{q})U_{\mathcal{B}_1\mathcal{B}_2}(\mathbf{q})$ has an eigenvalue $\lambda = -1$. This can be seen as a generalized Stoner criterion for PH instabilities.

A diverging susceptibility indicates an instability of the system with respect to this perturbation since infinitesimal fluctuations are sufficient to induce a finite response of the system. In this scenario our perturbative treatment of the interaction certainly breaks down. Fortunately, the diverging susceptibility of some operator A already provides us with an ansatz for a possible mean-field expansion of the interaction: $\langle A \rangle$. In order to obtain the ground state of the system one can now perform a self consistent calculation in the mean-field approximation. This is similar to the fRG, where the numerical evaluation of the RG flow may lead to a divergence in the (cutoff dependent) vertex function. At this point one has to stop the flow due to a breakdown of the one-loop expansion of the flow-equation and also resorts to a renormalized mean-field analysis that is motivated by the diverging coupling function.

In contrast to the fRG, however, our RPA analysis up to this point does not include any feedback between PP and PH fluctuations. While we accept this constraint for the analysis of particle-hole like instabilities, bare repulsive interactions will not induce a superconducting instability in the PP channel. We have seen this in our analysis of the wcRG and in particular from the RG equation in the PP channel for $\mathbf{Q} = \mathbf{0}$ (the Cooper channel) given by Equation 1.110. Repulsive (positive) couplings in the Cooper channel renormalize to zero and only attractive channels flow to strong coupling.

As stated in Sect. 1.3, the expansion of the Cooper pair scattering vertex up to second order in the bare interaction Equation 1.86 is justified by an appropriate choice of the interaction scale

U and introduction of a cutoff Ω_0 in the wcRG. In the RPA, this cutoff may be given by a finite temperature in the evaluation of $\aleph$ or neglected as one disregards the PP diagram. The requirement of a small enough interaction scale is fulfilled in the RPA approximation if not only U but also $\aleph^{\mathrm{RPA}}$ are sufficiently small to allow for a truncation of the perturbative expansion of Equation 1.86.

Because we are interested only in attractive interactions in the Cooper channel, it is sufficient to perform calculations for the PH diagrams and neglect the PP diagram as discussed in Sect. 1.3. The remaining contributions of the one-loop expansion U^{PH} and U^{cPH} give rise to longitudinal and exchange (transverse) fluctuations [124] respectively and describe the lowest order contributions to superconducting pairing from PH (spin or charge) fluctuations. In this way, the expansion given in Equation 1.86 forms the basis of RPA and FLEX calculations [24, 79, 125–128]. The key difference between wcRG and RPA is the inclusion of higher order diagrams in the evaluation of the relevant PH fluctuations. The effective Cooper pair interaction

$$U^{\mathrm{eff}}_{\{\alpha_i\}}(\mathbf{k}_F, \mathbf{q}_F) = U^{\mathrm{PH}}_{\{\alpha_i\}}(\mathbf{k}_F, \mathbf{q}_F) - U^{\mathrm{cPH}}_{\{\alpha_i\}}(\mathbf{k}_F, \mathbf{q}_F) \tag{1.179}$$

on RPA level is given by Equation 1.108 and Equation 1.109 (for U^{PH} and U^{cPH}) but inserting $\aleph^{\mathrm{RPA}}$ instead of $\aleph^0$. Since our formalism is set up to treat generic Hamiltonians, where the spin-degree of freedom does not decouple from other dynamical degrees of freedom, these formulas only vaguely resemble conventional expressions from Refs. [24, 47, 79] and is more closely related to recent results for the Rashba Hubbard model [32].

Specifically, for models with spin-rotation (SU(2)) symmetry, the bare susceptibility $\aleph_0 \propto \delta_{\eta\eta'}$ is identical for charge $\eta = 0$ and spin-like $\eta = 1, 2, 3 = x, y, z$ PH excitations. Combined with the results from Equation 1.168 and Equation 1.169 we see that the interacting susceptibility on RPA level will separate into a charge component

$$\chi^{\mathrm{RPA}}_C(\mathbf{Q}) \propto \chi\Big(A^\dagger_{\eta=0,m,f=0}(\mathbf{q}), A_{\eta=0,m',f'=0}(\mathbf{q})\Big) \tag{1.180}$$

that differs from the spin component

$$\chi^{\mathrm{RPA}}_S(\mathbf{Q}) \propto \chi\Big(A^\dagger_{\eta=\{x,y,z\},m,f=0}(\mathbf{q}), A_{\eta=\{x,y,z\},m',f'=0}(\mathbf{q})\Big). \tag{1.181}$$

The restriction to the constant form factor $f = f' = 0$ is also common for RPA calculations. Additionally, the SU(2) symmetry facilitates a separation of the Cooper pair scattering amplitudes into singlet and triplet channel. Using these identifications, our formulas reduce to the conventional expressions for the RPA and FLEX approximation [129].

In the general case, where we consider non-SU2 symmetric models with multiple orbital / sublattice degrees of freedom and non-trivial form factors, the distinction between charge and spin

susceptibility is not sufficient. Fortunately, a more general framework for the analysis of diverging susceptibility matrices exists in the form of a simple eigenmode decomposition. This allows us to identify the linear combination of particle-hole operators A with the largest susceptibility and therefore the leading instability of the system.

Here, a connection with self-consistent mean-field approaches to the solution of the interacting electron problem is natural. In Appendix B, we provide a self-contained derivation for such an approach to superconductivity in spin-orbit coupled systems. Note that the final result for the linearized gap equation

$$\Delta_i = U^{\text{eff}}_{ij} L^{\text{PP}}_{jk} \Delta_k \,, \tag{1.182}$$

can be easily converted into a criterion similar to the divergence of the RPA susceptibility

$$\begin{aligned} L^{\text{PP}}_{li}\Delta_i &= L^{\text{PP}}_{li} U^{\text{eff}}_{ij} L^{\text{PP}}_{jk} \Delta_k \\ 0 &= (\mathbb{1}_{lj} - L^{\text{PP}}_{li} U^{\text{eff}}_{ij}) L^{\text{PP}}_{jk} \Delta_k \,. \end{aligned} \tag{1.183}$$

In other words, diverging susceptibilities imply spontaneous symmetry breaking via the emergence of finite expectation values. The eigenmodes of the susceptibility tensor may provide insight into the structure of this expectation value, priming a self-consistent mean field ansatz.

1.5 Comparison of the RPA with wcRG and fRG

To round out this chapter on methodological approaches to unconventional superconductivity, we will now focus on similarities and differences between the wcRG and RPA. This comparison would not be complete without a discussion of the functional renormalization group (fRG) as both the wcRG and RPA can be understood as different simplifications of it.

Starting from a unified description for a systems action S^Λ at high $\Lambda \to \infty$ and low $\Lambda \to 0$ energy scales, one can derive an exact renormalization group (RG) flow equation that connects actions at high scales to ones at lower scales [82, 112, 122, 130]. The microscopic model given by Eqns. 1.1 and 1.6 defines the initial conditions for this flow equation. Similarly to the RPA and wcRG the evolution of S_Λ to lower energy scales yields a low-energy effective model that only accounts for modes close to the Fermi level, while the influence of higher energy modes are absorbed into the renormalized effective interaction terms. A key difference to the wcRG is the numerical evaluation of the RG flow.

The exact flow equation for the action can be rephrased an infinite set of *coupled*flow-equations for two-particle irreducible vertex functions. Then, the flow of each n-particle vertex function is connected to the $n+1$-particle vertex and an exact solution result for $S_{\Lambda\to 0}$ would require the

tracking of all two-particle irreducible vertex functions. The common solution of this problem lies in lies in a truncation of the flow equation *i.e.*, one neglects the effect of three-particle and higher order vertex functions. Further common simplifications that reduce computational cost are additionally neglecting changes of the one-particle vertex function (self energy corrections) and fixing the frequency dependence of the two-particle vertex to the static part. All of these approximations were justified in numerous places in the literature (see [82, 122] and references therein) and do not affect the methods capability for resolving the interplay between particle-hole (*e.g.* antiferromagnetic) and particle-particle (*e.g.* superconducting) fluctuations. The resulting integro-differential equation for the effective two-particle vertex has striking similarities to the perturbative expansion in Equation 1.83. The key difference is that the left hand side is replaced with a derivative of the scale dependent two-particle vertex U^Λ with respect to Λ while the Greens-functions on the right hand side are partially replaced by their scale derivatives. The differential equation for $U^\Lambda_{\{a_i\}}(\mathbf{k}_0, \mathbf{k}_1, \mathbf{k}_2)$ is then solved via standard techniques.

Analogous to the calculation of RPA susceptibilities at low temperatures, the vertex elements of U^Λ will generically grow during the flow to an effective theory. At some point, this results in the breakdown of the truncation conditions and the flow has to be stopped. A subsequent mean-field decomposition of the effective interaction allows the identification of a clear instability. Similar to the wcRG and RPA such an analysis goes beyond a simple treatment of the initial model on mean-field level, as most order parameter fluctuations at energies $> \Lambda$ are included in the analysis.

More specifically, the fRG constitutes the most rigorous perturbative treatment of such fluctuation effects in the limit of weak coupling when compared to the wcRG and RPA approaches. Similar to the analytical starting point of the wcRG, the fRG treats all two-particle instability channels on equal footing. Expanding on the notion of analytical rigour and in a similar spirit to the RPA, one may however allow for finite interaction scales, allowing approximate nesting vectors to drive the system under consideration into a magnetically or charge-ordered phase. The main advantage of the fRG lies in its iterative solution structure, furnishing a generic mixture of the particle-particle and particle-hole channels. While our RPA and wcRG approaches outlined above analyze the particle-hole renormalized interactions in the particle-particle (PP) channel, the fRG tracks the evolution of the full interaction vertex during the whole flow. Consequently, cross-channel contributions are naturally included in every single step of the differential equation's integration.

This advantage of the fRG is simultaneously it's biggest drawback. The treatment of magnetic, charge and PP interaction channels in an unbiased way necessitates the storage of the full two-particle vertex and it's three independent momentum dependencies. Using a naive momentum space discretization with n_k different momenta and considering a system with n_a degrees of freedom per unit cell [no. sublattices $\times$ no. orbitals ($\times$ 2 for spin-orbit coupled systems)] this function

scales as $n_k^3 \times n_a^4$. Assuming storage of $V_{\{a_i\}}(\{\mathbf{k}_i\})$ in terms of double precision complex floating point numbers a typical size a 3 band model in two-spatial dimensions without spin-orbit coupling would be $n_k = 40^2$, $n_a = 3$ and the size of V would be $\approx 5.3\,\mathrm{TB}$, making such calculations prohibitive without further approximations. One such approximation is given by the truncated-unity (TU) formulation of the fRG [123], which heavily inspired our approach to the treatment of bare long-range interactions in the wcRG and RPA. It is important to note that the expansion of the two-particle vertex in terms of formfactors, while exact for finite ranged interactions, poses an approximation in the fRG approach. During the flow non-local and highly non-local interactions can be generated, a process which is completely analogous to the generation of long-range Cooper pairing interactions from purley local bare interactions in the wcRG (see Section 1.3). Accordingly, the number of formfactors used for any TU-fRG calculation significantly exceeds the one needed for an exact representation of the bare interaction. Therefore, a limitation to model systems with limited complexity is present for the fRG, even in the TU approximation.

The RPA and wcRG approaches to unconventional superconductivity circumvent this problem by constraining the calculation to one single channel at a time. This allows for a more efficient vertex parametrization due to the limited range of the bare interaction and the constraint to the $\mathbf{Q} = 0$ case for the PP-channel (the Cooper channel). Accordingly, the potential complexity of the model system is enhanced at the cost of a more biased analysis. This bias is exemplified by the potential for fRG to resolve finite $\mathbf{Q}$ instability in the PP channel. Also the RPA allows for particle-hole fluctuations as a driver for Cooper pairing, while the feedback of particle-particle excitations into the magnetic and charge channel is completely neglected. While these omissions constitute a (physically motivated) approximation for the RPA, they are exact constraints on the effective interaction in the limit of vanishing bare interactions [23, 92]. In the limit of vanishing bare interactions $U/W \to 0$ and notwithstanding numerical implementation problems, the wcRG, fRG and RPA are formally equivalent. Under the assumption that spin and charge fluctuations of the unrenormalized electronic system drive phase transitions in the Fermi-liquid, the small set of resummable diagrams included in the RPA poses a sensible restriction and we can expect it to match results from a more involved fRG calculation [24, 125].

In order to properly compare the three methods, another numerical challenge has to be considered: the sharpness of the Fermi surface for zero temperature. On one hand, the introduction of a finite regularization scale Λ in the fRG circumvents the problem at the beginning of the flow. Furthermore, due to the start with a finite interaction scale, the flow is usually terminated before Λ becomes to small to allow for efficient loop integrations. In the RPA one can similarly enhance the ordering tendencies of the system via the introduction of a finite interaction, justifying an artificial temperature regularization to simplify the integration of the particle-hole bubble in Equation 1.103. On the other hand, the vanishing interaction strength constraint of the wcRG

necessitates an evaluation of this integral at zero temperature in order to achieve a conceptually consistent result. Due to this, numerical calculations of the wcRG may be significantly more involved when compared to seemingly similar RPA results for the same system. Such a comparison of the wcRG and RPA via the necessary effort for the loop integration is justified as the necessary matrix operations for the ladder resummation are dwarfed by the integration.

Finally we would like to comment on the feasibility of detailed phase-diagram mappings in all three methods. Changes to the single-particle Hamiltonian H_0, for example in order to compare of different doping levels, necessitate a complete recalculation in all three cases. In contrast, modifications of the interaction Hamiltonian parameters H_I do not alter Equation 1.103 *i.e.*, the results of this calculation may be re-used for scans in *e.g.* the overall interaction strength or different ratios between onsite and nearest-neighbour interactions. Due to this, the computational complexity of phase-diagram scans in the interaction parameters for wcRG and RPA is significantly reduced compared to the fRG as its iterative solution structure does not allow for significant re use of results for different initial conditions.

1.6 Conclusion and Outlook

In the pursuit of an efficient and reliable framework for the analysis of unconventional superconducting instabilities of correlated metals, we have identified the particle-hole bubble as the central quantity. We have unified the formulations of the wcRG and the RPA in terms of this object, which we introduced as the generalized susceptibility χ for local and it's generalization $\aleph$ for non-local interactions.

In combination with the numerical performance optimizations we presented in detail in [72], our work paves the way towards an efficient and reliable numerical toolbox, equipped for the *ab-inito* analysis of unconventional superconducting instabilities in real materials. We envision such a framework to be based on traditional density functional theory calculations, downfolding of the model to a tight-binding Hamiltonian via Wannierization and the presented analysis of its Fermi surface instabilities within the wcRG or RPA.

Future methodological improvements of this work may include the relaxation of various approximations. Clearly, a combination of our results with the inclusion of frequency dependent vertex functions as well as self energy corrections could be a worthwhile pursuit. The resulting framework, commonly known as fluctuation exchange approximation (FLEX) constitutes a conserving approximation and was established as a useful tool for the analysis of various toy-models[131–133]. Fusing it with our results could open up the possibility of studying the interplay of non-local

interactions and self-energy effects in the context of realistic material scenarios. In this context, a connection with dynamical mean field theory (DMFT) approaches may also be fruitful.

Benchmark calculations

Here we investigate the propensity towards unconventional surface superconductivity of the square and triangular Hubbard modes with and without Rashba spin-orbit coupling. Some results of this this part of the thesis have been published in Reference [72].

Benchmark calculations

In this chapter we will discuss the paradigmatic Hubbard model on the square and triangular lattice from a weak coupling perspective. Particularly, we will focus on the superconducting instabilities of these models and the influence of Rashba spin-orbit coupling on them. The square lattice model provides a perfect benchmark case, where our methodology can be compared to related approaches, and is accordingly the first place to establish the capabilities of our framework to include spin-orbit effects.

The Hubbard model on the triangular lattice features a different lattice geometry while avoiding the necessity for a sublattice basis, making it an ideal model to highlight the influence of the model geometry on superconductivity. Additionally the surface of LuPtBi we investigate in the next chapter features a triangular lattice of bismuth atoms.

2.1 SU(2) symmetric Hubbard models

Before concerning ourselves with the complications arising due spin-orbit coupling effects, we study models with an intact spin-rotation symmetry. We restrict our analysis to the simplest case *i.e.*, models with three parameters.

1. The nearest neighbour tunneling amplitude t.
2. A repulsive onsite interaction of strength U.
3. The average number of electrons per unit cell n.

For the lattices with a trivial unit cell considered here, $0 < n < 2$ due to the Pauli principle. We further note, that our methods are limited to a perturbative treatment of these models *i.e.*, $U \ll t$ as discussed in the previous chapter.

The general Hamiltonian describing the models in this section is therefore a particularization of Eqs. 1.1 and 1.6 that can be written as

$$H = t \sum_{\sigma} \sum_{\langle i,j \rangle} c^{\dagger}_{j,\sigma} c_{i,\sigma} - \mu \sum_{\sigma} \sum_{i} c^{\dagger}_{i,\sigma} c_{i,\sigma} + U \sum_{i} c^{\dagger}_{i,\downarrow} c^{\dagger}_{i,\uparrow} c_{i,\uparrow} c_{i,\downarrow} \,. \tag{2.1}$$

The chemical potential μ is chosen such that the groundstate $|0\rangle$ of H (for $U = 0$) yields

$$n = \frac{1}{N} \sum_{\sigma} \sum_{i} \langle 0 | \, c^{\dagger}_{i,\sigma} c_{i,\sigma} \, | 0 \rangle \tag{2.2}$$

for a system with N lattice sites. The operators $c^{\dagger}_{i,\sigma}$ create an electronic state at site i with spin σ.

The spin rotation symmetry of this model is given by the gauge-transformation

$$c^{\dagger}_{i,\sigma} \to \sum_{\sigma'} \mathcal{U}_{\sigma\sigma'} c^{\dagger}_{i,\sigma'} \quad , \quad c_{i,\sigma} \to \sum_{\sigma'} \mathcal{U}^{*}_{\sigma\sigma'} c_{i,\sigma'} \,, \tag{2.3}$$

where $\mathcal{U} \in \mathrm{SU}(2)$ is generated by the Pauli matrices $\boldsymbol{\sigma} = \{\sigma_x, \sigma_y, \sigma_z\}$ such that $\mathcal{U}(\boldsymbol{\Theta}) = \mathrm{e}^{-\mathrm{i}\boldsymbol{\Theta}\boldsymbol{\sigma}}$.

Clearly the model features an additional U(1) gauge-symmetry

$$c^{\dagger}_{i,\sigma} \to \mathrm{e}^{-\mathrm{i}\phi} c^{\dagger}_{i,\sigma} \quad , \quad c_{i,\sigma} \to \mathrm{e}^{+\mathrm{i}\phi} c_{i,\sigma} \,, \tag{2.4}$$

related to the conservation of particle-number. The implications of these symmetries for emergent low-energy effective interactions is discussed in detail in Ref. [120].

Therefore, we will be content with a brief discussion of Equation 2.3's implications for the bare susceptibilities introduced in Section 1.4.1. For the simple Bravais lattice models we discuss here, it is sufficient to discuss the local operators

$$n(\mathbf{Q}) = \sum_{\mathbf{k}} \sum_{\sigma} c^{\dagger}_{\mathbf{k}+\mathbf{Q},\sigma} c_{\mathbf{k},\sigma} \,, \tag{2.5}$$

$$\mathbf{S}(\mathbf{Q}) = \sum_{\mathbf{k}} \sum_{\sigma\sigma'} c^{\dagger}_{\mathbf{k}+\mathbf{Q},\sigma} \boldsymbol{\sigma}_{\sigma\sigma'} c_{\mathbf{k},\sigma'} \tag{2.6}$$

as well as their non-local generalization

$$A_{\eta,f}(\mathbf{Q}) = \sum_{\mathbf{k}} \sum_{\sigma\sigma'} \phi_f(\mathbf{k}) c^{\dagger}_{\mathbf{k}+\mathbf{Q},\sigma} \sigma^{\eta}_{\sigma\sigma'} c_{\mathbf{k},\sigma'} \tag{2.7}$$

discussed in Section 1.4. Due to the local nature of the presently discussed model class, we will refrain from discussing susceptibilities of non-local operators, as their RPA contributions vanish.

To keep notation general we introduce

$$\phi_0(\mathbf{k}) = 1\,, \tag{2.8}$$

a constant formfactor associated with index $f = 0$.

We recall from Equation 1.147 that

$$\chi^0(A^\dagger_{\eta,0}(\mathbf{Q}), A_{\eta',0}(\mathbf{Q}')) = \delta(\mathbf{Q}-\mathbf{Q}')\sum_{\{\sigma_i\}}\sigma^{\eta}_{\sigma_0\sigma_3}\sigma^{\eta'}_{\sigma_1\sigma_2}\aleph^{00}_{\sigma_0\sigma_1\sigma_2\sigma_3}(\mathbf{Q},\mathbf{0}) \tag{2.9}$$

and note that Equation 2.3 implies

$$\aleph^{00}_{\sigma_0\sigma_1\sigma_2\sigma_3}(\mathbf{Q},\mathbf{0}) \propto \delta_{\sigma_0\sigma_2}\delta_{\sigma_1\sigma_3}\,, \tag{2.10}$$

for the bare susceptibility, as the spin degree of freedom is conserved along each propagator line. Straightforward calculation

$$\sum_{\{\sigma_i\}}\sigma^{\eta}_{\sigma_0\sigma_3}\sigma^{\eta'}_{\sigma_1\sigma_2}\delta_{\sigma_0\sigma_2}\delta_{\sigma_1\sigma_3} = \sum_{\sigma_0\sigma_1}\sigma^{\eta}_{\sigma_0\sigma_1}\sigma^{\eta'}_{\sigma_1\sigma_0} = 2\delta^{\eta\eta'} \tag{2.11}$$

yields

$$\chi^0(A^\dagger_{\eta,f}(\mathbf{Q}), A_{\eta',f'}(\mathbf{Q})) \propto \delta_{\eta\eta'}\,. \tag{2.12}$$

As previously (compare Section 1.4.4) discussed, this only holds for the non-interacting susceptibilities and the spin (S) ($\eta = (1,2,3)$) and charge (C) ($\eta = 0$) sectors will split upon including interaction effects into the susceptibility calculation.

Finally, in order to simplify notation for the results presented here, we introduce the shorthand notations

$$\chi^{0,C} = \chi^{0,C}(\mathbf{Q}) = \chi^0(A^\dagger_{0,0}(\mathbf{Q}), A_{0,0}(\mathbf{Q})) \tag{2.13}$$

and

$$\chi^{0,ij} = \chi^{0,ij}(\mathbf{Q}) = \chi^0(A^\dagger_{i,0}(\mathbf{Q}), A_{j,0}(\mathbf{Q})) \tag{2.14}$$

with $i, j \in \{x, y, z\}$. In particular for the case of bare susceptibilities and intact spin-rotation symmetry we have $\chi^{0,C} = \chi^{0,ii} = \chi^0$ for all i. Note that in some figures we further abbreviate $\chi^0 = \chi$.

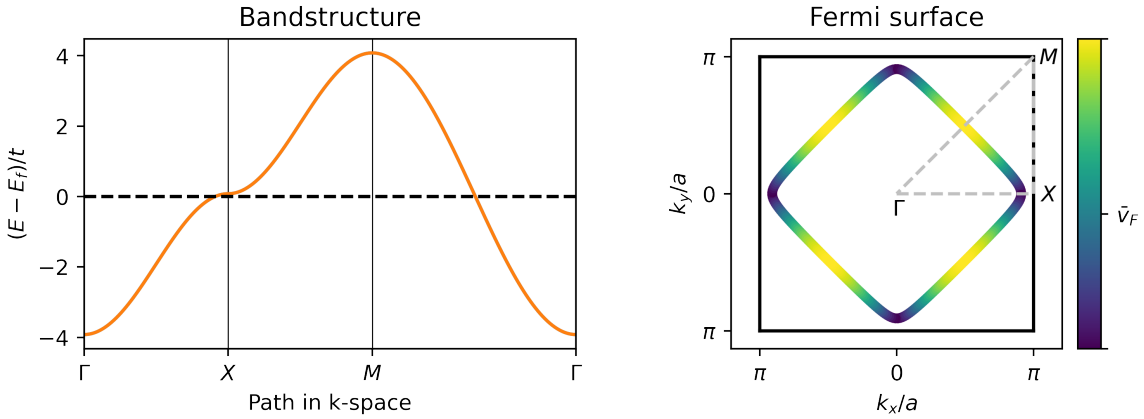

Figure 2.1: We show the energy dispersion of the nearest neighbour square lattice tight-binding Hamiltonian in the left panel. The energy-dispersion is measured relative to the Fermi energy implied by a filling of $n = 0.95$ electrons per unit cell and the Fermi level is indicated by a dashed line. The high symmetry path through momentum space is indicated by a dashed line in the right panel where we also depict the models Fermi surface for $n = 0.95$. The color coding of the Fermi surface illustrates the Fermi velocity $v_F = \partial E/\partial k$ along the Fermi surface and the ticked color corresponds to its reciprocal average $\bar{v}_F$ along the Fermi surface as defined in Equation 1.112.

2.1.1 Square lattice

The square lattice Hubbard model can be physically motivated in various ways, one of which is discussed in the introduction of this thesis. Here we will instead focus on the model as a simple testing ground for the methodological framework introduced in Chapter 1. In particular, the filling fraction n *i.e.*, the average number of electrons per unit cell, is taken as a completely variable input. While this is in stark contrast to most realistic experimental situations (with the notable exception of the recently discovered Moire hetero-structures [56, 60]), it allows us to track the influence of the system's Fermi surface shape on the superconducting pairing. In particular, the model at very low filling fractions maps to the Free electron model with a vanishing influence of the lattice chosen as a ultraviolet-regulator to the parabolic kinetic energy relation.

In the left panel of Figure 2.1, we show the band structure for the Hamiltonian's non-interacting part ($U = 0$). Notice the particle-hole symmetry of the band structure around the van-Hove filling at $\mu = 0$ ($n = 1$), as well as the SU(2) symmetry enforced two-fold degeneracy of the band. Here, we have chosen a slightly lower filling fraction of $n = 0.95$ electrons per unit cell, resulting in the depicted Fermi level and the Fermi surface shown in the adjacent panel. This way, we avoid the ideal nesting (and corresponding divergence in the $T = 0$ particle-hole (PH) susceptibility) at this special point in parameter space. The reciprocal of the Fermi velocity along the Fermi surface

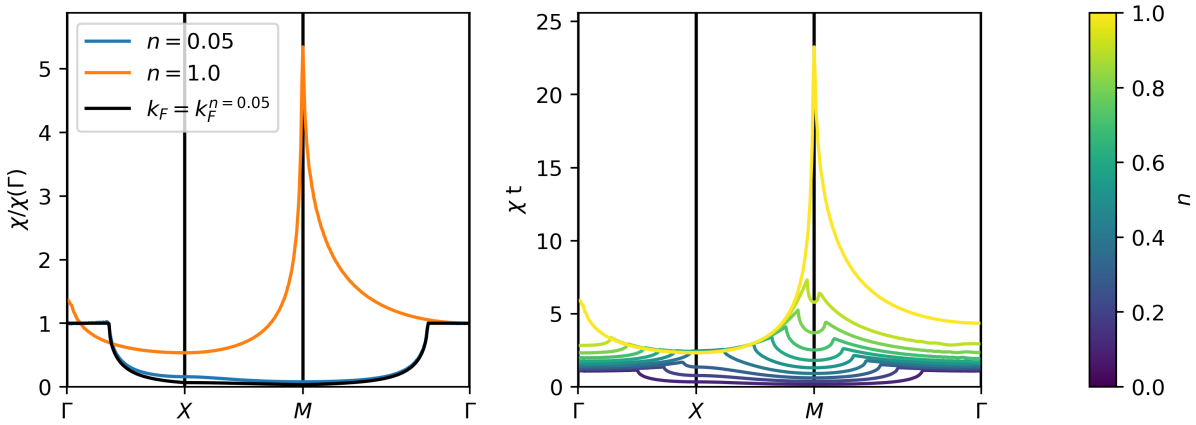

Figure 2.2: Comparison of the square lattice Hubbard model's bare particle hole susceptibility χ_0 for varying filling fractions n. In the left panel, we compare our results to the exact result for the free electron gas for a small filling $n = 0.05$, where lattice effects are negligible due to the mean electron separation exceeding the lattice constant significantly. The right panel shows the continuous evolution of the susceptibility as a function of n. We particularly emphasize the evolution of the maximum from Γ to X and finally M as n increases.

is proportional to the density of states at this point $\rho \propto 1/v_F$ so that the chosen setting is still influenced by the band structures van-Hove singularity at the $\mathbf{k} = X$ point, where $|\nabla_{\mathbf{k}} E|$ vanishes.

The influence of the square lattice geometry on the electronic structure becomes particularly important close to half-filling *i.e.*, $n = 1$. We illustrate this by comparing the PH susceptibility defined in Equation 1.99 for different fillings in Figure 2.2. Starting from a susceptibility profile matching the free electron gas for small filling fractions, one can clearly observe the emergence of additional features when the Fermi momentum approaches the Brillouin zone boundary $2k_F \approx \pi/a$ at $n \approx 0.4$.

We use this setting, where we only vary the filling n as the simplest benchmark scenario for the wcRG and RPA methods. We present the filling dependent phase diagram of this particle hole symmetric model (for the hole doped side $0 < n < 1$ only) in Figure 2.3. Not only do we reproduce the initial results by Raghu *et al.* [23] but also find the small region of spin triplet pairing in the E irreducible representation (Irrep) at $n \approx 0.5$ uncovered in [134]. Our quantitative deviation from the results in [23] by an overall factor has been resolved in private communication with the authors. Note that the emergence of a significant $V_{\text{eff}} t/U^2$ at $n \approx 0.4$ coincides with the introduction of lattice effects in the susceptibility as discussed in the previous paragraph. Following this line of argument, the B_1 / $d_{x^2-y^2}$-wave superconducting phase can be associated with the dominating PH susceptibility in the region around $\mathbf{Q} = (\pi, \pi)$.

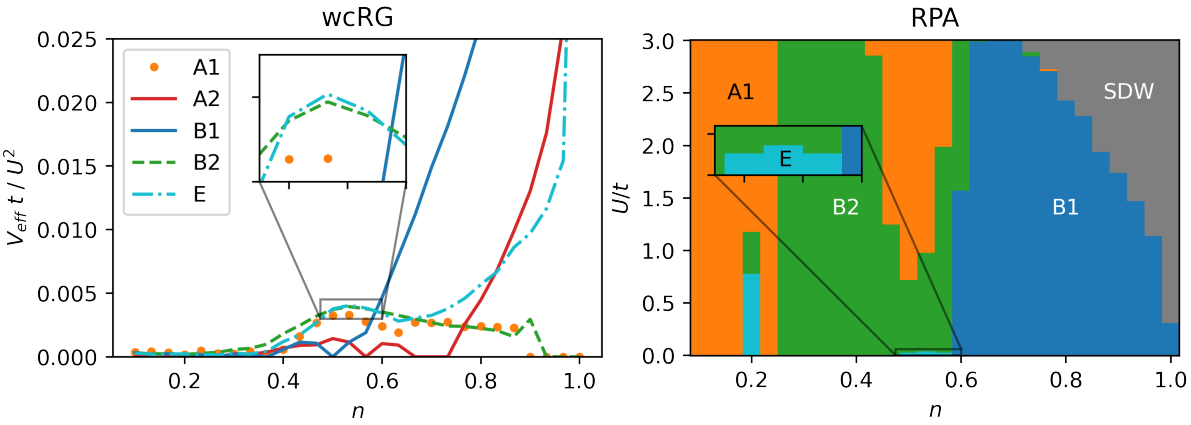

Figure 2.3: Results for the NN ($t' = 0$) Hubbard model on a square lattice. Most of the presented data has been previously reported in [23, 134, 135]. Wolf *et al.* [134] identified a small parameter region where triple superconductivity in the E irreducible representation (Irrep) is favoured in the wcRG. We reproduce their results by discretizing the Fermi surface with 80 distinct points and solving the critical susceptibility integral using an equally spaced grid of (800×800) points in the Brillouin zone. Nevertheless, the instability scales for fillings $n < 0.2$ are indistinguishable within the numerical error. The proximity of different phases close to $n = 0.5$ filling is highlighted in the inset. A generalization of these results for finite interaction strength is obtained in the RPA and shown in the right panel. Based on the bare susceptibility calculations obtained as an intermediate result of the left panel, the RPA resummation with varying onsite interaction reveals slight changes in the ordering of instabilities. In particular, the triplet state is suppressed via the enhanced antiferromagnetic spin fluctuations, giving rise to a double transition into the neighbouring B_2 Irrep and finally the extended s-wave solution A_1 for $U > t$. The inset shows that the E Irrep survives for very small interaction scales, demonstrating the equivalence of RPA and wcRG for infinitesimal interaction scales. We emphasize that our findings coincide with the results of Ref. [135] ($t' = 0$ line in Fig.3). The grey region around half filling signals the onset of a spin-density wave (SDW) instability due to a diverging RPA spin susceptibility as expected from the perfect (π, π) nesting of the FS at $n = 1$.

Using the generalized susceptibilities obtained from these calculations we perform RPA calculations for the same system at varying interaction scales $0 < U < 3t$ without any additional numerical integrations and present our findings in the right panel of Figure 2.3. As expected this does not affect the symmetry of the order parameter in regions of large separation between the eigenvalues of g but introduces qualitative changes at $n \approx 0.5$. In agreement with the results from [135] an extended s-wave A_1 state is favoured in this transition region between the common nearest neighbour B_1 / $d_{x^2-y^2}$-wave state around half filling and the next nearest neighbour B_2 / d_{xy}-wave state for $0.25 < n < 0.45$.

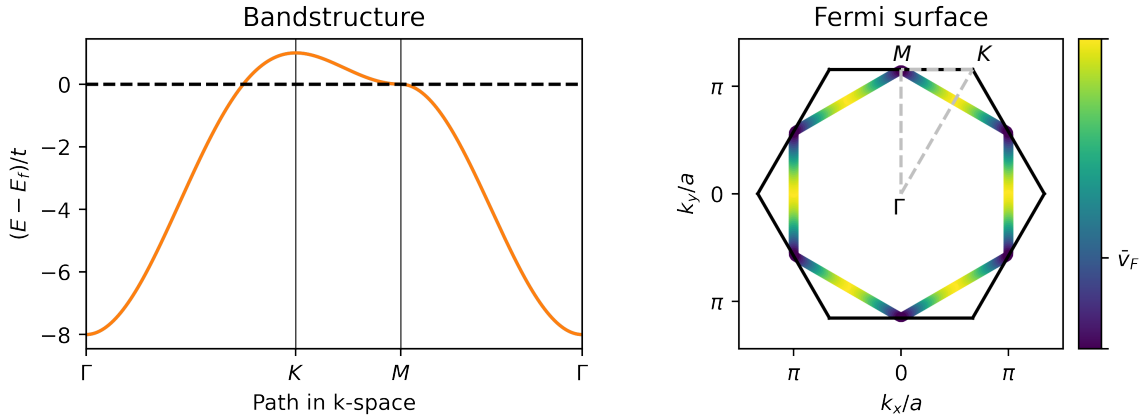

Figure 2.4: We show the energy dispersion of the nearest neighbour triangular lattice tight-binding Hamiltonian in the left panel. The energy-dispersion is measured relative to the Fermi energy implied by a filling of $n = 1.5$ electrons per unit cell and the Fermi level is indicated by a dashed line. The high symmetry path through momentum space is indicated by a dashed line in the right panel where we also depict the models Fermi surface for $n = 1.5$. The color coding of the Fermi surface illustrates the Fermi velocity $v_F = \partial E/\partial k$ along the Fermi surface and the ticked color corresponds to its reciprocal average $\bar{v}_F$ along the Fermi surface as defined in Equation 1.112. In contrast to Figure 2.1, this model does not feature a particle-hole symmetry for any filling fraction.

2.1.2 Triangular lattice

Similar to the previously discussed square lattice Hubbard model, the model on the triangular lattice features a single spin-degenerate bands as it is a pure Bravais lattice. The different space group symmetry of the lattice, therefore manifests itself only in a different point group symmetry: C_{6v} instead of C_{4v} for the square lattice. In Figure 2.4 one can see the appropriate hexagonal Brillouin zone (BZ) with the Fermi surface at van-Hove filling ($n = 1.5$ electrons per unit cell). From the band structure it also becomes clear that the bandstructure does not feature a particle-hole symmetry as expected for a non-bipartite lattice. Another interesting consequence of the hexagonal structure are the different Fermi surface topologies when hole doping or electron doping away from the van-Hove filling. For fillings $n < 1.5$ the Fermi surface is fully connected and shrinks around the Γ point. This finally results in a model that is well approximated by a free electron model with quadratic band dispersion for very small fillings, analogous to the discussion for the square lattice model. In contrast, for $n > 1.5$ the Fermi surface splits into two disconnected segments, conventionally named pockets. Both pockets center around the corners of the hexagon *i.e.*, the K points of the Brillouin zone. While the four corners of the BZ are identical modulo reciprocal lattice translations, this is not the case for the triangular lattice. Here only every second

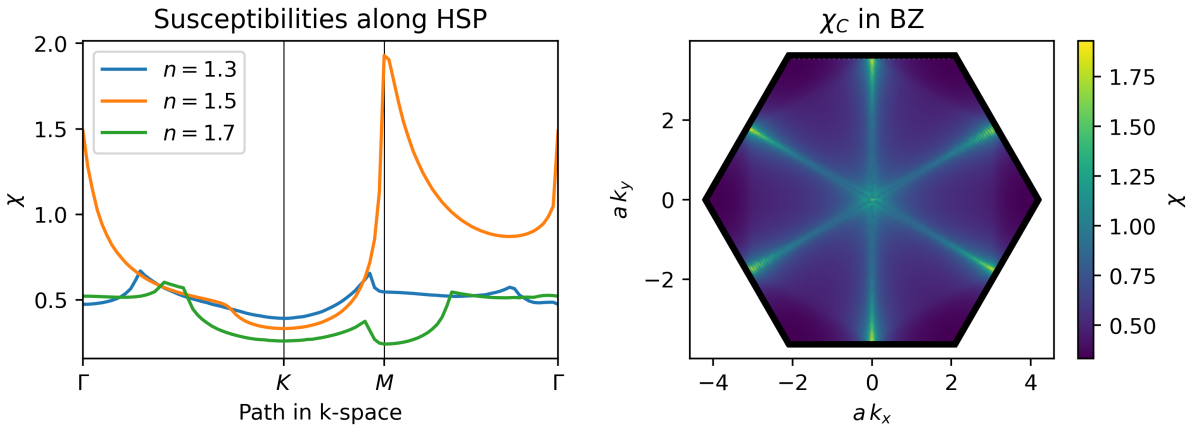

Figure 2.5: Comparison of the triangular lattice Hubbard model's bare particle hole susceptibility χ_0 for filling fractions $n \in \{1.3, 1.5, 1.7\}$. In the left panel, we compare the three scenarios along a high symmetry path through the Brillouin zone. We emphasize the strong increase of $\chi_0(\mathbf{0})$ and $\chi_0(M)$ for $n = 1.5$, *i.e.*, as the Fermi level coincides with the van-Hove singularity at M. The right panel shows the the bare susceptibility for this scenario in the complete first Brillouin zone. The results were obtained while employing a regularization temperature of $T = t/600$.

corner when traversing the hexagonal BZ can be identified with each other, resulting in two distinct K points related only via the C_{6v} point group symmetry but not via reciprocal lattice translations. Similarly, three distinct M points exist in any hexagonal lattice systems.

As we have seen previously, a systems particle-hole fluctuations near van-Hove filling are dominated by nesting vectors *i.e.*, non-trivial displacements between two Fermi surface copies that allow for good match between them. Visual inspection of the Fermi surface in Figure 2.4 quickly results in the insight, that every vector along the high symmetry line between Γ and M induces a strong nesting, maximising for $\mathbf{Q} = M$. The resulting bare susceptibility is depicted in Figure 2.5, where this feature can be seen clearly. We supplement the data for the van Hove filling by the results for $\approx 13\%$ hole and electron doping. One can clearly see that (i) particle-hole fluctuations are more strongly suppressed for electron doping compared to the hole doping case and (ii) the particle hole susceptibility for the electron doped scenario is largest for small momentum transfers. Both of these effects are nicely explained by the two smaller Fermi surface pockets in the electron doped case.

These differences influence the dominating superconducting instability strongly as shown in Fig. 8 of Ref. [23]. We refrain from plotting our own data for the complete scan in filling as the most interesting region around the van-Hove singularity is already contained as a special case in Figure 2.10 which we discuss below.

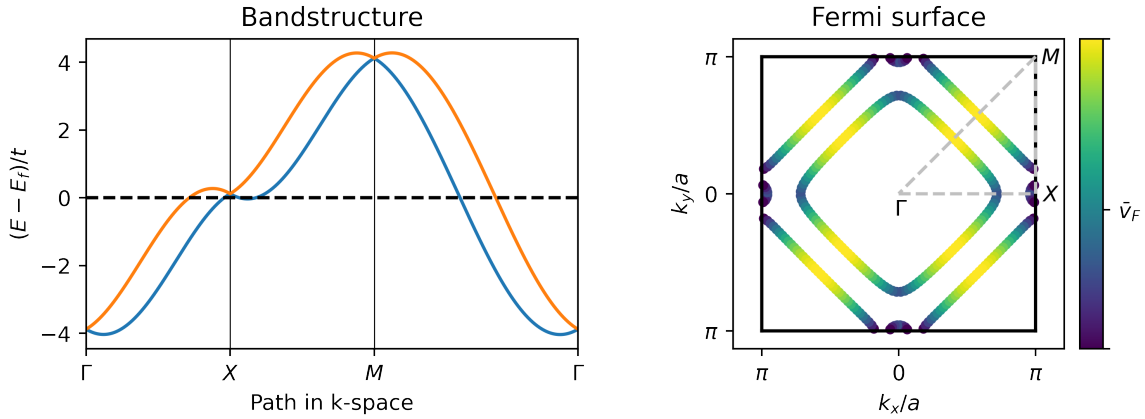

Figure 2.6: We show the energy dispersion of the nearest neighbour square lattice tight-binding Hamiltonian with Rashba spin-orbit coupling $\alpha_R = 0.4t$ in the left panel. The energy-dispersion is measured relative to the Fermi energy implied by a filling of $n = 0.95$ electrons per unit cell and the Fermi level is indicated by a dashed line. The right panel shows the four pocket Fermi surface resulting from the singly degenerate bands.

2.2 Rashba spin-orbit coupling

Having established the effect of lattice geometry on particle-hole fluctuations and the subsequent impact on superconducting pairing, we will now proceed to discuss the influence of spin-orbit coupling on static particle-hole fluctuations.

Spin-orbit coupling is a relativistic effect that is rooted in the Zeeman coupling $\mu_B \boldsymbol{\sigma} \mathbf{B}$ between the spin $\boldsymbol{\sigma}$ of an electron and the effective magnetic field $\mathbf{B}$ experienced by this electron in its rest frame. In this reference frame, an effective magnetic field $\mathbf{B} \sim \mathbf{E} \times \mathbf{p}/mc^2$ arises, whenever the electron moves in an electric field $\mathbf{E}$, inducing a finite Zeeman splitting $\boldsymbol{\sigma}(\mathbf{E} \times \mathbf{p})\mu_B/mc^2$ for vanishing external magnetic fields [27]. The required electric field is naturally present in the vicinity of heavy atomic nuclei, where its radial symmetry induces the well known $\mathbf{L}\boldsymbol{\sigma}$ term, coupling the electrons spin to its orbital angular momentum [136]. While this term can not induce an energy splitting in time-reversal preserving and inversion symmetric systems, it will still lead to an orbital admixture and energy shifts as exemplified in the unconventional superconductor Sr_2RuO_4 [137]. Nevertheless all bands in such a system are doubly degenerate.

A spin dependent energy splitting becomes possible in time-reversal invariant systems due to the presence of inversion symmetry breaking induced by the crystal structure, interfaces between different materials or simply at a crystals surface [138, 139]. This effect is known as Rashba spin-orbit coupling in the literature and leads to a variety of experimentally observed effects and is

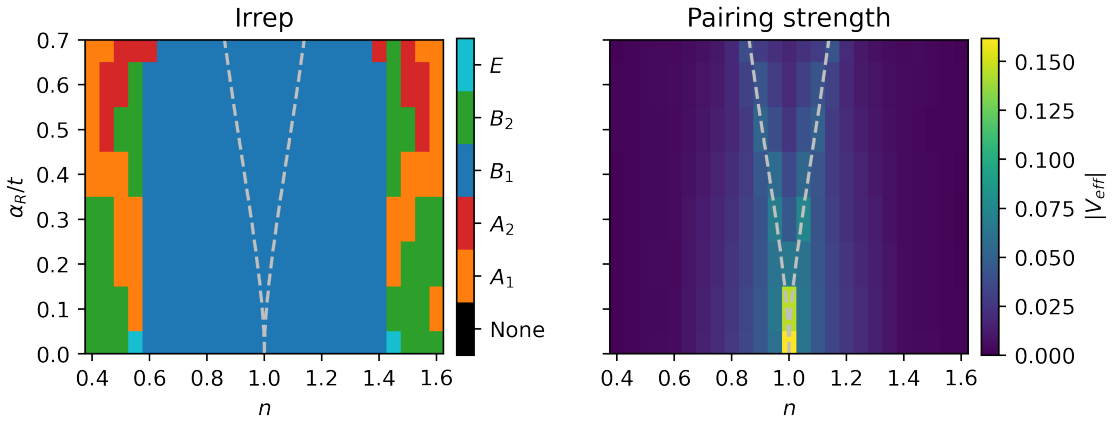

Figure 2.7: Phase diagram for a wcRG analysis of the unconventional superconducting instabilities induced by a local Hubbard repulsion on a nearest-neighbour square lattice tight-binding model with Rashba spin-orbit coupling α_R as a function of filling n. The right panel shows effective pairing strength described by Equation 1.115 and the grey dashed lines indicate the position of the van-Hove singularities as a function of α_R. In the left panel we can see that the symmetries of the superconducting order parameter do not change in the region around half filling. The slight particle-hole asymmetry for small and large filling fractions is an indication of numerical inaccuracies in this regime.

especially relevant in the context of spintronics [27]. In the following we will focus on the Rashba spin-orbit effect at interfaces.

Naively, one could assume that the electric field gradient at a crystal surface or epitaxial interface is the sole driver for the observed spin-splitting via the analogous effect discussed previously. The experimentally observed strength of spin-splitting is however underestimated by several orders of magnitude by this [140–142]. Ref. [141] resolves this discrepancy via a tight-binding model (in particular for an Au (111) surface including all sp^3 orbitals) and find that the spin-splitting is well described by a term of form $\alpha_R \boldsymbol{\sigma}(\mathbf{z} \times \mathbf{p})$. The coupling strength α_R is dominated by processes in perturbation theory that involve nearest neighbour hopping *and* matrix elements of the intra-orbital spin-orbit interaction, enhancing the effect for materials involving heavy elements.

Due to the single orbital nature and model character of our Hubbard models, we introduce Rashba spin-orbit coupling phenomenologically via an added term in the tight-binding Hamiltonian

$$H_{\mathrm{SOC}} = \alpha_R \sum_{\langle i,j \rangle} \sum_{\sigma\sigma'} c^{\dagger}_{j,\sigma} \mathbf{g}(\mathbf{r}_i - \mathbf{r}_j) \boldsymbol{\sigma}_{\sigma\sigma'} c_{i,\sigma'} \,. \tag{2.15}$$

As one can anticipate from our previous discussion

$$\mathbf{g}(\mathbf{r}) = \mathrm{i}\, t(|\mathbf{r}|)\, \mathbf{r} \times \mathbf{z} \tag{2.16}$$

for a 2d system in the xy plane, where $t(|\mathbf{r}|)$ parametrises the non-spin-orbit hopping element between sites separated by $\mathbf{r}$. An exemplary bandstructure and corresponding Fermi surface is shown in Figure 2.6.

Previous studies of unconventional superconducting instabilities in this system have relied on an analytical solution of this tight-binding Hamiltonian in order to circumvent the gauge problem posed by numerical matrix diagonalization [32, 33]. Since the Rashba term is not centrosymmetric, it lifts the spin degeneracy between the bands at all points in the Brillouin zone with the exception of time reversal invariant momenta and thereby making our gauge fixing procedure discussed in Chapter 1 unique. We validate our approach by successfully reproducing their results without relying on analytical eigenstates. Our resulting phase diagram is shown representatively in Figure 2.7. One can clearly see the splitting of the superconducting dome at $\alpha_R = 0.0$ and $n = 1$ into two separate domes following the new van Hove singularities established by the two spin-orbit separated Fermi surface sheets and observe an overall suppression of the superconducting pair strength V_{eff} with larger values of α_R. This result is expected due to the reduction of the systems nesting. In addition to this phase diagram, we provided extensive phase diagram scans in α_R and filling n for finite next nearest neighbour hybridizations in [72], further validating our implementation.

Due to the small effective pairing strength for small Fermi surfaces in the small and large n limit, which further decreases as the spin-orbit interaction is increased, the gap between leading and sub-leading instabilities drops beneath the numerical resolution of the applied scheme, which is a problem also present in other works (e.g. Ref. [33, 134]). Our results are therefore only strictly reliable in phase space regions of sizeable pairing strength, providing a natural explantation for the slight particle-hole asymmetry in Figure 2.7.

A superficial look at the presented phase diagram for the Rashba Hubbard model an a square lattice could lead to the conclusion that the influence of the spin-orbit coupling is a purely quantitative effect that is well explained by the splitting of the van-Hove singularity. This is not true as the broken inversion symmetry qualitatively changes the symmetry considerations for potential Cooper pairing states [31, 143, 144]. Similarly, the spin-orbit coupling invalidates our considerations for the symmetry between bare charge and spin fluctuations that resulted in Equation 2.12. It is true, however, that the implied changes are subtle on the square lattice. Due to this, we will now proceed with our discussion of these effects on the triangular lattice.

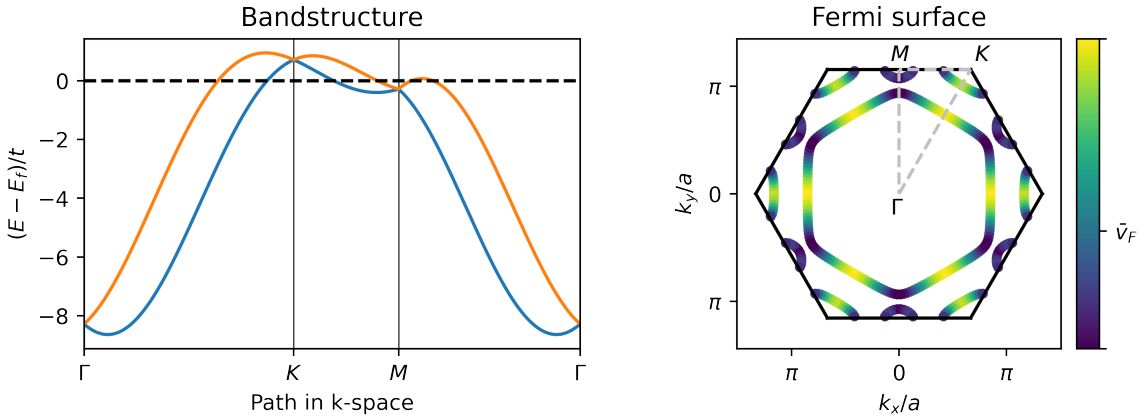

Figure 2.8: We show the energy dispersion of the nearest neighbour triangular lattice tight-binding Hamiltonian with Rashba spin-orbit coupling $\alpha_R = 0.5t$ in the left panel. The energy-dispersion is measured relative to the Fermi energy implied by a filling of $n = 1.5$ electrons per unit cell and the Fermi level is indicated by a dashed line. The right panel shows the six pocket Fermi surface resulting from the singly degenerate bands.

Triangular lattice

Let us start the discussion with a quick summary of the kinetic Hamiltonian on the triangular lattice. Analogous to the square lattice situation, the two previously spin degenerate bands split at all momenta that are not time-reversal invariant (TRI) (here the Kramers theorem protects the spin degeneracy for all time-reversal symmetric systems). The van-Hove singularity splits into asymmetrically due to the absent particle-hole symmetry and the hexagonal Brillouin zone leads to up to six distinct pockets as one can see in Figure 2.8, corresponding to the six distinct TRI momenta. We overlay the dependence of the new van-Hove fillings on the Rashba parameter α_R as grey lines over the phase diagrams in Figure 2.10.

Since the discussion of particle-hole fluctuations and unconventional superconductivity on the surface of a crystal are a central topic of this thesis, we refer the reader to the following Chapter 3 for a detailed discussion of Cooper pairing in these models and only summarize the main points here.

Since Equation 2.2 breaks spin-rotation symmetry, the spin of an electron moving on the lattice is not conserved in the presence of spin-orbit interactions. Accordingly, $\chi_{\{\sigma_i\}}$ is less constrained in this scenario. One can show that $\chi^{0,0i} = \chi^{0,i0})^* = 0$ with $i \in \{x, y, z\}$ vanishes for time-reversal invariant systems, *i.e.*, the total spin of a local particle-hole excitation $c^\dagger_{i\sigma} c_{i\sigma'}$ is conserved even in the presence of SOC. In contrast, the direction of such an excitations spin is not conserved and in general all $\chi^{0,ij}$ are finite and only constrained by hermiticity. Figure 2.9 shows the resulting diagonal elements of the particle-hole susceptibility along the high symmetry path through the BZ for

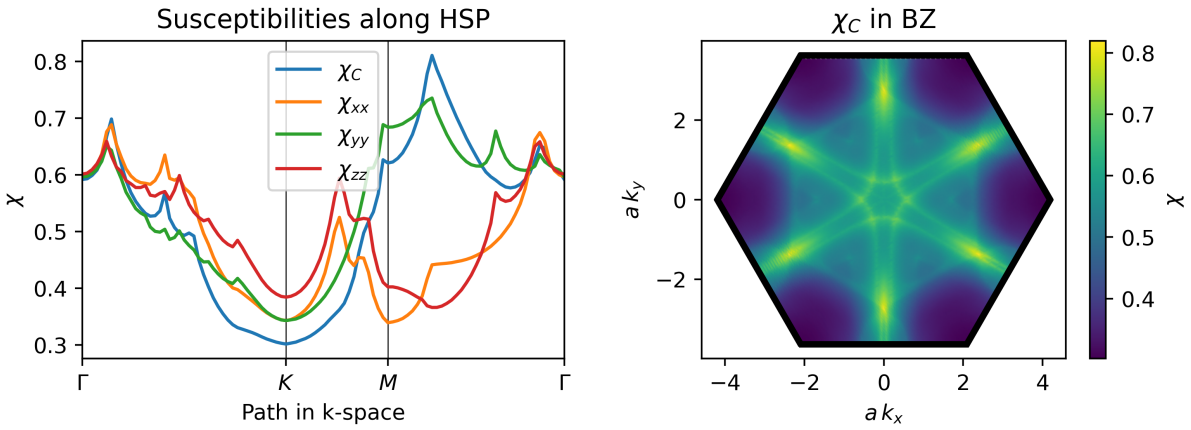

Figure 2.9: Bare particle hole susceptibilities χ_{xx}, χ_{yy}, χ_{zz} and χ_C on the triangular lattice for $n = 1.5$ and $\alpha_R = 0.5$. In the left panel, we compare the different diagonal spin contributions along scenarios along the high symmetry path through the Brillouin zone shown in Figure 2.8. We emphasize the strong increase of χ_{yy} at the $k_x = 0$ M point. The right panel shows the the charge susceptibility for this scenario in the complete first Brillouin zone. The results were obtained while employing a regularization temperature of $T = t/600$. Plots of the off diagonal components of the spin-susceptibility and complete Brillouin zone have been delegated to Appendix C. Readers are encouraged to check out the beautiful pictures :-).

exemplary fixed model parameters. One can clearly observe the influence of the spin-momentum locking for the large SOC case and the distinction between in plane xy and out of plane z spin alignments. While the off diagonal elements are finite, their absolute value is small compared to the diagonal components and we have decided to move additional plots into Appendix C for conciseness.

In addition to this modification of the particle-hole susceptibities, superconducting pairing in Rashba spin-orbit coupled systems is significantly modified by the spin-split Fermi surface. This effect is particularly strong in our calculations due to the static approximation for the pairing interaction. It implies the strict fixation of Cooper pair excitations to the Fermi surface that, when combined with the zero momentum condition $\mathbf{k}_0 = -\mathbf{k}_1$ constrains the potential pair wavefunctions to be of intra-band type $\Delta_{\lambda\lambda'} \propto \delta_{\lambda\lambda'}$. For the present case this fixes the complete spin-structure of a Cooper pair excitation with given relative momentum $\mathbf{k}$. A combination of time-reversal symmetry and fermionic antisymmetry then implies a constraint to even pairing functions $\Delta_{\lambda\lambda}(-\mathbf{k}) = \Delta_{\lambda\lambda}(\mathbf{k})$. For the case of the triangular lattice with point group C_{6v}, this means that only the three even (A_1, A_2, E_2) of the six irreps constitute energetically favourable pairing wavefunctions in the limit of string SOC $\alpha_R \gg \Delta$. Clearly this condition is fullfilled for arbitrarily small values of α_R in the wcRG limit, where U and correspondingly Δ is extremely small compared to all energy scales.

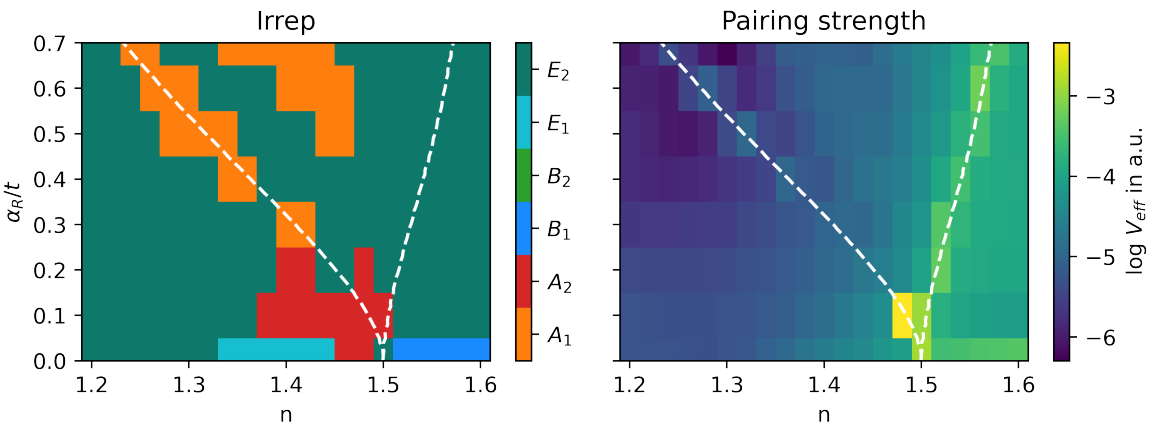

Figure 2.10: Phase diagram for a wcRG analysis of the unconventional superconducting instabilities induced by a local Hubbard repulsion on a nearest-neighbour triangular lattice tight-binding model with Rashba spin-orbit coupling α_R as a function of filling n. The right panel shows effective pairing strength described by Equation 1.115 and the grey dashed lines indicate the position of the van-Hove singularities as a function of α_R. The perceived enhancement of V_{eff} at *e.g.* $\alpha_R = 0.1$, $\alpha_R = 0.5$ and $n = 1.48$ is attributed to the almost perfect coincidence with the van Hove filling at this parameter. In the left panel we can see the constraint to even irreducible representations that is imposed by spin split Fermi surfaces in the limit of weak coupling.

Finally we present the phase diagram of unconventional superconductivity obtained from our wcRG calculation in the vicinity of the van-Hove singularity in Figure 2.10. The previously discussed point is clearly visible as the odd representations E_1 and B_1 are only supported for $\alpha_R = 0$ and the degenerate E_2 representation which was limited to the exact vHS at $\alpha_R = 0$ dominates the phase diagram for finite SOC. Interestingly, a new phase transforming under the A_1 irrep emerges along the lower vHS.

Unconventional surface superconductivity

Here we investigate the possibility of unconventional surface superconductivity. A particular focus is given to the half-Heusler compound LuPtBi, whose unusual surface state is a prime candidate for correlation induced Cooper pairing. The presented results are in preparation for publication [145].

Unconventional surface superconductivity

The analysis of many established unconventional superconductors has been predominantly focused on the bulk limit of quasi-two-dimensional (quasi-2D) such as the cuprates, ruthenates or certain families of iron-based superconductors [12, 137, 146–149]. This fact may be understood in terms of the generically reduced nesting features of three-dimensional (3D) Fermiologies compared to the quasi-2D case in these layered systems. In addition, a variety of superconducting systems with atomic scale thickness have been identified in recent years, some of which we already sketched in the introduction to this thesis. Noteworthy is, for instance, the case of twisted bilayer graphene (TWBLG) (and related systems), where the twisting angle between the graphene's layers affects the flatness of bands close to the Fermi level [56, 60]. Other examples include the deposition of adatoms on the surface of various insulating and semimetallic substrates such as Sn on Si(111) [54] or superconductivity (SC) between insulating oxide materials like the $LaAlO_3$ / $SrTiO_3$ or $KTaO_3$ based interfaces [55, 58, 150–152]. The true 2D nature of these systems allows for potentially topological superconducting condensates that can feature chiral Majorana fermions, the building blocks for topologically protected quantum computation [153–158]. Compared to SC at an interface, however, surface SC has significant advantages, as it may be prone to easier manipulation and investigation compared to interfaces hidden between two bulk materials. In particular, many widely applied experimental probes such as photoemission spectroscopy (ARPES) or scanning tunneling microscopy (STM) could be used to investigate surface SC.

While the 2D nature of SC between insulating oxides and on top of insulating or semiconducting substrates is experimentally well established, the distinction between surface and bulk SC in bulk (semi)metals is challenging. For phonon driven bulk superconductors, the distinction between surface and bulk SC deriving from a single material superconductor is especially hard, because

the SC 3D bulk transition sets all decisive energy scales due to its dominant density of states in generic settings.

Evidence of surface SC has been reported in a variety of 3D topological insulators as well as 3D Dirac semimetals [63–68]. While the superconducting transition temperature T_c in these systems reaches up to $\approx 9\,\mathrm{K}$, the comparatively small density of states (DOS) of linearly dispersing Dirac fermions inhibits even higher T_c's. In contrast, non-topologically protected (Shockley or Tamm) surface states may be characterized by small bandwidths and nearly-flat dispersions, indeed providing a promising avenue to increase T_c via the enhanced DOS.

In this chapter we will start by summarizing the literature on surface superconductivity and contrast it with our proposition for unconventional surface SC. We continue with a summary of symmetry considerations for superconducting pairing in the absence of inversion symmetry as it is relevant for a crystals surface. Subsequently, we discuss the crystal structure and electronic properties of the half-Heusler material LuPtBi in the context of its bulk SC and metallic surface state. Finally, we present an almost *ab-initio* Fermi surface instability analysis of this surface state and identify a condensate of Cooper pairs which spontaneously breaks time-reversal symmetry as the leading instability.

3.1 Surface superconductivity

In the introduction of this thesis we have discussed experimental investigations of two dimensional (2D) superconductivity in various systems. This section particularizes the discussion to the explicit case of surface superconductivity *i.e.*, 2D superconductors arising at the surface of a bulk material with critical transition temperature T_c^{surface} exceeding any bulk SC transition temperature $T_c^{\mathrm{bul}} < T_c^{\mathrm{surface}}$.

To the best of our knowledge, such a scenario was first discussed by Saint-James and de Gennes [159] in the context of conventional bulk superconductors in the presence of decreasing magnetic fields. The diamagnetic properties of superconductors implies that they expel magnetic fields H from their bulk. Clearly, the presence of such an external field raises the total system energy and for large enough values of $H > H_c$ [1], the superconducting state is no longer energetically favourable compared to a normal state that allows for a penetration of the field through the material [5]. Saint-James and de Gennes studied the Ginzburg Landau theory of a bulk superconductor in the presence of a plane boundary and magnetic fields parallel to this surface. They found that upon lowering the field from values $H > H_c$, superconductivity nucleates at the surface and

[1] For the sake of conciseness we do not discuss the difference between superconductors of the first and second kind here, and refer the reader to [5] for a general discussion and [159] for the implied differences for surface superconductivity.

not at the bulk. The critical field at which this nucleation occurs was named H_{c3} and found to be larger than the bulk value $H_c < H_{c3}$ for ideal superconductors. For superconductors of the second kind (type II superconductors), they established that the presence of such a magnetic field will lead to a superconducting layer near the surface of the sample *i.e.*, surface superconductivity. The theoretical prediction was quickly verified experimentally [160, 161] and their theory expanded to finite temperatures [162], more complicated surface geometries [163–165] and multi-band superconductors [166]. Measurements of this effect in the heavy-Fermion superconductor UPt_3 [167] lead to extensions of the theory to unconventional order parameters [168]. Finally, the influence of spin-orbit coupling on this type of surface superconductivity was also discussed [169]. In their study, the authors predict an enhancement of particle-particle condensation with finite center of mass momentum (FFLO[2] states) due to the interplay of in-plane magnetic field and spin-orbit coupling. Going forward, we will label all of these scenarios of surface superconductivity discussed in this paragraph as field induced. They do not depend on a specific electronic structure at the surface and are therefore not related to the scenario considered in this thesis.

A completely different approach to the idea of surface superconductivity is concerned with possibility of a modified electronic structure at a material's surface and accordingly does not require the presence of a magnetic field. Theoretically, zero-field surface superconductivity (in the following titled surface superconductivity) has been predominantly studied in the context of topological surface states. The literature includes superconductivity in flatband surface states at the surface of nodal fermionic systems [170, 171], phonon induced superconductivity in the metallic surface states of three-dimensional topological insulators [172, 173] and the influence of bulk superconductivity on topological surface states [174] to name a few. While experimental evidence for surface superconducting islands in the topological insulator Sb_2Te_3 has been reported in [63], conclusive evidence for a coherent superconducting condensate in the topological surface state is outstanding. The arena of 3D semimetals seems to be more promising, as a variety of groups have reported in evidence for surface superconductivity in a wide array of materials [64–68].

Our proposal for unconventional surface superconductivity, however, neither relies on magnetic fields nor non-trivial topology. Instead, we propose that an enhanced density of states at some crystal surfaces may conspire with the increased correlation effects in two spatial dimensions [14] and pronounced nesting features in the surface band structure to yield an unconventional mechanism for surface superconductivity. The first point was previously proposed by Weitzel and Micklitz [175], who claimed that their observation of superconductivity in rhombohedral bismuth clusters could be explained by the strongly increased density of states at the cluster surfaces,

[2] Fulde Ferrell Larkin Ovchinnikov

leading to surface superconductivity. We are, however, not aware of any proposals for surface superconductivity driven by electronic correlation effects inside the surface state itself.

Topologically trivial surface states are a widespread phenomenon in semiconducting materials and even metals as reported by numerous photoemission as well as scanning tunnelling microscopy studies [140, 176, 177]. Typically, the resulting surface bandstructure are well separated from the bulk, making these systems prototypical two-dimensional (2D) material platforms. As we discussed in Section 2.2, the broken inversion symmetry at the surface can conspire with the strong spin-orbit coupling (SOC) of heavy elements to yield spin-split Fermi surfaces. Finally, the relevance of correlation effects for such surface states has not only been predicted theoretically [178] but observed in experiment [179]. A related system class to these intrinsic surface band structures forming naturally on top of certain bulk materials, 2D band structures with strong SOC and correlation effects can be engineered by depositing a single layer of atoms on top of a clean substrate. This approach is even more flexible and both correlation effects and topological properties have been observed in this large class of systems [180–182]. In both cases, missing bond partners at a crystal termination are responsible for the formation of these surface band structures. Typically, electrons hopping through out-of-plane atomic orbitals (*i.e.*, perpendicular to the new surface) form $\pi-$bonds and experience the vacuum region's strong potential barrier. These conditions naturally lead to band dispersions flatter than for their in-plane-hopping counterparts. The resulting increase in the associated density-of-states forms a genuine proxy for stabilizing collective phenomena.

Having established the surface of bulk materials as an interesting platform for the realization of unconventional superconductivity, we will now proceed by studying the constraints on pairing imposed by the absent inversion symmetry at a surface. Particular focus is given to the relevance of spin-orbit coupling in this context.

3.2 Relativistic corrections to superconducting pairing

As we discussed before in the introduction of this thesis and in Section 2.2, the dominant relativistic correction in condensed matter systems stems from the effective magnetic field experienced by electrons in the vicinity of the strong potential gradient near atomic nuclei. The coupling between this effective field and the electrons intrinsic spin results in the well known spin-orbit interaction [183]. In the absence of inversion symmetry, this effect has dramatic qualitative consequences as it lifts the spin degeneracy of the electronic band structure and ties the electron's spin degree of freedom to it's lattice momentum. This effect was discovered by Rashba [139] and Dresselhaus [138] and was discussed by us in Section 2.2.

In the following section we will first discuss the general implications of time reversal symmetry on the electronic structure of Rashba spin-orbit coupled systems. We will then use the result to discuss the implications of spin-orbit coupling on superconducting pairing.

Time reversal symmetry in a spin-orbit coupled system without inversion symmetry

In a system of spin one half without orbital or sublattice degrees of freedom, we can write a generic Hamiltonian as

$$H = \sum_{\vec{k}} \psi_{\boldsymbol{k}}^{\dagger}(\epsilon(\boldsymbol{k}) + \boldsymbol{g}(\boldsymbol{k})\boldsymbol{\sigma})\psi_{\boldsymbol{k}} = \sum_{\boldsymbol{k}} \psi_{\boldsymbol{k}}^{\dagger} h(\boldsymbol{k})\psi_{\boldsymbol{k}}\,, \tag{3.1}$$

with the combined creation operator

$$\psi_{\boldsymbol{k}}^{\dagger} = (c_{\boldsymbol{k},\uparrow}^{\dagger}\,;\, c_{\boldsymbol{k},\downarrow}^{\dagger})\,,$$

for up (down) spin electrons $c_{\boldsymbol{k}\uparrow}^{\dagger}$ ($c_{\boldsymbol{k}\downarrow}^{\dagger}$) at momenta $\boldsymbol{k}$.

We define the helicity operator

$$\Lambda_{\boldsymbol{k}} = \frac{\boldsymbol{g}(\boldsymbol{k})\boldsymbol{\sigma}}{|\boldsymbol{g}(\boldsymbol{k})|} \tag{3.2}$$

squaring to the identity which trivially commutes with $h(\boldsymbol{k})$. Due to this we can label the eigenstates at each momentum $\boldsymbol{k}$ according to their eigenvalue $\lambda = \pm 1$ corresponding to this operator Λ. The given Hamiltonian is already diagonal in momentum so we define eigenstates of the problem defined by their eigenvalue equations

$$\begin{aligned} \hat{\boldsymbol{P}}\,|\boldsymbol{p};\lambda\rangle &= \boldsymbol{p}\,|\boldsymbol{p};\lambda\rangle\ , \\ \Lambda_{\boldsymbol{p}}\,|\boldsymbol{p};\lambda\rangle &= \lambda\,|\boldsymbol{p};\lambda\rangle\ . \end{aligned} \tag{3.3}$$

We can now diagonalize our Hamiltonian by introducing new operators creating these states

$$\Psi_{\boldsymbol{k}\lambda}^{\dagger} = (c_{\boldsymbol{k},\lambda=+}^{\dagger}\,;\, c_{\boldsymbol{k},\lambda=-}^{\dagger}) = \psi_{\boldsymbol{k}\sigma}^{\dagger}(U_{\lambda\sigma})^{\dagger}\,.$$

$$\Psi_{\boldsymbol{k}\lambda} = \begin{pmatrix} c_{\boldsymbol{k},+} \\ c_{\boldsymbol{k},-} \end{pmatrix} = U_{\lambda\sigma}(\boldsymbol{k})\psi_{\boldsymbol{k}\sigma}\,,$$

where we define operators $c^\dagger_{\boldsymbol{k}\lambda}$ that create electrons with momentum $\boldsymbol{k}$ and helicity λ on the vacuum

$$|\boldsymbol{k};\lambda\rangle = c^\dagger_{\boldsymbol{k}\lambda}|0\rangle \ .$$

We pick $U_{\lambda\sigma}(\boldsymbol{k})$ such that

$$U(\boldsymbol{k})_{\lambda\sigma}h(\boldsymbol{k})_{\sigma\sigma'}U^*(\boldsymbol{k})_{\sigma'\lambda'} = E_\lambda(\boldsymbol{k})\delta_{\lambda\lambda'} \ .$$

In the new basis Equation 3.1 reads

$$H = \sum_{\vec{k}}\sum_{\lambda} E_\lambda(\boldsymbol{k})c^\dagger_{\boldsymbol{k},\lambda}c_{\boldsymbol{k},\lambda}$$

and one possible solution for $U_{\lambda\sigma}(\boldsymbol{k})$ is given by

$$U(\boldsymbol{k}) = \begin{pmatrix} \frac{|\boldsymbol{g}(\boldsymbol{k})|+g_z(\boldsymbol{k})}{n_+} & \frac{g_x(\boldsymbol{k})-ig_y(\boldsymbol{k})}{n_+} \\ \frac{|\boldsymbol{g}(\boldsymbol{k})|-g_z(\boldsymbol{k})}{n_-} & \frac{-g_x(\boldsymbol{k})+ig_y(\boldsymbol{k})}{n_-} \end{pmatrix}, \tag{3.4}$$

with normalization factors

$$n_\pm = \sqrt{2|\boldsymbol{g}(\boldsymbol{k})|(|\boldsymbol{g}(\boldsymbol{k})| \pm g_z(\boldsymbol{k}))} \, .$$

Clearly this unitary transformation also diagonalizes Λ

$$U(\boldsymbol{k})\Lambda(\boldsymbol{k})U^\dagger(\boldsymbol{k}) = \begin{pmatrix} 1 & 0 \\ 0 & -1 \end{pmatrix},$$

and results in energy eigenvalues

$$E_\lambda = \epsilon(\boldsymbol{k}) + \lambda|\boldsymbol{g}(\boldsymbol{k})| \, . \tag{3.5}$$

Note that generically, operators in the helicity basis B can be obtained from operators in the spin basis A via

$$B(\boldsymbol{k})_{\lambda\lambda'} = U(\boldsymbol{k})_{\lambda\sigma}A(\boldsymbol{k})_{\sigma\sigma'}U(\boldsymbol{k})^*_{\sigma'\lambda'} \, , \tag{3.6}$$

resulting in the fact that operators constant in momentum acquire a momentum dependence from the unitary transformation.

Having found the energy eigenvalues of our Hamiltonian we continue with analysing the symmetry properties of our solution. In order to investigate the transformation behaviour of (time-independent) operators and states under time-reversal symmetry it is easiest and most transparent to start from the transformation behaviour of spin up and spin down states. In real space this

transformation behaviour is given by

$$\begin{aligned} Tc_{j\uparrow}T^{-1} &= c_{j\downarrow} \\ Tc_{j\downarrow}T^{-1} &= -c_{j\uparrow}\,, \end{aligned}$$

and the time reversal operation for our system can be represented in the spin basis as

$$Tc_{j\sigma}T^{-1} = \sum_{\sigma'} i(\sigma_y)_{\sigma\sigma'}c_{j\sigma'}\,.$$

While it is up to a choice of convention how the minus sign for this transformation is picked, we can't choose all signs to be positive since $T^2 = -1$ has to hold for spin $1/2$ particles. The time reversal operator in spin space can is conventionally written as

$$T = i\sigma_y\mathcal{K} = U_{\mathrm{TR}}\mathcal{K}\,, \tag{3.7}$$

where the complex conjugation $\mathcal{K}$ is necessary in order for T to be anti-unitary and U_{TR} is the unitary part of T. If the matrix U_{TR} is not real, it is important to notice that

$$T^{-1} = (U_{\mathrm{TR}}\mathcal{K})^{-1} = \mathcal{K}U_{\mathrm{TR}}^{-1} = (U_{\mathrm{TR}}^{-1})^{*}\mathcal{K} = (U_{\mathrm{TR}})^{T}\mathcal{K}\,.$$

Introducing a Fourier transformation to connect real space and momentum space we can compute the transformation behaviour of the creation and annihilation operators from the real space behaviour and find

$$\begin{aligned} c_{\boldsymbol{k}\sigma} &= \sum_{\boldsymbol{x}} e^{i\boldsymbol{k}\boldsymbol{x}}c_{\boldsymbol{x}\sigma} \\ Tc_{\boldsymbol{k}\uparrow}T^{-1} &= \sum_{\boldsymbol{x}} e^{-i\boldsymbol{k}\boldsymbol{x}}Tc_{\boldsymbol{x}\uparrow}T^{-1} = \sum_{\boldsymbol{x}} e^{i(-\boldsymbol{k})\boldsymbol{x}}c_{\boldsymbol{x}\downarrow} = c_{-\boldsymbol{k}\downarrow} \\ Tc_{\boldsymbol{k}\downarrow}T^{-1} &= \sum_{\boldsymbol{x}} e^{-i\boldsymbol{k}\boldsymbol{x}}Tc_{\boldsymbol{x}\downarrow}T^{-1} = \sum_{\boldsymbol{x}} e^{i(-\boldsymbol{k})\boldsymbol{x}}(-c_{\boldsymbol{x}\uparrow}) = -c_{-\boldsymbol{k}\uparrow}\,. \end{aligned}$$

This can be summarized into

$$T\psi_{\boldsymbol{k}}T^{-1} = i\sigma_y\psi_{-\boldsymbol{k}}\,. \tag{3.8}$$

We can now compute the transformation behaviour of the Hamiltonian under the time reversal operator

$$\begin{aligned} THT^{-1} &= \sum_{\boldsymbol{k}} T\psi_{\boldsymbol{k}}^\dagger h(\boldsymbol{k})\psi_{\boldsymbol{k}} T^{-1} = \sum_{\boldsymbol{k}} T\psi_{\boldsymbol{k}}^\dagger T^{-1} Th(\boldsymbol{k})T^{-1} T\psi_{\boldsymbol{k}} T^{-1} \\ &= \sum_{\boldsymbol{k}} \psi_{-\boldsymbol{k}}^\dagger (-i\sigma_y) Th(\boldsymbol{k})T^{-1}(i\sigma_y)\psi_{-\boldsymbol{k}} = \sum_{-\boldsymbol{k}} \psi_{\boldsymbol{k}}^\dagger (-i\sigma_y) Th(-\boldsymbol{k})T^{-1}(i\sigma_y)\psi_{\boldsymbol{k}} \,. \end{aligned}$$

Since $h(k)$ is not an operator on the Hilbert space but simply a matrix shorthand for prefactors of linear combinations of Hilbert space operators, time reversal simply acts on it as complex conjugation, $Th(k)T^{-1} = h^*(k)$. We find

$$THT^{-1} = \sum_{\boldsymbol{k}} \psi_{\boldsymbol{k}}^\dagger \sigma_y h^*(-\boldsymbol{k})\sigma_y \psi_{\boldsymbol{k}} \,.$$

We can generalize this statement for operators of the form $O_{\boldsymbol{k}} = \psi_{\boldsymbol{k}}^\dagger O_{\boldsymbol{k}} \psi_{\boldsymbol{k}}$ and general unitary symmetry operations $\mathcal{S}$ represented in the space of creation and annihilation operators by U_S

$$\begin{aligned} &\mathcal{S}\psi_{\boldsymbol{k}}\mathcal{S}^{-1} = U_S \psi_{R_S(\boldsymbol{k})} \\ &\mathcal{S}O_{\boldsymbol{k}}\mathcal{S}^{-1} = \psi_{R_S(\boldsymbol{k})}^\dagger U_S^\dagger O_{\boldsymbol{k}} U_S \psi_{R_S(\boldsymbol{k})} = \psi_{\boldsymbol{k}'}^\dagger U_S^\dagger O_{R_S^{-1}(\boldsymbol{k}')} U_S \psi_{\boldsymbol{k}'} = \psi_{\boldsymbol{k}'}^\dagger O'_{\boldsymbol{k}'} \psi_{\boldsymbol{k}'} = O'_{\boldsymbol{k}'} \\ &\text{with } O'_{\boldsymbol{k}} = U_S^\dagger O_{R_S^{-1}(\boldsymbol{k})} U_S \,. \end{aligned} \tag{3.9}$$

For the Hamiltonian in Equation 3.1 this result can be used to compute constraints on $g(\boldsymbol{k})$ and $\epsilon(\boldsymbol{k})$

$$\begin{aligned} THT^{-1} &= \sum_{\boldsymbol{k}} \psi_{\boldsymbol{k}}^\dagger \sigma_y (\epsilon^*(-\boldsymbol{k}) + \boldsymbol{g}^*(-\boldsymbol{k})\boldsymbol{\sigma}^*)\sigma_y \psi_{\boldsymbol{k}} \\ &= \sum_{\boldsymbol{k}} \psi_{\boldsymbol{k}}^\dagger (\epsilon(-\boldsymbol{k}) - \boldsymbol{g}(-\boldsymbol{k})\boldsymbol{\sigma})\sigma_y^2 \psi_{\boldsymbol{k}} \\ &= \sum_{\boldsymbol{k}} \psi_{\boldsymbol{k}}^\dagger (\epsilon(-\boldsymbol{k}) - \boldsymbol{g}(-\boldsymbol{k})\boldsymbol{\sigma})\psi_{\boldsymbol{k}} \\ &\overset{!}{=} \sum_{\boldsymbol{k}} \psi_{\boldsymbol{k}}^\dagger (\epsilon(\boldsymbol{k}) + \boldsymbol{g}(\boldsymbol{k})\boldsymbol{\sigma})\psi_{\boldsymbol{k}} = H \,. \end{aligned}$$

Here we used the fact that ϵ and g have to be real in order for H to be hermitian as well as the fact that while σ_y is the only Pauli matrix with imaginary components resulting in $\sigma_y^* = -\sigma_y$ it is also the only Pauli matrix commuting with σ_y. σ_x and σ_z on the other hand acquire a minus sign from the anti commutation relation with σ_y. In summary

$$\epsilon(-\boldsymbol{k}) - \boldsymbol{g}(-\boldsymbol{k})\boldsymbol{\sigma} \overset{!}{=} \epsilon(\boldsymbol{k}) + \boldsymbol{g}(\boldsymbol{k})\boldsymbol{\sigma} \,. \tag{3.10}$$

From Equation 3.10 we find that for H to be time reversal symmetric, $\boldsymbol{g}(\boldsymbol{k})$ has to be an odd function of $\boldsymbol{k}$ i.e. $-\boldsymbol{g}(-\boldsymbol{k}) = \boldsymbol{g}(\boldsymbol{k})$. Due to this we interpret Λ as a helicity operator. It further holds that

$$T\Lambda_{\boldsymbol{k}}T^{-1} = -\Lambda_{\boldsymbol{k}} = \Lambda_{-\boldsymbol{k}}\,, \tag{3.11}$$

and therefore

$$\Lambda_{\boldsymbol{k}}T\,|\boldsymbol{k};\lambda\rangle = -\Lambda_{-\boldsymbol{k}}T\,|\boldsymbol{k};\lambda\rangle = -T\Lambda_{\boldsymbol{k}}T^{-1}T\,|\boldsymbol{k};\lambda\rangle = -T\Lambda_{\boldsymbol{k}}\,|\boldsymbol{k};\lambda\rangle = -T\lambda\,|\boldsymbol{k};\lambda\rangle = -\lambda T\,|\boldsymbol{k};\lambda\rangle$$
$$\Lambda_{\boldsymbol{k}}T\,|\boldsymbol{k};\lambda\rangle = -\lambda T\,|\boldsymbol{k};\lambda\rangle$$

i.e. the time-reversal operator seems to connect states with different helicity. This of course is not correct since we also have to account for time-reversal changing the momentum of our state. If we act with the helicity operator at the "correct" momentum $-\boldsymbol{k}$ on a state $T\,|\boldsymbol{k};\lambda\rangle$ it holds that

$$\Lambda_{-\boldsymbol{k}}T\,|\boldsymbol{k};\lambda\rangle = \lambda T\,|\boldsymbol{k};\lambda\rangle\ . \tag{3.12}$$

Using this information we can now define states at $-\boldsymbol{k}$ via their time-reversal partners at $\boldsymbol{k}$

$$T\,|\boldsymbol{k};\lambda\rangle = e^{i\alpha_\lambda(\boldsymbol{k})}\,|-\boldsymbol{k};\lambda\rangle\ , \tag{3.13}$$

capturing the correct transformation behaviour for both momentum and helicity eigenvalues.

We can check that this is true and fix the phase by calculating $\langle -\boldsymbol{k},\lambda\,|\,T\,|\,\boldsymbol{k},\lambda'\rangle$ in the spin basis to be

$$\langle -\boldsymbol{k},\lambda\,|\,T\,|\,\boldsymbol{k},\lambda'\rangle = \lambda\frac{g_x(\boldsymbol{k}) - ig_y(\boldsymbol{k})}{\sqrt{g_x(\boldsymbol{k})^2 + g_y(\boldsymbol{k})^2}}\delta_{\lambda\lambda'}\delta_{\boldsymbol{k}\boldsymbol{k}'}\mathcal{K} = e^{i\alpha_\lambda(\boldsymbol{k})}\delta_{\lambda\lambda'}\delta_{\boldsymbol{k}\boldsymbol{k}'}\mathcal{K}\,,$$
$$e^{i\alpha_\lambda(\boldsymbol{k})} = \lambda\frac{g_x(\boldsymbol{k}) - ig_y(\boldsymbol{k})}{\sqrt{g_x(\boldsymbol{k})^2 + g_y(\boldsymbol{k})^2}}\,. \tag{3.14}$$

Notice that we did not compute the "time-reversal operator in the helicity representation" as it would be defined by Equation 3.6. This is not possible for the time reversal operator as a suitable representation for T has to fulfil Equation 3.11 *i.e.*, it is not diagonal in momentum space and connects states at different momenta. To see that Equation 3.14 is consistent with $T^2 = -1$ we

compute

$$\begin{aligned}\langle k,\lambda|T^2|k,\lambda\rangle &= \sum_{k',\lambda'}\langle k,\lambda|\,T\,|-k',\lambda'\rangle\langle -k',\lambda'|\,T\,|k,\lambda\rangle = \sum_{k',\lambda'} e^{i\alpha_\lambda(-\boldsymbol{k})}\delta_{\lambda\lambda'}\delta_{\boldsymbol{k}\boldsymbol{k}'}\mathcal{K}e^{i\alpha(\boldsymbol{k})}\mathcal{K}\\ &= e^{i\alpha(-\boldsymbol{k})}\left(e^{i\alpha(\boldsymbol{k})}\right)^*\mathcal{K}^2 = (\lambda)^2\frac{g_x(-\boldsymbol{k})-ig_y(-\boldsymbol{k})}{\sqrt{g_x(-\boldsymbol{k})^2+g_y(-\boldsymbol{k})^2}}\frac{g_x(\boldsymbol{k})+ig_y(\boldsymbol{k})}{\sqrt{g_x(\boldsymbol{k})^2+g_y(\boldsymbol{k})^2}}\\ &= -\frac{(g_x(\boldsymbol{k})-ig_y(\boldsymbol{k}))(g_x(\boldsymbol{k})+ig_y(\boldsymbol{k}))}{g_x(\boldsymbol{k})^2+g_y(\boldsymbol{k})^2}\\ &= -1\,.\end{aligned}$$

Using Equation 3.13 and $T^2 = -1$ we can also compute a generic constraint on the phase $e^{i\alpha_\lambda(\boldsymbol{k})}$ generated by the time reversal operation

$$-|\boldsymbol{k},\lambda\rangle = T^2\,|\boldsymbol{k},\lambda\rangle = Te^{i\alpha_\lambda(\boldsymbol{k})}\,|-\boldsymbol{k},\lambda\rangle = e^{i\alpha_\lambda(-\boldsymbol{k})}e^{-i\alpha_\lambda(\boldsymbol{k})}\,|\boldsymbol{k},\lambda\rangle$$

yielding

$$-e^{i\alpha_\lambda(\boldsymbol{k})} = e^{i\alpha_\lambda(-\boldsymbol{k})}\,. \tag{3.15}$$

Superconducting pairing in the absence of inversion symmetry

Having studied the single particle solution of the tight-binding Hamiltonian Equation 3.1, we proceed with investigating the symmetry properties of two-electron wave-functions, in particular of Cooper pairs. In a weak coupling theory we can constrain ourselves to Cooper pairs where the single electron states are time reversal partners since we assume the superconducting pairing to be much smaller than the band-splitting energy gap. The pair wave functions can thus be written in terms of two creation operators on the same band

$$\Psi_{\text{pair}}(\boldsymbol{k};\lambda) = c^\dagger_{\boldsymbol{k}\lambda}Tc^\dagger_{\boldsymbol{k}\lambda}T^{-1} = e^{i\alpha_\lambda(\boldsymbol{k})}c^\dagger_{\boldsymbol{k}\lambda}c^\dagger_{-\boldsymbol{k}\lambda}\,. \tag{3.16}$$

By introducing an additional term

$$H_{\text{SC}} = \frac{1}{2}\sum_{\lambda,\boldsymbol{k}}\Delta_\lambda(\boldsymbol{k})\Psi_{\text{pair}}(\boldsymbol{k};\lambda) + \text{h.c.} \tag{3.17}$$

into Equation 3.1, we add superconducting pairing on the mean field level to the Hamiltonian. The chosen form restricts our description to intra band pairing *i.e.*, Cooper pairs that consist of electrons with different helicities are excluded.

To compute the energy spectrum of such a mean field Hamiltonian, it is convenient to formulate the problem in terms of Nambu spinors

$$C_{\boldsymbol{k}}^{\dagger} = \left(c_{\boldsymbol{k},+}^{\dagger}\,, c_{\boldsymbol{k},-}^{\dagger}\,, c_{-\boldsymbol{k},+}\,, c_{-\boldsymbol{k},-}\right)$$

and its hermitian conjugate $C_{\boldsymbol{k}}$. The Bogoliubov-de Gennes Hamiltonian Hamiltonian for a single orbital superconductor with broken inversion symmetry restricted to intra band (=intra helicity) pairing can then be written in matrix form as

$$H = H_0 + H_{\mathrm{SC}} = \frac{1}{2}\sum_{\boldsymbol{k}} C_{\boldsymbol{k}}^{\dagger}\begin{pmatrix} E_+(\boldsymbol{k}) & 0 & \Delta_+(\boldsymbol{k}) & 0 \\ 0 & E_-(\boldsymbol{k}) & 0 & \Delta_-(\boldsymbol{k}) \\ \Delta_+^*(\boldsymbol{k}) & 0 & -E_+(-\boldsymbol{k}) & 0 \\ 0 & \Delta_-^*(\boldsymbol{k}) & 0 & -E_-(-\boldsymbol{k}) \end{pmatrix} C_{\boldsymbol{k}} + \mathcal{K}\,.$$

The spectrum of this Hamiltonian is given by the absolute value of the gap function $|\Delta_\lambda(\boldsymbol{k})|^2 = \Delta_\lambda^*(\boldsymbol{k})\Delta_\lambda(\boldsymbol{k})$ and the spectrum of the normal Hamiltonian $E_\lambda(\boldsymbol{k})$ to be

$$\mathcal{E}_\lambda(\boldsymbol{k}) = \pm\sqrt{E_\lambda^2(\boldsymbol{k}) + |\Delta_\lambda(\boldsymbol{k})|^2}\,. \tag{3.18}$$

One clearly sees the separation of the two helicity degrees of freedom, which can be treated in analogy to multi band superconductivity in our weak coupling approximation.

Implications of time reversal symmetry

In the absence of inversion symmetry, time reversal symmetry is an almost mandatory requirement for the formation of superconductivity. As we discussed in Chapter 1, the divergence of the particle particle susceptibility, or the related absence of phase space restrictions on the particle-particle scattering with total momentum $\mathbf{Q}$ ensures the existence of a superconducting Fermi surface instability. A necessary precondition for this is the existence of a zero energy pairing partner state $c^{\dagger}(-\mathbf{k})$ for Fermi surface excitation at $\mathbf{k}$. In the absence of inversion symmetry, time reversal is the only remaining symmetry enforcing the existence of such a state.

Here, we start by computing the transformation of Cooper pair states under time reversal in spin space

$$\begin{aligned}
T\Psi_{\text{pair}}(\boldsymbol{k};\text{sgt})T^{-1} &= T(c^\dagger_{\boldsymbol{k}\uparrow}c^\dagger_{-\boldsymbol{k}\downarrow} - c^\dagger_{\boldsymbol{k}\downarrow}c^\dagger_{-\boldsymbol{k}\uparrow})T^{-1} = (-c^\dagger_{-\boldsymbol{k}\downarrow}c^\dagger_{\boldsymbol{k}\uparrow} + c^\dagger_{-\boldsymbol{k}\uparrow}c^\dagger_{\boldsymbol{k}\downarrow}) = (c^\dagger_{-\boldsymbol{k}\uparrow}c^\dagger_{\boldsymbol{k}\downarrow} - c^\dagger_{-\boldsymbol{k}\downarrow}c^\dagger_{\boldsymbol{k}\uparrow}) \\
&= \Psi_{\text{pair}}(-\boldsymbol{k};\text{sgt}) \\
T\Psi_{\text{pair}}(\boldsymbol{k};\text{tpt},m=0)T^{-1} &= T(c^\dagger_{\boldsymbol{k}\uparrow}c^\dagger_{-\boldsymbol{k}\downarrow} + c^\dagger_{\boldsymbol{k}\downarrow}c^\dagger_{-\boldsymbol{k}\uparrow})T^{-1} = (-c^\dagger_{-\boldsymbol{k}\downarrow}c^\dagger_{\boldsymbol{k}\uparrow} - c^\dagger_{-\boldsymbol{k}\uparrow}c^\dagger_{\boldsymbol{k}\downarrow}) = (-c^\dagger_{-\boldsymbol{k}\uparrow}c^\dagger_{\boldsymbol{k}\downarrow} - c^\dagger_{-\boldsymbol{k}\downarrow}c^\dagger_{\boldsymbol{k}\uparrow}) \\
&= -\Psi_{\text{pair}}(-\boldsymbol{k};\text{tpt},m=0) \\
T\Psi_{\text{pair}}(\boldsymbol{k};\text{tpt},m=\pm1)T^{-1} &= Tc^\dagger_{\boldsymbol{k}\sigma}c^\dagger_{-\boldsymbol{k}\sigma}T^{-1} = c^\dagger_{-\boldsymbol{k}\sigma'}c^\dagger_{\boldsymbol{k}\sigma'} = -c^\dagger_{\boldsymbol{k}\sigma'}c^\dagger_{-\boldsymbol{k}\sigma'} \\
&= -\Psi_{\text{pair}}(-\boldsymbol{k};\text{tpt},m=\mp1)\,,
\end{aligned} \tag{3.19}$$

and perform the analogous calculation in helicity space

$$\begin{aligned}
T\Psi_{\text{pair}}(\boldsymbol{k};\lambda,\lambda')T^{-1} &= Te^{i\alpha_{\lambda'}(\boldsymbol{k})}c^\dagger_{\boldsymbol{k}\lambda}c^\dagger_{-\boldsymbol{k}\lambda'}T^{-1} = e^{-i\alpha_{\lambda'}(\boldsymbol{k})}e^{i\alpha_\lambda(\boldsymbol{k})}c^\dagger_{-\boldsymbol{k}\lambda}e^{i\alpha_{\lambda'}(-\boldsymbol{k})}c^\dagger_{\boldsymbol{k}\lambda'} \\
&= -e^{i\alpha_\lambda(\boldsymbol{k})}c^\dagger_{-\boldsymbol{k}\lambda}c^\dagger_{\boldsymbol{k}\lambda'} = e^{i\alpha_\lambda(-\boldsymbol{k})}c^\dagger_{-\boldsymbol{k}\lambda}c^\dagger_{\boldsymbol{k}\lambda'} \\
&= e^{i\alpha_\lambda(-\boldsymbol{k})}e^{-i\alpha_{\lambda'}(-\boldsymbol{k})}\Psi_{\text{pair}}(-\boldsymbol{k};\lambda,\lambda') \\
T\Psi_{\text{pair}}(\boldsymbol{k};\lambda,\lambda)T^{-1} &= \Psi_{\text{pair}}(-\boldsymbol{k};\lambda,\lambda) \\
T\Psi_{\text{pair}}(\boldsymbol{k};\lambda,\lambda'\neq\lambda)T^{-1} &= -\Psi_{\text{pair}}(-\boldsymbol{k};\lambda,\lambda')\,.
\end{aligned} \tag{3.20}$$

Notice that these calculations are independent of any specific form of the phase $e^{i\alpha_\lambda(-\boldsymbol{k})}$ but can be derived by the general properties of T and in particular Equation 3.15 only. Only the last statement about unequal helicity pairing makes explicit use of Equation 3.14.

We use this information to calculate properties of the intra helicity superconducting gap function by demanding that the Hamiltonian H_{SC} be time-reversal invariant

$$\begin{aligned}
TH_{\text{SC}}T^{-1} &\stackrel{!}{=} H_{\text{SC}} \\
\sum_{\lambda,\boldsymbol{k}}\Delta^*_\lambda(\boldsymbol{k})\Psi_{\text{pair}}(-\boldsymbol{k};\lambda) + \text{h.c.} &= \sum_{\lambda,\boldsymbol{k}}\Delta_\lambda(\boldsymbol{k})\Psi_{\text{pair}}(\boldsymbol{k};\lambda) + \text{h.c.} \\
\sum_{\lambda,\boldsymbol{k}}\Delta^*_\lambda(-\boldsymbol{k})\Psi_{\text{pair}}(\boldsymbol{k};\lambda) + \text{h.c.} &= \sum_{\lambda,\boldsymbol{k}}\Delta_\lambda(\boldsymbol{k})\Psi_{\text{pair}}(\boldsymbol{k};\lambda) + \text{h.c.} \\
\Delta^*_\lambda(-\boldsymbol{k}) &= \Delta_\lambda(\boldsymbol{k})\,.
\end{aligned} \tag{3.21}$$

The restriction to pairing of electrons on the same band, which as we emphasize again is a very sensible assumption for the case of large spin-orbit coupling, constrains the gap function Δ to even functions of $\mathbf{k}$. This clearly goes beyond constraints imposed by the point group of the crystal which, even in the absence of inversion symmetry, allows for $\mathbf{k}$ even and odd pairing.

Equation 3.21 does not hold for superconductors that break time reversal symmetry spontaneously as it is merely a statement on the Fermi surface instability level. It is sensible to require the pairing interaction responsible for the Cooper pair formation

$$H_I = \sum_{\boldsymbol{k},\boldsymbol{q},\lambda,\lambda'} V_{\lambda\lambda'}(\boldsymbol{k},\boldsymbol{q})\Psi^{\dagger}_{\text{pair}}(\boldsymbol{q};\lambda')\Psi_{\text{pair}}(\boldsymbol{k};\lambda) \tag{3.22}$$

to be time reversal invariant. This restricts the mean-field Hamiltonian to terms given in Equation 3.21. An explicit determination of this restriction is most easily done by assuming a mean-field expansion of H_I in terms of real and even basis functions

$$d_i(\mathbf{k}) = d_i^*(\mathbf{k}) = d_i(-\mathbf{k}) \tag{3.23}$$

yielding

$$V_{\lambda\lambda'}(\mathbf{k},\mathbf{q}) = \sum_{ij} V_{ij,\lambda\lambda'} d_i(\mathbf{k}) d_j(\mathbf{q})\,. \tag{3.24}$$

Using Equation 3.20 we find that the matrix elements of a time reversal invariant interaction have to be real $V_{ij,\lambda\lambda'} = V^*_{ij,\lambda\lambda'}$. The restriction to even functions is a direct result of the fermionic antisymmetry and our constraint to intra-band pairing and does not constitute a further approximation.

Spontaneous time-reversal symmetry breaking is still possible for superconducting instabilities transforming as a degenerate irreducible representation (Irrep) of the point group. In this case, the gap function may acquire a non-trivial phase factor between the different components of the Irrep, leading to a finite imaginary part violating $\Delta^*_\lambda(-\boldsymbol{k}) = \Delta_\lambda(\boldsymbol{k})$ for the even basis functions $\Delta(-\boldsymbol{k}) = \Delta(\boldsymbol{k})$.

The helical degree of freedom manifests itself in the possibility to have different pairing amplitudes for the different helicities, like it would be possible in a multiband superconductor. The helical degree of freedom is closely connected to the spin of the Cooper pairs, allowing us to calculate the spin-singlet / triplet nature of the condensate from this information [31]

$$\Delta_{\sigma\sigma'}(\boldsymbol{k}) = \frac{\Delta_{\lambda=+}(\boldsymbol{k}) + \Delta_{\lambda=-}(\boldsymbol{k})}{2}\left[i\sigma_y\right]_{\sigma\sigma'} + \frac{\Delta_{\lambda=+}(\boldsymbol{k}) - \Delta_{\lambda=-}(\boldsymbol{k})}{2}\boldsymbol{g}(\boldsymbol{k})\left[\boldsymbol{\sigma} i\sigma_y\right]_{\sigma\sigma'}. \tag{3.25}$$

The limit of strong spin-orbit coupling and or small pairing amplitudes, is by definition fulfilled in the weak coupling renormalization group approach for any finite SOC. It is then natural to expect a vanishing superconducting gap function $\Delta_\lambda(\boldsymbol{k})$ whenever $|E_\lambda(\mathbf{k})| \gg 0$. Under these conditions Equation 3.25 predicts an precisely equal mixing between the spin-singlet and spin-triplet nature of the pairing wavefunction in the limit of strong spin-orbit coupling and inversion symmetry

breaking. This statement is slightly weakened in the vicinity of band-crossings, which may either occur accidentally or in case of Fermi surfaces in proximity of time reversal invariant momenta.

In contrast, the presence of inversion symmetry not only implies a restoration of the band degeneracy and therefore simultaneous formation of gaps for helicities. The spin degenerate system also naturally allows for inter-helicity pairing. Most importantly, however, inversion symmetry implies that the parity of a Cooper pair remains a good quantum number. This allows a strict separation between the (pseudo) spin singlet and triplet pairing wave functions as scattering between them is forbidden by symmetry [31, 81].

While such scattering elements are symmetry allowed in the case of inversion symmetry breaking and strongly spin-orbit coupled systems, they are not necessarily large. In contrast to the energy considerations that lead to a mixed singlet and triplet pair amplitude, the seeding fluctuations leading to this result may be of pure type. Once could then state that the opposite parity pairing is induced by the low energy projection. In the next section, we will now discuss some general facts about the half-Heusler material LuPtBi before applying the presented analysis to it's surface state.

3.3 LuPtBi - a prime candidate for unconventional superconductivity

Named after Friedrich Heusler [184], the so called Heusler compounds are a diverse class of materials with roughly 500 members [26]. In particular, ternary half Heusler compounds of XYZ composition (X,Y denote transition metal or rare-earth metals and Z a main group element) have recently received considerable interest due to their relevance for spintronic applications. Their strong tendency towards covalent bonding allows for the prediction of semiconducting properties in these compounds from a valence electron counting argument alone. In general, XYZ materials can be considered as YZ zinc-blende lattices (analogous to III-V semiconductors) that are filled with an additional X atom as displayed in Figure 3.1. Here we have indicated the zinc-blende lattice with bonds between the Y (grey) and Z atoms (yellow). Systems with 18 valence electrons like LuPtBi can be considered as a "sum" of positively charged X atoms (Lu^{3+}) and negatively charged zinc-blende structures [$(PtBi)^{3-}$] [185]. Accordingly, these systems can be expected to have semiconducting or at least semimetallic properties with remarkable electronic tunability [26].

Here, we study the half-Heusler compound LuPtBi which crystallizes in the non-symmorphic space group (SG) F-43m (# 216) [69, 186]. At temperatures $T > T_c$, this material a semimetal and features a quadratic band touching point near the Fermi energy [187, 188]. More generally, bulk LnPtBi (Ln=La, Y,Lu) is a prime candidate for unconventional topological superconductivity

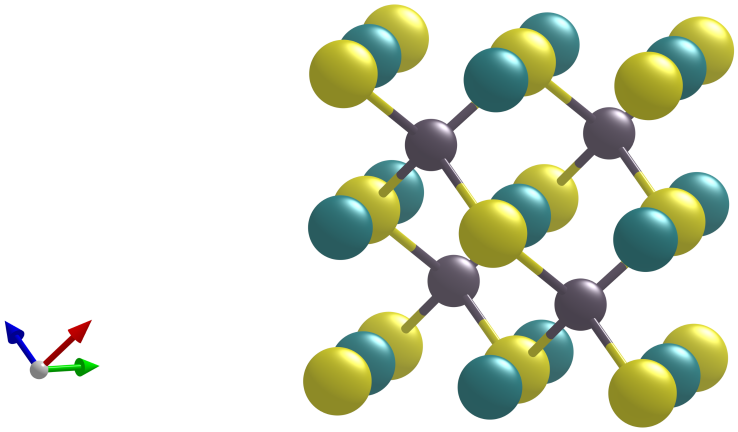

Figure 3.1: Crystal structure of the half-Heusler compound LnPtBi which crystallizes in the non-symmorphic space group F-43m (# 216). Yellow (grey) sites correspond to Bi (Pt) atoms forming a zinc-blende structure, while the green sites indicate the Ln site which is occupied by Lu and Y for LuPtBi and YPtBi respectively. Note that the arrows indicate the conventional crystal axes for half-Heusler structures and are distinct from those in Figure 3.2 (b).

with reported T_c's of ≈ 1 K [69, 189, 190]. While relativistic effects due to spin-orbit coupling are expected to be highly relevant in all of these compounds due to the presence of heavy elements Pt and Bi (with atomic numbers $Z = 78, 83$ respectively), LuPtBi is special in the sense that Lu ($Z = 71$) is the heaviest Lanthanide option for this half-Heusler system.

Several interesting bulk superconducting states for LnPtBi have already been proposed [70, 71, 187, 191–193] and even experimentally established for LuPdBi [194]. A common thread between all these proposals is the fusion of spin-orbit coupling induced $j = 3/2$ Fermion physics near the Fermi level and bulk inversion symmetry breaking due to the non-symmorphic crystal structure. This symmetry breaking generically leads to mixing between singlet and triplet pairing states as we discussed for surfaces in the previous section. The existence of fermionic quasi-particles with higher angular momentum (at least near the $\mathbf{k} = \mathbf{0}$, Γ point) can be understood from a combination of a p-orbital derived degeneracy and the two-fold spin-degeneracy at time-reversal invariant momenta. Strong spin-orbit coupling can then yield an effective $j = 3/2$ angular momentum excitation spectrum close to Γ: $(l = 1) \otimes (s = 1/2) = (j = 1/2) \oplus (j = 3/2)$. For or LnPtBi, the resulting four-fold degenerate state is in close proximity to the Fermi level, as one can see from band structure calculations [187].

The proximity of the Fermi level to this quadratic band touching point, combined with the absence of other bands at the Fermi level, explains the semimetallic properties of LnPtBi. Semimetals feature a small density of states, which is detrimental to high superconducting transition temperatures T_c as we have seen in Equation 1.115. This observation provoked Meinert [195] to ask the question whether the electron phonon coupling in LnPtBi is strong enough to explain the observed $T_c \approx 1\,\mathrm{K}$. While this transition temperature is small in absolute terms, making electron phonon coupling a likely candidate, it is large in relation to the observed small density of states. Based on *ab-initio* electron-phonon calculations for YPtBi, Meinert ruled out a phonon based mechanism and arrived at the strong statement that "it is safe to conclude that an unconventional mechanism is responsible for the superconductivity in YPtBi" [195]. Due to the strong structural similarities in the LnPtBi material class, it is most likely that these results hold for LuPtBi as well.

An at first glance completely unrelated, but nevertheless intriguing, experimental fact about YPtBi and LuPtBi is the existence of a (topologically trivial) metallic surface state. This flat metallic state emerges at the Bi terminated (111) crystal surface depicted in Figure 3.2 and has recently been observed by angle resolved photoemission spectroscopy (ARPES). It is well captured by conventional *ab-initio* electronic structure calculations [196]. Intuitively we can understand the existence with the absence of Pt atoms as covalent bond partners for the Bi atoms at the surface termination, leading to dangling bonds which then form the observed flat and surface localized bands.

Combining all this evidence with reports indicating that a small fraction of its electronic density of states undergoes a superconducting transition at $T_c \approx 6\,\mathrm{K}$ [197], we identify LuPtBi as a highly interesting instance of unconventional surface superconductivity. We suggest that the particularly flat surface bands for LuPtBi's Bi(111) termination could trigger a first superconducting transition T_c^{surface}, prior to the bulk superconducting transition at some lower T_c^{bulk}. A detailed analysis of the surface band structure and its symmetry properties is necessary, before continuing the analysis of unconventional superconductivity in this surface state.

Metallic surface state of LuPtBi

The Bi(111) surface termination (compare Figure 3.2) of LuPtBi features flat metallic surface states with strong spin-orbit coupling. Combined with the inversion symmetry breaking caused by the interface, a significant spin splitting of the surface bands, induced by Rashba spin-orbit coupling, can be expected.

In order to gain quantitative insight into this band structure, we employed density functional theory (DFT) based calculations from first principles for a slab of material. A non-primitive setting for the unit cell with broken translational symmetry in the $\boldsymbol{e}_z = \boldsymbol{a}_3$ direction was chosen, yield-

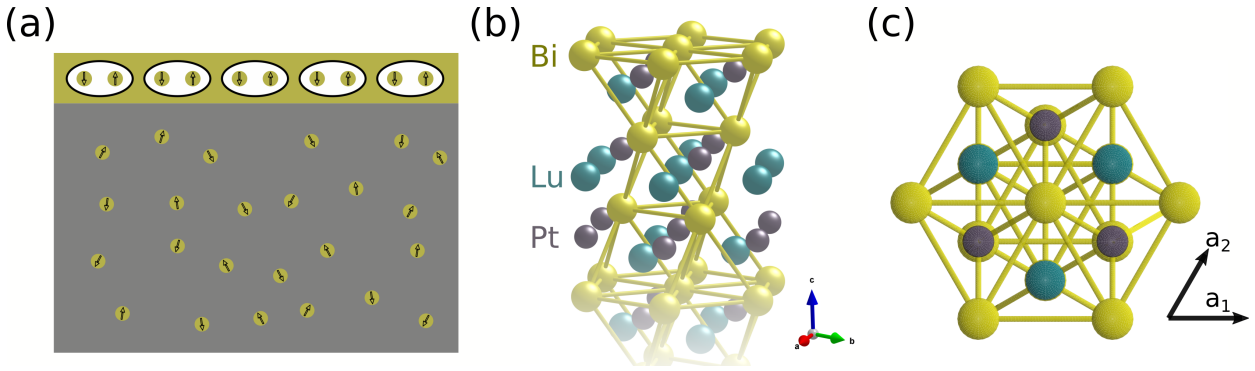

Figure 3.2: (a) Schematic representation of surface superconductivity. (b) Bulk crystal structure of LuPtBi. One can clearly see the half Heusler crystal structure along the (111) crystal direction chosen as the c-axis. (c) Sketch of the surface crystal structure constituted by a triangular lattice of Bi atoms, whose inversion symmetric C_{6v} point group symmetry is broken down to C_{3v} by the presence of Lu and Pt atoms in the layers below.

ing the two dimensional space group P3m1 (SG # 156 = plane group # 14). More precisely, the chosen hexagonal supercell consists of six unit cells and 22.5 Å of vacuum. The numerical calculation was performed by my collaborator Domenico di Sante [145], using a projector-augmented plane-wave method [30] for the DFT as it is implemented in the Vienna *ab-initio* simulation package (VASP) [198]. Employing the generalized gradient approximation (GGA) as parametrized by the Perdew, Burke and Ernzerhof (the PBE-GGA functional) for the exchange-correlation potential [199], the Kohn-Sham wave functions were expanded into plane waves up to an energy cutoff of 300 eV [200]. The Brillouin zone was sampled on a dense $16 \times 16 \times 1$ regular mesh and relativistic effects were included self-consistently. Figure 3.3 shows the resulting bands as grey lines along the high symmetry path of the surface Brillouin zone.

Our *ab-initio* calculation confirms the existence of metallic surface states. We find that the least dispersive low-energy bands emerge from dangling bonds of the Bi p_z orbitals at the crystals surface, as expected from a simple covalent bonding picture. Due to its dominant contribution to the density of states at the Fermi level as well as its highly non-trivial Fermi surface topology, we restrict our analysis to this band. The small Fermi surface pocket centred around Γ seen in experiment [196] is dominated by strongly dispersing Bi p_x and p_y orbitals. While it is well captured by our DFT calculation, we neglect its contribution to the surface low-energy model due to its small density of states at the Fermi level and nearly circular shape. The influence of non-trivial Fermi surface topology, as well as the comparative irrelevance of small circular pockets in the Brillouin center for unconventional superconductivity, becomes clear from our benchmark results presented in Chapter 2, where the pairing strength vanishes for small fillings.

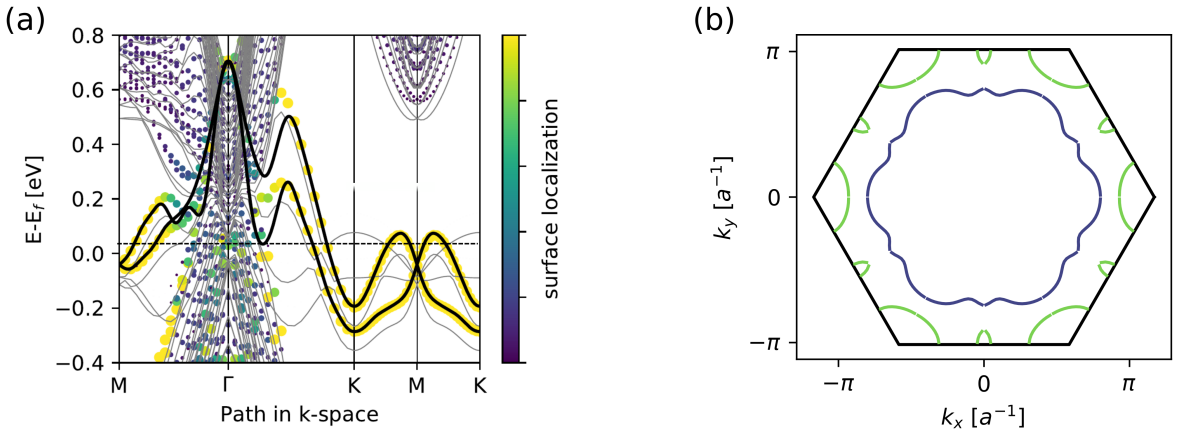

Figure 3.3: (a) The Bi(111) terminated surface band structure of LuPtBi as obtained by DFT as thin grey lines. The overlaid dots indicate the surface localization in the compuational supercell and continuous black lines represent a fit to the calculation obtained by using maximally localized Wannier functions on the Bi surface. Bands without any points overlaid are localized on the opposite surface with a different termination. (b) The resulting Fermi surface from the Wannier model presented in panel (a) features two helicity sheets highlighted in different colours. The conventional high symmetry points were introduced in Figure 2.4.

We use the framework of maximally localized Wannier functions as it is implemented in the VASP2WANNIER90 interface [201, 202] in order to obtain a best fit tight binding model for these bands, using a *single* Bi p_z orbital on the 1a Wyckoff position of the P3m1 space group as the starting point. Figure 3.3 shows the resulting band structure overlaid as a black line and in comparison to the *ab-initio* data. The resulting tight-binding Hamiltonian can be written as

$$\hat{H}_0 = \sum_{\boldsymbol{k}} \psi^\dagger_{\boldsymbol{k}} (\epsilon(\boldsymbol{k}) + \boldsymbol{g}(\boldsymbol{k})\boldsymbol{\sigma}) \psi_{\boldsymbol{k}} = \sum_{\boldsymbol{k}} \psi^\dagger_{\boldsymbol{k}} h(\boldsymbol{k}) \psi_{\boldsymbol{k}} , \tag{3.26}$$

with the combined creation operator

$$\psi^\dagger_{\boldsymbol{k}} = (c^\dagger_{\boldsymbol{k},\uparrow} , c^\dagger_{\boldsymbol{k},\downarrow}) , \tag{3.27}$$

for up (down) spin electrons $c^\dagger_{\boldsymbol{k}\uparrow}$ ($c^\dagger_{\boldsymbol{k}\downarrow}$) at momenta $\boldsymbol{k}$. The parameters for the functions $\epsilon(\boldsymbol{k})$ and $\boldsymbol{g}(\boldsymbol{k})$ based on these calculations are published in [145]. The strong spin-orbit coupling of Bi, modelled by $\boldsymbol{g}(\boldsymbol{k})$ in Equation 3.26 results in a significant splitting of the bands due to the broken inversion symmetry on the crystals surface. Kramers theorem protects a two-fold degeneracy of the band at the time-reversal invariant momenta Γ and M and a linear dispersion is realized in the vicinity of the latter. As before, we label the systems energy eigenstates with their helicity eigenvalue $\lambda = \pm 1$, where the helicity operator $\Lambda_{\boldsymbol{k}}$ is defined as the normalized spin-orbit coupling

term in the Hamiltonian. The colour of the Fermi surface pockets depicted in Figure 3.3 labels the helicity eigenvalue of different points on the Fermi surface, simultaneously indicating the opposite chirality of the spin texture of the corresponding pockets.

From a symmetry perspective, the Γ-point of the surfaces P3m1 SG is invariant under the C_{3v} point group (PG). While the the Bi atoms at the surface form a triangular lattice and one could accordingly expect a C_{6v} PG, the C_2 rotation symmetry of the surface is spoilt. This becomes clear upon considering Figure 3.2 (a) and realizing that, while the system is invariant under a mirror operation along the $\boldsymbol{a}_1 + \boldsymbol{a}_2$ direction, it exchanges the positions of Lu and Pt under the $\boldsymbol{a}_2 - \boldsymbol{a}_1$ mirror, resulting in a breaking of the C_{6v} symmetry of the triangular Bi lattice.

These symmetry considerations are not only crucial for the analysis of finite angular momentum Cooper pairing presented in the next section, but also allow for an additional term in the tight-binding Hamiltonian Equation 3.26. Most obvious is the absence of a second symmetry (beyond time reversal symmetry) that maps $\mathbf{k} \to -\mathbf{k}$ at the K point. For C_{6v} symmetric systems, the combination of C_2 rotation and time reversal enforces a Kramers degeneracy at the K point, even in the presence of spin-orbit coupling and spoilt inversion symmetry. Kane and Mele [203] pointed out, that spin-orbit coupling allows for an additional term (which preserves all symmetries in Graphene as the two sublattices interchange under C_2), that goes beyond Rashba spin-orbit coupling. In a triangular lattice, such a term is only present for models with the reduced C_{3v} PG symmetry.

Based on this symmetry analysis we now construct a symmetry respecting tight-binding model with ten parameters. Seven of these parameters describe a seventh nearest neighbour tight-binding model on a triangular lattice, while the remaining three describe relativistic effects. We employ two parameters for the nearest and second nearest neighbour Rashba spin-orbit coupling and the final parameter describes a Kane Mele term on the nearest neighbour bonds. Using this parametrization we write

$$\epsilon(\boldsymbol{k}) = 2 \sum_{n=1}^{7} t_n \sum_{\mathbf{d} \in \{\mathbf{d}_n\}} \cos(\mathbf{k}\mathbf{d}) \,, \tag{3.28}$$

where t_n are the hopping amplitude parameters and the $\mathbf{d}_n$ run over all (translation symmetry and C_2 rotation inequivalent) real space distance vectors separating nth nearest neighbours. Letting $\mathbf{a}_3 = \mathbf{a}_2 - \mathbf{a}_1$, we have

$$\{\mathbf{d}_1\} = \{\mathbf{a}_1, \mathbf{a}_2, \mathbf{a}_3\} \tag{3.29}$$

for nearest neighbours,

$$\{\mathbf{d}_2\} = \{\mathbf{a}_1 + \mathbf{a}_2, \mathbf{a}_2 + \mathbf{a}_3, \mathbf{a}_3 - \mathbf{a}_1\} \tag{3.30}$$

t_1	t_2	t_3	t_4	t_5	t_6	t_7
52.024	−21.341	−0.596	21.519	9.557	0.088	4.32

α_{R_1}	α_{KM}	α_{R_2}
23.887	11.283	−17.104

Table 3.1: Best fit tight-binding hopping matrix elements for a simple ten parameter model, approximating the Wannier model data presented in Figure 3.3. All values are given in meV.

for next nearest neighbours and so on. For the relativistic effects, we write

$$\boldsymbol{g}(\boldsymbol{k}) = \alpha_{R_1}\boldsymbol{g}_{R_1}(\boldsymbol{k}) + \alpha_{R_2}\boldsymbol{g}_{R_2}(\boldsymbol{k}) + \alpha_{KM}\boldsymbol{g}_{KM}(\boldsymbol{k})\,. \tag{3.31}$$

The Rashba spin-orbit coupling terms are given by

$$\boldsymbol{g}_{R_1}(\boldsymbol{k}) = \begin{pmatrix} -\sqrt{3}\sin(\mathbf{k}\mathbf{a}_2) - \sqrt{3}\sin(\mathbf{k}\mathbf{a}_3) \\ 2\sin(\mathbf{k}\mathbf{a}_1) + \sin(\mathbf{k}\mathbf{a}_2) - \sin(\mathbf{k}\mathbf{a}_3) \\ 0 \end{pmatrix} \tag{3.32}$$

and

$$\boldsymbol{g}_{R_2}(\boldsymbol{k}) = \begin{pmatrix} -\sqrt{3}\sin[\mathbf{k}(\mathbf{a}_1+\mathbf{a}_2)] - 2\sqrt{3}\sin[\mathbf{k}(\mathbf{a}_2+\mathbf{a}_3)] - \sqrt{3}\sin[\mathbf{k}(\mathbf{a}_3-\mathbf{a}_1)] \\ 3\sin[\mathbf{k}(\mathbf{a}_1+\mathbf{a}_2)] - 3\sin[\mathbf{k}(\mathbf{a}_3-\mathbf{a}_2)] \\ 0 \end{pmatrix}. \tag{3.33}$$

Finally, the Kane Mele term $\boldsymbol{g}_{KM}(\boldsymbol{k}) \parallel \mathbf{e}_z$ is given by

$$\left(\boldsymbol{g}_{KM}(\boldsymbol{k})\right)_z = -2(\sin(\mathbf{k}\mathbf{a}_1) - \sin(\mathbf{k}\mathbf{a}_2) + \sin(\mathbf{k}\mathbf{a}_3))\,. \tag{3.34}$$

Using this parametrization and the wannierized DFT data as a starting point, we performed a Monte Carlo parameter search, optimizing for an overlap between the energy eigenstates of H with special focus close to the Fermi level. The best fit model parameters are presented in Table 3.1. All following calculations were performed directly on the full Wannier model obtained from DFT as well as this minimal model, resulting in virtually identical results.

Having discussed the arena for the formation of unconventional surface superconductivity in LuPtBi, we now turn to the investigation of the obtained model via the wcRG and RPA methods as presented in Chapter 1.

3.4 Chiral surface superconductivity in LuPtBi

As a first step towards the analysis of electronic correlation effects in our model, this section starts with an analysis of the relevant particle-hole fluctuations in the non-interacting system. In a second step we will then discuss how these fluctuations modify the effective interaction in the Cooper channel within the RPA and wcRG discussed in Chapter 1. We find a chiral superconducting condensate featuring Majorana edge modes to be energetically favoured.

Particle-hole fluctuations in the LuPtBi surface state

Due to the absence of multiple orbital or sublattice degrees of freedom the most general (static and onsite) particle-hole excitations in the LuPtBi surface state are represented by the operator

$$S^{\eta}(\boldsymbol{q}) = \sum_{\boldsymbol{k}} \sum_{\sigma_0,\sigma_2} c^{\dagger}_{\boldsymbol{k}+\boldsymbol{q},\sigma_2} \sigma^{\eta}_{\sigma_2\sigma_0} c_{\boldsymbol{k},\sigma_0} \,. \tag{3.35}$$

Following Section 1.4.1, we calculate the static susceptibility matrix in the non-interacting limit as

$$\chi_{\eta\mu}(\boldsymbol{q}, \omega = 0) = \langle S^{\eta}(\boldsymbol{q}) S^{\mu}(-\boldsymbol{q}) \rangle_0 \,. \tag{3.36}$$

In contrast to systems without spin-orbit coupling, this matrix is neither diagonal nor proportional to the identity matrix. In a system where the spin and momentum degrees of freedom are coupled, it is intuitive that the magnetic response of the spin system depends on the alignment of the external magnetic field with respect to the crystal. In Figure 3.4, once can clearly see this effect.

For magnetic fields without any real space modulation, the susceptibility at $\mathbf{Q} = \mathbf{0}$ shows that the systems response differs between electric fields, in plane and out of plane magnetic fields, reflecting the inversion symmetry breaking along the $\mathbf{e}_z$ direction. Finite transfer momenta $\mathbf{Q}$ correspond to periodically modulated external fields in real space with the appropriate reciprocal length scale. The additional symmetry breaking of such an external field further splits the in plane response function. A second qualitative difference between finite $\mathbf{Q}$ response functions for systems with finite spin-orbit coupling and ones with SU(2) symmetry is the general finite value of off-diagonal response functions χ_{xy}, χ_{xz} and χ_{yz}. Since the associated energy scale for these is an order of magnitude smaller then their diagonal counterpart, we only present the obtained data

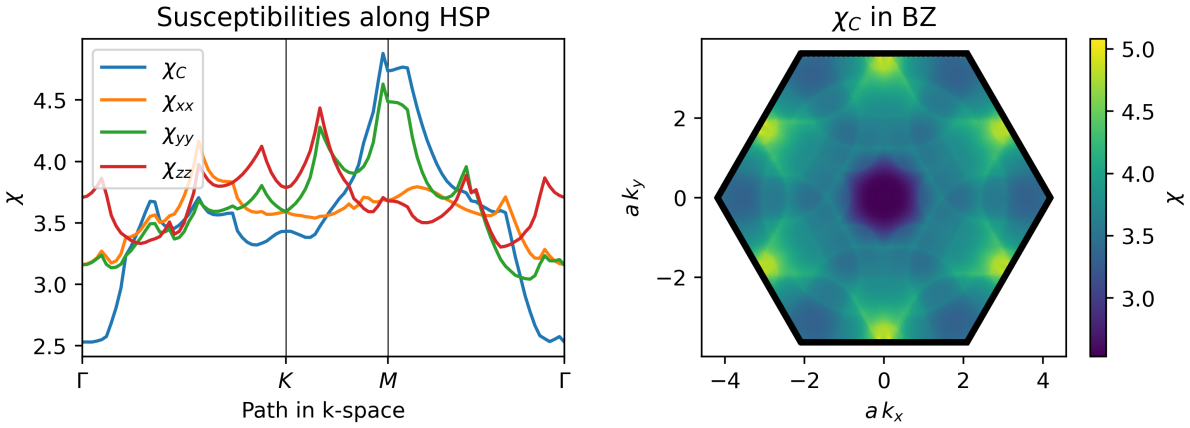

Figure 3.4: Bare particle hole susceptibilities χ_{xx}, χ_{yy}, χ_{zz} and χ_C of the LuPtBi surface state model for $n = 0.62$. In the left panel, we compare the different diagonal spin contributions along scenarios along the high symmetry path through the Brillouin zone. We emphasize the location of the maximum of χ_{yy} and χ_C close to the M point, especially in comparison to Figure 2.9. The right panel shows the $C_(6v)$ symmetric charge susceptibility for the surface state in the complete first Brillouin zone.

in Appendix C. We note that the residual time-reversal symmetry of our model forbids mixing between the onsite charge and spin fluctuations *i.e.*, $\chi_{0u} = 0$ for all $u \in \{x, y, z\}$.

Using these results, we can now employ a generalized Stoner criterion to obtain the energetically favoured particle-hole instability on RPA level as discussed in Section 1.4.4. Assuming a purely onsite Hubbard interaction U, we find that the RPA susceptibility diverges for all $U > 0.37\,\text{eV}$, approximately one third of the bandwidth W. Since the susceptibility first diverges at an incommensurate transfer momentum, the associated ordering vector $\mathbf{Q}$ is six (6) fold degenerate. One ordering vector associated with the smallest value of U that still results in a diverging magnetic susceptibility has an ordering vector $\mathbf{Q}_1 = [(1+\delta)\mathbf{b}_1 + (1-\delta)\mathbf{b}_2]/2$ with ($\delta \approx 0.016$). Accordingly, the magnetic instability is approximately associated with a commensurate ordering vector at the Brillouin zones three M points. In real space, this corresponds to nearest neighbour stripe antiferromagnetic order on the triangular lattice formed by the Bi atoms. The geometric frustration of the triangular lattice renders a true antiferromagnetic state impossible and three degenerate types of stripe magnetism are energeti[t]cally equivalent for triangular lattice Hubbard models close to the van Hove singularity (also compare Figure 2.5).

The imperfect nesting of the Fermi surface for this realistic material model induces a slight incommensurability which we parametrize by δ. In Figure 3.6 one can see the consequence of this in real space for one, arbitrarily chosen ordering vector $\mathbf{Q}_1 = (1.02, 0.55)\pi/a$ (with triangular lattice constant a). The close up view in the right panel reveals the approximate nearest neighbour

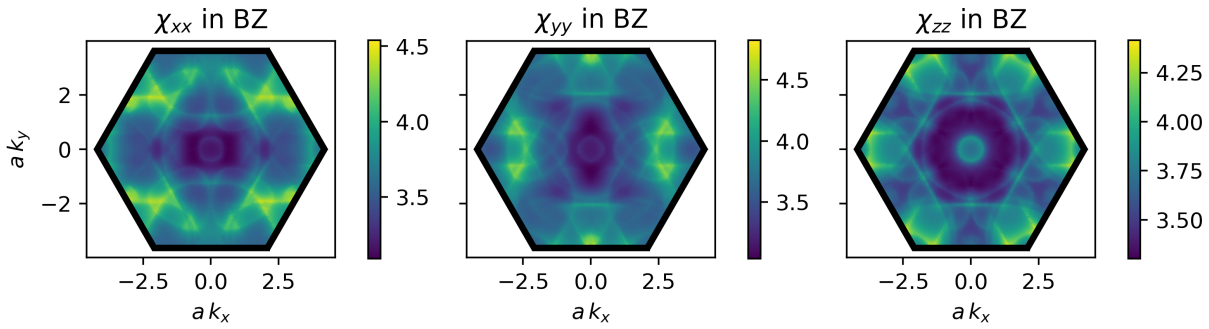

Figure 3.5: Bare particle hole susceptibilities $\chi_{xx}, \chi_{yy}, \chi_{zz}$ of the LuPtBi surface state model for $n = 0.62$ in the whole BZ as a function of transfer momentum $\mathbf{Q}$. We note the absence of C_3 rotation symmetry for in plane magnetic fields with finite transfer momentum.

stripe antiferromagnet, while the large scale overview on the left demonstrates the additional real space modulation of this magnetic order.

This is most clearly understood by first writing the transfer momentum as a sum of commensurate and incommensurate part

$$\begin{aligned} \mathbf{Q}_1 &= \mathbf{Q}_c + \mathbf{Q}_i \\ \mathbf{Q}_c &= \frac{\mathbf{b}_1 + \mathbf{b}_2}{2} \\ \mathbf{Q}_i &= \delta \frac{\mathbf{b}_1 - \mathbf{b}_2}{2}, \end{aligned} \tag{3.37}$$

in terms of the reciprocal lattice vectors $\mathbf{b}_1$ and $\mathbf{b}_2$. It is now natural to define real space vectors $\mathbf{R}_c$ and $\mathbf{R}_i$ such that $\mathbf{R}_c\mathbf{Q}_c = \pi$ and $\mathbf{R}_i\mathbf{Q}_i = \pi$ *i.e.*, vectors that define half period cycles of the orderings periodicity pattern. While these equations do not have a unique solution,

$$\begin{aligned} \mathbf{R}_c &= \frac{\mathbf{a}_1 + \mathbf{a}_2}{2} \\ \mathbf{R}_i &= \frac{1}{\delta} \frac{\mathbf{a}_1 - \mathbf{a}_2}{2} \end{aligned} \tag{3.38}$$

are a natural choice as they are the shortest vectors with this property. All other solutions correspond to rotated and elongated real space vectors that result in an identical oscillation pattern. The black arrow in the left (right) panel of Figure 3.6 corresponds to $\mathbf{R}_i$ ($\mathbf{R}_c$) respectively.

So far, the discussion would have been very similar for an incommensurate spin density wave order of a SU(2) symmetric model. In the case of spin-orbit coupling, the matrix structure of $\chi_{uu'}(\mathbf{Q}_1)$ is non-trivial. The eigenvector M_u of the matrix, with largest eigenvalue is associated with the instability, while the other two eigenvectors are energetically disadvantageous for the

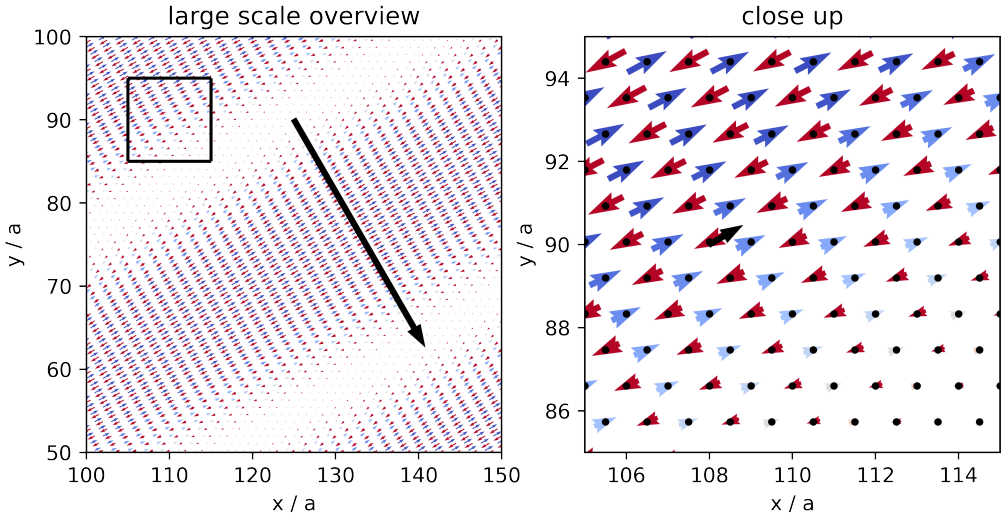

Figure 3.6: Example of a spin density wave instability of the LuPtBi surface state on RPA level as obtained from a general Stoner criterion. The spin spiral with $\mathbf{Q}_1 = [(1+\delta)\mathbf{b}_1 + (1-\delta)\mathbf{b}_2]/2$ is well approximated by a nearest neighbour stripe antiferromagnet as one can see in the right panel close up. The large scale overview shows the close up region as well as the long range incommensurate oscillation with real space period $\mathbf{R}_i$. Due to SOC, the spin degree of freedom is frozen to the real space magnetic pattern. The arrow on each lattice point was chosen proportional to the semi-classical in plane magnetization of the order parameter while the out of plane component in positive (negative) z direction is encoded by the red (blue) colour coding.

system. This allows us to predict an "easy"-axis for the present AFM state and plot the complete semi-classical spin spiral

$$\langle S^u(\mathbf{r})\rangle = |M_u|\cos(\mathbf{Q}\mathbf{r}+\varphi)\,, \tag{3.39}$$

with $M_u = |M_u|e^{i\varphi}$. We note that the necessity for a real expectation value constrains the ordering to simultaneously occur at $\mathbf{Q}_1$ and $-\mathbf{Q}_1$ and that the gauge degree of freedom in the choice of the eigenvector M_u is tied to the spontaneous translation symmetry breaking of the spin spiral. Since this work focuses on Fermi surface instabilities and superconductivity, we did not investigate the ground state magnetic solution further. Such an analysis would require the consideration of multi-Q magnetism in order to determine the precise point group symmetry breaking associated with the instability [204].

C_{3v}	A_1	A_2	E
$\mathbb{1}$	+1	+1	+2
C_3	+1	+1	−1
m_v	+1	−1	0
C_2			

$\langle\phi\rangle$	A_1	E_g	E'_g	A_2	E_u	E'_u
$\mathbb{1}$	+1	+1	+1	+1	+1	+1
C_3	+1	$-\frac{1}{2}$	$-\frac{1}{2}$	+1	$-\frac{1}{2}$	$-\frac{1}{2}$
m_v	+1	+1	−1	−1	−1	+1
C_2	+1	+1	+1	−1	−1	−1

Table 3.2: C_{3v} character table (left) and symmetry characters (right) of real space representations for the nearest neighbour form factors shown in Figure 3.7. The operation C_2 is not part of the C_{3v} point group (PG), therefore the corresponding line of the transposed character table is left empty. Nevertheless, we constructed real space representations with a defined transformation behaviour under this operation E_g and E_u. Note that these representations may generically mix under the C_{3v} PG.

Cooper pair symmery in a C_{3v} symmetric system with spin-orbit coupling

As a last preparation for the evaluation of the effective Cooper pair interaction mediated by the previously discussed particle-hole fluctuations, we will discuss constraints on the pairing wave function that can be deduced from locality of Cooper pair states and point group symmetry constraints alone.

In order for the superconducting mean field Hamiltonian in Equation 3.17 to be invariant under all point group symmetries of the free theory, the superconducting order parameter Δ has to transform according to irreducible representations of the crystallographic point group [82]. For the C_{3v} point group of the LuPtBi surface state we find three distinct possibilities for the representation of the gap function A_1, A_2 and E in the corresponding group theory tables [205]. While A_1 and A_2 are scalar representations, E is a two-fold degenerate representation. The C_{3v} character table as well as an overview of the symmetry operator expectation values for the presented basis functions is given in Table 3.2

Here, we present all form factor functions $\Phi(\mathbf{k})$ transforming as irreducible representations of C_{3v} up to nearest neighbour Cooper pairing. In addition to the onsite A_1 case, this requires us to give six (6) orthogonal basis functions, *i.e.*, we need to give more than one set of functions for one of the representations ($N_{A_1} + N_{A_2} + N_E = 1 + 1 + 2 = 4$). It turns out that it is possible to construct two additional basis functions in the E representation that are not trivially obtained via the routine

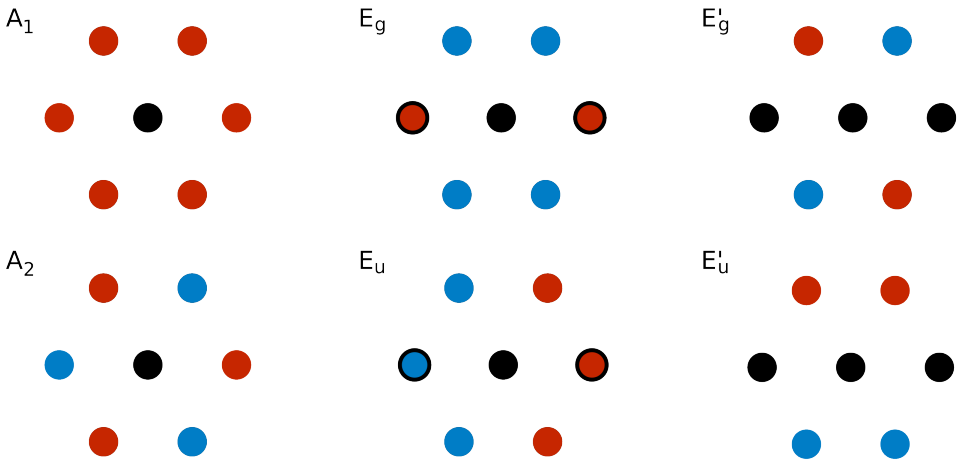

Figure 3.7: We present the real space structure of possible pairing wave functions as obtained from Table 3.2. Circles with black border are weighted twice, black circles indicate zero and blue (red) circles indicate a minus (plus) sign of the corresponding representation. Starting at the rightmost circle and in counter clockwise ordering, the states can be denoted as $A_1 = (+1,+1,+1,+1,+1,+1)$, $A_2 = (+1,-1,+1,-1,+1,-1)$, $E_g = (+2,-1,-1,+2,-1,-1)$, $E'_g = (0,-1,+1,0,-1,+1)$, $E_u = (+2,+1,-1,-2,-1,+1)$ and $E'_u = (0,+1,+1,0,-1,-1)$.

given by in the appendix of [82]:

$$
\begin{aligned}
\Phi^{A_1} &= 1\ ,\ \sqrt{\frac{2}{3}}\Big(\cos(k_x) + 2\cos(k_x/2)\cos\big(\sqrt{3}k_y/2\big)\Big)\\
\Phi^{A_2} &= \sqrt{\frac{2}{3}}\Big(\sin(k_x) - 2\sin(k_x/2)\cos\big(\sqrt{3}k_y/2\big)\Big)\\
\Phi^{E_g} &= \frac{2}{\sqrt{3}}\Big(\cos(k_x) - \cos(k_x/2)\cos\big(\sqrt{3}k_y/2\big)\Big)\\
\Phi^{E'_g} &= \cos\Big(k_x/2 + \sqrt{3}k_y/2\Big) - \cos\Big(k_x/2 - \sqrt{3}k_y/2\Big)\\
\Phi^{E_u} &= \frac{2}{\sqrt{3}}\Big(\sin(k_x) + \sin(k_x/2)\cos\big(\sqrt{3}k_y/2\big)\Big)\\
\Phi^{E'_u} &= \sin\Big(k_x/2 + \sqrt{3}k_y/2\Big) - \sin\Big(k_x/2 - \sqrt{3}k_y/2\Big)\,.
\end{aligned}
\tag{3.40}
$$

These form factors have been chosen to be real and orthonormal with respect to the scalar product

$$
\langle\Phi_1|\Phi_2\rangle = \frac{1}{A_{\mathrm{BZ}}}\int_{\mathrm{BZ}} \Phi_1^*(\boldsymbol{k})\Phi_2(\boldsymbol{k})\,\mathrm{d}\boldsymbol{k} \tag{3.41}
$$

and their corresponding real space configurations are displayed in Figure 3.7.

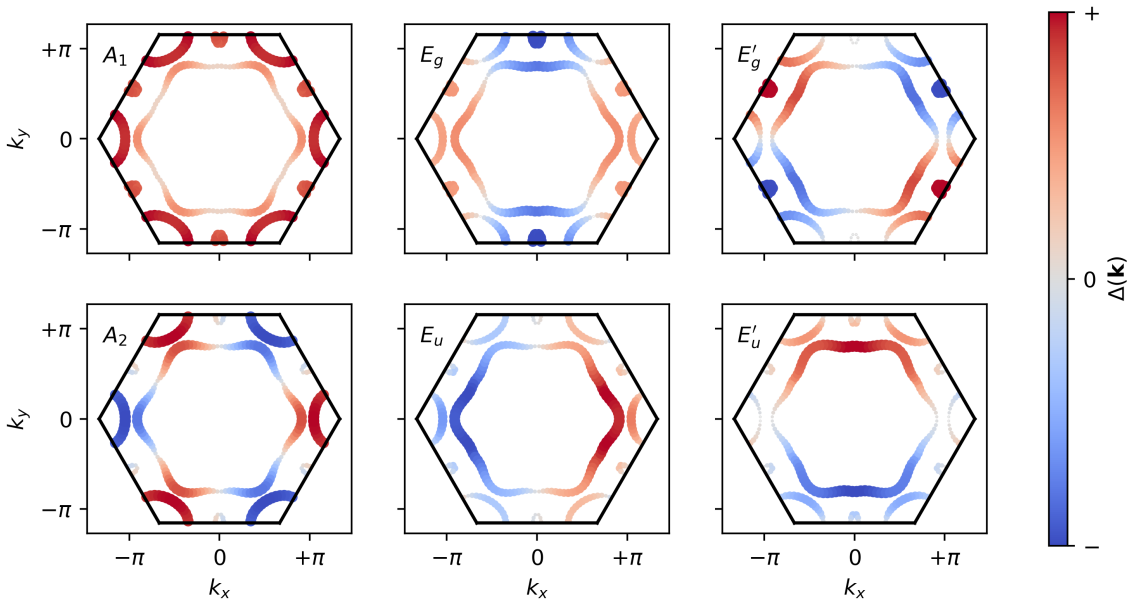

Figure 3.8: We present the evaluation of the analytically obtained gap functions from Figure 3.7 in momentum space, evaluated on the LuPtBi Fermi surface. The point size along the Fermi surface was chosen proportional to the order parameter (normalized over the complete BZ) value at that point. The color coding denotes the same information and additionally provides the sign of the (real) order parameter at each point. One can clearly see the different line nodes of the order parameters with finite angular momentum, while the A_1 line node is a circle inside the hexagonal center Fermi surface and therefore not visible.

In order to make a connection to the LuPtBi surface state, we present the resulting pairing wave function on the Fermi surface of our tight-binding model in Figure 3.8. We present the even pairing functions corresponding to the energetically favoured intra helicity pairing in the first line and note in passing that all considered gap functions are not affected by the bare on site Hubbard interaction.

Effective Cooper pair interaction

Following Section 3.2 we now introduce a basis of Cooper pair states for our model. Since a parametrization in terms of singlet and triplet states is not possible due to the lack of inversion symmetry, we consider pairs of electrons connected by the time-reversal operator $\hat{T} = i\sigma_y\mathcal{K}$, neglect inter-band pairing amplitudes due to $\alpha_R \gg \Delta$ and define

$$\Psi^\dagger_{\text{pair}}(\boldsymbol{k};\lambda) = c^\dagger_{\boldsymbol{k}\lambda} T c^\dagger_{\boldsymbol{k}\lambda} T^{-1} = \sum_{\sigma,\sigma'} \psi_{\lambda,\sigma\sigma'}(\boldsymbol{k}) c^\dagger_{\boldsymbol{k}\sigma} c^\dagger_{-\boldsymbol{k}\sigma'} , \tag{3.42}$$

with

$$\psi_{\lambda,\sigma\sigma'}(\boldsymbol{k}) = \sum_{\sigma''} u_{\lambda,\sigma}(\boldsymbol{k}) u^*_{\lambda,\sigma''}(\boldsymbol{k}) (i\sigma_y)_{\sigma''\sigma'} \,. \tag{3.43}$$

We emphasize again that our setup allows us to circumvent any issues arising from the global gauge freedom of $u_{\lambda,\sigma}(\boldsymbol{k})$ at different momenta that would arise from naively choosing $c^\dagger_{\boldsymbol{k}\lambda} c^\dagger_{-\boldsymbol{k}\lambda}$ as the basis for the pairing wave function.

Using this parametrization as a starting point we calculate the system's propensity towards different superconducting instabilities. To this end we implement a perturbative interaction term into our model Hamiltonian

$$\hat{H} = \hat{H}_0 + U_0 \sum_{\boldsymbol{k}} c^\dagger_{\boldsymbol{k},\uparrow} c^\dagger_{\boldsymbol{k},\downarrow} c_{\boldsymbol{k},\downarrow} c_{\boldsymbol{k},\uparrow} \,, \tag{3.44}$$

and calculate how it is screened by particle-hole excitations. In contrast to systems with SU(2) symmetry, the bare particle-hole (PH) susceptibility of our model can't be reduced to a single momentum dependent number as discussed before. For the analysis of superconductivity it is more convenient to consider the generalized particle-hole susceptibility without a conversion into the spin and charge operator basis

$$\chi^0_{\{\sigma_i\}}(\boldsymbol{k}, \tau) = \sum_{\boldsymbol{l}} \langle T_\tau c^\dagger_{\boldsymbol{l}+\boldsymbol{q},\sigma_2}(\tau) c_{\boldsymbol{l},\sigma_1}(\tau) c^\dagger_{\boldsymbol{l},\sigma_3}(0) c_{\boldsymbol{l}+\boldsymbol{q},\sigma_0}(0) \rangle \tag{3.45}$$

where we used the imaginary time-ordering operator T_τ. We calculate it's Fourier transform in the static limit using standard Matsubara summation techniques for the frequency integral and a discretized mesh containing $N_i = 1200^2$ points for the momentum space summation (compare Section 1.4). We have confirmed the convergence of our results at zero temperature by comparison with integration meshes containing $N_i = 2000$ points per direction and refrained from using any regularization for the susceptibility integral.

We have previously seen that a bare interaction U_0 of $U_c = 0.37\,\mathrm{eV}$ is sufficient to drive the system into an incommensurate magnetic phase on the RPA level. For U_0 below this critical value, the spin and charge fluctuations induce a superconducting phase transition [24, 79, 206]. We calculate the Cooper pair scattering amplitudes in the previously described basis

$$\Gamma_{\lambda\lambda'}(\boldsymbol{k}, \boldsymbol{q}) = \sum_{\{\sigma_i\}} \psi^{\mathrm{pair}}_{\lambda',\sigma_2\sigma_3}(\boldsymbol{q}) \Gamma_{\{\sigma_i\}}(\boldsymbol{k}, \boldsymbol{q}) \psi^{\mathrm{pair}}_{\lambda,\sigma_0\sigma_1}(\boldsymbol{k}) \,, \tag{3.46}$$

in the fluctuation exchange formulation generalized for spin-orbit coupled systems

$$\begin{aligned}
\Gamma_{\{\sigma_i\}}(\boldsymbol{k},\boldsymbol{q}) &= \Gamma^{(1)}_{\{\sigma_i\}} + \Gamma^{(2)}_{\{\sigma_i\}}(\boldsymbol{k},\boldsymbol{q})\,, \\
\Gamma^{(1)}_{\{\sigma_i\}} &= U_0(\delta_{\sigma_0\sigma_2}\delta_{\sigma_1\sigma_3} - \delta_{\sigma_0\sigma_3}\delta_{\sigma_1\sigma_2}) \quad \text{and} \\
\Gamma^{(2)}_{\{\sigma_i\}} &= \sum_{\{\tilde{\sigma}_i\}} \Gamma^{(1)}_{\sigma_0\tilde{\sigma}_2\sigma_2\tilde{\sigma}_1}\chi^{\mathrm{RPA}}_{\{\tilde{\sigma}_i\}}(\boldsymbol{k}-\boldsymbol{q})\Gamma^{(1)}_{\tilde{\sigma}_3\sigma_1\tilde{\sigma}_0\sigma_3} \\
&\quad - \sum_{\{\tilde{\sigma}_i\}} \Gamma^{(1)}_{\sigma_0\tilde{\sigma}_2\sigma_3\tilde{\sigma}_1}\chi^{\mathrm{RPA}}_{\{\tilde{\sigma}_i\}}(\boldsymbol{k}+\boldsymbol{q})\Gamma^{(1)}_{\tilde{\sigma}_3\sigma_1\tilde{\sigma}_0\sigma_2} \\
&\quad + \sum_{\{\tilde{\sigma}_i\}} \Gamma^{(1)}_{\sigma_0\sigma_1\tilde{\sigma}_0\tilde{\sigma}_1}\chi^{\mathrm{PP}}_{\{\tilde{\sigma}_i\}}(\boldsymbol{Q}=\boldsymbol{0})\Gamma^{(1)}_{\tilde{\sigma}_2\tilde{\sigma}_3\sigma_2\sigma_3}\,.
\end{aligned} \tag{3.47}$$

that we introduced in Chapter 1. The generalized RPA susceptibilities $\chi^{\mathrm{RPA}}_{\{\sigma_i\}}(\boldsymbol{Q})$ are calculated via the usual Dyson series resummation of all RPA diagrams and the momenta $\boldsymbol{k}$ and $\boldsymbol{q}$ are chosen from $N_p = 360$ unique Fermi surface points.

The resulting Cooper pair scattering amplitude serves as an input for the linearised superconducting gap equation

$$V_{eff}\Delta_\lambda(\boldsymbol{k}) = \sum_{\boldsymbol{q}} \Gamma_{\lambda\lambda'}(\boldsymbol{k},\boldsymbol{q})\Delta_{\lambda'}(\boldsymbol{q})\,, \tag{3.48}$$

whose solutions indicate the leading superconducting gap functions Δ which can be analysed in terms of irreducible representations of the model's point group. The most negative V_{eff} indicates the maximum paring strength. Despite the selective RPA resummation of diagrams, we would like to stress that this approach recovers the solution of the asymptotically exact weak coupling renormalization group in the limit of $U_0 \to 0$ [23].

For our model of the LuPtBi surface states, no qualitative changes Figure 3.9 are observed over the whole range $0 < U_0 < U_c$ and the leading eigenvalue is two-fold degenerate over the complete range of doping analysed. We emphasize this aspect since the changes in the filling of a surface state may be sensitive to adsorbates or other influences that are not present for bulk states. As expected from the performed symmetry analysis, we find a superconducting gap function transforming under the E irreducible representation of C_{3v} as shown in Figure 3.9. This is confirmed by the fact that the corresponding gap functions transform accordingly. Furthermore, the numerically obtained gap functions are almost perfectly fitted by linear combinations of Φ^{E_g} and $\Phi^{E'_g}$, highlighting the nearest-neighbour character of the superconducting pairing.

The absence of inversion symmetry on the LuPtBi surface allows for mixing of spin-singlet and spin-triplet Cooper pairs, which we analyse by comparing the fitted harmonics for the different helicity Fermi surfaces. From the almost identical fitting parameters for both helicities we infer the Cooper pair wavefunction to be well approximated by pure spin-singlet pairs. This result is again stable across a wide range of filling fractions.

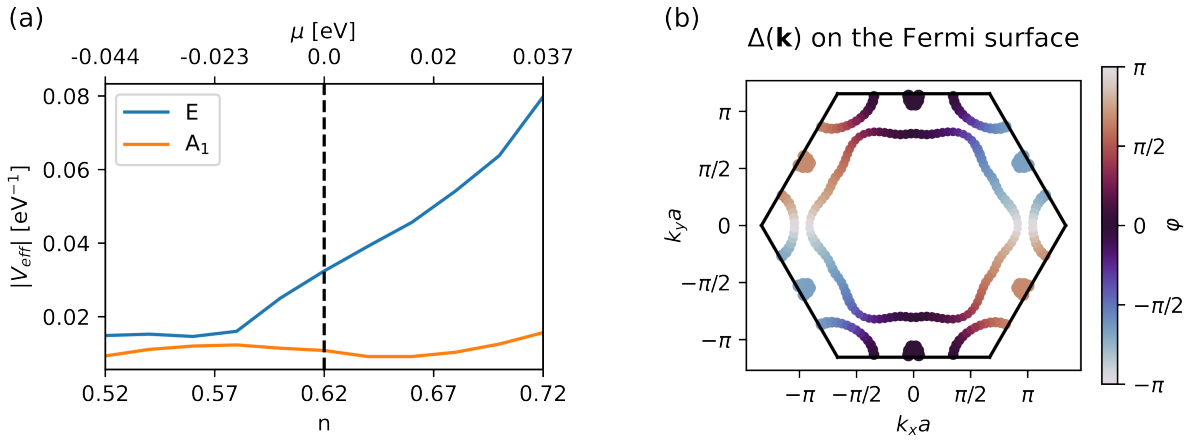

Figure 3.9: Panel (a) shows the superconducting pairing strength V_{eff} in the RPA as a function of the particle occupation n in the surface band. While this calculation was done for an intermediate value of $U_0 = 0.3$ eV, all qualitative features of this figure are preserved upon lowering U_0 to the analytically controlled limit $U_0 \to 0$. The filling of $n = 0.62$ corresponds to the DFT result and our result is rather insensitive to the variation of filling. The right panel (b) depicts the gap function $\Delta(\mathbf{k}) = |\Delta(\mathbf{k})|e^{i\varphi(\mathbf{k})}$ of the leading superconducting instability along the Fermi surface. The point size is chosen proportional to the absolute value of the gap size $|\Delta|$ while the colour represents the phase $\varphi(\mathbf{k})$ of the complex condensate. One can clearly see the approximately uniform magnitude of the chiral $d + id$ pairing as well as the phase winding of 4π.

We want to highlight the notion of two very distinct types of singlet-triplet mixing in inversion symmetry breaking unconventional superconductors. As discussed before, the superconducting state will mix singlet and triplet excitations due to the well defined spin polarization for each Fermi surface momentum in a spin-split system. In the limit of strong spin-orbit interaction this almost inevitably leads to a half and half admixture of singlet and triplet pairing as we discussed at the end of Section 3.2 and was recently observed in a truncated unity functional renormalization group (TU-fRG) study of the square lattice Rashba Hubbard model [34]. This has to be contrasted with the scattering of singlet and triplet Cooper pairs via the effective pairing interaction [31]. In the limit where the spin splitting energy significantly exceeds the superconducting gap size, one should actually distinguish three separate Cooper pair scattering amplitudes: singlet to singlet scattering, triplet to triplet scattering and the mixing singlet to triplet scattering. For $\Gamma_{\lambda\lambda'}(\boldsymbol{k}, \boldsymbol{q})$ this corresponds to the three independent scattering sectors Γ_{++}, Γ_{--} and Γ_{+-} which can be related to

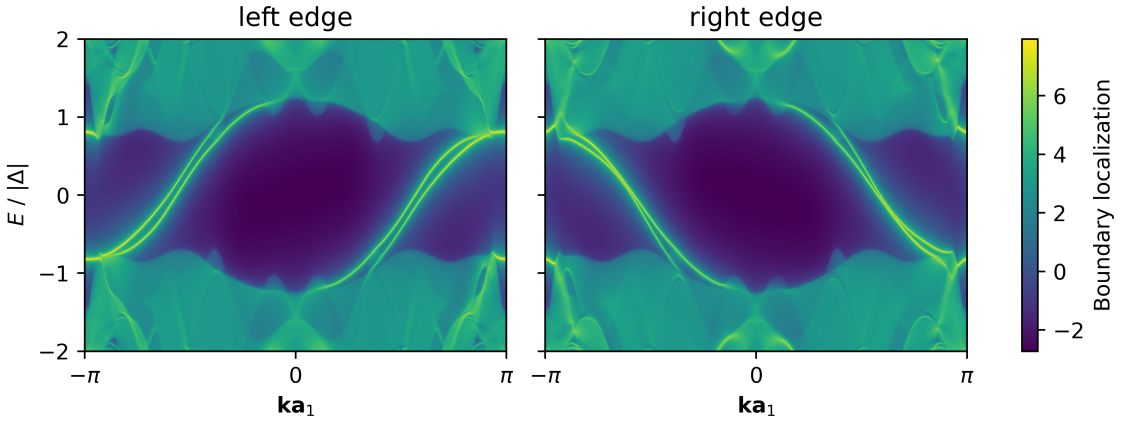

Figure 3.10: Excitation spectrum of the resulting Bogoliubov-de-Gennes Hamiltonian on a ribbon with periodic (open) boundary conditions along the $\boldsymbol{a}_2$ ($\boldsymbol{a}_1$) directions. We show the localization at the left and right boundaries of the ribbon respectively in order to demonstrate their different spectra due to the C_{3v} point group of the surface state.

Γ_{sgt}, Γ_{tpt} and Γ_{mix} via [31]

$$\begin{aligned}\Gamma_{\mathrm{sgt}} &= \frac{\Gamma_{++}+\Gamma_{--}+\Gamma_{+-}+\Gamma_{-+}}{4}\\ \Gamma_{\mathrm{tpt}} &= \frac{\Gamma_{++}+\Gamma_{--}-\Gamma_{+-}-\Gamma_{-+}}{4}\\ \Gamma_{\mathrm{mix}} &= \frac{\Gamma_{++}-\Gamma_{--}}{4}\,.\end{aligned} \tag{3.49}$$

Many choices exist for obtaining scalar objects from the two variable functions $\Gamma_{\lambda\lambda'}(\boldsymbol{k},\boldsymbol{q})$. For example, one can project onto the leading eigenvector, an arbitrary form factor or simply integrate all couplings.

From such an analysis, the pairing fluctuations in the surface state of LuPtBi are found to be of dominant singlet-singlet type. Nevertheless the large spin-splitting of the Fermi surface will induce triplet Cooper pairs via "proximity effect".

In order to distinguish among all possible linear combinations $\alpha\Phi^{E_g}+\beta\Phi^{E_g'}$ (with identical pairing potential) we compute the free-energy F of the resulting superconducting state according to the procedure we outline in Appendix B. We find that F is optimized for the chiral and time-reversal symmetry breaking linear combinations $\Phi^{E_g}\pm \mathrm{i}\Phi^{E_g'}$ shown in Figure 3.9. The physical intuition for this result lies in the formation of a full excitation gap across the Fermi surface and therefore a maximum gain in condensation energy [76, 207]. The superconducting condensate formed by the $\Phi^{E_g}\pm \mathrm{i}\Phi^{E_g'}$ combination is characterized by a topological Chern number $C=\pm 2$. One experimentally signature of this topological invariant would be the universal thermal and spin

Hall conductivity due to two low-energy edge modes [208–210], as we show in Figure 3.10. Using our ten parameter tight binding model we have confirmed the existence of this asymmetry in the absence of numerical disorder originating from the numerical minimization of the Wannier orbital spread. Additionally we have verified the necessity of spin-orbit coupling for the splitting between both boundary modes.

As we have discussed in the introduction of this thesis, the role of quantum fluctuations is enhanced in two dimensional systems. The time-reversal superconducting state is associated with discrete $\mathcal{Z}_2$ (time reversal symmetry) and continuous $U(1)$ (gauge symmetry resulting in particle conservation) symmetry. Despite the Mermin-Wagner-Hohenberg (MWH) theorem one expects the formation of a $U(1)$ symmetry breaking superconducting phase of matter with algebraically decaying correlation functions for two dimensional surface superconductors via a Kosterlitz-Thouless-Berezinskii (KTB) transition at a finite transition temperature T_c. On the mean field level, time reversal symmetry breaking sets in at exactly the same temperature. The quantum fluctuations neglected in the mean-field treatment are however sensitive to the distinction between the breaking of continuous and discrete symmetries and tend to split the transition [145, 211–214]. This effect is particularly relevant for systems with low carrier concentration like the LuPtBi surface state and results in a vestigial time reversal symmetry breaking above T_c.

Conclusion

Starting from an overview of literature about surface superconductivity we have highlighted strongly spin-orbit coupled surface bands as a novel and potentially diverse domain for superconducting instabilities driven by electronic correlation effects. In particular, we have formulated a theory on how LuPtBi might be reconciled as an instance of an unconventional chiral topological surface superconductor. Our proposition lends itself to several tangible experimental tests: First, any thermodynamic measurement sensitive to distinguish sub-extensive surface contributions from bulk contributions should be able to discriminate between a leading surface transition and a subsequent bulk transition. Second, we would expect a finite Kerr signal not only below T_c, but also above T_c due to low-dimensional order parameter fluctuations and resulting vestigial time-reversal symmetry breaking. Finally we suggest to the possible resolution of the topological edge modes or vortex spectra as a smoking gun signature of the theoretically predicted state. While it is likely that our theory will not universally apply to all half-Heuslers for all surface terminations, it might be promising to reconcile instances of hitherto observed SC in currently known half-Heuslers from the viewpoint of unconventional surface SC engineering.

Conclusion

At the start of the thesis we set out to develop a generic and computationally efficient way of analysing superconducting Fermi surface instabilities of real materials which we presented in Chapter 1. Following a brief overview of obtained benchmark results in the Chapter 2 we identified the metallic surface states of LuPtBi as a prime candidate for the observation of surface superconductivity driven by electronic correlation effects in Chapter 3 We summarize our results in the following.

Our framework for the analysis of unconventional superconductivity in realistic materials is based on a three step program. In the first step we analyse the electronic band structure of a material by performing standard *ab-initio* density functional theory calculations. After a qualitative analysis of the results we proceed with the building of a tight-binding model capable of describing the low-energy degrees of freedom *i.e.*, the bands around the materials Fermi level. This can be done either via the use of maximally localized Wannier orbitals or through fitting of an analytical tight-binding model that is based on the symmetries of the material and Wyckoff positions of the relevant orbital degrees of freedom to the band structure. Already from this intermediate result, one can analyse the models bare particle-hole susceptibility to get a first impression of the relevant nesting vectors of the Fermi surface, dominating spin- and charge fluctuations as well as the importance of matrix element effects arising from the interference of energy eigenstates with different orbital character.

In a second step, a basis for all possible Cooper pair states, *i.e.*, two-electron states with vanishing total momentum is set up via the use of a discretized Fermi surface. In Chapter 1 we outline a detailed algorithm for this task that is useable in the presence of spin-orbit coupling. The established tight-binding model can now be dressed with interactions terms, yielding an extended Hubbard type model.

Finally we complete the program by calculating the effective interactions between all classified Cooper pair states and identifying the most strongly bound pairing states. We propose a unified

formulation to analyse this effective interaction in the Cooper channel of these models using the weak coupling renormalization group (wcRG) method as well as the random phase approximation (RPA). The key insight of our formulation is the fact that both methods centrally rely on the generalized bare particle-hole susceptibility as the only computationally expensive ingredient, thus placing them in the same class of computational complexity. Our formulation is almost completely gauge-invariant and therefore allows for the analysis of arbitrary spin-orbit coupled systems. Further we introduce an efficient and conceptually simple way to treat non-local interaction terms in both approaches and show how the numerical effort can be managed via the use of hermiticity, Fermionic antisymmetry and spatial symmetries. Using these ingredients the third step can be performed efficiently and phase diagram scans in different interaction parameters do not require the recalculation of any integrals.

Using all of these methodological advances we were able to analyse possible superconducting instabilities of the metallic surface state of the bulk semimetal LuPtBi. The combination of bismuth's strong spin-orbit coupling and the broken inversion symmetry at the crystal surface require the use of our gauge invariant formulation of the RPA. We identified completely gapped, time-reversal symmetry breaking chiral d-wave superconductivity to be the dominant superconducting instability in the system independent of interaction strength or model details.

Appendices

Decomposition of long range interactions

We show that a generic translationally invariant two particle interaction

$$\begin{aligned} U_{\{a_i\}}(\{\mathbf{k}_i\}) = \; & \delta(\mathbf{k}_0 + \mathbf{k}_1 - \mathbf{k}_2 + \mathbf{k}_3) \\ & \sum_{\hat{\mathbf{r}}_1, \hat{\mathbf{r}}_2, \hat{\mathbf{r}}_3} U_{\{a_i\}}(\hat{\mathbf{r}}_1, \hat{\mathbf{r}}_2, \hat{\mathbf{r}}_3) \mathrm{e}^{+\mathrm{i}(\mathbf{k}_1\hat{\mathbf{r}}_1 - \mathbf{k}_2\hat{\mathbf{r}}_2 - \mathbf{k}_3\hat{\mathbf{r}}_3)} \,, \end{aligned} \tag{A.1}$$

involving a finite number of bonds can be rewritten in the D-channel representation

$$\begin{aligned} U_{\{a_i\}}(\{\mathbf{k}_i\}) = \; & \delta(\mathbf{k}_0 + \mathbf{k}_1 - \mathbf{k}_2 + \mathbf{k}_3) \\ & \sum_{i,j} U^{ij}_{\{a_i\}}(\mathbf{k}_0 - \mathbf{k}_2) f_i^*(\mathbf{k}_0) f_j(\mathbf{k}_3) \,, \end{aligned} \tag{A.2}$$

with a finite set of form factor functions $f_i(\mathbf{k})$.

This is accomplished by first rewriting the exponent in Equation A.1 by using momentum conservation for $\mathbf{k}_1$

$$\begin{aligned} & \mathbf{k}_1\hat{\mathbf{r}}_1 - \mathbf{k}_2\hat{\mathbf{r}}_2 - \mathbf{k}_3\hat{\mathbf{r}}_3 \\ = \; & (\mathbf{k}_3 + \mathbf{k}_2 - \mathbf{k}_0)\hat{\mathbf{r}}_1 + (\mathbf{k}_0 - \mathbf{k}_2)\hat{\mathbf{r}}_2 - \mathbf{k}_0\hat{\mathbf{r}}_2 - \mathbf{k}_3\hat{\mathbf{r}}_3 \\ = \; & (\mathbf{k}_0 - \mathbf{k}_2)(\hat{\mathbf{r}}_2 - \hat{\mathbf{r}}_1) - \mathbf{k}_0\hat{\mathbf{r}}_2 - \mathbf{k}_3(\hat{\mathbf{r}}_3 - \hat{\mathbf{r}}_1) \,, \end{aligned} \tag{A.3}$$

and introducing form factors

$$f_i(\mathbf{k}) = \mathrm{e}^{\mathrm{i}\mathbf{k}\hat{\mathbf{r}}_i} \,. \tag{A.4}$$

By shifting the summations via the use of translational invariance and defining

$$\begin{aligned} \hat{\mathbf{r}}_i &= \hat{\mathbf{r}}_2 - \hat{\mathbf{r}}_1 \,, \\ \hat{\mathbf{r}}_g &= \hat{\mathbf{r}}_2 \,, \\ \hat{\mathbf{r}}_h &= \hat{\mathbf{r}}_1 - \hat{\mathbf{r}}_3 \text{ and} \end{aligned} \tag{A.5}$$

we can then simply rewrite Equation A.1

$$
\begin{aligned}
U_{\{a_i\}}(\{\mathbf{k}_i\}) = \; & \delta(\mathbf{k}_0 + \mathbf{k}_1 - \mathbf{k}_2 + \mathbf{k}_3) \\
& \sum_{\hat{\mathbf{r}}_i, \hat{\mathbf{r}}_g, \hat{\mathbf{r}}_h} U_{\{a_i\}}(\hat{\mathbf{r}}_g - \hat{\mathbf{r}}_i, \hat{\mathbf{r}}_g, \hat{\mathbf{r}}_g - \hat{\mathbf{r}}_i - \hat{\mathbf{r}}_h) \\
& \qquad \mathrm{e}^{+\mathrm{i}(\mathbf{k}_0 - \mathbf{k}_2)\hat{\mathbf{r}}_i} \mathrm{e}^{-\mathrm{i}\mathbf{k}_0 \hat{\mathbf{r}}_g} \mathrm{e}^{+\mathrm{i}\mathbf{k}_3 \hat{\mathbf{r}}_h} \\
= \; & \delta(\mathbf{k}_0 + \mathbf{k}_1 - \mathbf{k}_2 + \mathbf{k}_3) \\
& \sum_{\hat{\mathbf{r}}_g, \hat{\mathbf{r}}_h} f_g^*(\mathbf{k}_0) f_h(\mathbf{k}_3) \\
& \sum_{\hat{\mathbf{r}}_i} U_{\{a_i\}}(\hat{\mathbf{r}}_g - \hat{\mathbf{r}}_i, \hat{\mathbf{r}}_g, \hat{\mathbf{r}}_g - \hat{\mathbf{r}}_i - \hat{\mathbf{r}}_h) \\
& \qquad \mathrm{e}^{+\mathrm{i}(\mathbf{k}_0 - \mathbf{k}_2)\hat{\mathbf{r}}_i} \\
= \; & \delta(\mathbf{k}_0 + \mathbf{k}_1 - \mathbf{k}_2 + \mathbf{k}_3) \\
& \sum_{\hat{\mathbf{r}}_g, \hat{\mathbf{r}}_h} f_g^*(\mathbf{k}_0) f_h(\mathbf{k}_3) U_{\{a_i\}}^{gh}(\mathbf{k}_0 - \mathbf{k}_2) \, .
\end{aligned}
\tag{A.6}
$$

The remaining interaction tensor can be identified as

$$
\begin{aligned}
& U_{\{a_i\}}^{gh}(\mathbf{k}_0 - \mathbf{k}_2) \\
& \quad = \sum_{\hat{\mathbf{r}}_i} U_{\{a_i\}}(\hat{\mathbf{r}}_g - \hat{\mathbf{r}}_i, \hat{\mathbf{r}}_g, \hat{\mathbf{r}}_g - \hat{\mathbf{r}}_i - \hat{\mathbf{r}}_h) \, \mathrm{e}^{+\mathrm{i}(\mathbf{k}_0 - \mathbf{k}_2)\hat{\mathbf{r}}_i} \\
& \quad = \sum_{\hat{\mathbf{r}}_j} U_{\{a_i\}}(\hat{\mathbf{r}}_j, \hat{\mathbf{r}}_g, \hat{\mathbf{r}}_j - \hat{\mathbf{r}}_h) \, \mathrm{e}^{-\mathrm{i}(\mathbf{k}_0 - \mathbf{k}_2)(\hat{\mathbf{r}}_j - \hat{\mathbf{r}}_g)} \, .
\end{aligned}
\tag{A.7}
$$

Note that the summations over $\mathbf{r}_g$ and $\mathbf{r}_h$ involve a very limited number of terms for short range interactions and that the complete derivation does not necessitate any approximations.

Mean field theory for spin-split Fermi surfaces

Starting from a quartic Hamiltonian with a superconducting interaction

$$H = \sum_{\mathbf{k},\lambda} \epsilon_\lambda(\mathbf{k}) c^\dagger_{\mathbf{k}\lambda} c_{\mathbf{k}\lambda} + \frac{1}{2} \sum_{\mathbf{k},\mathbf{q},\lambda,\lambda'} V_{\lambda\lambda'}(\mathbf{k},\mathbf{q}) c^\dagger_{\mathbf{q}\lambda'} \hat{T} c^\dagger_{\mathbf{q}\lambda'} \hat{T}^{-1} \hat{T} c_{\mathbf{k}\lambda} \hat{T}^{-1} c_{\mathbf{k}\lambda} \tag{B.1}$$

it is sensible to introduce pair creation operators

$$\Psi^\dagger_{\text{pair}}(\mathbf{k},\lambda) = c^\dagger_{\mathbf{q}\lambda} \hat{T} c^\dagger_{\mathbf{q}\lambda} \hat{T}^{-1} \,. \tag{B.2}$$

We perform a standard mean field decomposition of the interaction term followed by the neglection of order parameter fluctuations yielding

$$\begin{aligned}
2H_I &= \sum_{\mathbf{k},\mathbf{q},\lambda,\lambda'} V_{\lambda\lambda'}(\mathbf{k},\mathbf{q}) \Psi^\dagger_{\text{pair}}(\mathbf{q},\lambda') \Psi_{\text{pair}}(\mathbf{k},\lambda) \\
&= \sum_{\mathbf{k},\mathbf{q},\lambda,\lambda'} V_{\lambda\lambda'}(\mathbf{k},\mathbf{q}) \Big(\langle \Psi^\dagger_{\text{pair}}(\mathbf{q},\lambda') \rangle \Psi_{\text{pair}}(\mathbf{k},\lambda) + \Psi^\dagger_{\text{pair}}(\mathbf{q},\lambda') \langle \Psi_{\text{pair}}(\mathbf{k},\lambda) \rangle \\
&\qquad - \langle \Psi^\dagger_{\text{pair}}(\mathbf{q},\lambda') \rangle \langle \Psi_{\text{pair}}(\mathbf{k},\lambda) \rangle \\
&\qquad + (\Psi^\dagger_{\text{pair}}(\mathbf{q},\lambda') - \langle \Psi^\dagger_{\text{pair}}(\mathbf{q},\lambda') \rangle)(\Psi_{\text{pair}}(\mathbf{k},\lambda) - \langle \Psi_{\text{pair}}(\mathbf{k},\lambda) \rangle) \Big) \\
&\approx \sum_{\mathbf{k},\mathbf{q},\lambda,\lambda'} V_{\lambda\lambda'}(\mathbf{k},\mathbf{q}) \Big(\langle \Psi^\dagger_{\text{pair}}(\mathbf{q},\lambda') \rangle \Psi_{\text{pair}}(\mathbf{k},\lambda) + \Psi^\dagger_{\text{pair}}(\mathbf{q},\lambda') \langle \Psi_{\text{pair}}(\mathbf{k},\lambda) \rangle \\
&\qquad - \langle \Psi^\dagger_{\text{pair}}(\mathbf{q},\lambda') \rangle \langle \Psi_{\text{pair}}(\mathbf{k},\lambda) \rangle \Big)
\end{aligned} \tag{B.3}$$

From here we proceed by introducing a spectral decomposition of $V_{\lambda\lambda'}(\mathbf{k},\mathbf{q})$ using a set of real orthonormal functions $d_i(\mathbf{k})$ even in $\mathbf{k}$

$$V_{\lambda\lambda'}(\mathbf{k},\mathbf{q}) = \sum_{ij} V_{ij,\lambda\lambda'} d_i(\mathbf{k}) d_j(\mathbf{q}) \tag{B.4}$$

and introducing variational parameters

$$\Delta_{i,\lambda} = \sum_{j\lambda'} V_{ij,\lambda\lambda'} \sum_{\mathbf{q}} d_j(\mathbf{q}) \langle \Psi_{\text{pair}}(\mathbf{q},\lambda') \rangle \,. \tag{B.5}$$

Clearly this equates to the conventional choice

$$\Delta_\lambda(\mathbf{k}) = \sum_i \Delta_{i,\lambda} d_i(\mathbf{k}) = \sum_{\mathbf{q}\lambda'} V_{\lambda\lambda'}(\mathbf{k},\mathbf{q}) \langle \Psi_{\text{pair}}(\mathbf{q},\lambda') \rangle \,. \tag{B.6}$$

with the benefit of reducing the problem from a variational problem of a function to set of parameters. We now consider the quadratic Hamiltonian

$$H = \sum_{\mathbf{k},\lambda} \epsilon_\lambda(\mathbf{k}) c^\dagger_{\mathbf{k}\lambda} c_{\mathbf{k}\lambda} + \frac{1}{2} \sum_{i,\mathbf{k},\lambda} d_i(\mathbf{k}) \Big(\Delta^*_{i,\lambda} \Psi_{\text{pair}}(\mathbf{k},\lambda) + \Delta_{i,\lambda} \Psi^\dagger_{\text{pair}}(\mathbf{k},\lambda) - \Delta_{i,\lambda} \langle \Psi^\dagger_{\text{pair}}(\mathbf{k},\lambda) \rangle \Big) \,. \tag{B.7}$$

Introducing Nambu spinors

$$\Psi_{\mathbf{k}\lambda} = (c_{\mathbf{k},\lambda},\, \hat{T} c^\dagger_{\mathbf{k},\lambda})^T = (c_{\mathbf{k},\lambda},\, e^{i\alpha_\lambda(\boldsymbol{k})} c^\dagger_{-\mathbf{k},\lambda})^T \tag{B.8}$$

we rewrite this

$$H = \frac{1}{2} \sum_{\mathbf{k},\lambda} \Psi^\dagger_{\mathbf{k}\lambda} h^\lambda_{\text{BdG}}(\mathbf{k}) \Psi_{\mathbf{k}\lambda} + \frac{1}{2} \sum_{\mathbf{k}\lambda} \epsilon_\lambda(\mathbf{k}) - \frac{1}{2} \sum_{i,\mathbf{k},\lambda} d_i(\mathbf{k}) \Delta_{i,\lambda} \langle \Psi^\dagger_{\text{pair}}(\mathbf{k},\lambda) \rangle \,, \tag{B.9}$$

where we introduced matrices

$$h^\lambda_{\text{BdG}}(\mathbf{k}) = \begin{pmatrix} \epsilon_\lambda(\mathbf{k}) & \sum_i d_i(\mathbf{k}) \Delta_{i,\lambda} \\ \sum_i d_i(\mathbf{k}) \Delta^*_{i,\lambda} & -\epsilon_\lambda(\mathbf{k}) \end{pmatrix} . \tag{B.10}$$

Not that this structure neglects the possibility of inter band / inter helicity pairing. The hermitian 2x2 matrices with a symmetric spectrum due to the emergent particle hole symmetry are diago-

nalizable using

$$h^{\lambda}_{\mathrm{BdG}}(\mathbf{k}) = \begin{pmatrix} u^*_{0,\lambda}(\mathbf{k}) & u^*_{1,\lambda}(\mathbf{k}) \\ v^*_{0,\lambda}(\mathbf{k}) & v^*_{1,\lambda}(\mathbf{k}) \end{pmatrix} \begin{pmatrix} E_\lambda(\mathbf{k}) & 0 \\ 0 & -E_\lambda(\mathbf{k}) \end{pmatrix} \begin{pmatrix} u_{0,\lambda}(\mathbf{k}) & v_{0,\lambda}(\mathbf{k}) \\ u_{1,\lambda}(\mathbf{k}) & v_{1,\lambda}(\mathbf{k}) \end{pmatrix} \tag{B.11}$$

with eigenvalues

$$E_\lambda(\mathbf{k}) = \sqrt{\epsilon^2_\lambda(\mathbf{k}) + \Big|\sum_i d_i(\mathbf{k})\Delta_{i,\lambda}\Big|^2} \tag{B.12}$$

and orthonormal eigenvectors

$$\begin{aligned} u_{0,\lambda}(\mathbf{k}) &= \frac{1}{\sqrt{N_\lambda(\mathbf{k})}}\Big(E_\lambda(\mathbf{k}) + \epsilon_\lambda(\mathbf{k})\Big) \\ v_{0,\lambda}(\mathbf{k}) &= \frac{1}{\sqrt{N_\lambda(\mathbf{k})}} \sum_i d_i(\mathbf{k})\Delta^*_{i,\lambda} \\ N_\lambda(\mathbf{k}) &= \Big(E_\lambda(\mathbf{k}) + \epsilon_\lambda(\mathbf{k})\Big)^2 + \Big|\sum_i d_i(\mathbf{k})\Delta_{i,\lambda}\Big|^2 \\ u_{1,\lambda}(\mathbf{k}) &= -v^*_{0,\lambda}(\mathbf{k}) \\ v_{1,\lambda}(\mathbf{k}) &= u^*_{0,\lambda}(\mathbf{k}) \end{aligned} \tag{B.13}$$

it is natural to introduce quasi particle operators

$$\begin{aligned} \alpha^\dagger_{\mathbf{k}\lambda} &= u_{0,\lambda}(\mathbf{k})c_{\mathbf{k}\lambda} + v_{0,\lambda}(\mathbf{k})e^{i\alpha_\lambda(\boldsymbol{k})}c^\dagger_{-\mathbf{k}\lambda} \text{ and} \\ \gamma^\dagger_{\mathbf{k}\lambda} &= u_{1,\lambda}(\mathbf{k})c_{\mathbf{k}\lambda} + v_{1,\lambda}(\mathbf{k})e^{i\alpha_\lambda(\boldsymbol{k})}c^\dagger_{-\mathbf{k}\lambda}\,. \end{aligned} \tag{B.14}$$

Note that naturally

$$\begin{aligned} \alpha_{\mathbf{k}\lambda} &= u^*_{0,\lambda}(\mathbf{k})c^\dagger_{\mathbf{k}\lambda} + v^*_{0,\lambda}(\mathbf{k})e^{-i\alpha_\lambda(\boldsymbol{k})}c_{-\mathbf{k}\lambda} \\ &= -u_{1,\lambda}(\mathbf{k})e^{-i\alpha_\lambda(\boldsymbol{k})}c_{-\mathbf{k}\lambda} + v_{1,\lambda}(\mathbf{k})c^\dagger_{\mathbf{k}\lambda} \\ &= u_{1,\lambda}(\mathbf{k})e^{-i\alpha_\lambda(-\boldsymbol{k})}c_{-\mathbf{k}\lambda} + v_{1,\lambda}(\mathbf{k})c^\dagger_{\mathbf{k}\lambda} \\ &= e^{-i\alpha_\lambda(-\boldsymbol{k})}\Big(u_{1,\lambda}(-\mathbf{k})c_{-\mathbf{k}\lambda} + e^{+i\alpha_\lambda(-\boldsymbol{k})}v_{1,\lambda}(-\mathbf{k})c^\dagger_{\mathbf{k}\lambda}\Big) \\ &= e^{-i\alpha_\lambda(-\boldsymbol{k})}\gamma^\dagger_{-\mathbf{k}\lambda}\,. \end{aligned} \tag{B.15}$$

This allows us to connect the operators γ and α

$$\begin{aligned} \gamma^\dagger_{\mathbf{k}\lambda} &= -e^{+i\alpha_\lambda(-\boldsymbol{k})}\alpha_{-\mathbf{k}\lambda} \\ \gamma_{\mathbf{k}\lambda} &= -e^{-i\alpha_\lambda(-\boldsymbol{k})}\alpha^\dagger_{-\mathbf{k}\lambda}\,, \end{aligned} \tag{B.16}$$

and to further simplify

$$\begin{aligned}\frac{1}{2}\sum_{\mathbf{k},\lambda}\Psi^{\dagger}_{\mathbf{k}\lambda}h^{\lambda}_{\mathrm{BdG}}(\mathbf{k})\Psi_{\mathbf{k}\lambda} &= \frac{1}{2}\sum_{\mathbf{k},\lambda}\begin{pmatrix}\alpha^{\dagger}_{\mathbf{k}\lambda} & \gamma^{\dagger}_{\mathbf{k}\lambda}\end{pmatrix}\begin{pmatrix}E_{\lambda}(\mathbf{k}) & 0\\ 0 & -E_{\lambda}(\mathbf{k})\end{pmatrix}\begin{pmatrix}\alpha_{\mathbf{k}\lambda}\\ \gamma_{\mathbf{k}\lambda}\end{pmatrix}\\ &= \frac{1}{2}\sum_{\mathbf{k},\lambda}E_{\lambda}(\mathbf{k})\Big(\alpha^{\dagger}_{\mathbf{k}\lambda}\alpha_{\mathbf{k}\lambda}-\gamma^{\dagger}_{\mathbf{k}\lambda}\gamma_{\mathbf{k}\lambda}\Big) = \frac{1}{2}\sum_{\mathbf{k},\lambda}E_{\lambda}(\mathbf{k})\Big(\alpha^{\dagger}_{\mathbf{k}\lambda}\alpha_{\mathbf{k}\lambda}-\alpha_{-\mathbf{k}\lambda}\alpha^{\dagger}_{-\mathbf{k}\lambda}\Big)\\ &= \frac{1}{2}\sum_{\mathbf{k},\lambda}E_{\lambda}(\mathbf{k})\Big(\alpha^{\dagger}_{\mathbf{k}\lambda}\alpha_{\mathbf{k}\lambda}+\alpha^{\dagger}_{-\mathbf{k}\lambda}\alpha_{-\mathbf{k}\lambda}-1\Big) = \sum_{\mathbf{k},\lambda}E_{\lambda}(\mathbf{k})\alpha^{\dagger}_{\mathbf{k}\lambda}\alpha_{\mathbf{k}\lambda}-\frac{1}{2}\sum_{\mathbf{k},\lambda}E_{\lambda}(\mathbf{k})\,.\end{aligned} \tag{B.17}$$

In summary we can write the Hamiltonian as

$$H = \sum_{\mathbf{k},\lambda}E_{\lambda}(\mathbf{k})\alpha^{\dagger}_{\mathbf{k}\lambda}\alpha_{\mathbf{k}\lambda}-\frac{1}{2}\sum_{\mathbf{k},\lambda}E_{\lambda}(\mathbf{k})+\frac{1}{2}\sum_{\mathbf{k}\lambda}\epsilon_{\lambda}(\mathbf{k})-\frac{1}{2}\sum_{i,\mathbf{k},\lambda}d_i(\mathbf{k})\Delta_{i,\lambda}\langle\Psi^{\dagger}_{\mathrm{pair}}(\mathbf{k},\lambda)\rangle\,. \tag{B.18}$$

The free energy of this system is now given by

$$\Omega_T = -T\sum_{\mathbf{k},\lambda}\log\Big(1+\exp\big(-\beta E_{\lambda}(\mathbf{k})\big)\Big)-\frac{1}{2}\sum_{\mathbf{k},\lambda}E_{\lambda}(\mathbf{k})+\frac{1}{2}\sum_{\mathbf{k}\lambda}\epsilon_{\lambda}(\mathbf{k})-\frac{1}{2}\sum_{i,\mathbf{k},\lambda}d_i(\mathbf{k})\Delta_{i,\lambda}\langle\Psi^{\dagger}_{\mathrm{pair}}(\mathbf{k},\lambda)\rangle\,. \tag{B.19}$$

For a system in thermodynamic equilibrium the value of the order parameter is defined by the minimum of the Free energy

$$0 = \frac{\partial\Omega_T}{\partial\langle\Psi^{\dagger}_{\mathrm{pair}}(\mathbf{k},\lambda)\rangle} \tag{B.20}$$

To recast this into a more useful form we calculate some intermediate results:

$$\frac{\partial}{\partial\langle\Psi^{\dagger}_{\mathrm{pair}}(\mathbf{k},\lambda)\rangle}\Delta_{i,\lambda''} = \frac{\partial}{\partial\langle\Psi^{\dagger}_{\mathrm{pair}}(\mathbf{k},\lambda)\rangle}\sum_{j\lambda'}V_{ij,\lambda''\lambda'}\sum_{\mathbf{q}}d_j(\mathbf{q})\langle\Psi_{\mathrm{pair}}(\mathbf{q},\lambda')\rangle = 0 \tag{B.21}$$

$$\frac{\partial}{\partial\langle\Psi^{\dagger}_{\mathrm{pair}}(\mathbf{k},\lambda)\rangle}\Delta^{*}_{i,\lambda''} = \frac{\partial}{\partial\langle\Psi^{\dagger}_{\mathrm{pair}}(\mathbf{k},\lambda)\rangle}\sum_{j\lambda'}V_{ij,\lambda''\lambda'}\sum_{\mathbf{q}}d_j(\mathbf{q})\langle\Psi^{\dagger}_{\mathrm{pair}}(\mathbf{q},\lambda')\rangle = \sum_{j}V_{ij,\lambda''\lambda}d_j(\mathbf{k}) \tag{B.22}$$

$$\begin{aligned}\frac{\partial}{\partial\langle\Psi^{\dagger}_{\mathrm{pair}}(\mathbf{k},\lambda)\rangle}E_{\lambda'}(\mathbf{q}) &= \frac{1}{2E_{\lambda'}(\mathbf{q})}\frac{\partial}{\partial\langle\Psi^{\dagger}_{\mathrm{pair}}(\mathbf{k},\lambda)\rangle}\Big(\sum_{i}d_i^2(\mathbf{q})\Delta_{i,\lambda'}\Delta^{*}_{i,\lambda'}\Big)\\ &= \frac{1}{2E_{\lambda'}(\mathbf{q})}\Big(\sum_{i}d_i^2(\mathbf{q})\Delta_{i,\lambda'}\sum_{j}V_{ij,\lambda'\lambda}d_j(\mathbf{k})\Big)\,.\end{aligned} \tag{B.23}$$

We apply everything to Ω_T and find

$$\begin{aligned}
0 &= \frac{\partial}{\partial\langle\Psi^\dagger_{\text{pair}}(\mathbf{k},\lambda)\rangle}\Omega_T \\
&= \sum_{\mathbf{q}\lambda'} \frac{\exp\left(-\beta E_{\lambda'}(\mathbf{q})\right)}{1+\exp\left(-\beta E_{\lambda'}(\mathbf{q})\right)} \frac{\partial}{\partial\langle\Psi^\dagger_{\text{pair}}(\mathbf{k},\lambda)\rangle} E_{\lambda'}(\mathbf{q}) - \frac{1}{2}\sum_{\mathbf{q}\lambda'} \frac{\partial}{\partial\langle\Psi^\dagger_{\text{pair}}(\mathbf{k},\lambda)\rangle} E_{\lambda'}(\mathbf{q}) - \frac{1}{2}\sum_i d_i(\mathbf{k})\Delta_{i,\lambda} \\
&= \sum_{\mathbf{q}\lambda'} \Big(f\big(\beta E_{\lambda'}(\mathbf{q})\big) - \frac{1}{2}\Big) \frac{\partial}{\partial\langle\Psi^\dagger_{\text{pair}}(\mathbf{k},\lambda)\rangle} E_{\lambda'}(\mathbf{q}) - \sum_i d_i(\mathbf{k})\Delta_{i,\lambda}
\end{aligned} \tag{B.24}$$

$$\sum_j d_j(\mathbf{k})\Delta_{i,\lambda} = \sum_{\mathbf{q}\lambda'} \Big(f\big(\beta E_{\lambda'}(\mathbf{q})\big) - \frac{1}{2}\Big) \frac{1}{2E_{\lambda'}(\mathbf{q})} \Big(\sum_i d_i^2(\mathbf{q})\Delta_{i,\lambda'} \sum_j V_{ij,\lambda'\lambda} d_j(\mathbf{k})\Big) \tag{B.25}$$

$$\Delta_{j,\lambda} = \sum_{\mathbf{q}\lambda'} \Big(f\big(\beta E_{\lambda'}(\mathbf{q})\big) - \frac{1}{2}\Big) \frac{1}{2E_{\lambda'}(\mathbf{q})} \sum_i d_i^2(\mathbf{q})\Delta_{i,\lambda'} V_{ij,\lambda'\lambda} \tag{B.26}$$

$$\Delta_{i,\lambda} = \sum_{\lambda' j} V^*_{ij,\lambda\lambda'} \sum_{\mathbf{q}} \frac{d_j^2(\mathbf{q})}{2E_{\lambda'}(\mathbf{q})} \Big(f\big(\beta E_{\lambda'}(\mathbf{q})\big) - \frac{1}{2}\Big)\Delta_{j,\lambda'} \,. \tag{B.27}$$

Finally we define the integral

$$\Lambda_{i,\lambda}(\mathbf{\Delta}) = \sum_{\mathbf{q}} \frac{d_i^2(\mathbf{q})}{2E_\lambda(\mathbf{q})} \Big(f\big(\beta E_\lambda(\mathbf{q})\big) - \frac{1}{2}\Big) \tag{B.28}$$

and rewrite the non-linear gap equation as

$$\Delta_{i,\lambda} = \sum_{\lambda' j} V^*_{ij,\lambda\lambda'} \Lambda_{j,\lambda'}(\mathbf{\Delta})\Delta_{j,\lambda'} \tag{B.29}$$

and remember that we reduced everything to the positive energy solution

$$E_\lambda(\mathbf{k}) = \sqrt{\epsilon_\lambda^2(\mathbf{k}) + \Big|\sum_i d_i(\mathbf{k})\Delta_{i,\lambda}\Big|^2} \,. \tag{B.30}$$

Note that the RHS of the non-linear gap equation is, in contrast to its linear approximated version, not hermitian. Also the dependence of Λ on Δ makes a solution via the eigenvalue problem alone impossible. Our strategy for solution therefore contains multiple steps

- Use singular value decomposition of the matrix $V\Lambda$ to identify its singular values.
- Use the right hand side eigenvactors as guesses for the shape of the gap function.

- Calculate a critical interaction parameter α such that $\alpha V\Lambda$ has a singular eigenvalue of exactly 1 for a given gap and temperature.
- The function $\alpha(T, \Delta) - 1$ is monotonous in both temperature and gap size. We search for its roots via the divide and conquer method.
- These roots are solutions to the non linear gap equation.

From here we can calculate the Free energy F of the system at a given temperature by inserting into

$$\Omega_T = -T \sum_{\mathbf{k},\lambda} \log\left(1 + \exp\left(-\beta E_\lambda(\mathbf{k})\right)\right) - \frac{1}{2}\sum_{\mathbf{k},\lambda} E_\lambda(\mathbf{k}) + \frac{1}{2}\sum_{\mathbf{k}\lambda} \epsilon_\lambda(\mathbf{k}) - \frac{1}{2}\sum_{i,\mathbf{k},\lambda} d_i(\mathbf{k})\Delta_{i,\lambda}\langle\Psi^\dagger_{\text{pair}}(\mathbf{k},\lambda)\rangle\,, \tag{B.31}$$

where we calculate

$$\langle\Psi^\dagger_{\text{pair}}(\mathbf{k},\lambda)\rangle = \left[\sum_i d_i(\mathbf{k}) \sum_{j\lambda'} V^{-1}_{ij,\lambda\lambda'}\Delta_{j,\lambda'}\right]^*. \tag{B.32}$$

For superconducting instabilities with a gap function transforming like a two fold degenerate irreducible representation, we may label two orthogonal solutions by $i = 0, 1$. We then minimize Ω_T by solving Equation B.29 for $\Delta_{0,\lambda}$ at each temperature and subsequenty varying the complex superposition of possible gap functions with identical amplitude and helicity distribution

$$\Delta_{i,\lambda} = (\cos(\theta)\delta_{i0} + \sin(\theta)e^{i\varphi}\delta_{i1})\Delta_{0,\lambda} \tag{B.33}$$

to find the minima of Ω_T in terms of φ and θ. For $T = 0.67T_c$ we find that $\theta = \pi/4$ and $\varphi = \pi/2$ to minimize the free energy for both the rashba Hubbard and LuPtBi models. We present the amplitude of the gap function as a function of temperature as well as the gap function at $T/T_c = 2/3$ for both models.

Additional susceptibilities

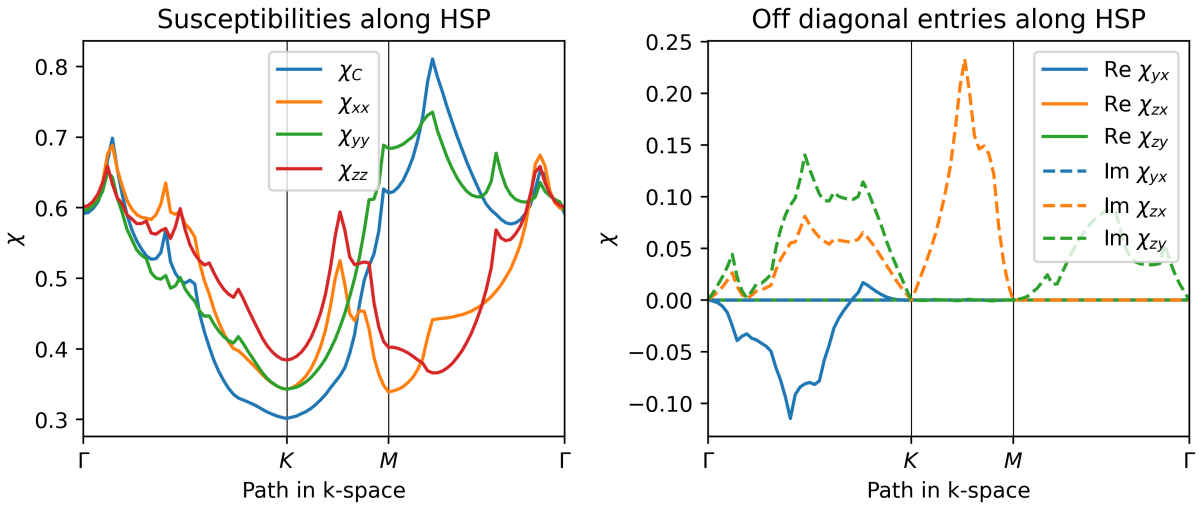

Figure C.1: Bare particle hole susceptibilities on the triangular lattice for $n = 1.5$ and $\alpha_R = 0.5$. In the left panel, we compare the different diagonal spin contributions $\chi_{xx}, \chi_{yy}, \chi_{zz}$ and χ_C along the high symmetry path through the Brillouin zone shown in Figure 2.8. The right panel shows the real and imaginary part of the three independent off diagonal spin contributions $\chi_{yx}, \chi_{zy}, \chi_{zx}$ along the same high symmetry path.

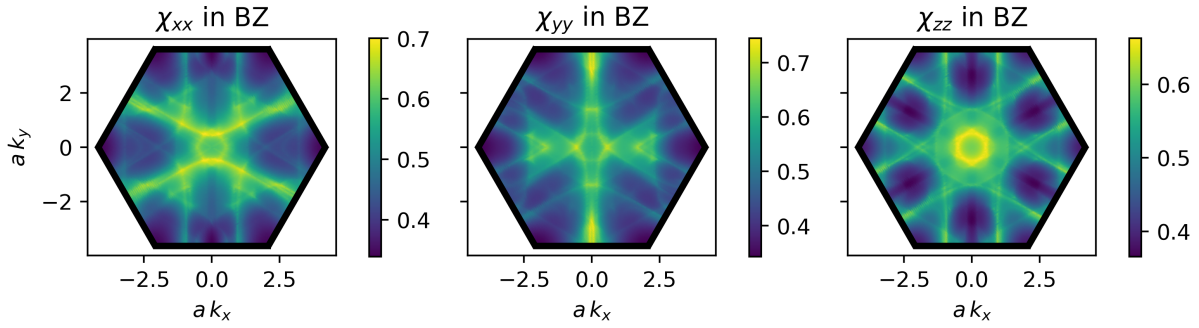

Figure C.2: Bare particle hole susceptibilities on the triangular lattice for $n = 1.5$ and $\alpha_R = 0.5$. We present the different diagonal spin contributions $\chi_{xx}, \chi_{yy}, \chi_{zz}$ in the complete Brillouin zone.

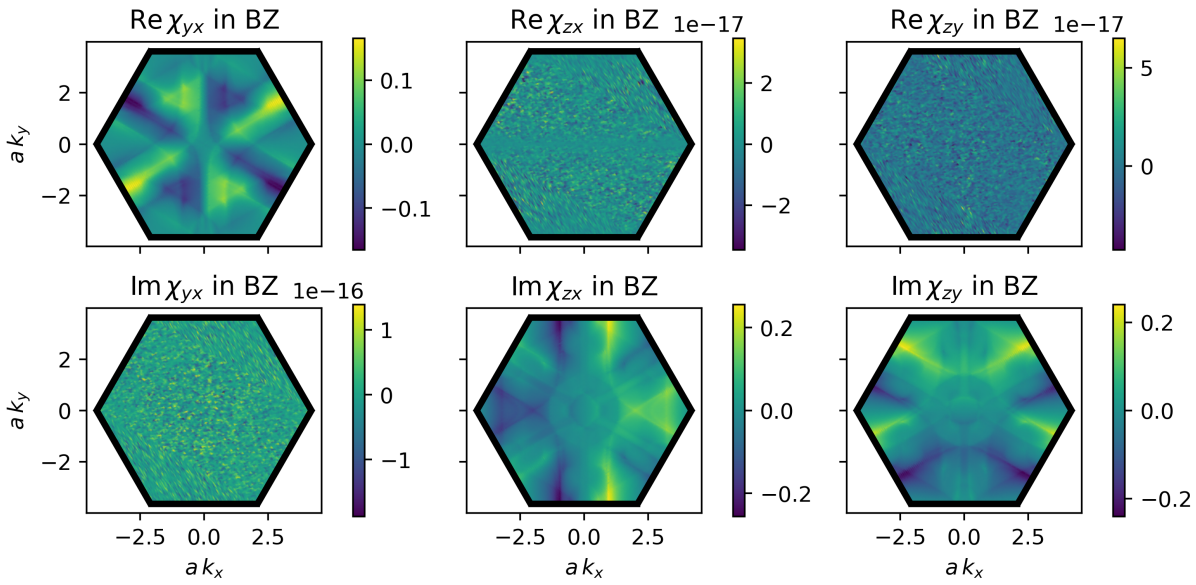

Figure C.3: Bare particle hole susceptibilities on the triangular lattice for $n = 1.5$ and $\alpha_R = 0.5$. We present the real and imaginary part of the three independent off diagonal spin contributions $\chi_{yx}, \chi_{zy}, \chi_{zx}$ in the complete Brillouin zone.

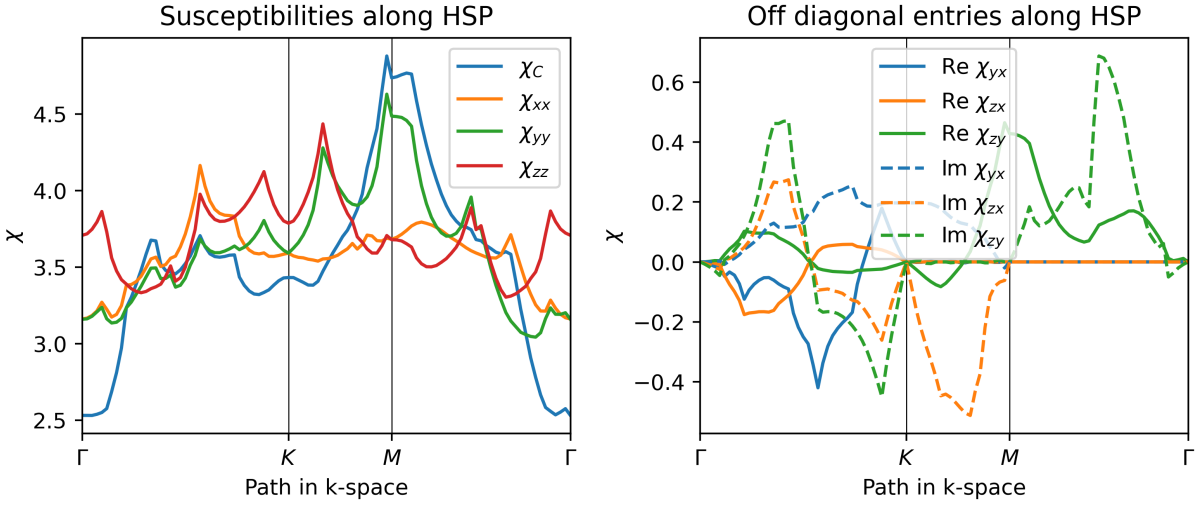

Figure C.4: Bare particle hole susceptibilities of the LuPtBis surface state model for $n = 0.62$. In the left panel, we compare the different diagonal spin contributions $\chi_{xx}, \chi_{yy}, \chi_{zz}$ and χ_C along the high symmetry path through the Brillouin zone shown in Figure 2.8. The right panel shows the real and imaginary part of the three independent off diagonal spin contributions $\chi_{yx}, \chi_{zy}, \chi_{zx}$ along the same high symmetry path.

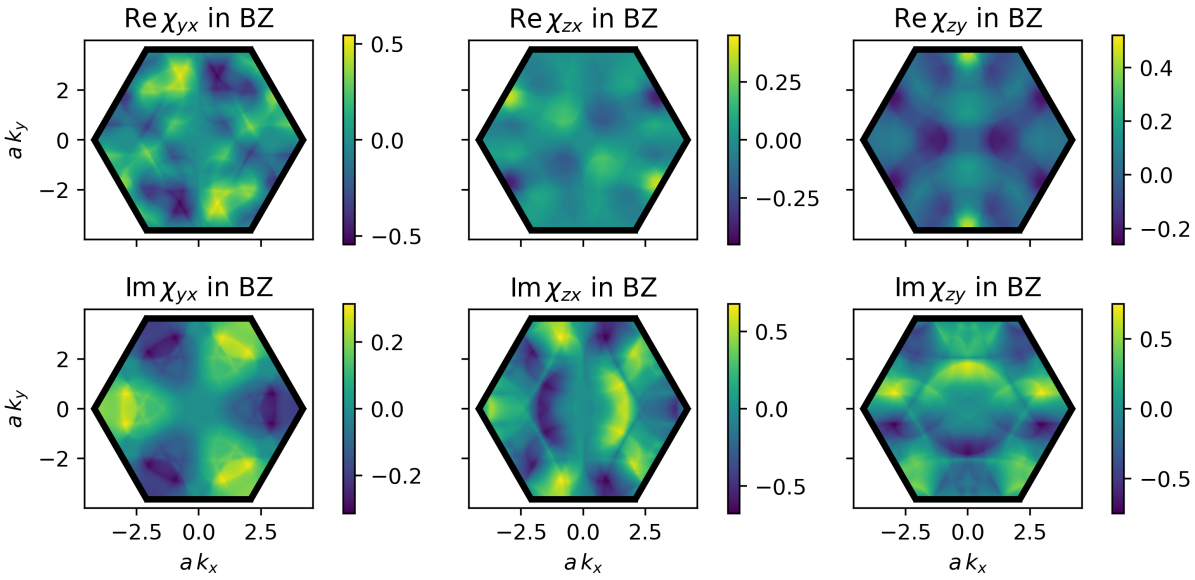

Figure C.5: Bare particle hole susceptibilities of the LuPtBis surface state model for $n = 0.62$. We present the real and imaginary part of the three independent off diagonal spin contributions $\chi_{yx}, \chi_{zy}, \chi_{zx}$ in the complete Brillouin zone.

Bibliography

[1] H. K. Onnes, "*The resistance of pure mercury at helium temperatures*", Leiden Comm. **120b** (1911).

[2] Siemens, *MAGNETOM Vida Environmental Product Declaration*, Website, Healthineers, 2022.

[3] S. Weinberg, *Lectures on Quantum Mechanics*, en, (Cambridge University Press, 2015)

[4] J. Bardeen, L. N. Cooper, and J. R. Schrieffer, "*Theory of Superconductivity*", Physical Review **108**, 1175 (1957).

[5] J. R. Schrieffer, *Theory Of Superconductivity*, en, (Avalon Publishing, 1999)

[6] E. Maxwell, "*Isotope Effect in the Superconductivity of Mercury*", Physical Review **78**, 477 (1950).

[7] L. Boeri, O. V. Dolgov, and A. A. Golubov, "*Is $LaFeAsO_{1-x}F_x$ an Electron-Phonon Superconductor?*", Phys. Rev. Lett. **101**, 026403 (2008).

[8] J. G. Bednorz and K. A. Müller, "*Possible highTc superconductivity in the Ba-La-Cu-O system*", Zeitschrift für Physik B Condensed Matter **64**, 189 (1986).

[9] W. Kohn and J. M. Luttinger, "*New Mechanism for Superconductivity*", Phys. Rev. Lett. **15**, 524 (1965).

[10] M. Sigrist and K. Ueda, "*Phenomenological theory of unconventional superconductivity*", Reviews of Modern Physics **63**, 239 (1991).

[11] P. A. Lee, N. Nagaosa, and X.-G. Wen, "*Doping a Mott insulator: Physics of high-temperature superconductivity*", Reviews of Modern Physics **78**, 17 (2006).

[12] I. I. Mazin and J. Schmalian, "*Pairing symmetry and pairing state in ferropnictides: Theoretical overview*", Physica C: Superconductivity, Superconductivity in Iron-Pnictides **469**, 614 (2009).

[13] T. Ito, H. Takagi, S. Ishibashi, T. Ido, and S. Uchida, "*Normal-state conductivity between CuO2 planes in copper oxide superconductors*", Nature **350**, 596 (1991).

[14] A. Isihara, "*Electron Correlations in Two Dimensions*", en, ed. by H. Ehrenreich and D. Turnbull, vol. 42, Superconductivity Quasicrystals two Dimensional Physics, (Academic Press, 1989) pp. 271–402.

[15] N. D. Mermin and H. Wagner, "*Absence of Ferromagnetism or Antiferromagnetism in One- or Two-Dimensional Isotropic Heisenberg Models*", Physical Review Letters **17**, 1133 (1966).

[16] P. C. Hohenberg, "*Existence of Long-Range Order in One and Two Dimensions*", Physical Review **158**, 383 (1967).

[17] S. Coleman, "*There are no Goldstone bosons in two dimensions*", Communications in Mathematical Physics **31**, 259 (1973).

[18] Y. Kamihara *et al.*, "*Iron-Based Layered Superconductor: LaOFeP*", Journal of the American Chemical Society **128**, 10012 (2006).

[19] H. Takahashi *et al.*, "*Superconductivity at 43 K in an iron-based layered compound* $LaO_{1-x}F_xFeAs$".

[20] J. Hubbard and B. H. Flowers, "*Electron correlations in narrow energy bands*", Proceedings of the Royal Society of London. Series A. Mathematical and Physical Sciences **276**, 238 (1963).

[21] D. P. Arovas, E. Berg, S. A. Kivelson, and S. Raghu, "*The Hubbard Model*", Annual Review of Condensed Matter Physics **13**, 239 (2022).

[22] D. J. Scalapino, "*A common thread: The pairing interaction for unconventional superconductors*", Reviews of Modern Physics **84**, 1383 (2012).

[23] S. Raghu, S. A. Kivelson, and D. J. Scalapino, "*Superconductivity in the repulsive Hubbard model: An asymptotically exact weak-coupling solution*", Phys. Rev. B **81**, 224505 (2010).

[24] D. J. Scalapino, E. Loh, and J. E. Hirsch, "*d-wave pairing near a spin-density-wave instability*", Physical Review B **34**, 8190 (1986).

[25] C. Honerkamp, "*Density Waves and Cooper Pairing on the Honeycomb Lattice*", Phys. Rev. Lett. **100**, 146404 (2008).

[26] S. Chadov *et al.*, "*Tunable multifunctional topological insulators in ternary Heusler compounds*", Nature Materials **9**, 541 (2010).

[27] A. Manchon, H. C. Koo, J. Nitta, S. M. Frolov, and R. A. Duine, "*New perspectives for Rashba spin–orbit coupling*", Nature Materials **14**, 871 (2015).

[28] L. D. Landau and E. M. Lifshitz, *Quantum Mechanics: Non-Relativistic Theory*, en, (Elsevier, 2013)

[29] K. V. Shanavas, Z. S. Popović, and S. Satpathy, "*Theoretical model for Rashba spin-orbit interaction in $ d$ electrons*", Physical Review B **90**, 165108 (2014).

[30] G. Kresse and J. Furthmüller, "*Efficient iterative schemes for ab initio total-energy calculations using a plane-wave basis set*", Physical Review B **54**, 11169 (1996).

[31] K. V. Samokhin and V. P. Mineev, "*Gap structure in noncentrosymmetric superconductors*", Physical Review B **77**, 104520 (2008).

[32] A. Greco and A. P. Schnyder, "*Mechanism for Unconventional Superconductivity in the Hole-Doped Rashba-Hubbard Model*", Phys. Rev. Lett. **120**, 177002 (2018).

[33] S. Wolf and S. Rachel, "*Spin-orbit coupled superconductivity: Rashba-Hubbard model on the square lattice*", Phys. Rev. B **102**, 174512 (2020).

[34] J. Beyer *et al.*, *Rashba spin-orbit coupling in the square lattice Hubbard model: A truncated-unity functional renormalization group study*, tech. rep., arXiv:2210.09384 [cond-mat] type: article, arXiv, 2022.

[35] M. L. Kiesel, C. Platt, and R. Thomale, "*Unconventional Fermi Surface Instabilities in the Kagome Hubbard Model*", Phys. Rev. Lett. **110**, 126405 (2013).

[36] W.-S. Wang, Z.-Z. Li, Y.-Y. Xiang, and Q.-H. Wang, "*Competing electronic orders on kagome lattices at van Hove filling*", Phys. Rev. B **87**, 115135 (2013).

[37] B. R. Ortiz *et al.*, "*New kagome prototype materials: discovery of KV_3Sb_5,RbV_3S_5, and CsV_3S_5*", Phys. Rev. Materials **3**, 094407 (2019).

[38] B. R. Ortiz *et al.*, "*CsV_3S_5: A Z_2 Topological Kagome Metal with a Superconducting Ground State*", Phys. Rev. Lett. **125**, 247002 (2020).

[39] Y.-X. Jiang *et al.*, "*Unconventional chiral charge order in kagome superconductor KV3Sb5*", Nature Materials **20**, 1353 (2021).

[40] H. Zhao *et al.*, "*Cascade of correlated electron states in the kagome superconductor CsV3Sb5*", Nature **599**, 216 (2021).

[41] B. R. Ortiz *et al.*, "*Superconductivity in the Z_2 kagome metal KV_3S_5*", Phys. Rev. Materials **5**, 034801 (2021).

[42] Q. Yin *et al.*, "*Superconductivity and Normal-State Properties of Kagome Metal RbV_3Sb_5 Single Crystals*", Chinese Physics Letters **38**, 037403 (2021).

[43] X. Wu *et al.*, "*Nature of Unconventional Pairing in the Kagome Superconductors AV_3Sb_5 (A=K,Rb,Cs)*", Physical Review Letters **127**, 177001 (2021).

[44] M. L. Kiesel and R. Thomale, "*Sublattice interference in the kagome Hubbard model*", Phys. Rev. B **86**, 121105 (2012).

[45] W. M. Li *et al.*, "*Superconductivity in a unique type of copper oxide*", Proceedings of the National Academy of Sciences **116**, 12156 (2019).

[46] Y. Nomura *et al.*, "*Formation of a two-dimensional single-component correlated electron system and band engineering in the nickelate superconductor $NdNiO_2$*", Physical Review B **100**, 205138 (2019).

[47] X. Wu *et al.*, "*Robust $d_{x^2-y^2}$-wave superconductivity of infinite-layer nickelates*", Physical Review B **101**, 060504 (2020).

[48] P. Hansmann *et al.*, "*Turning a Nickelate Fermi Surface into a Cupratelike One through Heterostructuring*", Phys. Rev. Lett. **103**, 016401 (2009).

[49] J. M. Kosterlitz and D. J. Thouless, "*Ordering, metastability and phase transitions in two-dimensional systems*", Journal of Physics C: Solid State Physics **6**, 1181 (1973).

[50] P. Minnhagen, "*Kosterlitz- Thouless transition for a two-dimensional superconductor: Magnetic-field dependence from a Coulomb-gas analogy*", Physical Review B **23**, 5745 (1981).

[51] T. Uchihashi, "*Two-dimensional superconductors with atomic-scale thickness*", Superconductor Science and Technology **30**, 013002 (2016).

[52] D. B. Haviland, Y. Liu, and A. M. Goldman, "*Onset of superconductivity in the two-dimensional limit*", Physical Review Letters **62**, 2180 (1989).

[53] A. F. Hebard and A. T. Fiory, "*Critical-Exponent Measurements of a Two-Dimensional Superconductor*", Physical Review Letters **50**, 1603 (1983).

[54] X. Wu *et al.*, "*Superconductivity in a Hole-Doped Mott-Insulating Triangular Adatom Layer on a Silicon Surface*", Physical Review Letters **125**, 117001 (2020).

[55] L. Li, C. Richter, J. Mannhart, and R. C. Ashoori, "*Coexistence of magnetic order and two-dimensional superconductivity at LaAlO3/SrTiO3 interfaces*", Nature Physics **7**, 762 (2011).

[56] Y. Cao *et al.*, "*Unconventional superconductivity in magic-angle graphene superlattices*", Nature **556**, 43 (2018).

[57] Q.-Y. Wang *et al.*, "*Interface-Induced High-Temperature Superconductivity in Single Unit-Cell FeSe Films on $SrTiO_3$*", Chinese Physics Letters **29**, 037402 (2012).

[58] C. Liu *et al.*, "*Two-dimensional superconductivity and anisotropic transport at $KTaO_3$ (111) interfaces*", Science **371**, 716 (2021).

[59] S. He *et al.*, "*Phase diagram and electronic indication of high-temperature superconductivity at 65 K in single-layer FeSe films*", Nature Materials **12**, 605 (2013).

[60] Y. Cao *et al.*, "*Correlated insulator behaviour at half-filling in magic-angle graphene superlattices*", Nature **556**, 80 (2018).

[61] S. Wolf, D. Di Sante, T. Schwemmer, R. Thomale, and S. Rachel, "*Triplet Superconductivity from Nonlocal Coulomb Repulsion in an Atomic Sn Layer Deposited onto a Si(111) Substrate*", Physical Review Letters **128**, 167002 (2022).

[62] S. G. Davison and M. Stęślicka, *Basic Theory of Surface States*, en, (Clarendon Press, 1996)

[63] L. Zhao *et al.*, "*Emergent surface superconductivity in the topological insulator Sb2Te3*", Nature Communications **6**, 8279 (2015).

[64] O. O. Shvetsov, V. D. Esin, A. V. Timonina, N. N. Kolesnikov, and E. V. Deviatov, "*Surface superconductivity in a three-dimensional Cd3As2 semimetal at the interface with a gold contact*", Physical Review B **99**, 125305 (2019).

[65] Y. Xing *et al.*, "*Surface Superconductivity in the type II Weyl Semimetal TaIrTe4*", National Science Review **7**, arXiv:1805.10883 [cond-mat], 579 (2020).

[66] D. Shen *et al.*, "*Two-dimensional superconductivity and magnetotransport from topological surface states in AuSn4 semimetal*", Communications Materials **1**, 1 (2020).

[67] J. Song *et al.*, "*Coexistence of Surface Superconducting and Three-Dimensional Topological Dirac States in Semimetal KZnBi*", Physical Review X **11**, 021065 (2021).

[68] Q. Liu *et al.*, *Observation of surface superconductivity in a three-dimensional Dirac material*, tech. rep., arXiv:2206.03405 [cond-mat] type: article, arXiv, 2022.

[69] F. F. Tafti *et al.*, "*Superconductivity in the noncentrosymmetric half-Heusler compound LuPtBi: A candidate for topological superconductivity*", Physical Review B **87**, 184504 (2013).

[70] C. Timm, A. P. Schnyder, D. F. Agterberg, and P. M. R. Brydon, "*Inflated nodes and surface states in superconducting half-Heusler compounds*", Physical Review B **96**, 094526 (2017).

[71] Q.-Z. Wang, J. Yu, and C.-X. Liu, "*Unconventional superconductivity and surface pairing symmetry in half-Heusler compounds*", Physical Review B **97**, 224507 (2018).

[72] M. Dürrnagel, J. Beyer, R. Thomale, and T. Schwemmer, "*Unconventional superconductivity from weak coupling - A unified perspective on formalism and numerical implementation*", The European Physical Journal B **95**, 112 (2022).

[73] R. Shankar, "*Renormalization-group approach to interacting fermions*", Reviews of Modern Physics **66**, 129 (1994).

[74] S. Raghu, E. Berg, A. V. Chubukov, and S. A. Kivelson, "*Effects of longer-range interactions on unconventional superconductivity*", Physical Review B **85**, 024516 (2012).

[75] W. Cho, R. Thomale, S. Raghu, and S. A. Kivelson, "*Band structure effects on the superconductivity in Hubbard models*", Phys. Rev. B **88**, 064505 (2013).

[76] R. Nandkishore, L. S. Levitov, and A. V. Chubukov, "*Chiral superconductivity from repulsive interactions in doped graphene*", Nature Physics **8**, 158 (2012).

[77] T. Scaffidi and S. H. Simon, "*Large Chern Number and Edge Currents in Sr_2RuO_4*", Physical Review Letters **115**, 087003 (2015).

[78] P. W. Anderson, "*Random-Phase Approximation in the Theory of Superconductivity*", Phys. Rev. **112**, 1900 (1958).

[79] S. Graser, T. A. Maier, P. J. Hirschfeld, and D. J. Scalapino, "*Near-degeneracy of several pairing channels in multiorbital models for the Fe pnictides*", New Journal of Physics **11**, 025016 (2009).

[80] J. Beyer, J. B. Hauck, and L. Klebl, "*Reference results for the momentum space functional renormalization group*", The European Physical Journal B **95**, 65 (2022).

[81] M. Fink, "*Unconventional and topological superconductivity in correlated non-centrosymmetric systems with spin-orbit coupling*", PhD thesis, Universität Würzburg, 2019.

[82] C. Platt, W. Hanke, and R. Thomale, "*Functional renormalization group for multi-orbital Fermi surface instabilities*", Advances in Physics **62**, 453 (2013).

[83] D. S. de la Peña, J. Lichtenstein, and C. Honerkamp, "*Competing electronic instabilities of extended Hubbard models on the honeycomb lattice: A functional renormalization group calculation with high-wave-vector resolution*", Physical Review B **95**, 085143 (2017).

[84] D. S. de la Peña, J. Lichtenstein, C. Honerkamp, and M. M. Scherer, "*Antiferromagnetism and competing charge instabilities of electrons in strained graphene from Coulomb interactions*", Physical Review B **96**, 205155 (2017).

[85] J. B. Hauck and D. M. Kennes, "*TU^2FRG: a scalable approach for truncated unity functional renormalization group in generic fermionic models*", The European Physical Journal B **95**, 60 (2022).

[86] X.-G. Wen, *Quantum Field Theory of Many-Body Systems*, (Oxford University Press, 2007)

[87] N. Marzari, A. A. Mostofi, J. R. Yates, I. Souza, and D. Vanderbilt, "*Maximally localized Wannier functions: Theory and applications*", Rev. Mod. Phys. **84**, 1419 (2012).

[88] E. Şaşioğlu, C. Friedrich, and S. Blügel, "*Effective Coulomb interaction in transition metals from constrained random-phase approximation*", Physical Review B **83**, 121101 (2011).

[89] R. Feynman and A. Hibbs, *Quantum mechanics and path integrals*, International series in pure and applied physics, (McGraw-Hill, 1965)

[90] A. Altland and B. D. Simons, *Condensed Matter Field Theory*, en, (Cambridge University Press, 2010)

[91] P. Coleman, *Introduction to Many-Body Physics*, en, (Cambridge University Press, 2015)

[92] T. Schwemmer, "*Superconducting instabilities in correlated quantum materials*", MA thesis, Universität Würzburg, 2019.

[93] H. Bruus and K. Flensberg, *Many-Body Quantum Theory in Condensed Matter Physics: An Introduction*, en, (OUP Oxford, 2004)

[94] G. C. Wick, "*The Evaluation of the Collision Matrix*", Phys. Rev. **80**, 268 (1950).

[95] J. Polchinski, "*Effective Field Theory and the Fermi Surface*", arXiv:hep-th/9210046, arXiv: hep-th/9210046 (1999).

[96] L. Wang and O. Vafek, "*Unconventional superconductivity in a two-dimensional repulsive gas of fermions with spin–orbit coupling*", Physica C: Superconductivity and its Applications **497**, 6 (2014).

[97] W.-S. Wang *et al.*, "*Functional renormalization group and variational Monte Carlo studies of the electronic instabilities in graphene near* 1/4 *doping*", Physical Review B **85**, 035414 (2012).

[98] J. Lichtenstein, "*Functional renormalization group studies on competing orders in the square lattice*", Veröffentlicht auf dem Publikationsserver der RWTH Aachen University; Dissertation, RWTH Aachen University, 2018, Dissertation, Aachen: RWTH Aachen University, 2018, 1 Online–Ressource (104 Seiten) : Illustrationen, Diagramme.

[99] G. Esirgen and N. E. Bickers, "*Fluctuation-exchange theory for general lattice Hamiltonians*", Phys. Rev. B **55**, 2122 (1997).

[100] A. T. Rømer, D. D. Scherer, I. M. Eremin, P. J. Hirschfeld, and B. M. Andersen, "*Knight Shift and Leading Superconducting Instability from Spin Fluctuations in* Sr_2RuO_4", Phys. Rev. Lett. **123**, 247001 (2019).

[101] D. Bohm and D. Pines, "*A Collective Description of Electron Interactions. I. Magnetic Interactions*", Physical Review **82**, 625 (1951).

[102] D. Pines and D. Bohm, "*A Collective Description of Electron Interactions: II. Collective v Individual Particle Aspects of the Interactions*", Physical Review **85**, 338 (1952).

[103] D. Pines, "*A Collective Description of Electron Interactions: IV. Electron Interaction in Metals*", Physical Review **92**, 626 (1953).

[104] D. Bohm and D. Pines, "*A Collective Description of Electron Interactions: III. Coulomb Interactions in a Degenerate Electron Gas*", Physical Review **92**, 609 (1953).

[105] M. Gell-Mann and K. A. Brueckner, "*Correlation Energy of an Electron Gas at High Density*", Physical Review **106**, 364 (1957).

[106] C. Nayak, "*Density-wave states of nonzero angular momentum*", Phys. Rev. B **62**, 4880 (2000).

[107] Y. Yanase *et al.*, "*Theory of superconductivity in strongly correlated electron systems*", Physics Reports **387**, 1 (2003).

[108] K. G. Wilson, "*Renormalization Group and Critical Phenomena. II. Phase-Space Cell Analysis of Critical Behavior*", Physical Review B **4**, 3184 (1971).

[109] D. S. Fisher, "*Random fields, random anisotropies, nonlinear \ensuremath{\sigma} models, and dimensional reduction*", Physical Review B **31**, 7233 (1985).

[110] G. Benfatto and G. Gallavotti, "*Perturbation theory of the Fermi surface in a quantum liquid. A general quasiparticle formalism and one-dimensional systems*", Journal of Statistical Physics **59**, 541 (1990).

[111] R. Shankar, "*Renormalization group for interacting fermions in d > 1*", Physica A: Statistical Mechanics and its Applications **177**, 530 (1991).

[112] C. Wetterich, "*Exact evolution equation for the effective potential*", Physics Letters B **301**, 90 (1993).

[113] D. Zanchi and H. J. Schulz, "*Weakly correlated electrons on a square lattice: A renormalization group theory*", Europhysics Letters **44**, 235 (1998).

[114] A. V. Chubukov and J. P. Lu, "*Pairing instabilities in the two-dimensional Hubbard model*", Physical Review B **46**, 11163 (1992).

[115] A. V. Chubukov, "*Kohn-Luttinger effect and the instability of a two-dimensional repulsive Fermi liquid at T=0*", Physical Review B **48**, 1097 (1993).

[116] S. Maiti and A. V. Chubukov, "*Renormalization group flow, competing phases, and the structure of superconducting gap in multiband models of iron-based superconductors*", Physical Review B **82**, 214515 (2010).

[117] R. Nandkishore, R. Thomale, and A. V. Chubukov, "*Superconductivity from weak repulsion in hexagonal lattice systems*", Phys. Rev. B **89**, 144501 (2014).

[118] C. J. Halboth and W. Metzner, "*d-Wave Superconductivity and Pomeranchuk Instability in the Two-Dimensional Hubbard Model*", Physical Review Letters **85**, 5162 (2000).

[119] C. Honerkamp and M. Salmhofer, "*Magnetic and Superconducting Instabilities of the Hubbard Model at the Van Hove Filling*", Physical Review Letters **87**, 187004 (2001).

[120] P. Kopietz and T. Busche, "*Exact renormalization group flow equations for nonrelativistic fermions: Scaling toward the Fermi surface*", Physical Review B **64**, 155101 (2001).

[121] J. Reiss, D. Rohe, and W. Metzner, "*Renormalized mean-field analysis of antiferromagnetism and d-wave superconductivity in the two-dimensional Hubbard model*", Physical Review B **75**, 075110 (2007).

[122] W. Metzner, M. Salmhofer, C. Honerkamp, V. Meden, and K. Schönhammer, "*Functional renormalization group approach to correlated fermion systems*", Reviews of Modern Physics **84**, 299 (2012).

[123] J. Lichtenstein *et al.*, "*High-performance functional Renormalization Group calculations for interacting fermions*", Computer Physics Communications **213**, 100 (2017).

[124] A. T. Rømer *et al.*, "*Pairing in the two-dimensional Hubbard model from weak to strong coupling*", Phys. Rev. Research **2**, 013108 (2020).

[125] N. F. Berk and J. R. Schrieffer, "*Effect of Ferromagnetic Spin Correlations on Superconductivity*", Phys. Rev. Lett. **17**, 433 (1966).

[126] N. E. Bickers, D. J. Scalapino, and S. R. White, "*Conserving Approximations for Strongly Correlated Electron Systems: Bethe-Salpeter Equation and Dynamics for the Two-Dimensional Hubbard Model*", Phys. Rev. Lett. **62**, 961 (1989).

[127] N. E. Bickers and S. R. White, "*Conserving approximations for strongly fluctuating electron systems. II. Numerical results and parquet extension*", Phys. Rev. B **43**, 8044 (1991).

[128] T. Takimoto, T. Hotta, and K. Ueda, "*Strong-coupling theory of superconductivity in a degenerate Hubbard model*", Phys. Rev. B **69**, 104504 (2004).

[129] M. Dürrnagel, "*Emergent order in correlated Fermiliquids: A diamagnetic perspective*", MA thesis, Universität Würzburg, 2022.

[130] M. Salmhofer and C. Honerkamp, "*Fermionic Renormalization Group Flows: Technique and Theory*", Progress of Theoretical Physics **105**, 1 (2001).

[131] J. J. Quinn and R. A. Ferrell, "*Electron Self-Energy Approach to Correlation in a Degenerate Electron Gas*", Physical Review **112**, 812 (1958).

[132] M. Gell-Mann, "*Specific Heat of a Degenerate Electron Gas at High Density*", Physical Review **106**, 369 (1957).

[133] R. Akashi, "*Revisiting homogeneous electron gas in pursuit of properly normed ab initio Eliashberg theory*", Physical Review B **105**, 104510 (2022).

[134] S. Wolf, T. L. Schmidt, and S. Rachel, "*Unconventional superconductivity in the extended Hubbard model: Weak-coupling renormalization group*", Physical Review B **98**, 174515 (2018).

[135] A. T. Rømer *et al.*, "*Pairing symmetry of the one-band Hubbard model in the paramagnetic weak-coupling limit: A numerical RPA study*", Phys. Rev. B **92**, 104505 (2015).

[136] W. Nolting, *Grundkurs Theoretische Physik 5/2: Quantenmechanik - Methoden und Anwendungen*, de, (Springer-Verlag, 2011)

[137] A. P. Mackenzie, T. Scaffidi, C. W. Hicks, and Y. Maeno, "*Even odder after twenty-three years: the superconducting order parameter puzzle of Sr_2RuO_4*", npj Quantum Materials **2**, 40 (2017).

[138] G. Dresselhaus, "*Spin-Orbit Coupling Effects in Zinc Blende Structures*", Physical Review **100**, 580 (1955).

[139] E. Rashba, "*Properties of semiconductors with an extremum loop. 1. Cyclotron and combinational resonance in a magnetic field perpendicular to the plane of the loop*", Sov. Phys. Solid State **2**, 1109 (1960).

[140] S. LaShell, B. A. McDougall, and E. Jensen, "*Spin Splitting of an Au(111) Surface State Band Observed with Angle Resolved Photoelectron Spectroscopy*", Physical Review Letters **77**, 3419 (1996).

[141] L. Petersen and P. Hedegård, "*A simple tight-binding model of spin–orbit splitting of sp-derived surface states*", Surface Science **459**, 49 (2000).

[142] G. Bihlmayer, Y. M. Koroteev, P. M. Echenique, E. V. Chulkov, and S. Blügel, "*The Rashba-effect at metallic surfaces*", Surface Science, Berlin, Germany: 4–9 September 2005 **600**, 3888 (2006).

[143] P. A. Frigeri, D. F. Agterberg, and M. Sigrist, "*Spin susceptibility in superconductors without inversion symmetry*", New Journal of Physics **6**, arXiv:cond-mat/0405179, 115 (2004).

[144] P. A. Frigeri, D. F. Agterberg, A. Koga, and M. Sigrist, "*Superconductivity without Inversion Symmetry: MnSi versus CePt3Si*", Physical Review Letters **92**, 097001 (2004).

[145] T. Schwemmer, D. Di Sante, J. Schmalian, and R. Thomale, *Chiral surface superconductivity in half-Heusler semimetals*, tech. rep., arXiv:2212.09786 [cond-mat] type: article, arXiv, 2022.

[146] C. Proust and L. Taillefer, "*The Remarkable Underlying Ground States of Cuprate Superconductors*", Annual Review of Condensed Matter Physics **10**, 409 (2019).

[147] Q. Si, R. Yu, and E. Abrahams, "*High-temperature superconductivity in iron pnictides and chalcogenides*", Nature Reviews Materials **1**, 1 (2016).

[148] G. R. Stewart, "*Superconductivity in iron compounds*", Reviews of Modern Physics **83**, 1589 (2011).

[149] H.-H. Wen and S. Li, "*Materials and Novel Superconductivity in Iron Pnictide Superconductors*", Annual Review of Condensed Matter Physics **Vol. 2:121-140** (2011).

[150] N. Reyren *et al.*, "*Superconducting Interfaces Between Insulating Oxides*", Science **317**, 1196 (2007).

[151] J. A. Bert *et al.*, "*Direct imaging of the coexistence of ferromagnetism and superconductivity at the LaAlO3 / SrTiO3 interface*", Nature Physics **7**, 767 (2011).

[152] A. Gozar *et al.*, "*High-temperature interface superconductivity between metallic and insulating copper oxides*", Nature **455**, 782 (2008).

[153] L. Fu and C. L. Kane, "*Superconducting Proximity Effect and Majorana Fermions at the Surface of a Topological Insulator*", Physical Review Letters **100**, 096407 (2008).

[154] L. Fu and E. Berg, "*Odd-Parity Topological Superconductors: Theory and Application to* $Cu_xBi_2Se_3$", Physical Review Letters **105**, 097001 (2010).

[155] X.-L. Qi, T. L. Hughes, S. Raghu, and S.-C. Zhang, "*Time-Reversal-Invariant Topological Superconductors and Superfluids in Two and Three Dimensions*", Physical Review Letters **102**, 187001 (2009).

[156] J. Linder, Y. Tanaka, T. Yokoyama, A. Sudbø, and N. Nagaosa, "*Unconventional Superconductivity on a Topological Insulator*", Physical Review Letters **104**, 067001 (2010).

[157] X.-L. Qi, T. L. Hughes, and S.-C. Zhang, "*Topological invariants for the Fermi surface of a time-reversal-invariant superconductor*", Physical Review B **81**, 134508 (2010).

[158] X.-L. Qi and S.-C. Zhang, "*Topological insulators and superconductors*", Reviews of Modern Physics **83**, 1057 (2011).

[159] D. Saint-James and P. D. de Gennes, "*Onset of superconductivity in decreasing fields*", Physics Letters **7**, 306 (1963).

[160] C. F. Hempstead and Y. B. Kim, "*Resistive Transitions and Surface effects in Type-II Superconductors*", Physical Review Letters **12**, 145 (1964).

[161] M. Strongin, A. Paskin, D. G. Schweitzer, O. F. Kammerer, and P. P. Craig, "*Surface Superconductivity in Type I and Type II Superconductors*", Physical Review Letters **12**, 442 (1964).

[162] A. A. Abrikosov, "*Concerning surface superconductivity in strong magnetic fields*", Soviet Physics JETP **20**, 480 (1965).

[163] H. J. Fink and W. C. H. Joiner, "*Surface Nucleation and Boundary Conditions in Superconductors*", Physical Review Letters **23**, 120 (1969).

[164] V. A. Schweigert and F. M. Peeters, "*Influence of the confinement geometry on surface superconductivity*", Physical Review B **60**, 3084 (1999).

[165] E. Montevecchi and J. O. Indekeu, "*Effects of confinement and surface enhancement on superconductivity*", Physical Review B **62**, 14359 (2000).

[166] D. A. Gorokhov, "*Surface Superconductivity of Dirty Two-Band Superconductors: Applications to MgB_2*", Physical Review Letters **94**, 077004 (2005).

[167] N. Keller, J. L. Tholence, A. Huxley, and J. Flouquet, "*Angular Dependence of the Upper Critical Field of the Heavy Fermion Superconductor UPt_3*", Physical Review Letters **73**, 2364 (1994).

[168] D. F. Agterberg and M. B. Walker, "*Effect of diffusive boundaries on surface superconductivity in unconventional superconductors*", Physical Review B **53**, 15201 (1996).

[169] V. Barzykin and L. P. Gor'kov, "*Inhomogeneous Stripe Phase Revisited for Surface Superconductivity*", Physical Review Letters **89**, 227002 (2002).

[170] N. B. Kopnin, T. T. Heikkilä, and G. E. Volovik, "*High-temperature surface superconductivity in topological flat-band systems*", Physical Review B **83**, 220503 (2011).

[171] N. B. Kopnin, M. Ijäs, A. Harju, and T. T. Heikkilä, "*High-temperature surface superconductivity in rhombohedral graphite*", Physical Review B **87**, 140503 (2013).

[172] S. Das Sarma and Q. Li, "*Many-body effects and possible superconductivity in the two-dimensional metallic surface states of three-dimensional topological insulators*", Physical Review B **88**, 081404 (2013).

[173] D. Li, B. Rosenstein, B. Y. Shapiro, and I. Shapiro, "*Quantum critical point in the superconducting transition on the surface of a topological insulator*", Physical Review B **90**, 054517 (2014).

[174] Y. Wang and R. M. Nandkishore, "*Topological surface superconductivity in doped Weyl loop materials*", Physical Review B **95**, 060506 (2017).

[175] B. Weitzel and H. Micklitz, "*Superconductivity in granular systems built from well-defined rhombohedral Bi-clusters: Evidence for Bi-surface superconductivity*", Physical Review Letters **66**, 385 (1991).

[176] E. Rotenberg, J. W. Chung, and S. D. Kevan, "*Spin-Orbit Coupling Induced Surface Band Splitting in Li/W(110) and Li/Mo(110)*", Physical Review Letters **82**, 4066 (1999).

[177] L. Petersen *et al.*, "*Direct imaging of the two-dimensional Fermi contour: Fourier-transform STM*", Physical Review B **57**, R6858 (1998).

[178] J. Ortega, F. Flores, and A. L. Yeyati, "*Electron correlation effects in the Si(111)-7x7 surface*", Physical Review B **58**, 4584 (1998).

[179] R. Losio, K. N. Altmann, and F. J. Himpsel, "*Fermi surface of Si(111) 7x7*", Physical Review B **61**, 10845 (2000).

[180] R. Cortés *et al.*, "*Competing charge ordering and Mott phases in a correlated Sn/Ge(111) two-dimensional triangular lattice*", Physical Review B **88**, 125113 (2013).

[181] F. Reis *et al.*, "*Bismuthene on a SiC substrate: A candidate for a high-temperature quantum spin Hall material*", Science **357**, 287 (2017).

[182] F. Adler *et al.*, "*Correlation-Driven Charge Order in a Frustrated Two-Dimensional Atom Lattice*", Physical Review Letters **123**, 086401 (2019).

[183] L. H. Thomas, "*The Motion of the Spinning Electron*", Nature **117**, 514 (1926).

[184] F. Heusler, "*Ueber magnetische Manganlegierungen*", Verhandlungen der Deutschen Physikalischen Gesellschaft **5.** S. 219 ff. (1903).

[185] H. C. Kandpal, C. Felser, and R. Seshadri, "*Covalent bonding and the nature of band gaps in some half-Heusler compounds*", Journal of Physics D: Applied Physics **39**, 776 (2006).

[186] P. C. Canfield *et al.*, "*Magnetism and heavy fermion-like behavior in the RBiPt series*", Journal of Applied Physics **70**, 5800 (1991).

[187] P. M. R. Brydon, L. Wang, M. Weinert, and D. F. Agterberg, "*Pairing of $j = 3/2$ Fermions in Half-Heusler Superconductors*", Physical Review Letters **116**, 177001 (2016).

[188] R. Majumder and M. M. Hossain, "*First-principles study of structural, electronic, elastic, thermodynamic and optical properties of topological superconductor LuPtBi*", Computational Condensed Matter **21**, e00402 (2019).

[189] G. Goll *et al.*, "*Thermodynamic and transport properties of the non-centrosymmetric superconductor LaBiPt*", Physica B: Condensed Matter **403**, 1065 (2008).

[190] N. P. Butch, P. Syers, K. Kirshenbaum, A. P. Hope, and J. Paglione, "*Superconductivity in the topological semimetal YPtBi*", Physical Review B **84**, 220504 (2011).

[191] L. Savary, J. Ruhman, J. W. F. Venderbos, L. Fu, and P. A. Lee, "*Superconductivity in three-dimensional spin-orbit coupled semimetals*", Physical Review B **96**, 214514 (2017).

[192] I. Boettcher and I. F. Herbut, "*Unconventional Superconductivity in Luttinger Semimetals: Theory of Complex Tensor Order and the Emergence of the Uniaxial Nematic State*", Physical Review Letters **120**, 057002 (2018).

[193] M. Bahari, S.-B. Zhang, and B. Trauzettel, "*Intrinsic finite-energy Cooper pairing in $j = 3/2$ superconductors*", Physical Review Research **4**, L012017 (2022).

[194] K. Ishihara *et al.*, "*Tuning the Parity Mixing of Singlet-Septet Pairing in a Half-Heusler Superconductor*", Physical Review X **11**, 041048 (2021).

[195] M. Meinert, "*Unconventional Superconductivity in YPtBi and Related Topological Semimetals*", Physical Review Letters **116**, 137001 (2016).

[196] Z. K. Liu *et al.*, "*Observation of unusual topological surface states in half-Heusler compounds LnPtBi (Ln=Lu, Y)*", Nature Communications **7**, 12924 (2016).

[197] A. Banerjee *et al.*, "*Evidence for a superconducting surface state in the half-heusler alloy LuPtBi*", *Bulletin of the American Physical Society*, vol. Volume 60, Number 1, (APS March Meeting 2015, 2015)

[198] P. E. Blöchl, "*Projector augmented-wave method*", Physical Review B **50**, 17953 (1994).

[199] J. P. Perdew, K. Burke, and M. Ernzerhof, "*Generalized Gradient Approximation Made Simple*", Physical Review Letters **77**, 3865 (1996).

[200] W. Kohn and L. J. Sham, "*Self-Consistent Equations Including Exchange and Correlation Effects*", Phys. Rev. **140**, A1133 (1965).

[201] A. A. Mostofi *et al.*, "*wannier90: A tool for obtaining maximally-localised Wannier functions*", Computer Physics Communications **178**, 685 (2008).

[202] C. Franchini *et al.*, "*Maximally localized Wannier functions in LaMnO3 within PBE + U, hybrid functionals and partially self-consistent GW: an efficient route to construct ab initio tight-binding parameters for eg perovskites*", Journal of Physics: Condensed Matter **24**, 235602 (2012).

[203] C. L. Kane and E. J. Mele, "*Quantum Spin Hall Effect in Graphene*", Physical Review Letters **95**, 226801 (2005).

[204] I. Martin and C. D. Batista, "*Itinerant Electron-Driven Chiral Magnetic Ordering and Spontaneous Quantum Hall Effect in Triangular Lattice Models*", Physical Review Letters **101**, 156402 (2008).

[205] M. S. Dresselhaus, G. Dresselhaus, and A. Jorio, *Group Theory: Application to the Physics of Condensed Matter*, en, (Springer Berlin Heidelberg, 2009)

[206] A. F. Kemper *et al.*, "*Sensitivity of the superconducting state and magnetic susceptibility to key aspects of electronic structure in ferropnictides*", New Journal of Physics **12**, 073030 (2010).

[207] M. L. Kiesel, C. Platt, W. Hanke, D. A. Abanin, and R. Thomale, "*Competing many-body instabilities and unconventional superconductivity in graphene*", Physical Review B **86**, 020507 (2012).

[208] N. Read and D. Green, "*Paired states of fermions in two dimensions with breaking of parity and time-reversal symmetries and the fractional quantum Hall effect*", Physical Review B **61**, 10267 (2000).

[209] T. Senthil, J. B. Marston, and M. P. A. Fisher, "*Spin quantum Hall effect in unconventional superconductors*", Physical Review B **60**, 4245 (1999).

[210] B. Horovitz and A. Golub, "*Superconductors with broken time-reversal symmetry: Spontaneous magnetization and quantum Hall effects*", Physical Review B **68**, 214503 (2003).

[211] R. M. Fernandes, P. P. Orth, and J. Schmalian, "*Intertwined Vestigial Order in Quantum Materials: Nematicity and Beyond*", Annual Review of Condensed Matter Physics **10**, 133 (2019).

[212] A. M. Polyakov, "*Interaction of goldstone particles in two dimensions. Applications to ferromagnets and massive Yang-Mills fields*", Physics Letters B **59**, 79 (1975).

[213] D. Friedan, "*Nonlinear Models in* $2 + \epsilon$ *Dimensions*", Physical Review Letters **45**, 1057 (1980).

[214] P. P. Orth, P. Chandra, P. Coleman, and J. Schmalian, "*Emergent criticality and Friedan scaling in a two-dimensional frustrated Heisenberg antiferromagnet*", Physical Review B **89**, 094417 (2014).

Acknowledgements

This thesis would not have been possible without the support of many colleagues, friends and loved ones.

First of all I want to thank Ronny Thomale for sparking my enthusiasm for quantum physics in general and condensed matter theory in particular, as well as providing me with endless opportunities during my PhD. I want to thank Domenico di Sante for all of his advice, and his friendship. My time at the institute for theoretical physics I would not have been the same if Tobias Müller and Michael Klett wouldn't have welcomed the next generation of PhD students with open arms and all of their support, for which I am immensely grateful. There are many other people I have been discussing and working with during the last four years who supported me and provided me important insights. I especially wish to thank Prof. Dr. Dr. h.c. Werner Hanke, Xianxin Wu, Pratyay Ghosh, Janik Potten, Stephan Rachel, Martin Greiter, Armando Consiglio, David Riegler, Mario Fink, Florian Goth, Srinivas Raghu, Matthew Bunney, Richard Schielein, Peter Wahl, Giorgio Sangiovanni, Jonas Hauck and Lennart Klebl. In particular I want to thank my friends Jacob, Matteo and Hendrik for their endless patience in discussing physics and software with me and Tobias Helbig and Tobias Hofmann for being the best office mates.

I thank all members of the Institute of physics I met during my time in Würzburg. In particular, I wish to mention Philipp Kagerer, Philipp Eck, Johannes Beierlein, Lukas Elter, Riccardo Sorbello, Jonas Schwab, Anja Wenger, Janis Seufert, Nora Taufertshöfer, Alex Stegmaier, Alex Fritzsche and our secretary Madalina Koch.

Finally I want to thank Lukas for his shoreless friendship, my family for their constant support and Laura for her endless patience and everything else.